Fundamental Studies on Wave Propagation Characteristics through Soils(Dissertation_全文)

AUTHOR(S):

Hori, Masayuki

FUNDAMENTAL STUDIES
ON
WAVE PROPAGATION CHARACTERISTICS
THROUGH SOILS

By

MASAYUKI HORI

FEBRUARY, 1974

FUNDAMENTAL STUDIES
ON
WAVE PROPAGATION CHARACTERISTICS
THROUGH SOILS

By

MASAYUKI HORI

FEBRUARY, 1974

SUMMARY

The main purposes of this thesis are: (1) to develop new experimental laboratory technique for study on stress wave propagation through soils; (2) to investigate the wave characteristics in soils and to offer the useful data of dynamic properties of soils for earthquake response analyses of a ground and design of foundations of machines; and (3) to develop methods for analyzing the earthquake response of an inhomogeneous ground.

Much efforts have been directed toward the development of the shock tube technique for studying the stress wave propagation through soils. In order to measure the dynamic soil strain, the condenser-type soil strain meter is devised by the author. The experimental apparatus of the shock tube technique has been accomplished with various measuring systems enough to observe accurately aspects of wave characteristics in soils.

The dynamic modulus of elasticity is calculated from the velocity of wave front and considered with respect to the void ratio and the confining pressure of the soils. The relationship among the modulus, the void ratio and the confining pressure agrees with those obtained from previous studies. The attenuation of stress wave is considered with respect to the stress or strain amplitude. It is confirmed that when the stress or strain amplitude is less than a certain level, the attenuation with distance is scarcely little. This stress or strain level corresponds to 20-25 % of the compressive strength of the soil or to 0.1 % strain, respectively. In the range of this strain level, the soil is assumed as the spring-Voigt model and its viscoelastic constants are obtained from the experimental results.

The approximate method for analyzing the earthquake response of an inhomogeneous ground is developed on the basis of multiple reflection theory of waves. By this technique, the response of a particular inhomogeneous

elastic soil layer can be calculated simply with a satisfactory accuracy and short computation time. The numerical examples are given for Osaka ground site and the results are examined with respect to maximum accelerations and shear strains in the ground.

ACKNOWLEDGMENT

The author wishes to express his deepest gratitude to Professor Koichi Akai of Kyoto University for his stimulating discussions and continuous guidance and encouragement. A grateful acknowledgment is made to Assistant Professor Toshihisa Adachi for his helpful advices, criticisms and encouragement.

The author is also indebted to Assistant Professor Kenzo Toki of Disaster Prevention Research Institute of Kyoto University and Mr. Yoshinori Iwasaki, Chief Engineer of Osaka Soil Test Laboratory, for their providing adequate advices concerned with the earthquake response analyses of grounds; Messrs. Tamio Shimogami and Fusao Oka, graduate students at the Professor Akai's Laboratory, for their stimulating discussions andsupport; Dr. Yuzo Ohnishi, Research Assistant of Kyoto University, for his kind help of the translation into English as well as offering helpful suggestions to accomplish this thesis; Mr. Hisayoshi Yoshikawa for typing the manuscript so quickly; Mr. Koji Hirobe for his drawing the figures; and Miss Yoko Maruyama for her assistance in the final preparation of this thesis.

The author also wishes to express sincere thanks to Professor Goro Kamimoto in the Department of Aeronautic Engineering of Kyoto University who advised him in designing the shock tube.

NOTATIONS

A	cross sectional area of a conductor(in Chapter 2)
A	stress amplitude(in Chapter 4)
A_H, A_s	amplitudes of sinusoidal steady-state displacement at base rock and surface
A_o, A_x	amplitudes of stress wave at reference point and at arbitrary distance from reference point
$A(x)(A(\xi))$	function of transmission coefficient
$B(x)(B(\xi))$	function of reflection coefficient
C, C_1, C_2	
C_3, C_4,	
C_A, C_B,	
C_a, C_b,	
C_o	electrostatic capacities
$C_i(x)$	cosine integral
C_Q, C_R	constants
D	spacing of two conductors
D_i	descending wave in i*th* layer
$D(t, x)$	descending wave in inhomogeneous soil layer
E	Young's modulus or spring constant in viscoelastic model
E'	constant of free spring in spring-Voigt model or Burgers model
E_c	chord modulus
E_d	dynamic Young's modulus
E_i	initial tangent modulus
E_s	static modulus of elasticity
$F(e), F'(e)$	functions of void ratio
$F(\epsilon)$	function of strain
G	shear modulus(or Lamé's constant)
G_d	dynamic shear modulus
G_i	shear modulus of i*th* layer
G_s	specific gravity
$G(x)(G(\xi))$	distribution function of shear modulus
H	thickness of inhomogeneous soil layer
H_i	thickness of i*th* layer
$J_1(\frac{\sigma}{q}, t)$	initial compliance
K	bulk modulus
M	modulus of deformation

$1/Q$	specific dissipation function
S_r	degree of saturation
$S_i(x)$	sine integral
T'	dimensionless rise time
T_o	a time
T_p	prominent period
U_i	displacement component of fluid(in Chapter 4)
U_i	ascending wave in i*th* layer(in Chapter 5)
$U(t, x)$	ascending wave in inhomogeneous soil layer
$U_1(i\omega)$, ..	Fourier transformations of $u_1(t)$, ...
$U_{s1}(i\omega)$, ..	Fourier transformations of $u_{s1}(t)$, ...
$U_c(i\omega)$, $U_s(i\omega)$,	
$U_x(i\omega)$	Fourier transformations of $u_c(t)$, $u_s(t)$, $u_x(t)$
V	electric voltage
V_C, V_H	phase velocities of compressional and shear waves
V_d	phase velocity at infinite frequency of compressional wave of the second kind
V_l, V_s	phase velocities at zero frequency of compressional and shear waves
V_n, V_p	phase velocities at infinite frequency of compressional and shear waves
W	potential energy stored per cycle
ΔW	energy dissipated per cycle
Y_1, Y_2	real and imaginary parts of complex modulus
a	a constant(in Chapter 2)
a	amplitude of sinusoidal steady-state displacement of incident motion(in Chapter 5)
a_o	dimensionless frequency
b	a coefficient
c	velocity
c_P	velocity of compressional wave
c_R	velocity of rod wave
c_S	velocity of shear wave
c_i	shear wave velocity in i*th* layer
c_g	group velocity
c_o	phase velocity of rod wave at zero frequency(in Chapter 4)
c_o	shear wave velocity at ground surface(in Chapter 5)
$c(x)$($c(\xi)$)	distribution function of shear wave velocity
c_p	phase velocity

e	volumetric strain
e	void ratio
e_{ij}	component of strain tensor
$\bar{e}$, $\bar{e}$	dilatations of elastic structure and fluid
f	frequency
$f(t - T)$	memory function
$f(\xi)$	normalized distribution function of shear wave velocity
g	acceleration of gravity
$g(1)$	a functional value
h	damping ratio
i	imaginary unit
k	a constant(in Chapter 2)
k	ratio of spring constant of Voigt element to free spring in spring-Voigt model(in Chapter 4)
n	porosity
p	consolidation pressure ; total pressure acting on fluid per unit area of cross section of porous material(in Chapter 4)
p_c	effective confining pressure
p_i	pre-consolidation pressure
q, q_u	unconfined compressive strengths
q_{max}	triaxial compressive strength
r	radius of rod
s_u	shear strength
t	time
t_c, t_x	rise times of input wave and wave at a certain distance
u	displacement
u_i	displacement component of solid
$u(x, t)$	displacement
u	displacement vector
$u_s(t)$	earthquake motion at ground surface
$u_o(t)$	incident earthquake motion
$u_i(t, z)$	displacement in ith layer
$u_{s1}(t)$, ..	surface motions
$u_1(t)$, ...	motions at base rock
w	moisture content
x	coordinate
z_i	coordinate of ith layer
α	attenuation constant

α_C, α_H	attenuation constants of compressional and shear waves
α_i	impedance ratio of i*th* layer
β	a parameter
β_i, β_i'	reflection coefficients of i*th* layer
β_n, β_n'	reflection coefficients at interface of base rock
γ_d	dry density
γ_w	specific mass density of fluid
γ_o	amplitude of shear strain
γ_i, γ_i'	transmission coefficients of i*th* layer
γ_n	transmission coefficient at interface of base rock
γ_{ij}	component of deviatoric strain tensor
$\gamma(t, x)$	shear strain at arbitrary depth
δ_C, δ_H	logarithmic decrements of compressional and shear waves
δ_T	logarithmic decrement
ϵ	normal strain
$\dot{\epsilon}$	strain rate
$\bar{\epsilon}$	dilatation
ϵ_1	major principal strain
ϵ_o	dielectric constant
ϵ_s	specific dielectric constant
$\epsilon(T)$	strain at time T
η	fluid viscosity
θ_{sV}, θ_C, θ_H	square of ratio of phase velocity at zero frequency to that at infinite frequency of rod wave, compressional wave, shear wave in spring-Voigt material
λ	Lamé's constant ; wavelength
μ	rheological constant of dashpot in viscoelastic models
ν	Poisson's ratio
ξ	dimensionless distance
ρ, ρ_{11}, ρ_{12}, ρ_{22}	mass densities
ρ_1, ρ_2	masses of solid and fluid per unit volume of aggregate
ρ_{12}	additional apparent mass
ρ_a	additional mass
ρ_s, ρ_f	mass densities of solid and fluid
ρ_i	density of i*th* layer

$\rho(x)$	distribution function of density in inhomogeneous soil layer
Σ'	dimensionless stress
σ	normal stress
σ_o	amplitude of cyclic stress
σ_1, σ_3	principal stresses
σ'_m	mean effective principal stress
$\sigma(\varepsilon, t)$	stress at time t
σ_{ij}	component of stress tensor
τ	dimensionless time
τ_C, τ_H	time constants of compressional and shear waves
τ_o	amplitude of shear stress
τ_i	traveling time of wave in ith layer
τ_M	relaxation time of Maxwell model
τ_V	retardation time of Voigt model
τ_{sV}	time constant of spring-Voigt model
ϕ_s	phase characteristic at ground surface
ϕ	wave number
$\chi(x)(\chi(\xi))$	distribution function of characteristic impedance
ψ	specific damping capacity
ω	angular frequency
ω_c	characteristic frequency
$\bar{\omega}_i$	component of rotation
ω	rotation of displacement vector u
∇^2	Laplacian

CONTENTS

Title	*page*
Summary	i
Acknowledgment	iii
Notations	iv
Chapter 1 Introduction	1
1.1 Introduction	1
1.2 Review of Previous Studies	7
1.2.1 Studies on Dynamic Modulus and Damping of Soils	8
1.2.2 Studies on Stress Wave Propagation	10
1.2.3 Studies on Earthquake Response Analyses of Ground	13
1.3 Scope of Study	14
References	17
Chapter 2 Device of Condenser-Type Soil Strain Meter	20
2.1 Introduction	20
2.2 Principle of Operation in the Meter	22
2.2.1 Apparatus	22
2.2.2 Principle of Operation	22
2.3 Calibration	26
2.4 Applications	30
2.4.1 One-Dimensional Stress Wave Propagation Test	30
2.4.2 Unconfined Compression Test	32
2.5 Conclusions	37
References	38
Chapter 3 Experimental Study on Stress Wave Propagation through Soils	39

3.1 Introduction 39
3.2 Waves in the Linear Elastic Body 39
3.3 Experimental Apparatus 42
3.3.1 Shock Tube 42
3.3.2 Apparatus for Compressional Wave Propagation Test 47
3.3.3 Triaxial Compression Chamber 47
3.4 Measuring Equipment 51
3.4.1 Measurement of Dynamic Soil Stress 54
3.4.2 Measurement of Dynamic Soil Strain 54
3.4.3 Measurement of Pore Water Pressure 54
3.5 Experimental Procedure 55
3.5.1 Compressional Wave Propagation Test 55
3.5.2 Rod Wave Propagation Test 56
3.6 Experimental Results and Discussions 61
3.6.1 Compressional Wave Velocity in Partially Saturated Soil 61
3.6.2 Rod Wave Velocity and Dynamic Modulus of Elasticity of the Saturated Clayey Soil 63
3.6.3 Relationship between Rod Wave Velocity and Dynamic Stress-Strain Curves during Stress Wave Propagation 72
3.6.4 Attenuation of Wave 77
3.7 Conclusions 85
References 88
Chapter 4 Viscoelastic Approach to Stress Wave Propagation through Soils 90
4.1 Introduction 90

4.2 Wave Characteristics of Spring-Voigt Model 91
4.2.1 Selection of Model 91
4.2.2 General Behaviors of the Spring-Voigt Model .. 100
4.2.3 Wave Characteristics 103
4.3 Similarity of Wave Characteristics in Viscoelastic Materials and Saturated Porous Elastic Media 109
4.3.1 Biot's Approach 111
4.3.2 Ishihara's Approach 113
4.3.3 Comparison with the Wave Characteristics of Spring-Voigt Model 115
4.4 Experimental Results and Discussions 120
4.4.1 Determination of the Viscoelastic Constants of the Spring-Voigt Model 120
4.4.2 Estimation of E' 127
4.4.3 Estimation of the Time Constant 128
4.4.4 Estimation of k 132
4.4.5 Estimation of the Logarithmic Decrement 132
4.5 Conclusions 134
References 140
Chapter 5 Analysis of Earthquake Motions of Inhomogeneous Elastic Surface Layer with Application of Multiple Reflection Theory 144
5.1 Introduction 144
5.2 Definition of Base Rock 147
5.3 Basic Equations of Multiple Reflection Theory in Multi-layered System 149
5.4 Calculation of Underground Motion from Surface Record of Earthquake Motion 152
5.4.1 Derivation of Approximate Equations 152

5.4.2 Discussion about $A(x)$ and $B(x)$ 155
5.4.3 Characteristics of the Ground Shaking and Considerations on Accuracy of the Approximate Equations 157
5.4.4 Numerical Examples 166
5.4.5 Conclusions 170
5.5 Response of Inhomogeneous Surface Layer Subjected to Excitation of Earthquake Motion 173
5.5.1 Derivation of Equations for Response Motion .. 175
5.5.2 Numerical Example 180
5.5.3 Conclusions 201
References 205
Chapter 6 Conclusions 208

Chapter 1 Introduction

1.1 Introduction

Japan is located in the seismic zone around the Pacific Ocean and has experienced many strong earthquakes. On all such a strong earthquake, a great many of lives, houses and civil structures have been sacrificed. Furthermore, the concentration of population, business and industry into a few great cities has promoted the increase in the damage potential of earthquakes. In the field of seismology, the source mechanism and the prediction of occurrence of earthquake and its magnitude are mainly investigated from the viewpoint of the "prediction of earthquake". On the other hand, from the viewpoint of the "minimization of earthquake damage", the studies on the development of the rational design of the earthquake resistant buildings and the accurate prediction of the ground motion are desired in the field of earthquake engineering. However, because of the complexity of dynamic behaviors of soils and the highly irregularity of geometrical configuration in surface layers, there are many unknown factors in analyzing the earthquake response of grounds compared with the analyses of the upper structures.

The prosperity of traffics and the expansion of highways have been rapidly continued as the growth of economy in our country. As a consequence, some highways are unavoidably constructed into a town and near a residental section. These circumstances cause that noises and vibrations from the traffics trouble inhabitants in the neighborhood of the highways. Also, sometimes the vibrations from machines trouble mankinds. Therefore, in constructing the highway and the foundation of machines, we must be careful to prevent the propagation of such uncomfortable vibrations knowing the dynamic properties and wave characteristics of the foundations.

These phenomena are due to wave propagation through the earth ground, and are mainly investigated in soil dynamics. In order to understand the conditions of various problems, Ishihara's classification with the time rate (or duration time) of loading and the number of repeated cycles is very useful. It is shown in Fig.1.1[1]. In order to solve the soil dynamics problems, we must concentrate our attention on the following subjects;

(1) to observe in detail the real phenomena and at the same time to investigate the local geological configurations of the site under considerations.

(2) to investigate the dynamic behaviors of soils and establish the constitutive equations under universal state.

(3) to develop the rational analytical method for the soil dynamics problems, in which we can take into account the detailed local geological configurations and the dynamic properties of soils.

This thesis discusses the fundamental approaches to (2) and (3) of the above subjects. The first study is to investigate the dynamic properties of soil from its wave characteristics. The second is to present the approximate analytical method of earthquake response of an inhomogeneous elastic layer.

The problems on the wave propagation in a solid have been studied in the field of mathematical physics and applied mechanics for a long time. Most of them are based on the theory of elasticity. However, the real mechanical behaviors of soils are far from the elasticity and the wave characteristics are different from those in elastic body. In general, the mechanical behaviors of soils are classified with the strain levels as shown in Fig. 1.2[2].

The general treatment for the wave propagation in soil is schematically shown in Fig.1.3[3]. Grain size, degree of saturation and void ratio are realized as the most important physical properties of soil which are to influence the wave characteristics. Fundamental equations in the study on

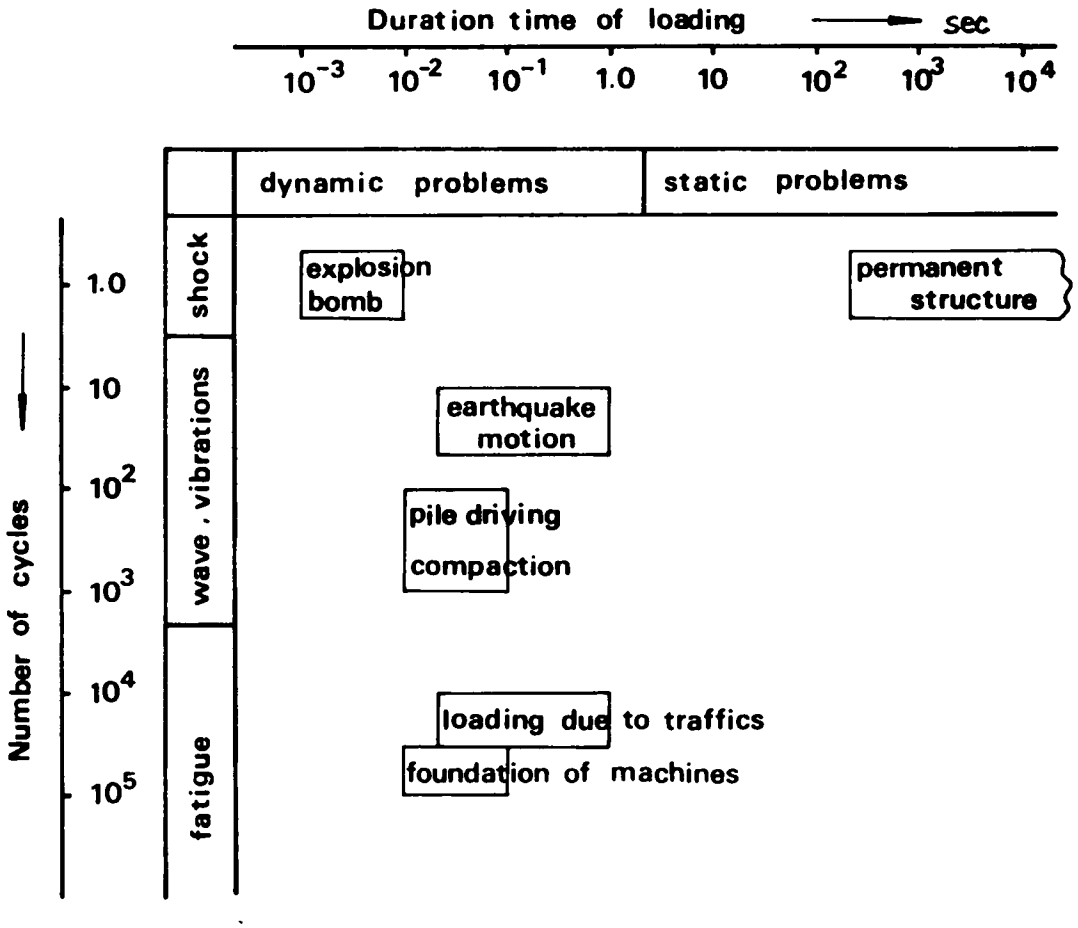

Fig.1.1 Classification of soil dynamics problems with duration time and number of cycles(after Ishihara[1]).

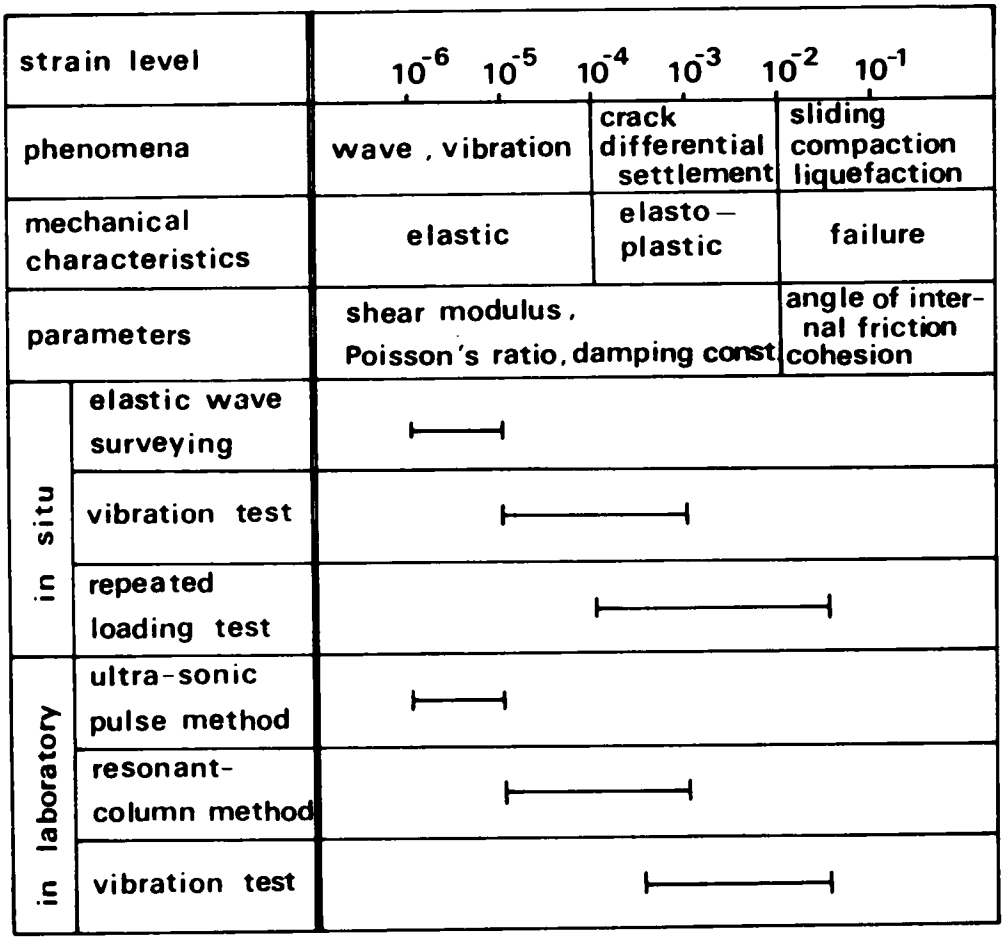

Fig.1.2 Classification of mechanical behaviors of soil and way of test with strain level(after Ishihara[2]).

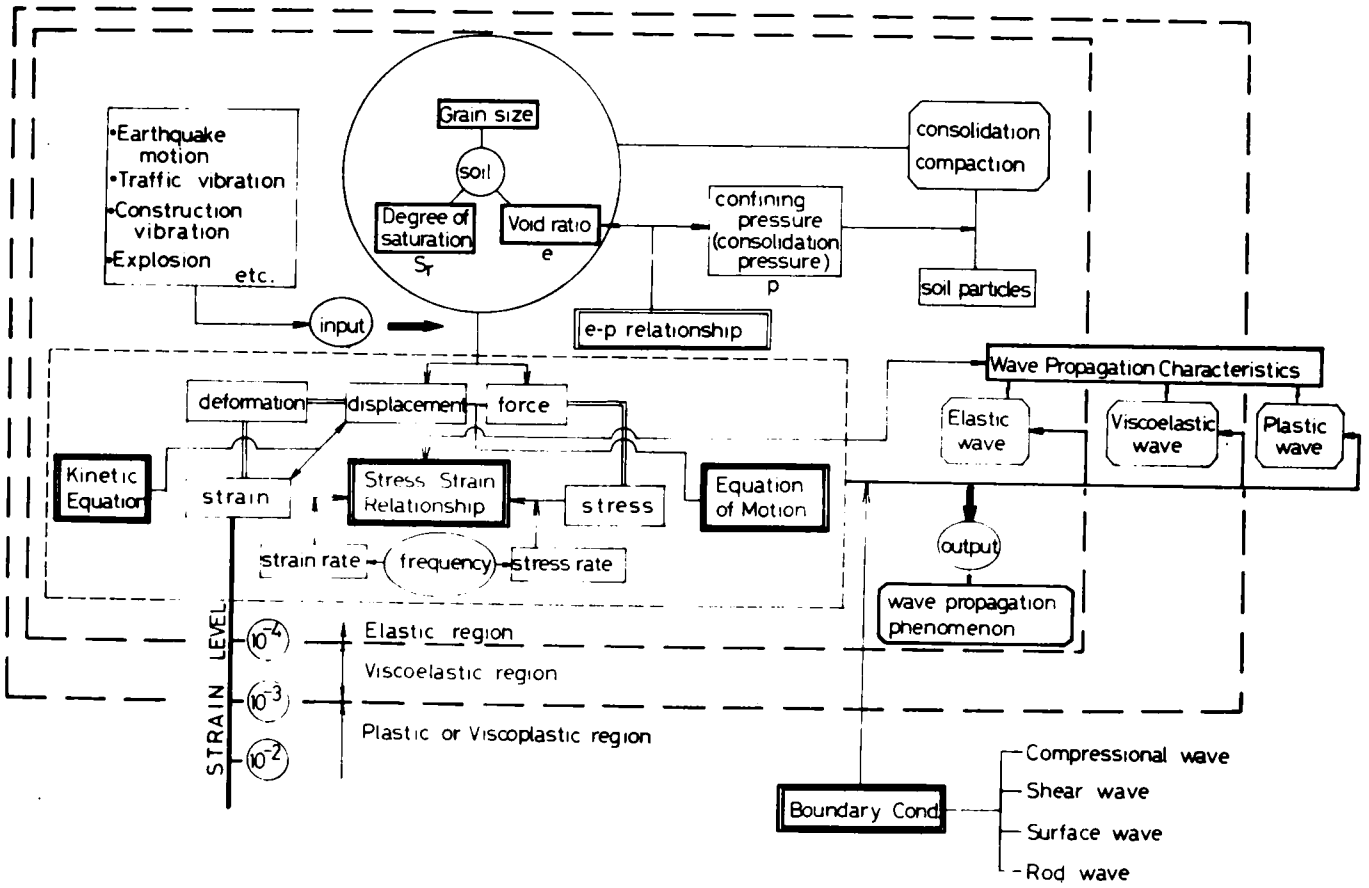

Fig.1.3 General concepts of treatment for the problems of wave propagation in soil.

wave propagation are equation of motion, kinetic equation and constitutive equation. If only the wave with the infinitesimally small amplitude is considered, the first two equations always hold. Therefore, the constitutive equation is most important to determine the wave characteristics. In other words, as long as the constitutive equation under universal state is not established, it is impossible to throughly express the entire characteristics of wave in soil. However, taking into account that the soil strain generated by earthquakes and vibrations from traffics and machines is at most about 10^{-3} in order, the assumption that soil is linear elastic or viscoelastic would not create much contradiction to the real situation. The author considers that the behaviors of soil are elastic in the strain level less than 10^{-4}, viscoelastic in the range of 10^{-4}-10^{-3} and plastic or viscoplastic more than 10^{-3}. In last, under boundary conditions, a particular type of wave is determined.

In order to investigate experimentally the wave propagation through soils, the author has made an effort for accomplishment of a wave propagation test in a laboratory and designed the special apparatus for the compressional and rod wave propagation tests. In both tests, the shock tube is used as the loading apparatus, and the propagation of stress pulse through the soil specimens is observed. These tests are called as the "shock tube technique". The obtained wave characteristics are examined with respect to the dynamic modulus and the energy damping of soils. Owing to this technique, the useful experimental data for analyses of soil dynamics problems are offered.

The other investigation in this thesis is concerned with the earthquake response analysis of a ground. In designing the earthquake resistant buildings and underground structures subjected to earthquake motion, first of all we must investigate the characteristics of earthquake motion in the site under consideration. In general, the ground formation near the surface is very complicated and the dynamic properties of earth materials change with

depth. When we take into account such a complex geological condition for the response analysis, it is often convenient for the dynamic properties and densities of system to distribute with the continuous function which increases monotonously with depth. For such a special case of the inhomogeneous surface layer, an approximate technique of earthquake response analysis is presented and its accuracy is examined in comparison with the exact solutions. By this technique, we can easily obtain the characteristics of an inhomogeneous ground motion and, at the same time, calculate the transient motion on and under the ground with a short computation time.

1.2 Review of Previous Studies

An earthquake motion involves various components of frequency between 0.1 and 10 *cps*. In the foundation of machines and railways, the frequency of loading sometimes comes to 100 *cps*. Furthermore, in the neighborhood of an explosion, the frequency becomes higher still more. On the other hand, the phenomena of creep and relaxation of soils are extremely slow. Therefore, the frequency range treated in soil mechanics is considerably wide. For the purposes of true settlement of soil mechanics problems including soil dynamics problems, we do not persist in studies on the soil behaviors in a particular time region but we must contribute to make the mechanical characteristics of soils clear over all the wide region of time and to establish the applicable constitutive equation under the universal state.

When we consider the previous studies on the soil dynamics problems, it is convenient to classify them into the following groups;

(a) Studies on dynamic modulus and damping of soils.

(b) Studies on earthquake response analyses of ground.

The objects of the studies in (a) are to investigate the dynamic characteristics of soils and at the same time, to offer the useful data for the earth-

quake response analyses of a ground and for the design of foundation of machines. While, the objects of the studies in (b) are to develop rational techniques of the response analyses and to predict the accurate earthquake motions of a ground taking into account the geological formation and the dynamic properties.

1.2.1 Studies on Dynamic Modulus and Damping of Soils

Hardin and Black[4] considered that the dynamic shear modulus of clay, G_d, is a function of the following factors;

$$G_d = f(\sigma'_{oct}, e, H, S_r, \tau_{oct}, c, A, f, t, \theta, T) \qquad (1.1)$$

where, σ'_{oct} denotes the effective octahedral normal stress, e the void ratio, H the ambient stress history and vibration history, S_r the degree of saturation, τ_{oct} the octahedral shear stress, c the grain characteristics such as grain shape, size and grading mineralogy A the amplitude of strain, f the frequency of vibration, t the secondary effect which is a function of time and magnitude of load increment, θ the soil structure and T the temperature. They also reported that, especially in the case of sand, G_d is independent of the factors except σ'_{oct} and e in the strain level less than 10^{-4}. Furthermore, Hardin and Richart[5] reported that the grain size, arrangement and shape of sands at the strain level of 10^{-4} do not influence upon G_d, and that the degree of saturation influences a little upon G_d only at low pressure level and G_d is independent of the frequency less than 2500 *cps*.

The dynamic tests are classified under three major types:

(a) Direct Method.

(b) Quasi-Direct Method.

(c) Indirect Method.

In the direct method, the stress-strain relationships are directly

obtained under various stress condition, and the appropriate modulus of deformation is defined by the ratio of stress to strain. In this case, there are several ways of loading; the static, repeated, rapid transient and steady-state loadings. Also in the quasi-direct method, the stress-strain relationships are directly obtained under various loading conditions, but the relationships are idealized to have certain characteristics of a suitable model, for example, the elasto-plastic solid. The bi-linear model by Thiers and Seed[6] and the equivalent linear model by Jacobsen[7] are typical examples of this method. In the equivalent linear model, the hysteretic stress-strain curve under a cyclic loading is represented by the equivalent shear modulus and the equivalent damping ratio. The entire damping ratio is given by a sum of the equivalent damping ratio and the viscous damping ratio. Idriss and Seed[8] introduced this concept into the lumped-mass modal analysis in order to take into account the non-linearity of soil properties in earthquake response of a ground. They used the value of 0.20 as the entire damping ratio in the analysis of the ground in Niigata. Furthermore, they arranged the many experimental data from various researchers concerning with the dynamic shear modulus and the damping ratio with respect to the amplitude of strain[9]. As a consequence, they pointed out that these dynamic properties remarkably change with the strain level and that, as increasing in the strain, the dynamic shear modulus decreases while the damping ratio increases.

In the third method, namely the indirect method, parameters other than stress and strain are used, including natural frequency, logarithmic decrement and velocity of propagation of stress wave. To interpret these measurements it is necessary to select an appropriate model or idealized medium to which the parameters can be assigned. Examples of this method of testing include the free vibration, resonant vibration and wave propagation tests. Especially the resonant vibration test and the wave propagation test have played important roles in determining the dynamic moduli of elasticity in extremely

small strain level less than 10^{-4}. As one of the resonant vibration tests, the method devised by Hardin is well known as the "resonant-column method"[10]. On the other hand, the wave propagation test using the ultra-sonic wave is well known as the "ultra-sonic pulse method".

By these two method, the elastic properties of soils have been investigated. Hardin and Richart[5] derived the important conclusions from the resonant-column method for granular soils that the elastic shear wave velocity c_s is only dependent upon the void ratio e and the applied mean effective principal stress σ_m' and is given by the relation as

$$c_s = F(e)\sigma_m'^{\,0.25} \tag{1.2}$$

where, $F(e)$ is a linear function of e. Also, the dynamic shear modulus is

$$G_d = F'(e)\sigma_m'^{\,0.5} \tag{1.3}$$

where, $F'(e)$ is a function of e. These relations are very useful in estimating the elastic modulus of a soil. After then, by Hardin *et al.*[4] and Marcuson *et al.*[11], it is found out that the same relations as Eqs.(1.2) and (1.3) also hold for cohesive soils.

1.2.2 Studies on Stress Wave Propagation

Most problems in soil mechanics can be classified phenomenologically into three major types with its governing differential equation. The first of all is the elliptic type differential equation represented by the steady-state flow in a ground. The second is the parabolic one represented by the consolidation. The third is the hyperboric one represented by the wave propagation in soils. Akai[12] has intended to clarify the characteristics of each problem and at the same time to reveal the correlation among these problems. There are many uncertainties especially in the phenomena of wave

propagation in soils. In experimentally investigating the entire wave characteristics through soils, many difficulties exist in the laboratory test, because the wave characteristics are influenced by many conditions such as boundary conditions, stress condition, frequency or wavelength and so on. The relation of wavelength and length of specimen through which the wave propagates, is important in observing the phenomena of wave propagation. That is, only when the length of specimen is long enough compared with the wavelength, we can observe the entire phenomena of wave propagation. Because of limitation of dimensions of specimen in a laboratory, however, the wavelength must be shotened; in other words, the wave with high frequency must be used. By this reason, the manner of testing with use of a stress pulse or shock is often used in the laboratory.

Akai *et al.*[13] initiated the new type of wave propagation test for the first time in Japan. By hitting one end of the rod of clayey specimen with suspended horizontally by means of a small steel ball, they observed the phenomena of wave propagation of the generated stress pulse through the specimen, and confirmed that the wave attenuated rapidly with distance. The shock tube technique described in this thesis modifies their technique in order to measure more accurately the wave phenomena through soils. Throughout these studies on the stress wave propagation[3),14),15)], the instantaneous elasticity of soils is considered from the velocity of wave front, while the characteristics of non-elasticity including the retardation elasticity, the energy loss and the time dependency are considered from the attenuation of stress wave and the change of wave form as the wave propagates. Furthermore, these wave characteristics are considered in relation to the soil properties and from the viewpoint of viscoelasticity[16),17)].

On the other hand, in foreign countries, the study on stress wave propagation has been carried out for the purpose of designing nondestructive underground structures as a military research and the purpose of mathematically

expression of a mechanism of energy damping in soils as well as the investigation of the dynamic soil properties.

Seaman[18] studied soil behavior during stress wave propagation through sand and clay specimens with five meter long column. Attempts were made to predict this behavior by determining soil properties in dynamic compression tests on small samples and by using these properties in a variety of mathematical models for soil. Two theoretical soil models were analyzed in this study; one to investigate the effect of combined time-dependent and time-independent dissipation and another to study the effects of nonlinear stress-strain relationships and geostatic stress. They were termed as viscoelastic compacting model and S-hysteretic model, respectively. A comparison of wave propagation results and of theoretical predictions based on compression test properties showed that the arrival time of stress wave could be predicted from the compression modulus of the soil, and that the stress attenuation could be predicted from the dissipative soil parameters found in the compression tests.

Vey and Strauss[19] conducted the experiments on triaxial specimens of Kaolin clay, 2.8 *inches* in diameter by 64 *inches* long, to measure the stress-strain relationship of the soil under the loading produced by a stress wave propagating through the specimen. Lateral confining pressures from 5 to 15 *psi* were used with an air shock loading on the end of the specimen from 5 to 35 *psi*. They found that the initial tangent modulus of dynamic stress-strain curve was one-half to one-quarter of the dynamic modulus calculated from the velocity of wave front.

Hampton and Wetzel[20] studied on the stress wave propagation through EPK clay and Ottawa sand specimens by the shock tube technique. They concluded that the results from the experiments considerably agree with the theoretical results by a constant tangent delta viscoelastic model in the case of EPK clay while by a linear hysteretic model in the case of Ottawa

sand.

1.2.3 Studies on Earthquake Response Analyses of Ground

In 1930, Sezawa and Kanai pointed out the possible effects of superfical soil layers on observed ground motions[21),22)]. By considering a simple layered model, namely, two-layered strata composed of a base rock and a superficial soil layer, they explained the possibility of prominent vibration of the superficial layer caused by the multiple reflections of the body waves in it. Since then, extensive research works have been carried out both theoretically and experimentally to study this problem[23),24)]. This approach is called as the "multiple reflection theory of waves" or the "wave propagation method". Although this approach is limited to the elasticity of the ground, this is excellent since to be able to calculate the underground and base rock motions from the surface record and to be simple. Furthermore, Kagami and Kobayashi[25)] developed the numerical technique for the response of the elastic multi-layered system in applying the multiple reflection theory of waves. Also, the analyses for viscoelastic grounds based on the theory of wave propagation have been carried out by Kanai[26)] and Tsai[27)].

In general, the ground formation near the surface is very complicated and also, the non-linearity of dynamic prpoperties of earth materials is remarkable as increasing with the strain level. In order to take into account these conditions in analyzing the response of a ground, Parmelee *et al.*[28)], and Idriss and Seed[8)] presented the lumped-mass modal analysis. As growth of computers, this analysis has been rapidly developed and today, has become a powerful technique to analyze the earthquake response of grounds. Since the ground is replaced by the finite discrete lumped masses and the base rock is assumed as a rigid base, some diffrences from the wave propagation method appear in the numerical results. However, the accuracy of

modal superposition in this analysis is examined by Whitman *et al.*[29], and the comparison of numerical results obtained by this analysis and the wave propagation method is investigated by Arango and Dietrich[30]. According to their conclusions, although the calculated maximum accelerations at the ground surface are almost identical between two analyses, there appear some differences in time histories of accelerations, and the values of stress and strain in the ground also show relatively poor agreement.

These two analyses are based on the theory of the one-dimensional wave propagation and in most cases, its assumption is valid because the earthquake motion is incident almost vertically to the surface soft layer at the base rock. However, when the assumption is impossible, the three-dimensional analyses must be taken into. For this purpose, the finite element method will become a powerful tool[31].

Since the phenomena of earthquakes are strongly influenced by the particular locality of a site, we must take into account the detailed local geological condition and at the same time the dynamic properties of earth materials under the considering site. Therefore, for accurate prediction of response ground motion, it is necessary to investigate the ground formations in detail and the dynamic properties of earth materials.

1.3 Scope of Study

This thesis is devoted to the study on the stress wave propagation through soils. The shock tube technique is presented to investigate experimentally the wave characteristics of soils in the laboratory. From the obtained experimental data, the dynamic properties of soils and the mechanism of energy loss in them are discussed with respect to the physical properties of the soils from a standpoint of wave propagation. Another effort is contributed to the development of earthquake response analysis of an in-

homogeneous ground.

Chapter 2 deals with the condenser-type soil strain meter to measure the dynamic soil strain during wave propagation. The principle of operation, the manner of calibration test and the application of this meter are described and its sensitivities and accuracy are discussed with some examples of application.

In Chapter 3, the experimental apparatus and procedure by the shock tube technique are described in detail. Two wave propagation tests, the compressional wave and the rod wave, are performed for the soil samples of sandy loam and silty loam, respectively. Especially for the rod wave propagation test, the special triaxial compression chamber is used and the tests are carried out under various confining pressures. In the considerations of wave characteristics of the soils, the dynamic modulus of elasticity is calculated from the velocity of wave front in the stress wave propagation, and the damping characteristics are considered from the attenuation of stress wave and the change in wave form with travelling distance. The dynamic modulus and the attenuation constants are discussed with respect to the physical properties and the attenuation constants are discussed with respect to the physical properties and the confining pressure, and also compared with the results of the other investigations.

Chapter 4 is devoted to the viscoelastic approach to the stress wave propagation through soils. From some analytical considerations such as one-dimensional wave propagation of spike pulse through viscoelastic materials, the spring-Voigt model is selected to follow the mechanical characteristics of soils at small strain level. Furthermore, this chapter deals with the comparison of wave characteristics in between viscoelastic materials and the saturated elastic porous media treated by Biot and Ishihara, and with the discussions on the physical natures of the defined material constants in these media. The viscoelastic constants of the spring-Voigt model are

calculated by using the experimental data of the rod wave propagation test in Chapter 3, and they are discussed with respect to the confining pressure and the frequency.

Chapter 5 is concerned with the earthquake response analysis of an inhomogeneous ground. The approximate analytical approach to obtain the underground or base rock motion from the surface record is presented by applying the multiple reflection theory of waves. The accuracy of this approximation is examined in comparison with the exact solusions. Furthermore, the numerical examples of earthquake response analysis are given for the Osaka ground and the distribution of underground accelerations and shear strains is considered.

References

1) Ishihara, K. : Dynamic Strength of Soils, Lecture of Dynamic Properties of Soils, Soil Mechanics and Foundations Engineering, Vol.20, No.7, July, 1972, pp.73-79(in Japanese).

2) Ishihara, K. : Dynamic Properties of Cohesive Soils, Preprint, 26th Conf. JSCE, Part 3, 1971, pp.III(1)-III(3)(in Japanese).

3) Akai, K. and M. Hori : Considerations of Wave Characteristics in Soil Assumed as Viscoelastic Material, Proc. of JSCE, No.221, Jan., 1974.

4) Hardin, B. O. and W. L. Black : Vibration Modulus of Normally Consolidated Clay, Proc. ASCE, Vol.94, No.SM2, Feb., 1968, pp.353-369.

5) Hardin, B. O. and F. E. Richart, Jr. : Elastic Wave Velocities in Granular Soils, Proc. ASCE, Vol.89, No.SM1, Jan., 1963, pp.33-65.

6) Thiers, G. R. and H. B. Seed : Cyclic Stress-Strain Characteristics of Clay, Proc. ASCE, Vol.94, No.SM2, Feb., 1968, pp.555-569.

7) Jacobsen, L. S. : Damping in Composite Structures, Proc. 2nd WCEE, Tokyo, 1960.

8) Idriss, I. M. and H. B. Seed : Seismic Response of Horizontal Soil Layers, Proc. ASCE, Vol.94, No.SM4, April, 1968, pp.1003-1031.

9) Seed, H. B. and I. M. Idriss : Soil Moduli and Damping Factors for Dynamic Response Analyses, Report No.EERC-70-10, Univ. of Calif., Berkeley, Calif., 1970, pp.1-15.

10) Richart, F. E. Jr., J. R. Hall and R. D. Woods: Vibrations of Soil Foundations, Prentice-Hall, Inc., 1970, pp.300-307.

11) Marcuson, W. F. and H. E. Wahls : Time Effects on Dynamic Shear Modulus of Clays, Proc. ASCE, Vol.98, No.SM12, Dec., 1972, pp.1359-1373.

12) Akai, K. : Advanced Theory of Soil Mechanics, Morikita Shuppan, 1974, pp.103-118(in Japanese).

13) Akai, K., M. Tokuda and T. Kiuchi : Experimental Study on the Propa-

gation of Stress Wave in Cohesive Soils, Proc. of JSCE, No.161, Jan., 1969, pp.59-67.

14) Akai, K., M. Hori, N. Ando and T. Shimogami : Shock Tube Study on Stress Wave Propagation in Confined Soils, Proc. of JSCE, No.200, April, 1972, pp.127-141.

15) Akai, K., M. Hori and T. Shimogami : Study on Stress Wave Propagation through Saturated Cohesive Soils by Means of Triaxial Shock Tube(under contribution to Proc. of JSCE).

16) Akai, K. and M. Hori : A Viscoelastic Approach to the Problem of Stress Wave Propagation in Cohesive Soils, Proc. of JSCE, No.185, Jan., 1971, pp.95-103.

17) Akai, K. and M. Hori : Analytical Study on Stress Wave Propagation in Viscoelastic Materials Subjected to Spike Pulse, Proc. of JSCE, No.195, Nov., 1971, pp.101-108.

18) Seaman, L. : One-Dimensional Stress Wave Propagation in Soils, Stanford Research Inst., AD-632106, DASA1757, 1966.

19) Vey, E. and L. V. Strauss : Stress-Strain Relationships in Clay Due to Propagating Stress Waves, Proc. Int. Symp. Wave Propagation and Dynamic Properties of Earth Materials, Univ. New Mexico, 1967, pp.575-586.

20) Hampton, D. and R. A. Wetzel : Stress Wave Propagation in Confined Soils, Proc. Int. Symp. Wave Propagation and Dynamic Properties of Earth Materials, Univ. New Mexico, 1967, pp.433-442.

21) Sezawa, K. and K. Kanai : Possibility of Free Oscillations of Strata Excited by Seismic Waves, Bull. Earthq. Res. Inst., Vol.8, 1930, pp.1-11, and Vol.10, 1932, pp.1-18 and pp.273-298.

22) Sezawa, K. and K. Kanai : Decay Constant of Seismic Vibrations of a Surface Layer, Bull. Earthq. Res. Inst., Vol.13, 1935, pp.251-265.

23) Kanai, K., T. Tanaka and S. Yoshizawa : Comparative Studies of Earthquake Motions on the Ground and Underground(Multiple Reflection Problem),

Bull. Earthq. Res. Inst., Vol.37, 1959, pp.53-87.

24) Kanai, K., T. Tanaka, S. Yoshizawa, T. Morishita, K. Osada and T. Suzuki : Comparative Studies of Earthquake Motions on the Ground and Underground, 2nd Report, Bull. Earthq. Res. Inst., Vol.44, 1966, pp.609-643.

25) Kagami, H. and H. Kobayashi : A Method for Local Seimic Intensity Zoning Maps on the Basis of Subsoil Conditions, Proc. Int. Conf. on Microzonation for Safer Construction Research and Applications, Vol.2, Seattle, 1972, pp.515-528.

26) Kanai, K. : Relation between the Nature of Surface Layer and the Amplitudes of Earthquake Motions, Bull. Earthq. Res. Inst., Vol.30, 1952, pp.31-37.

27) Tsai, N. C. : Influence of Local Geology on Earthquake Ground Motion, Ph.D. Thesis, California Institute of Technology, Pasadena, 1969.

28) Parmelee, R. A., J. Penzien, C. F. Scheffey, H. B. Seed and G. R. Thiers : Seismic Effects on Structures Supported on Piles Extending through Deep Sensitive Clays, Report No.64-2, Inst. of Eng. Res., Univ. of Calif., Berkeley, California, 1964.

29) Whitman, R. V., J. M. Roesset, R. Dobry and L. Ayestaran : Accuracy of Modal Superposition for One-Dimensional Soil Amplification Analysis, Proc. Int. Conf. on Microzonation for Safer Construction Research and Application, Vol.2, Seattle, 1972, pp.483-498.

30) Arango, I. and R. J. Dietrich : Soil and Earthquake Uncertainties on Site Response Studies, Proc. Int. Conf. on Microzonation for Safer Construction Research and Application, Vol.2, Seattle, 1972, pp.629-647.

31) Dynamic Interaction between Soils and Structures, Edition of JSSM & JSFE, Library of Soil Foundation Engineering, No.9, 1973, pp.165-257 (in Japanese).

Chapter 2 Device of Condenser-Type Soil Strain Meter[1)]

2.1 Introduction

It is of great importance in the field of soil mechanics to measure exactly local strains as local stresses in soil without any disturbance. Since soil stress gauge instrumentations have been developed so much, it is fairly easy to measure stresses in natural state of the ground. On the other hand, an appropriate instrumentation to measure local strains in soil has not been established in this country. Especially, it has been impossible to measure local dynamic strains in soil.

In U.S.A., soil strain gage instrumentation has been developed by IITRI to measure transient soil deformations in both laboratory and field applications. This strain sensor consists of two flat-coil disks which are embedded in soil in near parallel and concentric orientation without physical connection between them. The remainder of the gage hardware consists of a second set of coil disks, identical to those used as the strain sensor, and specially designed electronic driving, amplifying, balancing, and recording circuitly. Soil deformations are measured by the resulting changes in the spacing of embedded coils which are sensed as changes in the mutual inductance of the coils[2)]. This strain sensor is used so many kinds of soil testing, for example, tri-axial compression test[2)], wave propagation studies in soil[3),4)] and so on. However, this strain sensor has disadvantages as follows;

(1) Since the size of the coil disk is relatively large (laboratory gage: 3/4 inch in diameter and 1/16 inch in thickness, field gage: 4 inches in diameter and 1/4 inch in thickness), soil sample seems to be considerably disturbed in embedding the coil disks, and

(2) the equipment is expensive.

Nishigaki[5)] emphasizes that the measurements of microscopic strain are

very important to obtain the elastic constants of soils and tries to paste a strain gage on the side of soil sample of unconfined compression test. By this procedure, he obtains Young's modulus of clay in microscopic strain level. This procedure is very available with relatively stiff clay such as diluvial clay but unavailable with sandy soils or relatively soft clay such as alluvial one.

The condenser-type soil strain meter in order to measure the one-dimensional soil deformations during stress wave propagation has been devised. This type of strain meter has been used in the air but has not been used in soil as a dielectric substance. The advantages of this type of strain meter are as follows[6];

(1) able to measure such a large strain that cannot be messured by strain gages,

(2) able to measure strains as well as displacement and vibrating amplitudes as it is operated without physical connection between two electrode plates, and

(3) the construction is very simple and inexpensive.

However, this meter has also disadvantages as follows;

(1) since radio frequency is used in this meter, it is influenced by a man approaching or things without shielding,

(2) it is very difficult to calibrate the relationship between the spacing of two electrode plates in soil and change in capacity, and

(3) we have a chance to disturb soil condition in burying two electrode plates in a sample.

The above disadvantages are removed by using the needles instead of the plates as the condenser constructed in the soil. One-dimensional microscopic strains of soil can be measured simply and exactly by means of this type of soil strain meter.

2.2 Principle of Operation in the Meter

2.2.1 Apparatus

In the device of this condenser-type soil strain meter, 'Infinitesimal Displacement Meter MD-31' (Iwasaki Communication Apparatus Co.LTD.), is used. This meter, as shown in Photo.2.1, consists of a meter MD-31, a probe MDG-643 and a condenser embedded in soil. A main variable condenser (100 pF), a fine variable condenser (20 pF) and a subcondenser (20 pF) are contained in the probe MDG-643. The size, shape and material of the electrode plates as a condenser embedded in soil are optional. In the previous paper[7], the rectangular thin copper plates (2.5 cm x 1.5 cm) with coated by enamel (see Photo.2.2) so as to use even in wet soils were used. Recently, however, two needles (6 cm in length and 0.5 mm in diameter) with enveloped by a vinyl tube, as shown in Photo.2.3, are used as two electrodes in order to decrease disturbance of soil sample in embedding into soil. In experiments, as shown in Photo.2.4, these two needles are embedded in parallel in soil. Soil deformations are measured by the resulting changes in the spacing of embedded two needles which are sensed as changes in the electrostatic capacity of them.

2.2.2 Principle of Operation

For simplicity, consider two flat rectangular electrode plates but not two needles to explain the principle of operation in this type of soil strain meter. When two conductors are placed in parallel as shown in Fig.2.1, the resulting electrostatic capacity is given by

$$C = \frac{A \varepsilon_0 \varepsilon_s}{D} = 8.885 \times 10^{-12} \times \frac{A \varepsilon_s}{D} \quad [F]$$

$$= 8.885 \times \frac{A \varepsilon_s}{D} \quad [\mu F] \qquad (2.1)$$

where, A denotes the cross sectional area (a x b (m^2)) of the conductors, D the spacing of two conductors (m), ε_0 the dielectric constant and ε_s the specific dielectric constant. Eq.(2.1) implies that if ε_s is assumed to be constant

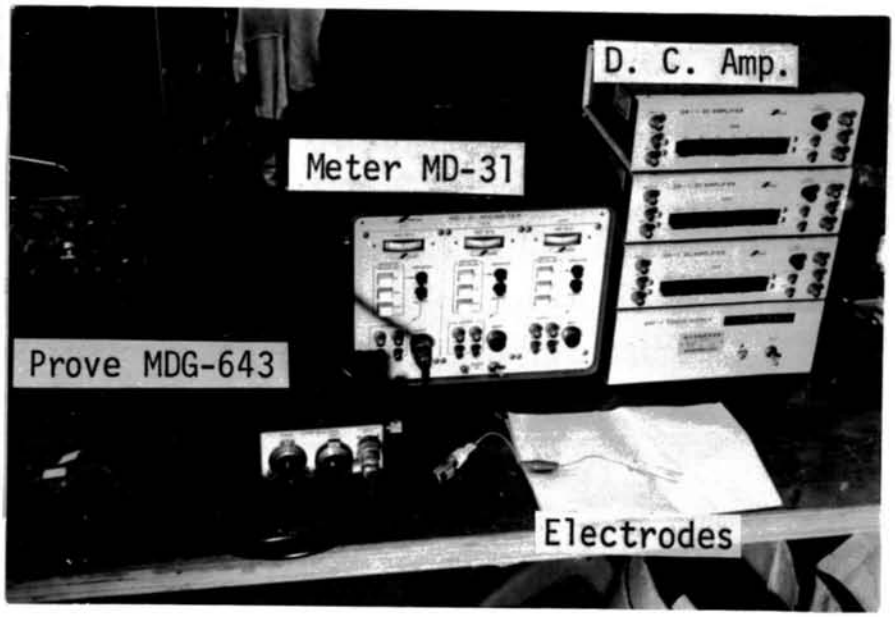

Photo.2.1 Apparatus of the condenser-type soil strain meter.

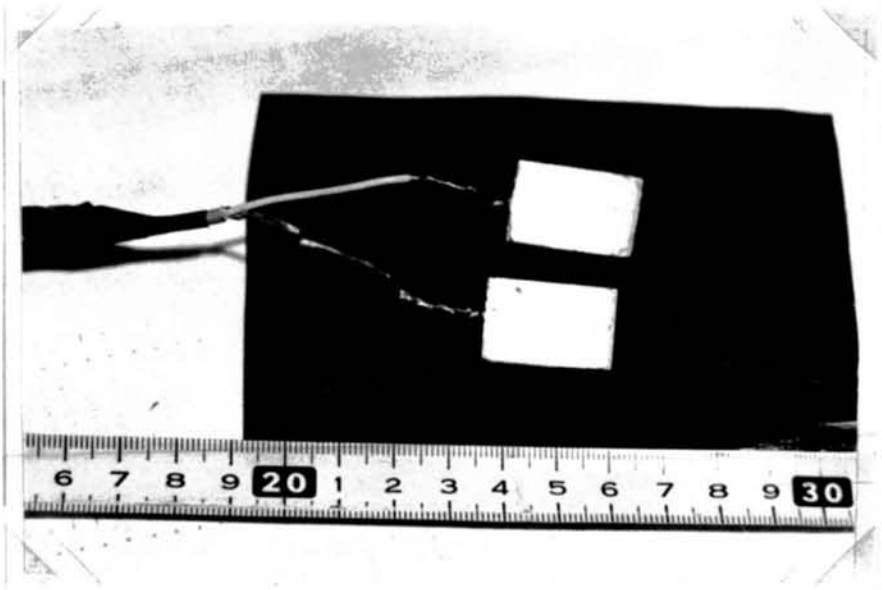

Photo.2.2 The rectangular thin electrode plates with coated by enamel.

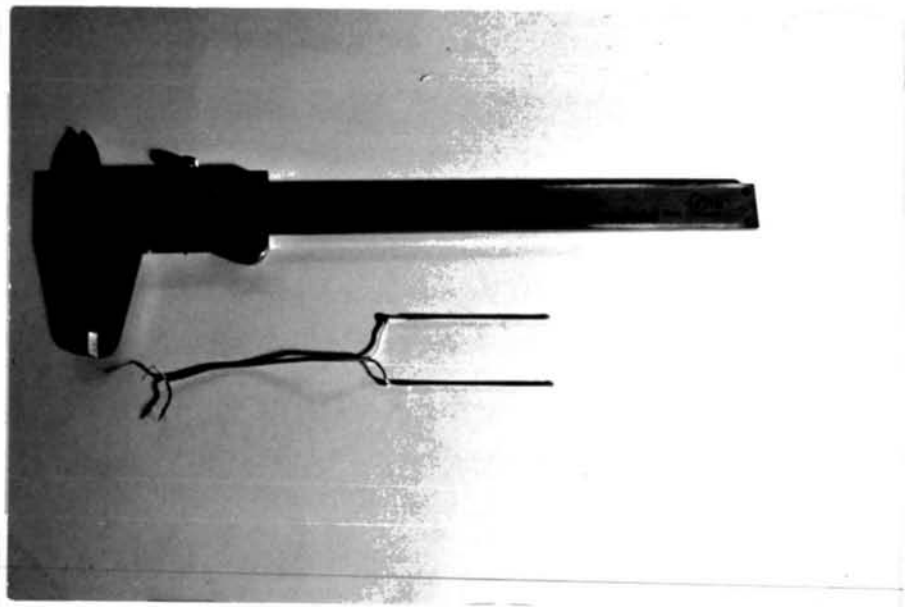

Photo.2.3 The electrode needles enveloped by a vinyl tube.

Photo.2.4 The electrode needles embedded in soil sample.

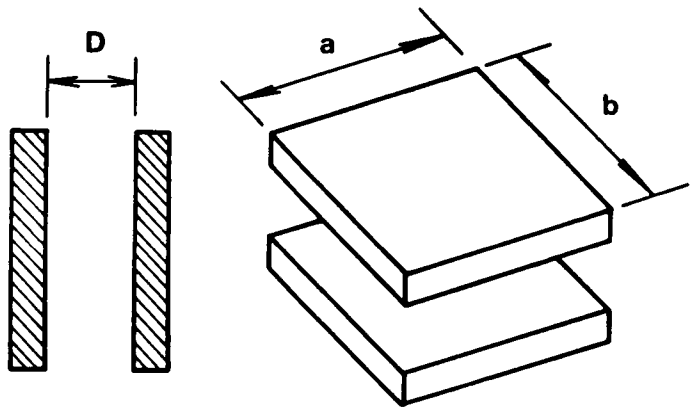

Fig.2.1 Two conductors in parallel.

through testing, the variation in the spacing ΔD of two conductors results in the change in capacity ΔC:

$$\Delta C = \frac{\partial C}{\partial D}\Delta D = -8.885 \times \frac{A\varepsilon_s}{D^2}\Delta D \qquad (2.2)$$

The strain meter consists of the bridge circuit indicated in Fig.2.2, where C_3 and C_4 denote the fixed condensers and have also equal capacity, the variable condenser for balance, C_a the measuring condenser embedded in soil and C_b the variable subcondenser which is used when C_a is less than 20 pF. If $C_a + C_b$ is replaced by C_1, a balance condition for this bridge circuit due to these four condensers (C_1, C_2, C_3 and C_4) is given by

$$\frac{C_1}{C_2} = \frac{C_3}{C_4} = 1 \qquad (2.3)$$

i.e., if C_2 is so controlled that it is equal to C_1 for measurement, no electric current occurs in the meter M. When C_1 changes, however, a potential difference occurs between the point A and B shown in Fig.2.2, and an electric current flows in meter M.

2.3 Calibration

A relationship between a change in spacing of two electrode plates and a resulting potential difference should be obtained by a calibration test. The previous manner of calibration[7] was that the soil sample was packed in a ring made of vinyl-chloride of which inside diameter and height were 5.2 cm and 2.0 cm, respectively. Two electrode plates were put on the upper and the lower surface of the packed soil sample in concentric orientation so that the initial spacing between two plates was about 2.0 cm. The initial spacing of them was accurately measured by the travelling microscope. After setting up the apparatus and balancing the bridge circuit in the prove MDG-643, soil sample was compressed by means of unconfined compression apparatus and, at the same time, the resulting potential difference was measured by means of a synchroscope. This manner of calibration test, however, was rather primitive

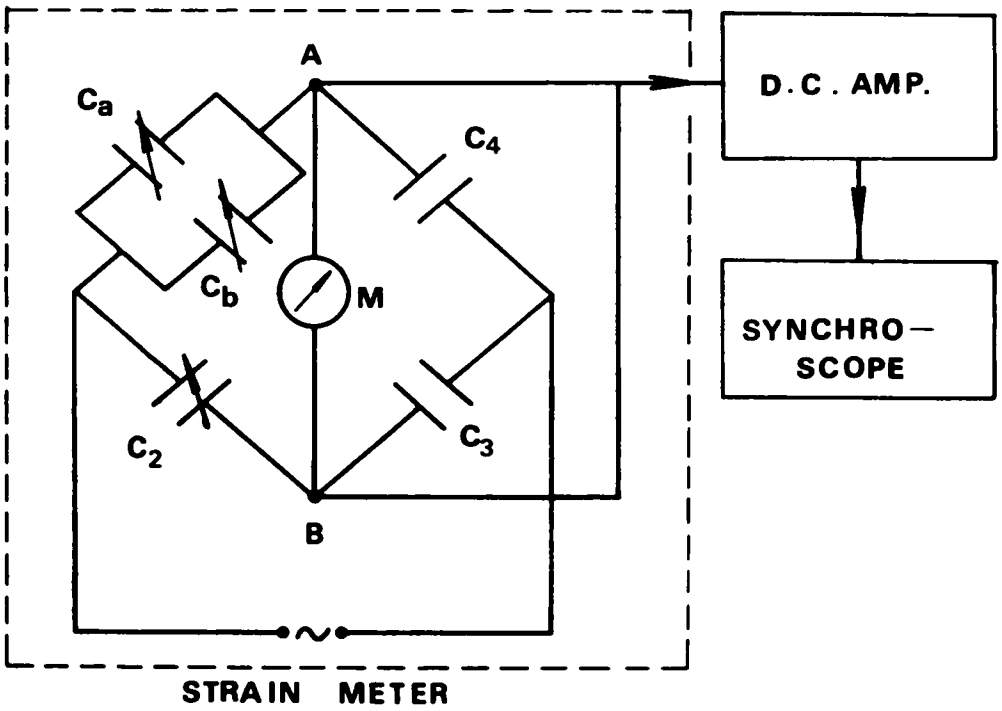

Fig.2.2 Bridge circuit in the strain meter.

so that the measurement of soil strain was relatively inaccurately. It was found that such a calibration test was needless.

When a pair of electrode needles is embedded in the soil sample in parallel, the electrostatic capacity stored in this condenser can be expressed by the expression same as Eq.(2.1) to the rectangular electrode plates,

$$C_o = \frac{a}{D_o} \tag{2.4}$$

where, C_0 denotes the initial capacity stored in the condenser (pF), D_0 the initial spacing of the two needles (m) and a the constant which is determined by the size and shape of the electrode needles. When the soil sample deforms and ΔD changes in the spacing of the two needles, the corresponding change of the capacity ΔC is expressed by the following equation if ΔD is very small,

$$\Delta C = -\frac{a}{D_o^2}\Delta D = -\frac{a}{D_o}\cdot\frac{\Delta D}{D_o}$$

$$= -C_o\frac{\Delta D}{D_o} \tag{2.5}$$

Since $\frac{\Delta D}{D_0}$ is a quantity of soil strain, Eq.(2.5) means that the corresponding change in capacity ΔC with the change in spacing ΔD is proportional to the soil strain. Namely, if the initial capacity C_0 is known, the soil strain is calculated from Eq.(2.5). The initial capacity C_0 is easily obtained by the following equation;

$$C_o = C_A - C_B \tag{2.6}$$

where, C_A denotes the capacity with the condenser embedded in the soil and C_B the capacity without it.

When we observed the strain record by means of a synchroscope or an electromagnetic oscillograph, we must obtain the relationship between the change in capacity ΔC and the corresponding voltage ΔV from calibration test. This relationship depends on the initial capacity. Typical test results are shown in Fig.2.3 as ΔC=1 pF. If the relationship between ΔC and ΔV at a certain initial capacity C_0 is expressed by the following equation;

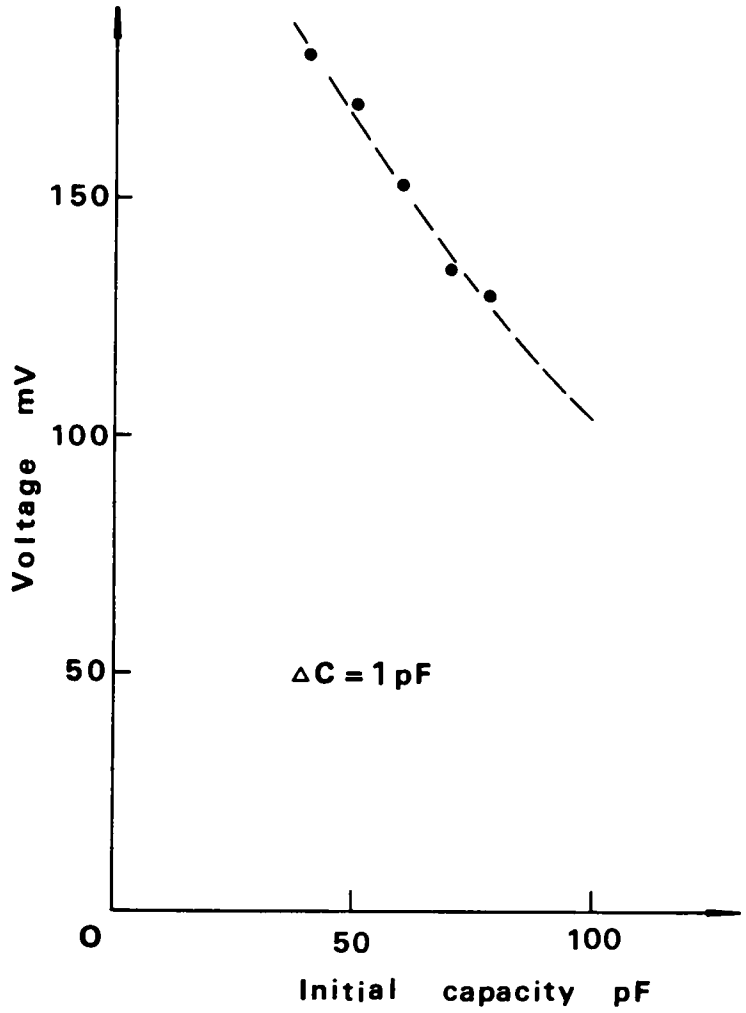

Fig.2.3 Typical results of the relationship between the initial capacity and the corresponding voltage.

$$\Delta V = \frac{1}{k}\Delta C \tag{2.7}$$

where, k denotes a constant, then the strain ε can be calculated from,

$$\varepsilon = \frac{\Delta D}{D_o} = -\frac{\Delta C}{C_o} = -\frac{k}{C_o}\Delta V \tag{2.8}$$

It has been confirmed by experiments that the linearity between strain ε and voltage ΔV exists in the range of strain less than 2%[8].

2.4 Applications

2.4.1 One-Dimensional Stress Wave Propagation Test

The soil strain meter is used in the one-dimensional stress wave propagation test as described in Chapter 3 in clay in order to obtain the stress-strain relationships during rod wave propagation. The rod of clay is 135 cm in length and 7.5 cm in diameter which is consolidated at confining pressure P_c=1.06 and 0.54 kg/cm^2 in the specially designed acryl cell[9]. Then the cell is relieved and a pair of needles as a strain meter is embedded in parallel with the initial spacing of about 1 cm. At the one end of the rod, the pulsative stress is applied by means of the shock tube. When the applied dynamic stress is propagating in the rod as a rod wave, the stress and the strain are at the same time measured by the soil stress gauge embedded in the sample and the strain meter, respectively. Figs.2.4(a) and (b) show the typical records of the stress and strain forms recorded by a synchroscope. The observation depth, and the ratio of the proportional constant k to the initial capacity C_0 as expressed in Eq.(2.8) are entered in that figure. Although the phenomena of the stress and strain in this wave propagation test by the shock tube are considerably rapid, it is found that the responsibility of this condenser-type strain meter is excellent.

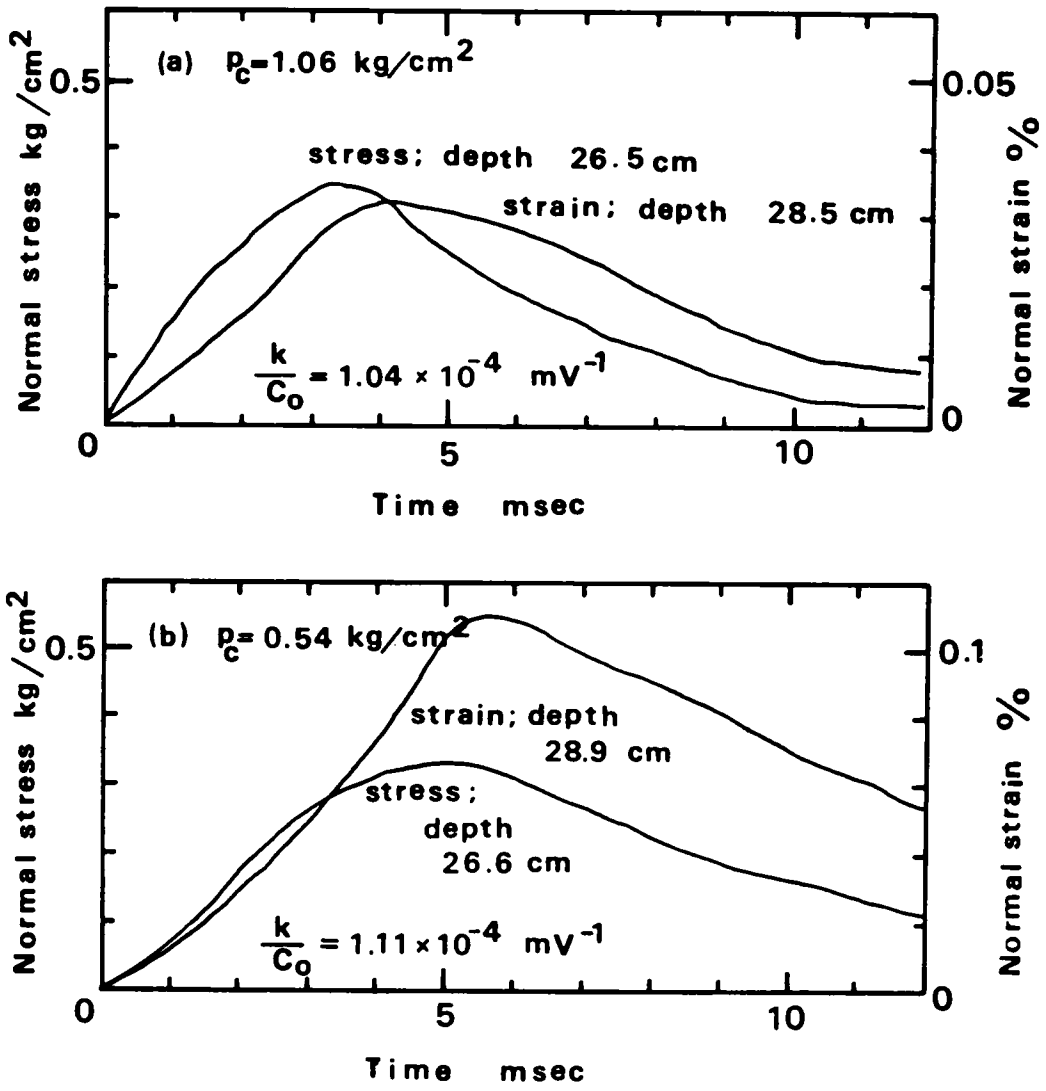

Fig.2.4 Typical records of the stress and the strain.

Fig.2.5 shows the stress-strain curves which are constructed by picking up the stress and the strain values corresponding to the same instant of time in Fig.2.4. Though the stress-strain curve expresses a large hysteresis loop for a given dynamic stress cycle, the plastic deformation does not seem to occur. Consequently, the physical behavior of the clay sample is considered viscoelastic at the range of a given strain level less than 10^{-3}. The initial tangent moduli E_i obtained from the stress-strain curve, the Young's moduli E_d calculated from rod wave velocity c_R and density ρ by the following equation;

$$E_d = \rho C_R^2 \tag{2.9}$$

and the initial tangent moduli E_s obtained from corresponding static stress-strain curve are summarized in Table 2.1. E_i and E_d are almost identical, and it is considered that this type of strain meter has an enough confidence.

2.4.2 Unconfined Compression Test

A distribution of normal strain in soil sample in unconfined compression test is observed by using this type of soil strain meter. The procedure of the strain meter is same as that described in 2.4.1.

In order to know the strain distribution in soil sample, needles are in each test embedded in one of upper, middle and lower parts of soil sample as shown in Fig.2.6. Fig.2.7(a) shows the relationship between the local strain measured by the soil strain meter and the average strain by a dial gauge. The soil samples used are relatively soft clay with 5.2 cm in diameter and about 10 cm in height. Their failure forms are ductile. It is found from this figure that the distribution of normal strain is nearly uniform up to the strain of 0.8%, and non-uniform for much more strain level. The local strain in a middle part of sample is same as the average strain up to about 2.5%, and much more compressed, the local strain does not increase and the soil in this part flows in lateral.

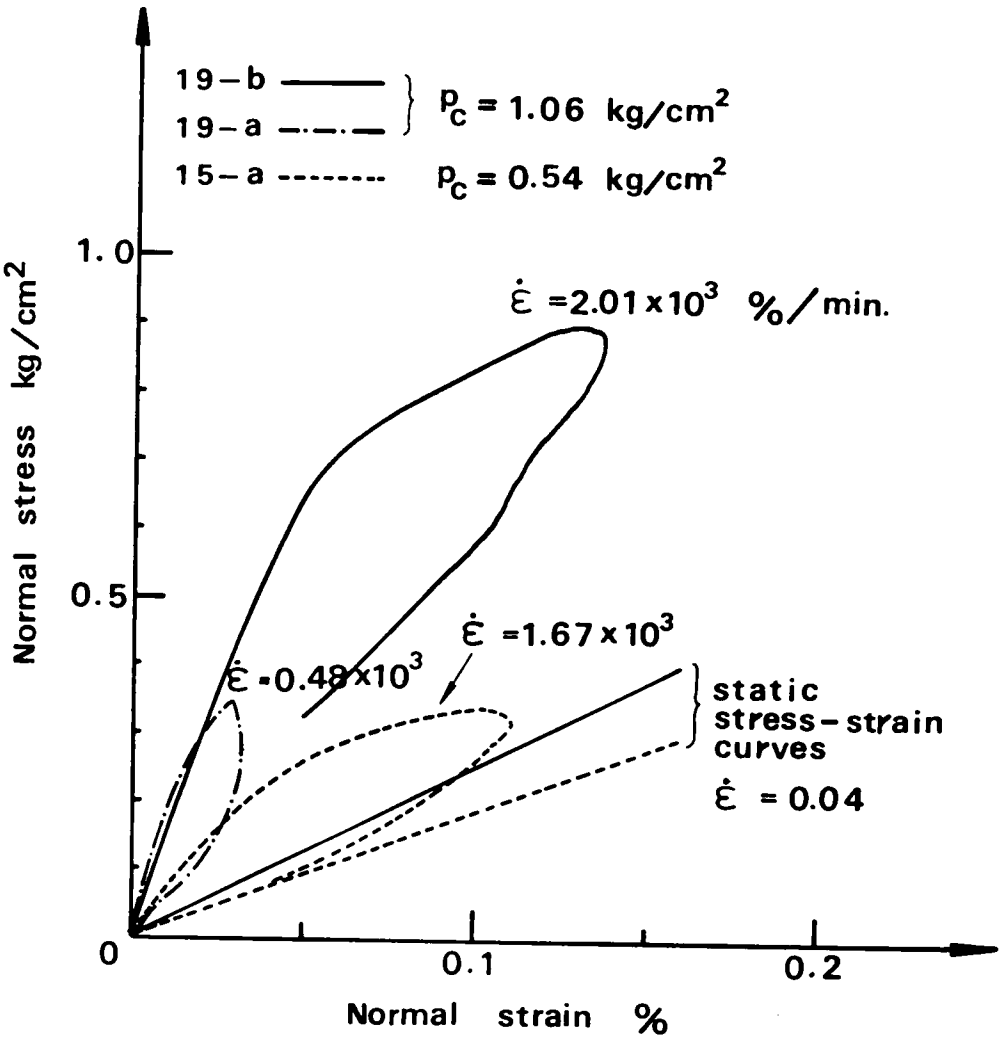

Fig.2.5 The stress-strain curves.

Table 2.1 Comparison of E_s, E_d and E_i.

No.	P_c kg/cm^2	E_s kg/cm^2	E_d kg/cm^2	E_i kg/cm^2
19-a	1.06	252	1730	1700
19-b			1640	1400
15-a	0.54	184	695	600

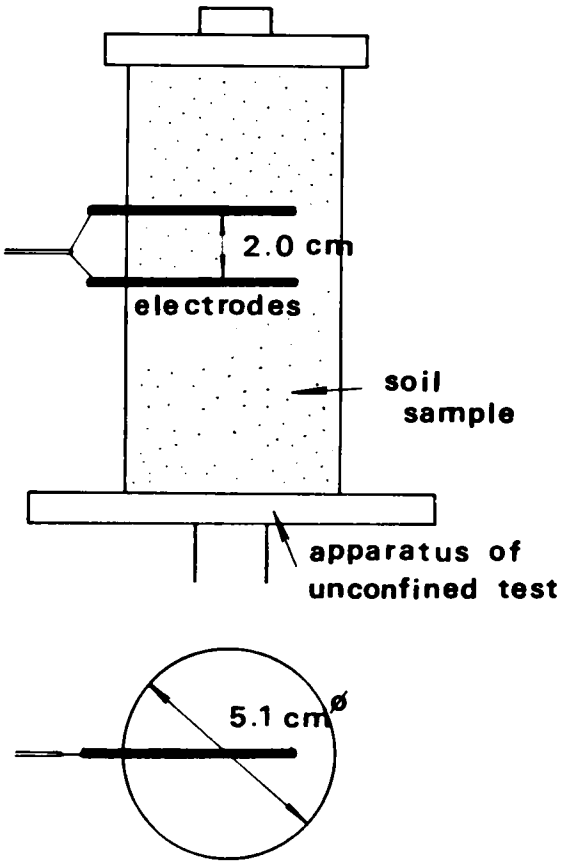

Fig.2.6 The manner of embedding needles into the sample of unconfined compression test.

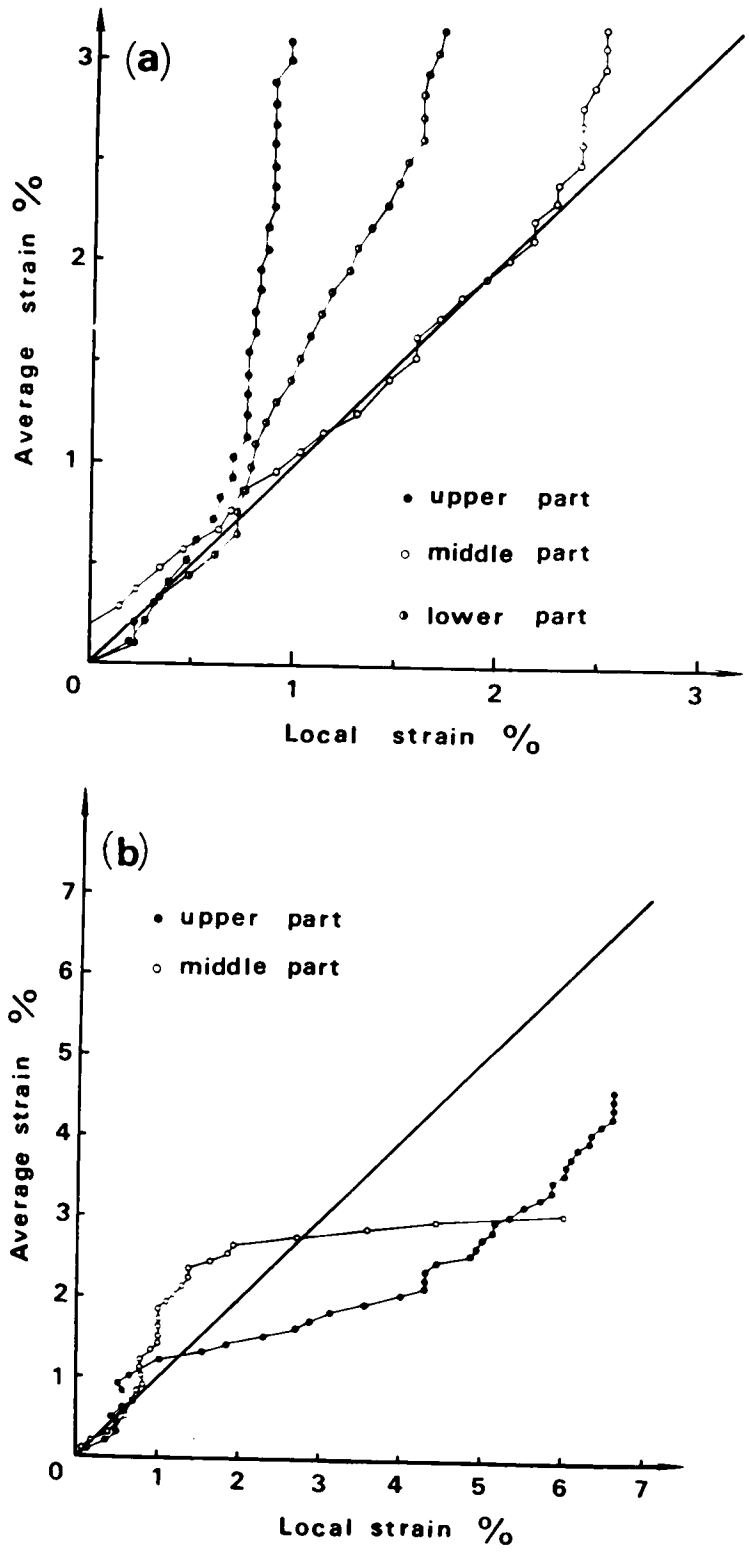

Fig.2.7 The relationships between the local strain and the average strain in (a) soft clay samples and (b) stiff clay samples.

Fig.2.7(b) is the results for a relatively stiff clay. Failure form in this case is brittle. The strain distribution is also uniform up to strain 0.8% same as above described one. Under further compression the local strain in middle part increases gradually and the one in upper part increases rapidly. This is due to that the samples are broken down.

2.5 Conclusions

It is found through this chapter that the condenser-type infinitesimal displacement meter can be used to measure the one-dimensional normal strain in soil. By using the thin needles as the electrodes of a condenser embedded in soil, the disturbance in soil sample can be decreased and the soil strain can be measured much more accurately. The troublesome calibration test described in the previous paper[7] is needless and when a pair of needles is embedded in soil, it does not need to read the initial spacing of them, provided the initial capacity C_0 and the constant k are examined from Eq.(2.8). Since the responsibility of this meter is excellent even in higher frequency range, it is suitable to measure the dynamic strain in soil.

References

1) Akai, K. and M. Hori: Device of Condenser-Type Soil Strain Meter, Proc. of JSCE, No.219, Nov., 1973, pp.115-120.

2) Truesdale, W. B. and R. B. Schwab: Soil Strain Gage Instrumentation, Proc. Int. Symp. Wave Propagation and Dynamic Properties of Earth Materials, Univ. of New Mexico, 1967, pp.931-941.

3) Vey, E. and L. V. Strauss: Stress-Strain Relationships in Clay due to Propagating Stress Waves, Proc. Int. Symp. Wave Propagation and Dynamic Properties of Earth Materials, Univ. of New Mexico, 1967, pp.575-586.

4) Deroock, B. and A. W. Cooper: Relation between Propagation Velocity of Mechanical Waves through Soil and Soil Strength, Proc. Int. Symp. Wave Propagation and Dynamic Properties of Earth Materials, Univ. of New Mexico, 1967, pp.905-912.

5) Nishigaki, Y.: Changes of Young's Modulus of Clay with Strain Level, Preprint, 26th Conf. of JSCE, 1971, pp.93-96(in Japanese).

6) Takenaka, J.: Measurements of Stress, Asakura Shoten, 1964, pp.261-285 (in Japanese).

7) Akai, K., Hori, M., Ando, N. and T. Shimogami: Shock Tube Study on Stress Wave Propagation in Confined Soils, Proc. of JSCE, No.200, April, 1972, pp.127-141.

8) Hori, M. and F. Oka: On the Measurement of Soil Strain (the second report), Preprint, Conf. of JSCE, Kansai Branch, 1972, III-34(in Japanese).

9) Shimogami, T.: Study on Stress Propagation through Cohesive Soils by Means of Triaxial Shock-Tube, Master Thesis of Kyoto University, 1973(in Japanese).

Chapter 3 Experimental Study on Stress Wave Propagation through Soils

3.1 Introduction

This chapter deals with the shock tube technique for the stress wave propagation test of soils. The shock tube is used as a loading apparatus which applies a pulsative stress to the soil specimen. For simplicity, only the one-dimensional wave propagation is considered in the experiments. Two types of wave through soils, compressional wave and longitudinal rod wave, are used. Although both waves cause the movement of particles parallel to the direction of wave propagation with compression of the soil, the lateral deformation of the soil rod is restrained in the former and is allowed in the latter. Sandy loam was used as the soil sample in the case of the compressional wave propagation test and the wave characteristics were mainly investigated with respect to its water content and degree of saturation. Meanwhile, in the case of the rod wave propagation test, saturated cohesive soil was used and its dynamic properties were examined under different confining pressures[1), 2)].

As already described in Chapter 1, the dynamic moduli and the material damping of the earth materials strongly depend on the strain level as well as the strain rate. The experiments were carried out in the range of strain level below 10^{-3} strain.

3.2 Waves in the Linear Elastic Body

Wave phenomena through earth materials ——— earthquakes and vibrations from sources of foundation of machines, traffics and explosions, are often encountered. These wave phenomena are essentially dependent upon the elastic properties of the earth materials, because they are generated by the interaction between the inertia force and the return force of the material.

That is, the wave can not propagate unlimitedly through the materials which do not create any return forces due to their deformations. The major features of seismic wave propagation will be expected on the basis of purely elastic properties of materials. Practically, the observations of the seismic wave propagation in the field can be often explained by the theory of elasticity. In order to investigate the wave propagation in a solid and to know the analytical treatment for it, the study on the waves in the linear elastic body is urgent.

There exist two body waves, *i.e.* compressional wave and shear wave, in an infinite linear elastic body. The wave equation of the former is expressed as

$$(\lambda + 2G)\nabla^2\bar{\varepsilon} = \rho\ddot{\bar{\varepsilon}} \tag{3.1}$$

where, λ and G are Lamè's constants, ρ the mass density, $\bar{\varepsilon}$ the dilatation and ∇^2 the Laplacian. Then the wave velocity is given by

$$c_p = \sqrt{\frac{\lambda + 2G}{\rho}} \tag{3.2}$$

When the plane one-dimensional compressional wave propagates, no lateral movement to the direction of wave propagation occurs.

While the shear wave distorts an element transversely to the direction of wave propagation, and propagates without volume change, the wave equation of this wave is expressed as

$$G\nabla^2\bar{\omega}_i = \rho\ddot{\bar{\omega}}_i \qquad (i = 1, 2, 3) \tag{3.3}$$

where, $\bar{\omega}_i$ denotes the component of the rotation, and the wave velocity is given by

$$c_s = \sqrt{\frac{G}{\rho}} \tag{3.4}$$

On the other hand, three independent kinds of wave motion are possible in an elastic rod: longitudinal, torsional and flexural waves. It is well known that the wave equation for the longitudinal wave of a rod is expressed as follows:

$$E \frac{\partial^2 u}{\partial x^2} = \rho \frac{\partial^2 u}{\partial t^2} \tag{3.5}$$

where, E is the Young's modulus, t the time, x the coordinate in the axial direction of the rod and u the displacement of the x-direction. Then the wave velocity is given by

$$C_R = \sqrt{\frac{E}{\rho}} \tag{3.6}$$

Eq.(3.5) is derived under the two assumptions, which are that the transverse sections of the rod remain plane during the passage of waves, and that the stress acts uniformly over each section. Furthermore, the inertia force due to lateral deformations of the rod during the passage of waves is neglected. Pochhammer initiated the research on the wave propagation in a rod and obtained the exact solutions for these problems. According to his exact solutions, the ratio of the phase velocity c_p of a sinusoidal wave to c_R obtained from Eq.(3.6) is simply given as[3)]

$$\frac{c_p}{c_R} = 1 - \nu^2 \pi^2 \left(\frac{r}{\lambda}\right)^2 \tag{3.7}$$

where, ν is the Poisson's ratio, r the radius of the rod and λ the wavelength. Moreover, the ratio of group velocity c_g to c_R is given by

$$\frac{c_g}{c_R} = 1 - 3\nu^2 \pi^2 \left(\frac{r}{\lambda}\right)^2 \tag{3.8}$$

So that, if the wavelength is large enough comparing to the radius of the rod such as the experiments described later, the wave is not too far from

representing the real situation of the rod wave as expressed by Eq.(3.5).

In the torsional wave of a rod, each transverse section rotates around its center. It is known that this wave propagates in a rod with a velocity $\sqrt{G/\rho}$ same as the shear wave velocity given in Eq.(3.4). Furthermore, in the flexural wave, flexural moment propagates along a rod, and the velocity depends on its wavelength. These problems are treated in detail by Kolsky[3].

The relationship between the shear modulus G and the Young's modulus E is given by

$$G = \frac{E}{2(1+\nu)} \tag{3.9}$$

Assuming volume change does not occur during the wave propagation in the saturated soils such as used in the experiments(that means $\nu=0.5$), Eq.(3.9) yields

$$G = \frac{E}{3} \tag{3.10}$$

Accordingly, by using the experimental data of the rod wave velocity, the shear wave velocity and shear modulus of the specimen can be examined.

3.3 Experimental Apparatus

3.3.1 Shock Tube

The history of shock tube is very old and its theory has been sufficiently elaborated in the field of aerodynamics. In 1899 Vielle invented a shock tube, 22 *mm* in diameter and 6 *m* long, for the first time. After then, it has been used throughout in many branches of science not only in the field of supersonic aerodynamics, but also in chemistry in order to solve dynamic problems for the mixture of gases.

A shock tube consists of two chambers; a high pressure cell(the driving

chamber) and a low pressure cell(the driven chamber) separated by a thin diaphragm. The principle of shock tube is very simple. The high pressure chamber is pressurized until the diaphragm breaks. At that instant, the air shock wave propagates along the low pressure chamber as the expansion wave. As long as the gas in the high pressure chamber is expanding, the shock wave is continued to travel. When the pressure in the high pressure chamber decreases to that in the low pressure chamber, the shock wave vanishes. The air shock wave has a sharp wave front and its pressure gradually decays behind the shock front. The more detailed explanation and the theory of shock tube are found in reference 4).

The schematic diagram of the shock tube used in the present study is shown in Fig.3.1. It consists of high pressure chamber(Photo.3.1), middle pressure chamber(Photo.3.2) and low pressure chamber(Photo.3.3). All chambers are made of cylindrical steel tube with the inside diameter of 7.76 *cm* and 1.2 *cm* in thickness. In general, it is known that if the length of low pressure chamber is more than ten times of the inside diameter, uniform shock wave can be obtained at the end of tube. Therefore, the 2 *m* long low pressure chamber was designed and built. At the distance of 5 *cm* from the end of the tube, a semi-conductor type pressure transducer is equipped in order to measure the shock pressure.

In experiments the low pressure chamber is atmospheric, while compressed air is used for the high and middle pressure chambers. Two thin aluminium sheets with 17.5 *cm* in diameter and 0.05 *mm* in thickness are used as the diaphragms to separate the high, middle and low pressure chambers. These diaphragms can be broken with pressure difference of about 3.5 kg/cm^2. At that time, the shock pressure of 1 to 2 kg/cm^2 is obtained at the end of the low pressure chamber. Photo.3.4 shows a typical shock pressure form measured by the pressure transducer at the end of the low pressure chamber.

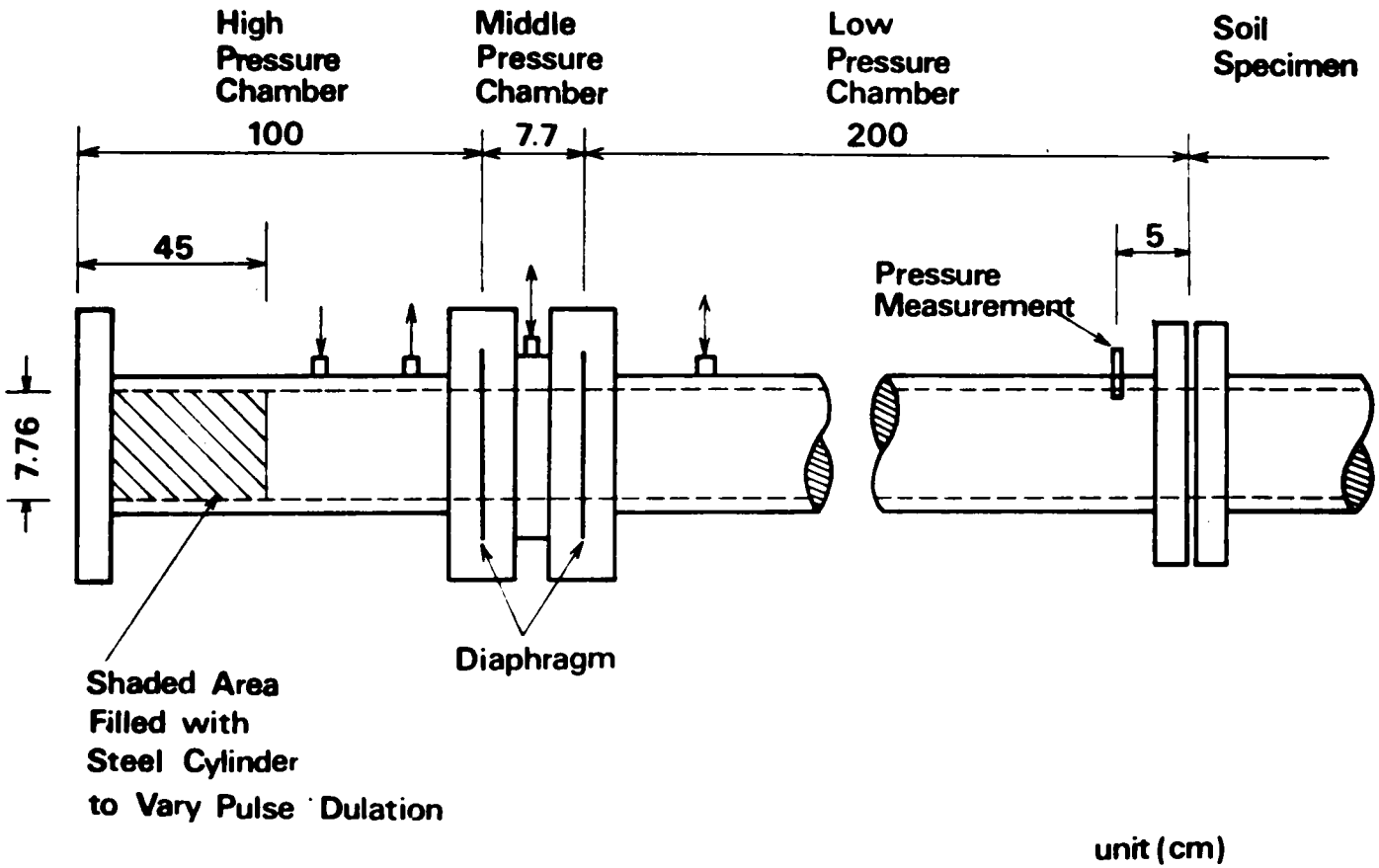

Fig.3.1 Schematic diagram of the shock tube used.

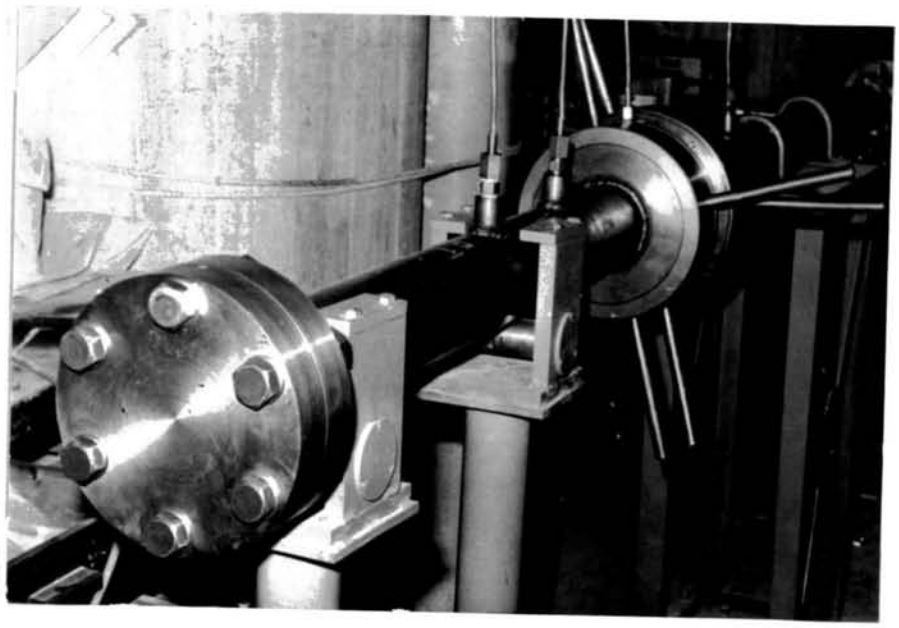

Photo.3.1 High pressure chamber.

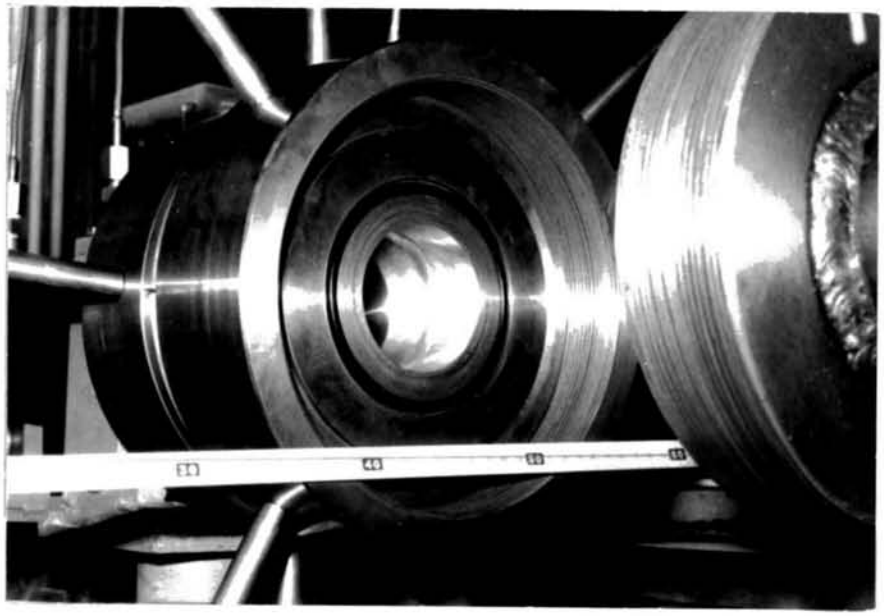

Photo.3.2 Middle pressure chamber.

Photo.3.3 Low pressure chamber.

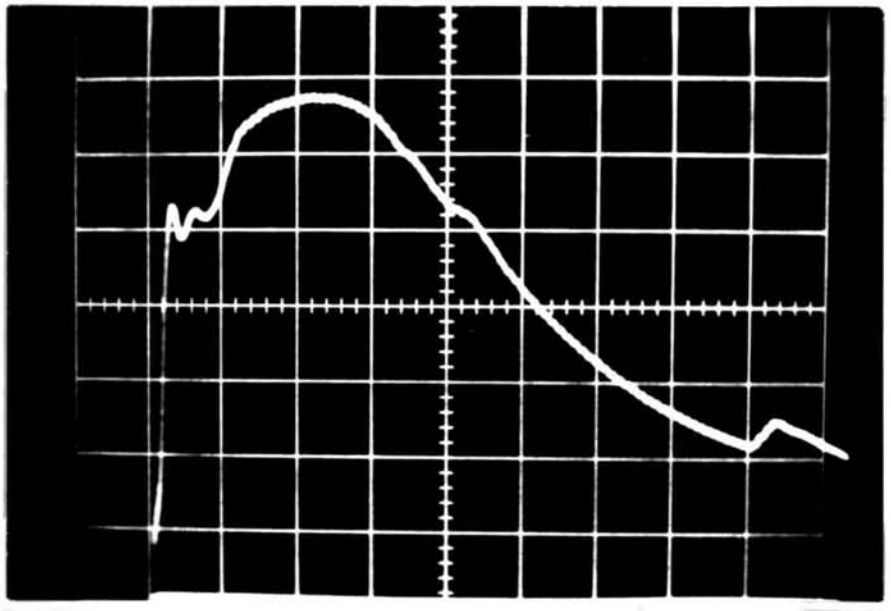

Photo.3.4 Typical shock pressure form (sweep: 2*msec/div.*, pressure: 0.2*kg/cm²/div.*).

3.3.2 Apparatus for Compressional Wave Propagation Test

Fig.3.2 shows the apparatus to confine soil specimens for one-dimensional compressional wave propagation test. This confining tube made of steel with an inside diameter of 7.6 *cm*, wall thickness of 6.5 *mm* and 2 *m* long, was horizontally connected with the shock tube. It is long enough to neglect the influence of a reflected stress wave at the reflection end of the tube, marked as *R* in the figure.

The cross section of the tube is perfectly circular. In putting the soil column in the tube, one can take off the upper half of it, marked as *A* in Fig.3.2(b). The upper half of the tube consists of five segments. As shown in Fig.3.2(c), each segment is 40 *cm* long and has splits at the both ends through which we can take out electric wires of various measuring equipments embedded in the soil specimen.

In this test, the air shock pressure generated by the shock tube was directly applied to the end surface of the soil specimen.

3.3.3 Triaxial Compression Chamber

This apparatus was designed for the rod wave propagation tests under different confining pressures. Fig.3.3 schematically shows the shock tube, the triaxial chamber, the pressure system and the water supply and drainage system. The triaxial cell consists of three lucite tubes, two aluminum rings and two end plates(see Photo.3.5). The dimensions of tubes are; outer diameter 32.4 *cm*, inner diameter 28.4 *cm* and length 50 *cm*. The two rings are sandwitched by tubes in between and the end plates are fixed by two steel pipes and the steel angle. The triaxial cell is horizontally connected to the end of the shock tube with bolts as shown in Fig.3.3. The air shock pressure generated in the shock tube is once received by a brass plate placed near the end of the low pressure chamber. Photo.3.6 shows the

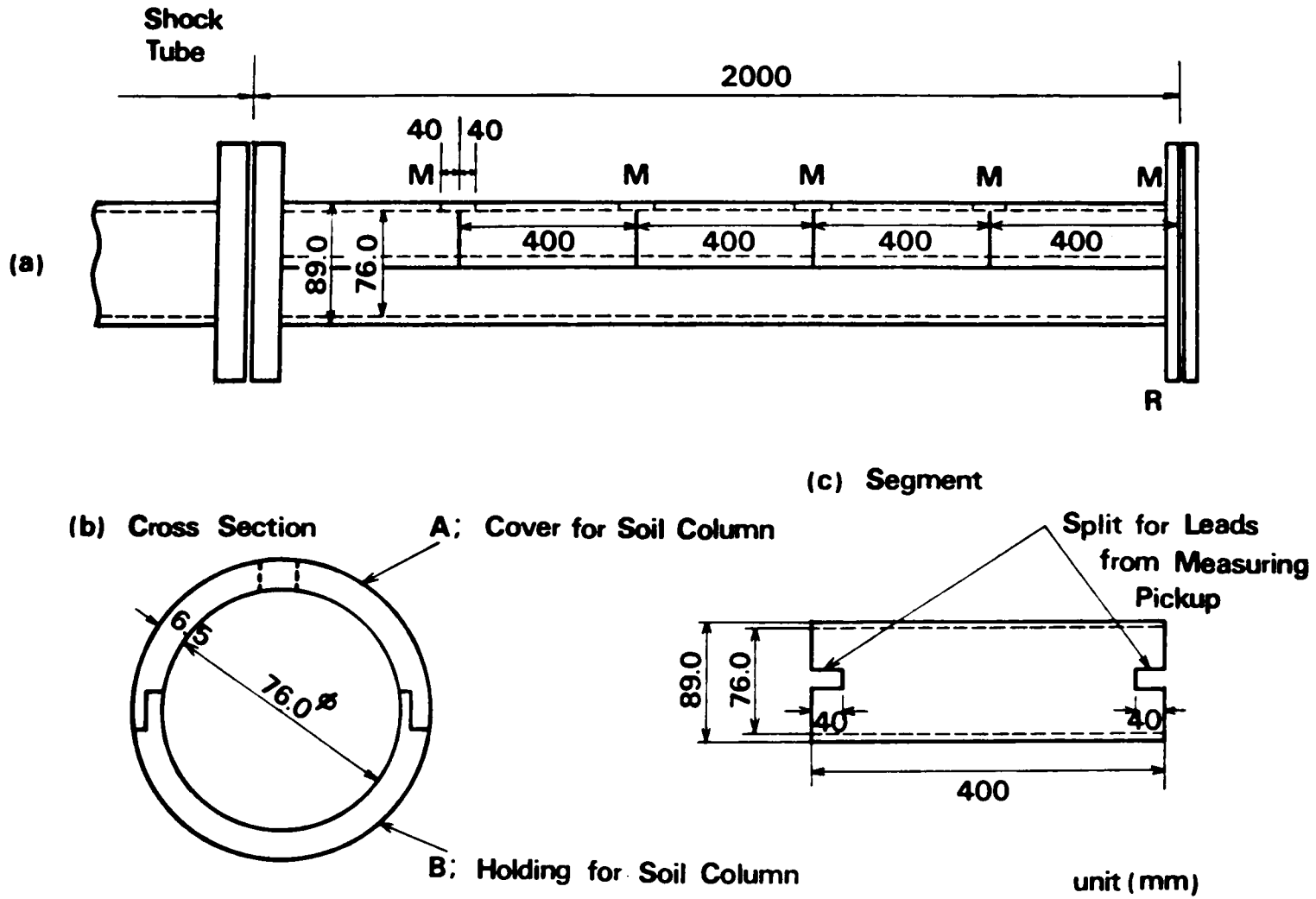

Fig.3.2 Apparatus for compressional wave; (a) confining tube of soil specimen, (b) cross section and (c) segment.

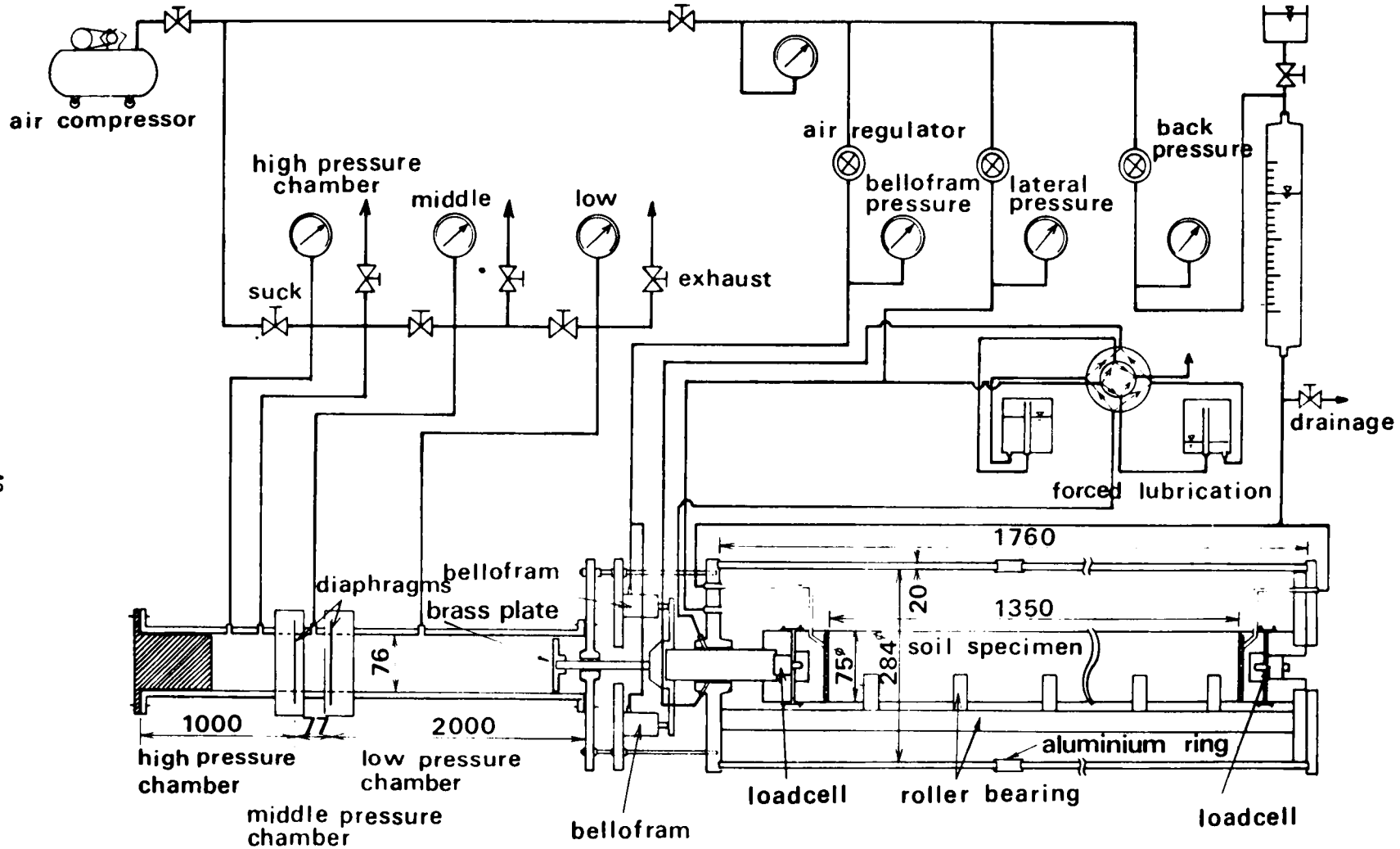

Fig.3.3 Schematic diagram of the shock tube, the triaxial compression chamber, the pressure system and the water supply and drainage system.

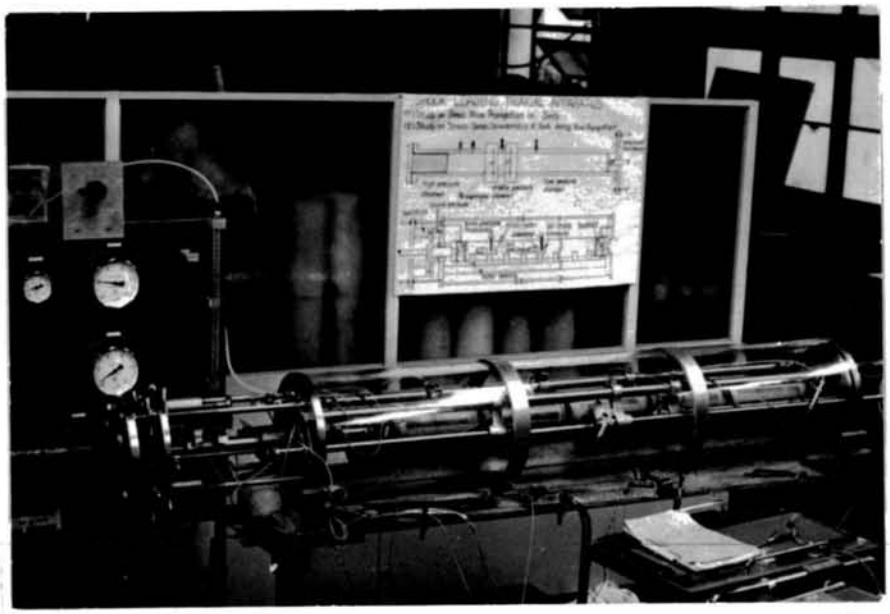

Photo.3.5 Triaxial compression chamber.

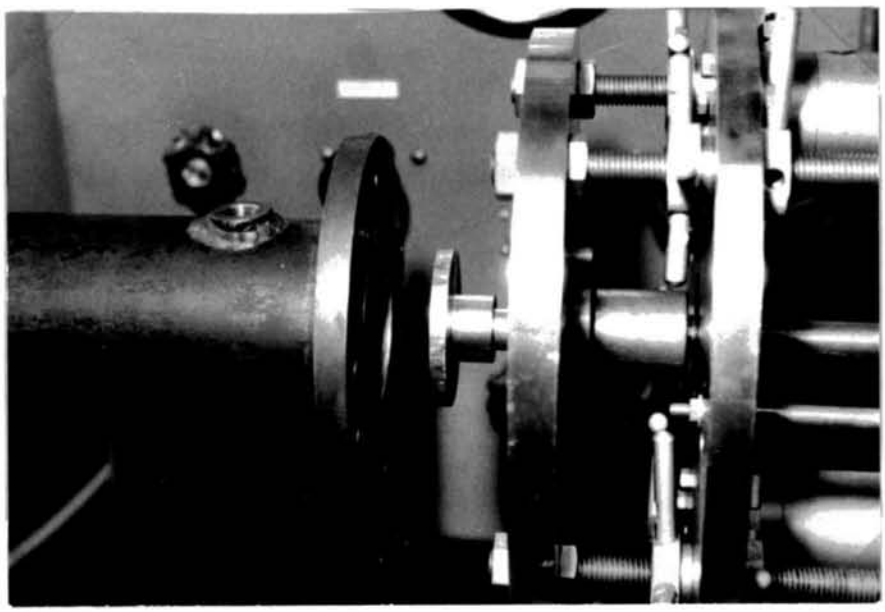

Photo.3.6 Brass plate subjected to the air shock pressure.

brass plate. It is transmitted to a piston supported by bearings in the center of the end plate and comes to the cap at the end of the specimen. This cap generates a pressure on the specimen. The shock pressure is monitored by a small transducer at the center of the brass plate. In order to reduce friction and air leak around the piston, the forced lubrication system is built in the bearings. The pressure applied on the cross section of the piston when the cell is pressurelized, is balanced by the force of two bellofram cylinders.

Fig.3.4 shows a schematic section through the triaxial cell. A soil sample is placed on the rotational roller bearings which are sitting on the axial roller bearing as shown in Fig.3.4. The bearings reduce the friction of the sample both in axial and rotational directions(see Photo.3.7). The dimensions of the sample are diameter 7.5 *cm* and length 135 *cm*. The axial bearings can be adjusted to match the specimen center and the piston center when the specimen is consolidated and moves its center.

A cohesive soil specimen is consolidated prior to the wave propagation test. The water collected through the filtering paper around the specimen is drained through the caps at the end of the specimen. A back pressure is also applied through the drainage pipe. The controls on the confining pressure, bellofram cylinder pressure and back pressure are done by regulators made by Fairchild Co. Ltd., U.S.A.. Those regulators can maintain the pressure constant steadly for a long time. The wires for the soil pressure gauges, pore water pressure gauges and the soil strain gauges placed in the specimen are taken out through two steel pipes to prevent the air leak as shown in Fig.3.4.

3.4 Measuring Equipment

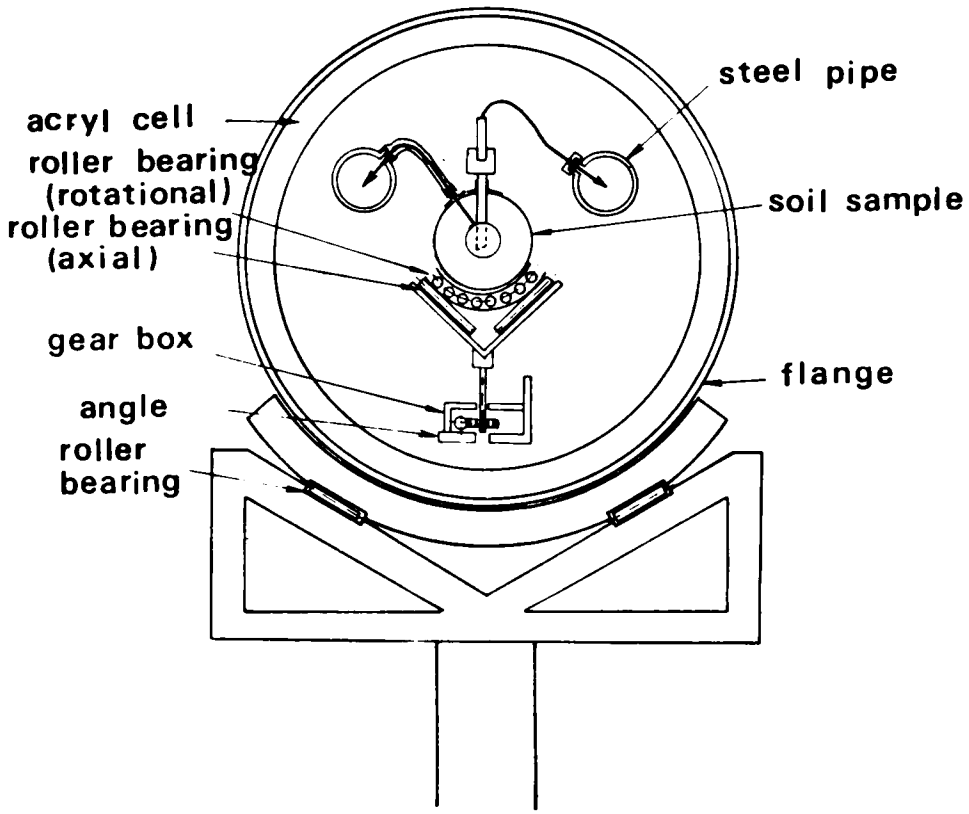

Fig.3.4 Section of the triaxial compression chamber.

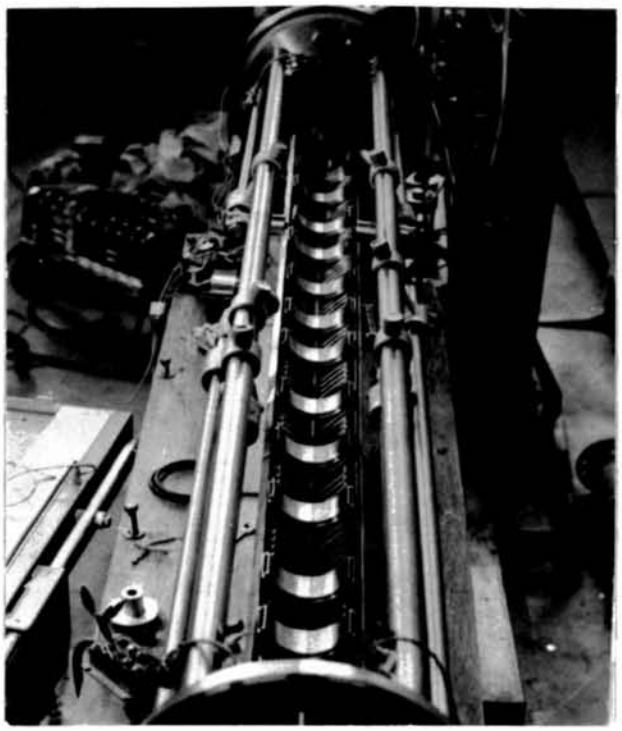

Photo.3.7 Roller bearings in the triaxial compression chamber.

Photo.3.8 Soil strain meter embedded in soil specimen.

3.4.1 Measurement of Dynamic Soil Stress

The dynamic stresses were measured by soil stress gauges buried at four different places in the specimen when the stress wave propagates. The stress gauge is a disk plate of 25 *mm* diameter and 5 *mm* thick. This gauge is made of a semi-conductive strain gauge and has a relatively high sensitivity. It can measure the pressure up to 10 kg/cm^2 but the maximum pressure ever recorded throughout the experiments is 1.2 kg/cm^2 and at this stress level, its calibration curve is linear and the sensitivity and precision of this gauge are excellent[5]. In the rod wave propagation test, the gauges were submerged into the saturated clay for a week to test the durability but did not cause any trouble.

3.4.2 Measurement of Dynamic Soil Strain

In order to measure the dynamic strain of soil when the wave propagates, the condenser-type soil strain meter described in detail in Chapter 2 was used. Two needles as the condenser were embedded in parallel with penetrated through the rubber sleeve as seen in Photo.3.8.

3.4.3 Measurement of Pore Water Pressure

Since in the rod wave propagation tests the specimen is consolidated prior to the test, the change of the pore water pressure in the specimen is monitored at the middle of the specimen where the pore water pressure gauge is pierced(see Photo.3.9). This gauge used here is a needle-like tube partially filled with the porous stone between 7 *mm* and 27 *mm* from the end. Its length is 55 *mm* and its diameter is 3 *mm*. The cross section of the porous stone is about $1cm^2$. The pore pressure is sensed by a small pressure transducer at the other end of the tube.

All measurements described above were carried out by three synchroscopes simultaneously triggered by a signal generated by a pressure transducer at the end of the shock tube.

3.5 Experimental Procedure

3.5.1 Compressional Wave Propagation Test

Sandy loam($G_s = 2.66$) was selected as the soil sample. It was sieved by 2 *mm* net and a part which passed through it was used. The mean diameter is about 0.3 *mm* and the uniformity coefficient is 22.5. The optimum moisture content is about 12%, which gives the maximum dry density of 1.89 g/cm^3. The tests were performed for three kinds of water content; dry, 5-7% and 11-13%, and the range of bulk density of 1.7-2.1 g/cm^3. The degree of saturation was in the wide range of 20-80%.

For the preparation of soil samples, a special mold with an inside diameter of 7.45 *cm* and a height of 40 *cm* was used. The inside wall of the mold was made very smoothly. In the mold a sandy loam was compacted by means of 2.5 *kg* rammer with 30 *cm* free-fall. In the stage of this compaction, the soil stress gauges were embedded in the soil. Five pieces of specimen prepared by the mold were necessary to make a complete soil specimen of 2 *m* length.

In this one-dimensional compressional wave propagation test, not only the lateral deformation should be prefectly confined, but also the friction force between the inside wall of confining tube and the soil specimen should be taken away. Although it is very difficult to completely reduce the friction, in order to minimize the friction the soil specimen was rolled by two teflon sheets of 0.1 *mm* and 0.4 *mm* thickness.

By these procedure the two-meter long confined soil column was made up

as shown in Photo.3.10.

3.5.2 Rod Wave Propagation Test

The physical properties of a silty loam used as a specimen are tabulated in Table 3.1. The specimen is made of Fukakusa dry clay which is sieved by a 400 μ net, kneaded with water, and consolidated at 1.8 kg/cm^2 surcharge in a consolidation cylinder box(diameter 60 *cm* and height 1 *m*). Fig.3.5 shows a typical result of the consolidation tests. It is seen that the pre-consolidation pressure of the specimen is about 0.7 kg/cm^2. Its unconfined compressive strength q_u is about 0.4 kg/cm^2. After the consolidation is completed, the specimen is taken out by a thin-walled sampler of which inner diameter is 75 *mm*. Paraffin is poured at each end of the tube to form a seal.

Since a soil specimen is a cylinder of 135 *cm* long and 7.5 *cm* diameter, five segments taken out from the thin-walled sampler of which each length is about 27 *cm*, are necessary to make a complete soil specimen. Those segments are put together, after placing soil stress gauges at the both ends as shown in Photo.3.11. The specimen is rolled by a sheet of filtering paper and furthermore covered by a rubber sleeve. Since the specimen is consolidated prior to the test, the problems of connection of each segment, disturbance around the soil stress gauges and fitting problem of gauges to the soil seem to be minute. The electric wires of the gauges are taken out through pores specially made on the rubber jacket(see Photo.3.9). Therefore the trouble of air leak into the specimen can be avoided. Photo.3.12 shows the complete soil specimen set up in the apparatus.

The pressures of each test series are listed in Table 3.2, where in the series-*a*, relatively low input peak preseure is applied to the soil specimen while relatively high pressure in the series-*b*.

Photo.3.9 Measurement of pore water pressure.

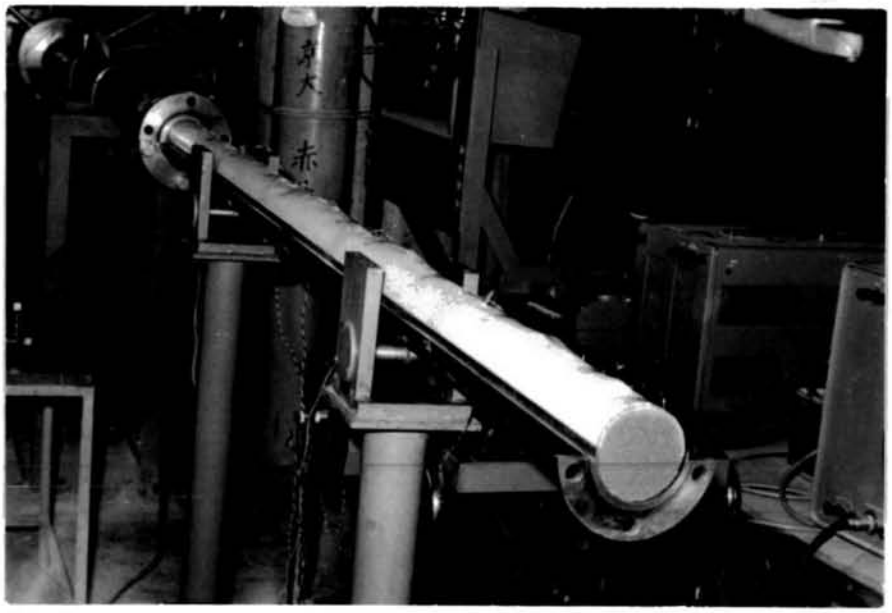

Photo.3.10 Soil column rolled by two teflon sheets.

Table 3.1 Physical properties of the silty loam used.

specific gravity	2.68
L. L.	48.6 %
P. L.	27.6 %
P. I.	21.0
uniformity coefficient	4.5
water content	31~34 %
bulk density	1.88~1.91 g/cm^3
coefficient of permeability	7.3×10^{-8} cm/sec

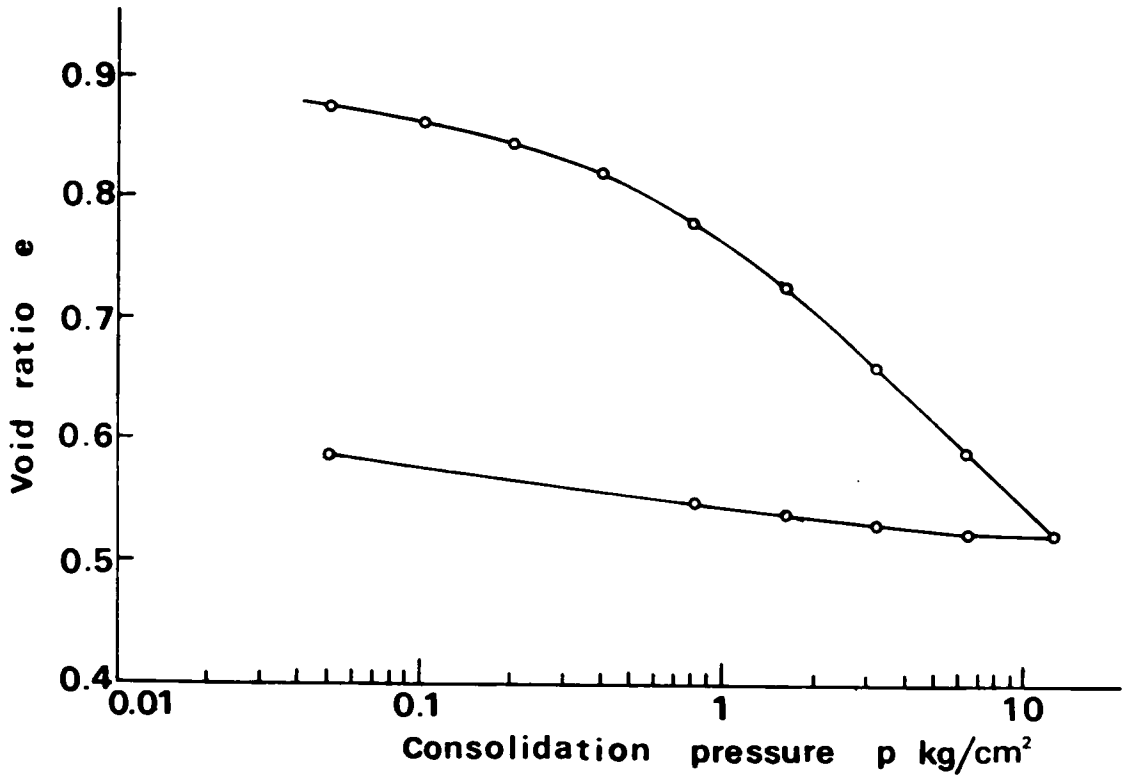

Fig.3.5 Typical e-log p curve.

Photo.3.11 Embedding the soil stress gauge in the soil specimen.

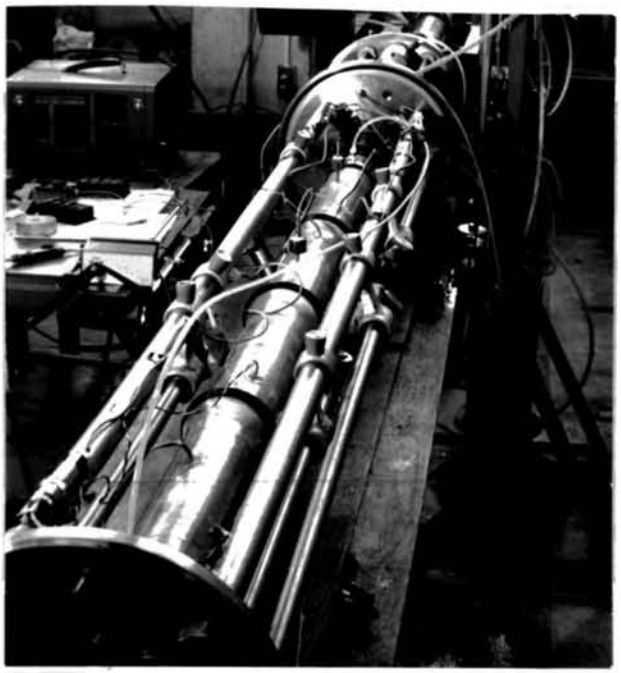

Photo.3.12 Complete soil specimen set up in the apparatus.

Table 3.2 Test series of the rod wave propagation test.

No.	confining pressure p_o kg/cm^2	back pressure p_b kg/cm^2	effective confining pressure p_c kg/cm^2	input peak pressure kg/cm^2
11-a	3.46	1.35	2.11	0.73
11-b	3.46	1.43	2.03	1.18
12-a	2.89	1.52	1.37	0.52
12-b	2 89	1.58	1.31	0.98
13-a	2.30	1.09	1.21	0.54
13-b	2.30	1.30	1.00	1.06
14-a	1.76	0.86	0.90	0.69
14-b	1.76	0.93	0.83	1.03
15-a	1.50	0.96	0.54	0.50
16-a	1.50	1.10	0.40	0.43
17-a	1.50	1.24	0.26	0.38
18-a	1.50	1.34	0.16	0.32
19-a	2.20	1.14	1.06	0.64
19-b	2.20	1.14	1.06	1.14

3.6 Experimental Results and Discussions

Propagating stress wave forms at four points in the soil specimen recorded by a synchroscope are shown schematically in Fig.3.6. These features of wave forms are almost same in both tests of the compressional wave and the rod wave. The pressure form picked up by the soil stress gauge buried in the specimen in the distance of 3 *cm* from the end, was considered as the input pressure form. The input pressure form is like a spike pulse, that is, its pressure steeply increases to the peak value and decays exponentially. The rise time of the input pressure was almost constant throughout the experiments; in the range of 0.6 to 1.4 *msec.* in the compressional wave propagation test and 2.2 to 3.0 *msec.* in the rod wave propagation test. The magnitude of the peak pressure was controled to be less than half or two-third of the unconfined compressive strength or triaxial compressive strength of the soil specimen.

Generally speaking, as the stress wave is propagating through the soil specimen, its wave form gradually changes as shown in Fig.3.6. To say that, the rise time and the duration time are increasing and, the peak stress attenuates as the wave propagates. These phenomena characterize the dynamic properties of soils. The wave velocity can be calculated from arrival time of the stress wave front and then, the dynamic modulus of elasticity can be known. Furthermore, the attenuation constant which is a parameter of energy loss absorbed into the soil during wave propagation, can be obtained from the peak stress attenuation.

3.6.1 Compressional Wave Velocity in Partially Saturated Soil

It is known that the presence of the fluid exerts an important influence on the compressional wave velocity but produces only a minor effect on the shear wave velocity. Biot[6] treated theoretically the wave propagation in

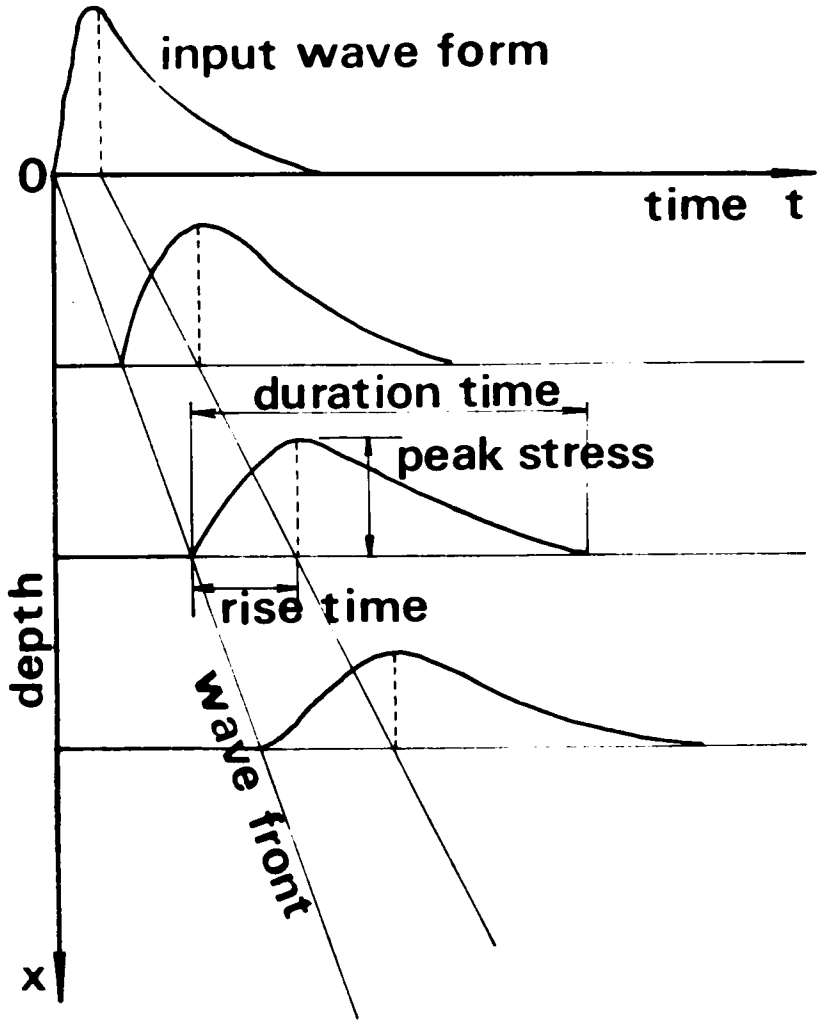

Fig.3.6 Propagating stress wave forms.

a fluid-saturated porous medium and described the influence of the fluid on the compressional wave velocity in the porous medium. On the other hand, Hardin and Richart[7] investigated the influence of the degree of saturation on the shear wave velocity for a sample made of 20-30 % Ottawa sand. They concluded that the presence of the fluid affected the shear wave velocity only by adding the mass of the fluid in motion and that much of the difference between the experimental results in the dry and saturated conditions could be caused by the effect of the weight of the water.

Fig.3.7 shows the relationship between the compressional wave velocities and the void ratio with parameters of the degree of saturation, by using the soil sample of sandy loam. The distinct experimental conclusions are drawn from this figure that the velocities decrease with increase in the void ratio for the same degree of saturation and with increase in the degree of saturation for the same void ratio. The rigidity of the soil structure becomes low with increase in the void ratio, and as a consequence, the wave velocity decreases. Since the increase in the degree of saturation increases the mass of the particles in motion and also weakens the bonds among the soil particles, the wave velocity decreases[8].

3.6.2 Rod Wave Velocity and Dynamic Modulus of Elasticity of the Saturated Clayey Soil

Rod Wave Velocity and Shear Wave Velocity

The relationship between the rod wave velocity, c_R and the confining pressure, p_c, is plotted in the log-log scale as shown in Fig.3.8. It is seen that the relationship is linear in log-log scale and it is expressed in the following equation:

$$c_R = m \cdot p_c^{\,n} \qquad (3.11)$$

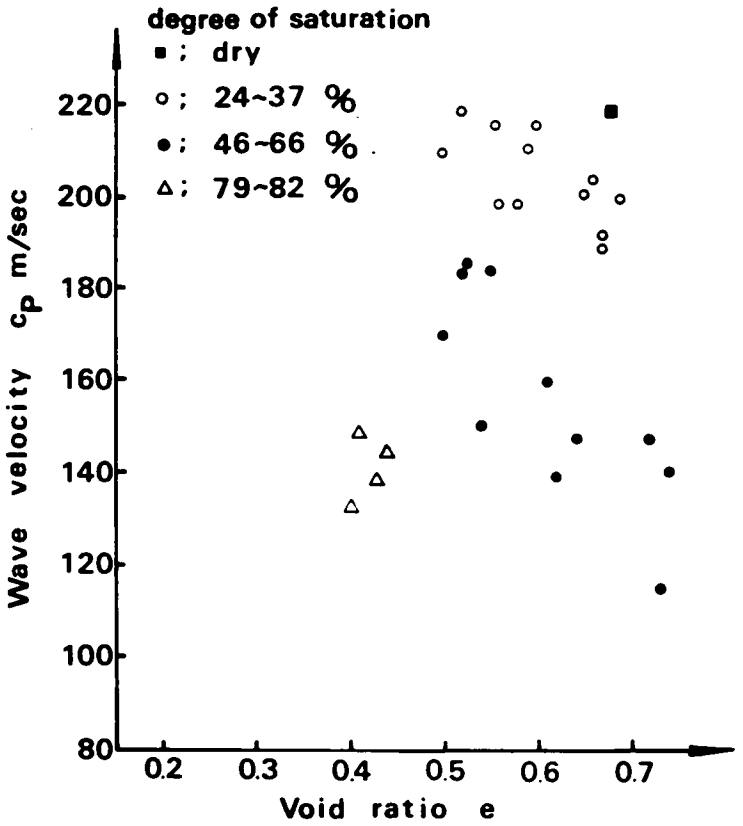

Fig.3.7 Relationship between the compressional wave velocity and the void ratio with the parameter of degree of saturation.

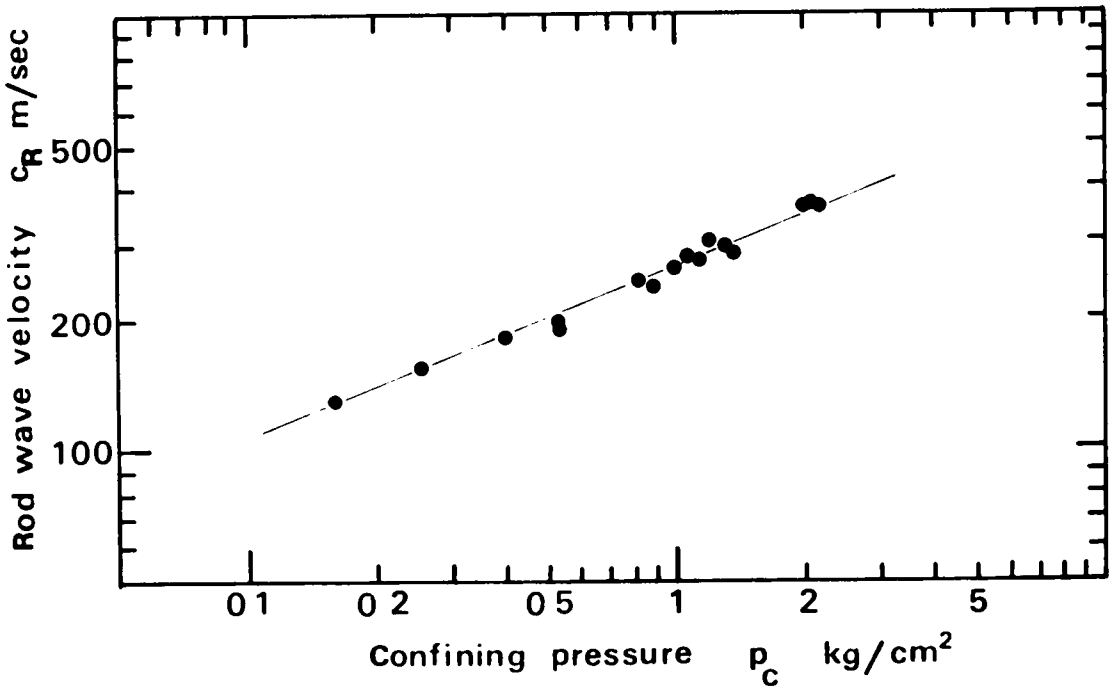

Fig.3.8 Relationship between c_h and p_c.

where, m and n are constants and, $m=280$ and $n=0.39$ from Fig.3.8(c_R: m/sec., p_c: kg/cm^2). As described in Section 3.2, if the soil is assumed to be fully saturated and not to change its volume during wave propagation, *i.e.*, $\nu=0.5$, the rod wave velocity c_E and shear wave velocity c_S satisfy the following equation:

$$c_S = \frac{1}{\sqrt{3}} c_R \tag{3.12}$$

By using the results of Fig.3.8 and Eq.(3.12), the relation of shear wave velocity and confining pressure is obtained as shown in Fig.3.9. Ishiguro[9] found that the shear wave velocity depended upon the structural inhomogeneity of clay and he obtained the results shown in Fig.3.9 from the experiments by the ultra-sonic pulse method, with "H-sample", in which wave travels perpendicular to the bedding direction of clay particle and "V-sample", in which wave travels parallel to the bedding direction. The consolidation pressures are from 1 to 32 kg/cm^2 in his tests. According to his results, n value in Eq.(3.11) is 0.44 for the "V-sample" and 0.38 for the "H-sample". They are similar to the author's results. In other words, the shear wave velocity of a clayey specimen is proportional to about the two-fifth power of p_c.

Relationship between Shear Wave Velocity and Void Ratio

Hardin and Richart[7] revealed from the resonant-column method for Ottawa sand and crushed quartz the important experimental fact that the shear wave velocity was dependent only upon the void ratio, e, and the mean effective principal stress, σ_m', and was proportional to the one-fourth power of σ_m' and was also linear to the void ratio, that is,

$$c_S = F(e) \cdot \sigma_m'^{0.25} \tag{3.13}$$

where, $F(e)$ is a linear function of e. By the cross-hole method in situ,

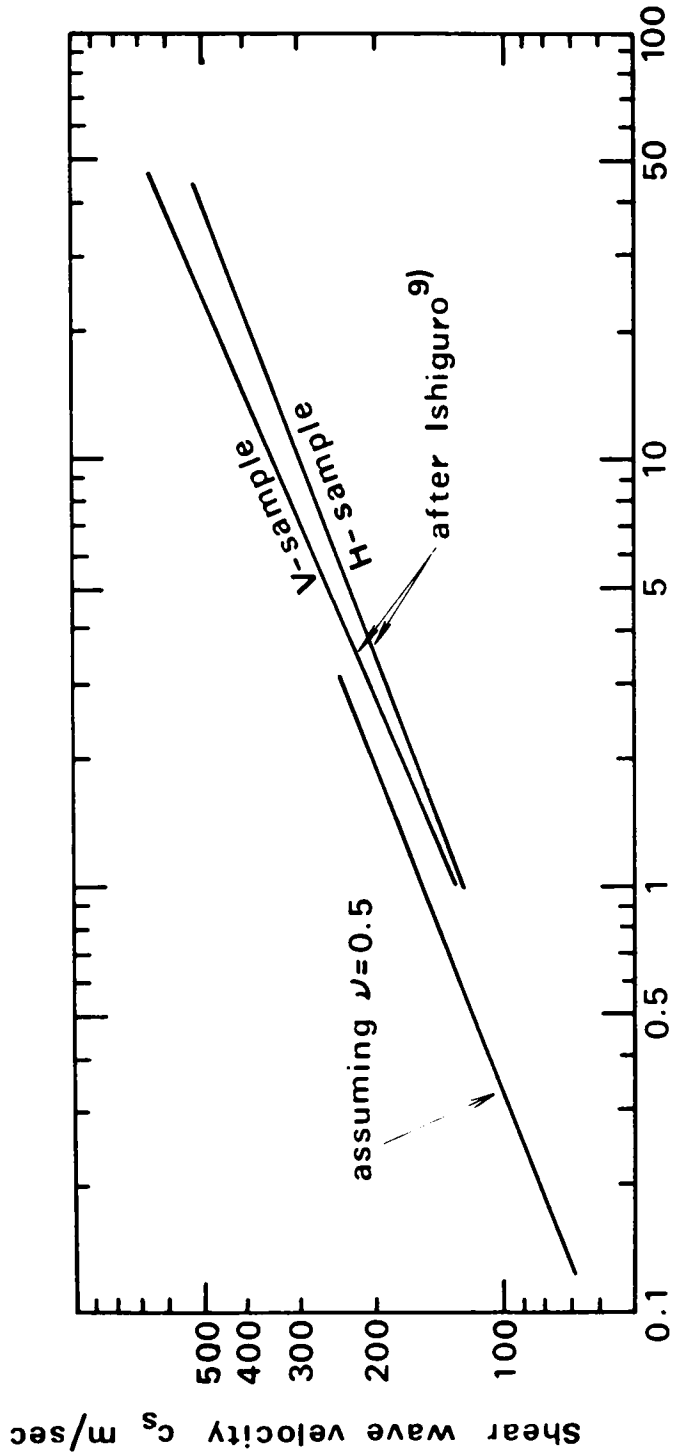

Fig.3.9 Relationship between c_S and p_c.

Stokoe and Woods confirmed the relation as expressed by Eq.(3.13) for silty sand. Furthermore, Hardin and Black[11] and, Marcuson and Wahls[12] found that also the similar relation as Eq.(3.13) held for clay such as Kaolinite, Bentonite and Boston Blue Clay.

Fig.3.10 shows the relation between the ratio, $c_S/p_c^{0.25}$, and the void ratio. It is clearly seen that the relationship is linear and the function $F(e)$ in Eq.(3.13) is determined, that is, $F(e)=-550e+602$, from our experimental results. In this case, in stead of the mean effective principal stress σ_m', the notation of p_c is used.

Dynamic Modulus of Elasticity

The dynamic modulus of elasticity, E_d, can be obtained by

$$E_d = \rho c_R^2 \tag{3.14}$$

The values of E_d and p_c are plotted in Fig.3.11(solid circles) and it is found that E_d and p_c are linearly dependent. From Fig.3.11,

$$E_d = 1220 \cdot p_c + 100 \tag{3.15}$$

is obtained (E_d and p_c in kg/cm^2).

The static triaxial compression tests were also carried out under the same confining pressure with the same soil as used in the rod wave propagation test. In these tests, the strain rate was as slow as 0.04 %/min. and the values of the initial tangent modulus of elasticity, E_s, in the stress-strain curves were determined. The open circles in Fig.3.11 show the relation between E_s and p_c and, this figure indicates that the values of E_s is almost 1/3 - 1/6 of the values of E_d, and the modulus of elasticity of the clay is strongly strain rate dependent.

Fig.3.12 shows the correlation between the shear strength under the consolidated undrained condition, and E_d, E_s and the dynamic shear modulus, G_d. In this case, G_d was calculated from E_d by Eq.(3.10). It is seen that

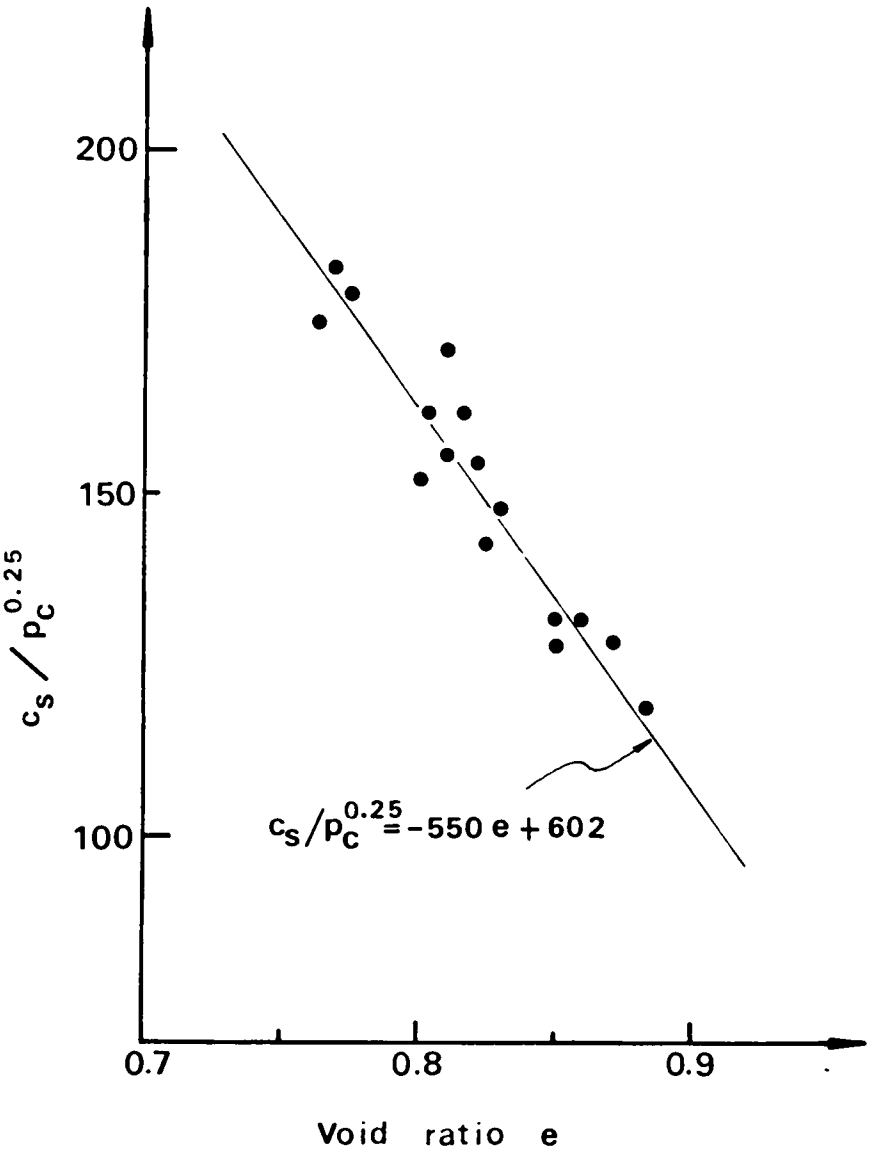

Fig. 3.10 Relationship between $c_s/p_c^{0.25}$ and the void ratio e.

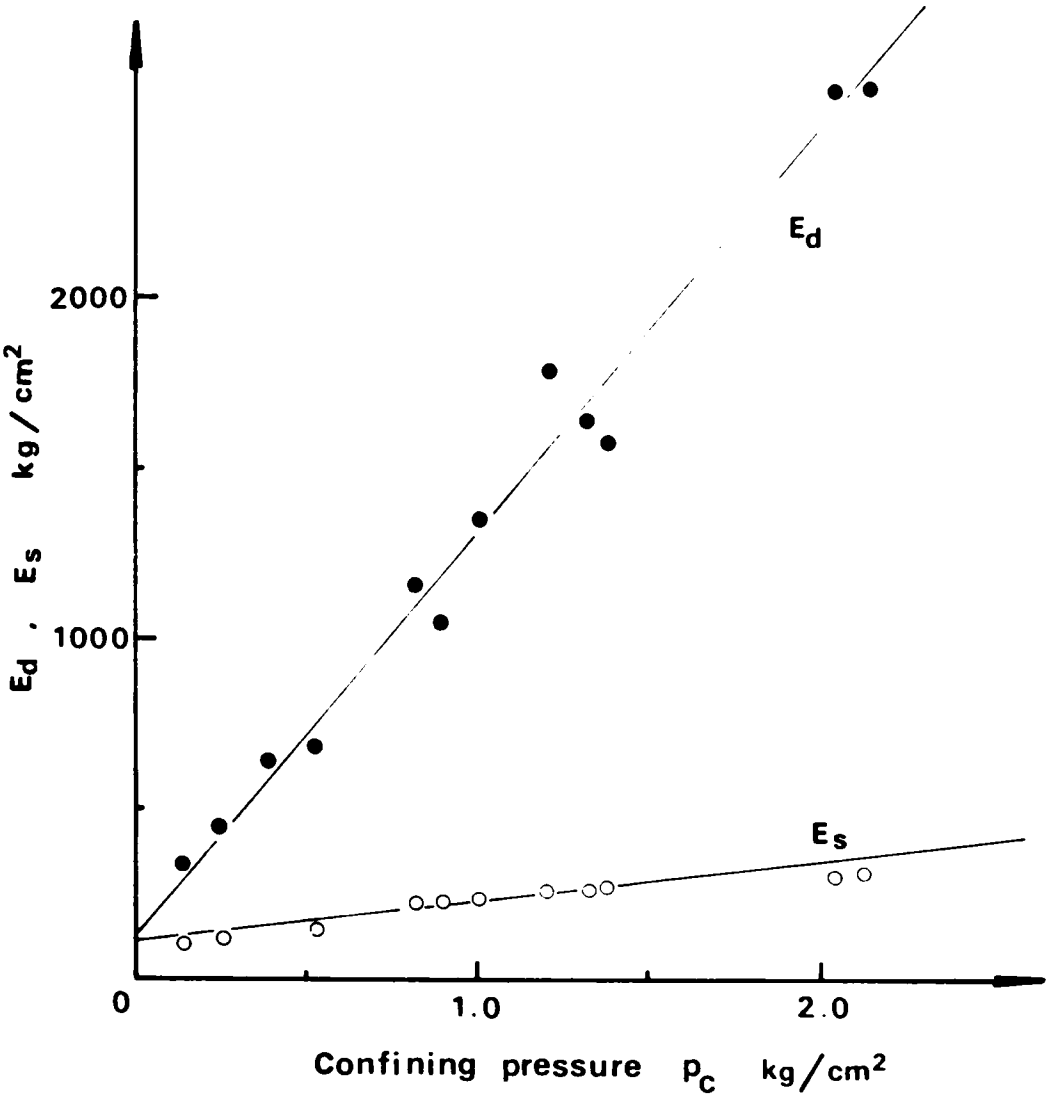

Fig.3.11 Variation of dynamic and static modulus of elasticity with confining pressure.

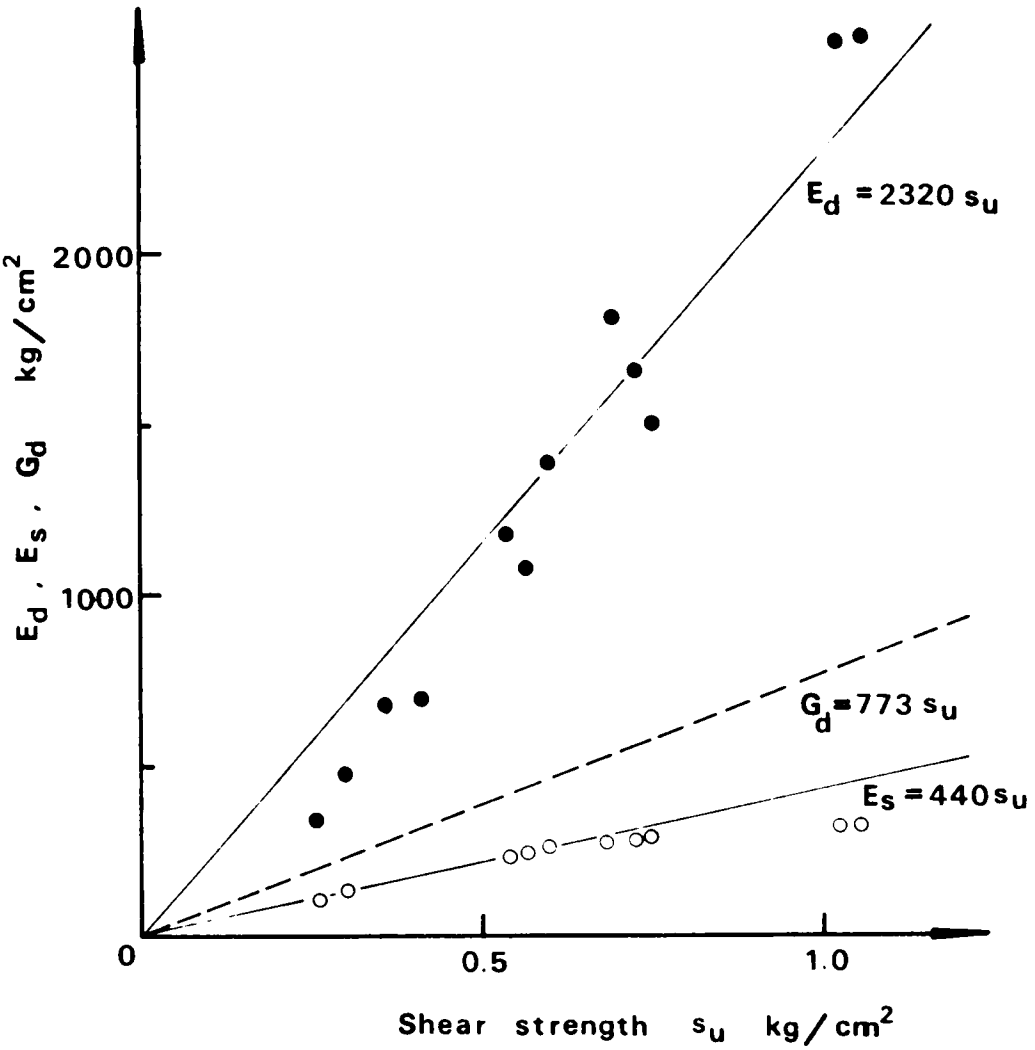

Fig.3.12 Correlation between the shear strength, and E_d, E_s and G_d.

the values of E_s can be corresponded to the relation

$$E_s = 480\, s_u \qquad (3.16)$$

proposed by Nishigaki[13], where s_u is the cohesive strength which is equal to $q_u/2$. Both E_d and E_s are linearly dependent upon s_u.

It has been clarified by many investigations[7),11),12),14)] that the main factors which influence the dynamic shear modulus of soils at small strain level are the void ratio and the mean effective principal stress, and that the dynamic shear modulus is proportional to the square of the mean effective principal stress, as listed in Table 3.3. It is found from this table that the values of the dynamic shear modulus change with the soil, though its functional form is almost identical. On the other hand, Seed and Idriss[15] initiated to point out that the shear modulus of soils reduced with increase in the amplitude of shear strain. By plotting the data by a number of investigators in the relationship between the ratio of the shear modulus to the undrained shear strength and the amplitude of shear strain, they obtained the distinct relation as shown in Fig.3.13. In this figure, the dashed lines represent the range of the scattered data and the solid line represents the average values. The author's result in Fig.12, $G_d/s_u=773$, corresponds to the value at 10^{-4} strain level according to Fig.3.13. Shibata and Ishiguro[16] also investigated the dependency of the dynamic shear moduli on the amplitude of shear strain, and concluded that the maximum dynamic shear modulus could be obtained by the the experiments with the amplitude of shear strain level less than $(0.9 - 2.0)\times10^{-4}$ in sands and $(2.0 - 7.0)\times10^{-4}$ in cohesive soils, and that the ratio of G_d/s_u was about 700 at that strain level.

3.6.3 Relationship between Rod Wave Velocity and Dynamic Stress-Strain Curves during Stress Wave Propagation

Table 3.3 Experimental results of the dynamic shear modulus of soils proposed by investigators.

Investigators	Soil Samples	Experimental Results (G_d:kg/cm^2, σ_m' and p_c:kg/cm^2)	Note
Hardin and Richart[7]	round-grained Ottawa sand	$G_d = \frac{695(2.17 - e)^2}{1 + e}\sqrt{\sigma_m'}$	$e<0.80$
	angular-grained crushed quartz	$G_d = \frac{325(2.97 - e)^2}{1 + e}\sqrt{\sigma_m'}$	
Hardin and Black[11]	kaolinite	$G_d = \frac{354(2.97 - e)^2}{1 + e}\sqrt{\sigma_m'}$	
Marcuson and Wahls[12]	kaolinite	$G_d = \frac{452(2.97 - e)^2}{1 + e}\sqrt{\sigma_m'}$	
	bentonite	$G_d = \frac{45(2.97 - e)^2}{1 + e}\sqrt{\sigma_m'}$	
Shibata[14]	sand and clay	$G_d = 4200(0.97 - n)\sqrt{\sigma_m'}$	n:porosity
The author	silty loam	$G_d = \frac{330(2.97 - e)^2}{1 + e}\sqrt{\sigma_m'}$	

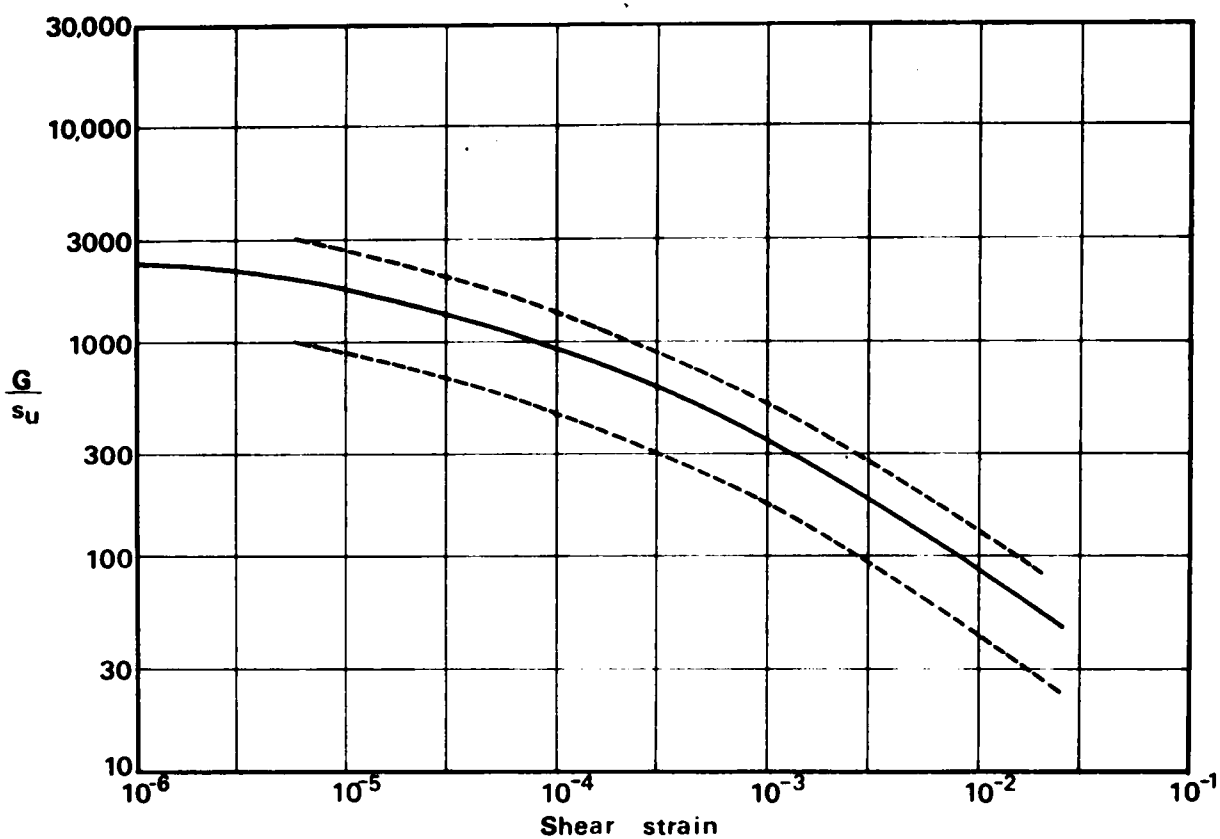

Fig.3.13 Variation of G_d/s_u with the amplitude of shear strain(after Seed and Idriss[15]).

In a clayey specimen, time histories of stress and strain were measured at the same position. Fig.3.14 shows a typical result of measurements; the peak of strain wave delays about 0.5 *msec.* from that of stress wave. This time lag of the strain was found in most of the tests, throughout which the peak strain was in the range of $(0.3 - 1.4)\times10^{-3}$ strain. The dynamic stress-strain curves in Fig.3.15 were constructed by reading the stress and strain values at the same instant of time in their time histories. In this figure, the static stress-strain curves under the same confining pressure are also shown. The dynamic stress-strain curve is steeper than the static one, from which the strain rate dependency of the stress-strain curve is clearly concluded. When one compares the curves at the same confining pressure (σ_3=*1.06 kg/cm*^{2}), the curve at the higher stress level(solid line) is nearly bi-linear whereas the curve at the lower stress level(chain line) does not show any clear turning point and is nearly parabolic. The magnitude of strain at the turning point of the former is about $(3 - 4)\times10^{-4}$. That is found also in the another stress-strain curve (σ_3=*0.54 kg/cm*^{2} as expressed by a dotted line). It should be noted in Fig.3.15 that at a small strain level the stress-strain curve shows hysteresis loop and nevertheless the specimen does not create any permanent strain after the load is off. It may be allowed that this behavior of the clayey specimen is considered to be viscoelastic at these strain levels.

It is well known that the wave velocity through soil is decided by ρ, the mass density and M, the modulus of deformation in the formula of $\sqrt{M/\rho}$. This theory, however, has not been confirmed as the experimental fact. For example, Vey *et al.*[17] reported that the dynamic modulus of elasticity, E_d^*, obtained from wave front velocity was 2 to 4 times of initial tangent modulus of elasticity, E_i obtained from the stress-strain curve due to wave propagation. In order to check and examine the above relation, the value of E_i was tried to compare with E_d. The results are in Table 3.4 and the initial

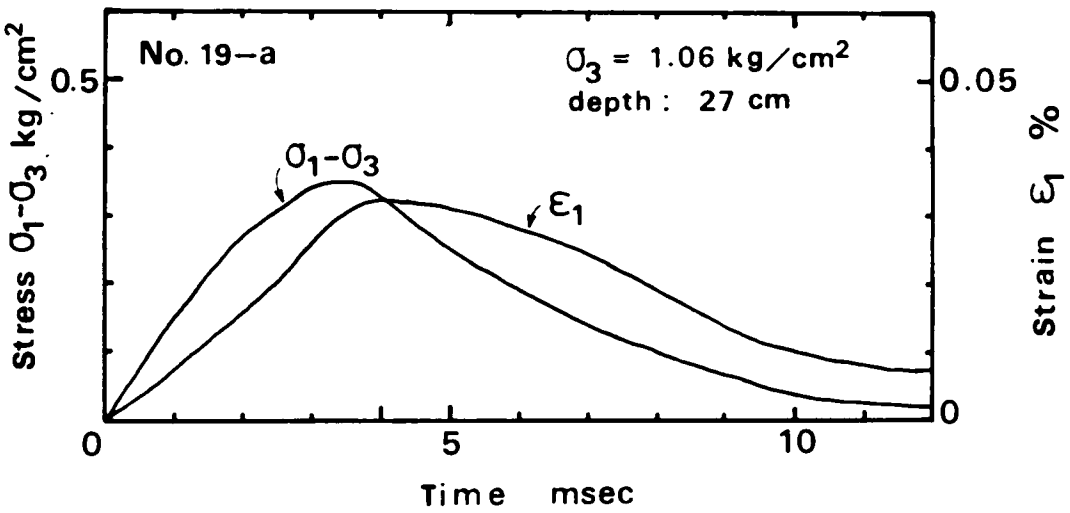

Fig.3.14 Typical result of dynamic stress and strain time histories recorded by a synchroscope.

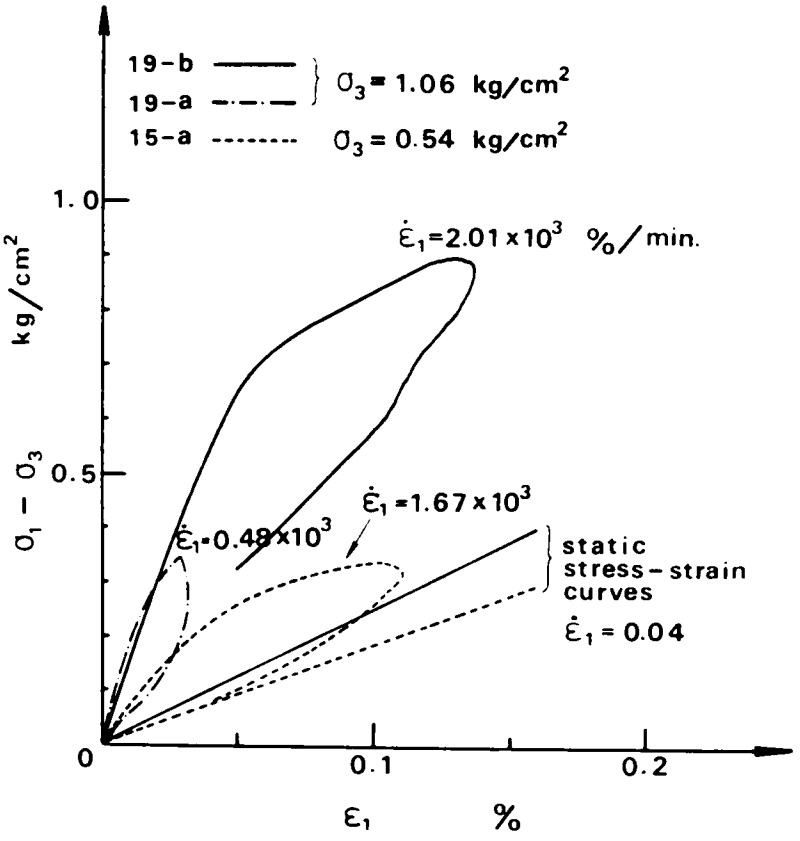

Fig.3.15 Dynamic and static stress-strain curves of the clayey specimen.

tangent modulus of elasticity E_s from a static stress-strain curve is also shown. It was found that the values of E_d and E_i were almost identical.

Table 3.4 Comparison of E_s, E_d and E_i.

No.	σ_3 kg/cm^2	Es kg/cm^2	Ed kg/cm^2	Ei kg/cm^2
19-a	1.06	252	1730	1700
19-b			1640	1400
15-a	0.54	184	695	600

3.6.4 Attenuation of Wave

The another notable feature of wave in observing the stress wave forms in soils is attenuation of amplitude of the wave with traveling. The mechanism of attenuation, in other words, energy loss, is due to an internal friction. Although this problem concerning the internal friction has not been solved sufficiently, it is obvious from observations of waves both in situ and in laboratory that the amplitude of a plane wave traveling through soils attenuates exponentially with distance, as expressed in mathematical symbols by

$$A_x = A_0 \exp(-\alpha x) \tag{3.17}$$

where, A_0 and A_x denote the amplitudes of wave at an arbitrary reference point and at distance, x, from the reference point, respectively. α is an attenuation constant and a parameter which expresses the damping characteristics of soils.

It is well known that the attenuation constant depends of the frequency of the wave, and therefore, it is necessary to examine the attenuation constants by using the wave with a constant frequency. On the other hand,

since the pulse like wave used in the present experiments consists of various frequency components, it is necessary to divide the pulse into the each frequency component(for example, the Fourier spectrum[18),19)]) in order to examine the dependency of the attenuation constant on the frequency. In the present study, however, the attenuation constant was simply determined by the attenuation of the amplitude of stress pulse in order to know the relationship between the attenuation and the physical properties of soils.

Attenustion of Compressional Wave through the Sandy Loam

Fig.3.16 shows the relationship between the dry density γ_d and the attenuation constant α. Due to increase in the dry density the soil strengthens its structure in the case of the samples with moisture content of 5-7 % and the attenuation constant decreases. While, in case of 11-13 % moisture content the soil structure is strongest and the attenuation constant is smallest at the dry density of about 1.75 g/cm^3. These tendencies represent the characteristics of compaction for sandy loam. Furthermore, the quantity of the wave energy absorbed in the soil is minimum in the sample with the dry density which is slightly smaller than the maximum dry density at the optimum water content[8)].

The traveling wave form becomes gently round and its rise time and duration time grow longer during wave propagation. In order to estimate quantitatively the increase in the rise time, the dimensionless rise time T' is defined by

$$T' = \frac{t_x}{t_0} \tag{3.18}$$

where t_0 denotes the rise time of the input wave($msec.$) and t_x the rise time at a certain distance($msec.$). Fig.3.17 shows the relationship between T' at various distances(40, 80 120 and 160 cm) and the dry density γ_d. The relationship between α and γ_d shown in Fig.3.16 is also drawn in this figure

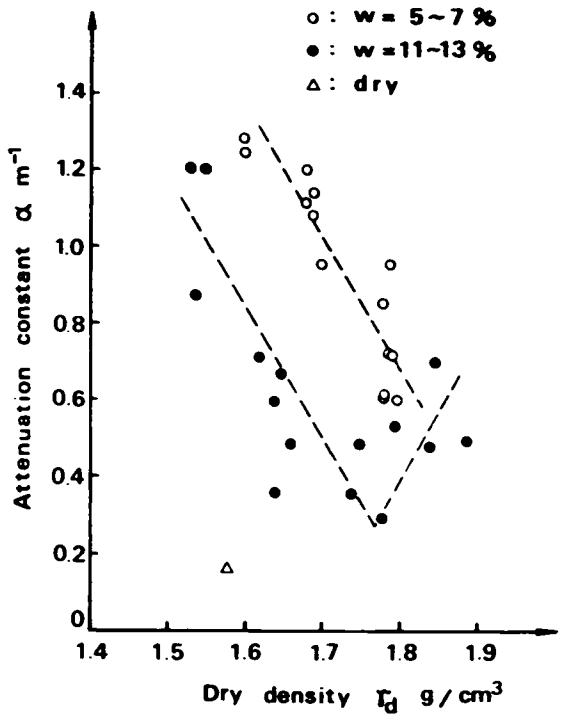

Fig.3.16 Relationship between the dry density γ_d of sandy loam and the attenuation constant α.

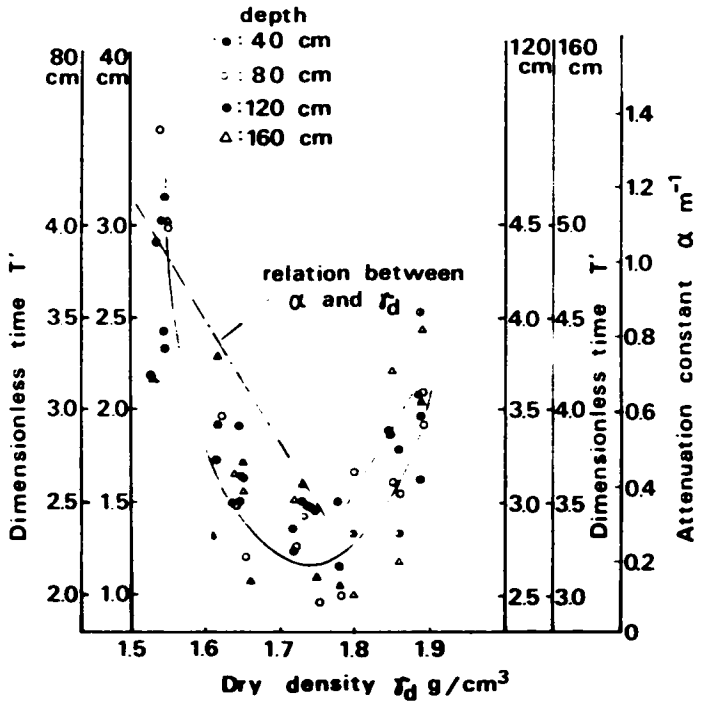

Fig.3.17 Relationship between the dimensionless rise time, the attenuation constant and the dry density.

for reference. It can be understood that the tendency for the change of wave form is similar to that for the stress attenuation.

Attenuation of Rod Wave through the Cohesive Soil

Figs.3.18(a) and (b) show the peak stresses of the pulse with the propagation distance. Most of data show that the stress attenuates almost 30-40 % by the distance of 23 cm from the end of the specimen and thereafter the attenuation rate slows down, that is, there exists a turning point where the rate changes. Furthermore, we found from our experiments that the higher the input peak stress is, the longer the distance becomes where the turning point appears. The turning point is considered to be observed when the peak stress attenuates with distance and becomes below the critical stress level where the machanical behaviors of the soil are considered to be elastic or viscoelastic. Fig.3.19 shows the relationship between the stress level at which the rate of the peak stress attenuation changes and the confining pressure applied to the soil specimen. In this figure, for reference, the triaxial compressive strength q_{max} is also given. It is found that the stress level at the critical point is less than 20 to 25 % of q_{max}. This stress level corresponds to about 0.1 % of the strain in the static stress-strain curve.

Relationship between the Attenuation Constant and the Void Ratio

Fig.3.20 shows the relationship between the attenuation constants obtained by the both tests of the compressional and rod wave and the void ratio of the soils. It is found from this figure that there exists an almost linear relationship between them on the log-log scale, and the void ratio is very important factor for the energy absorption of soils. The amount of the attenuation changes with moisture content in the case of the sandy loam. At the same void ratio, the attenuation in the soil sample with moisture content of 11-13 % is smaller than that of 5-7 %. Furthermore, the attenuation constant for the dry sample is $\alpha=0.16m^{-1}$ at the void ratio

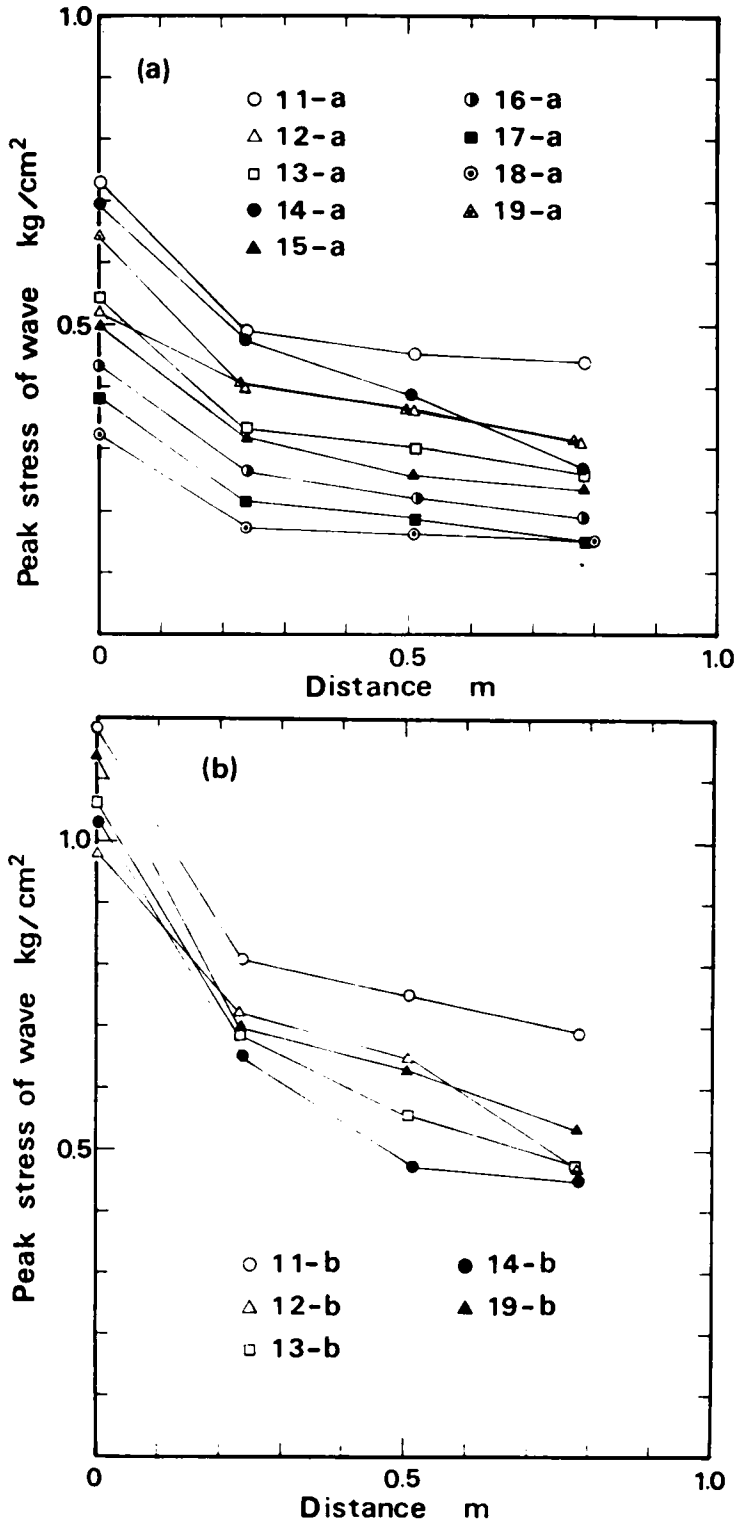

Fig.3.18 Attenuation of peak stress with travelling distance in the rod wave propagation test; (a) a-series and (b) b-series.

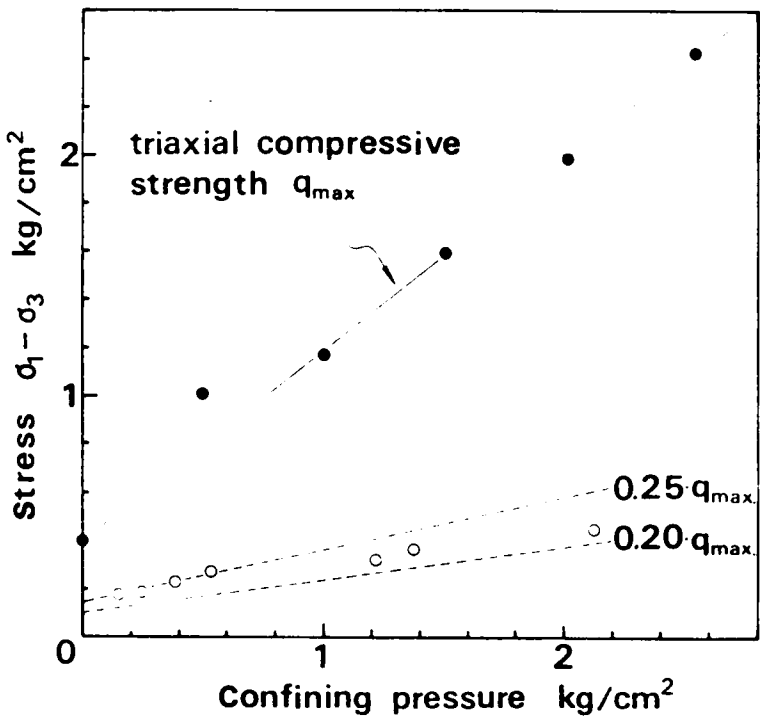

Fig.3.19 Stress level below which the soil is considered to behave as an elastic or viscoelastic material.

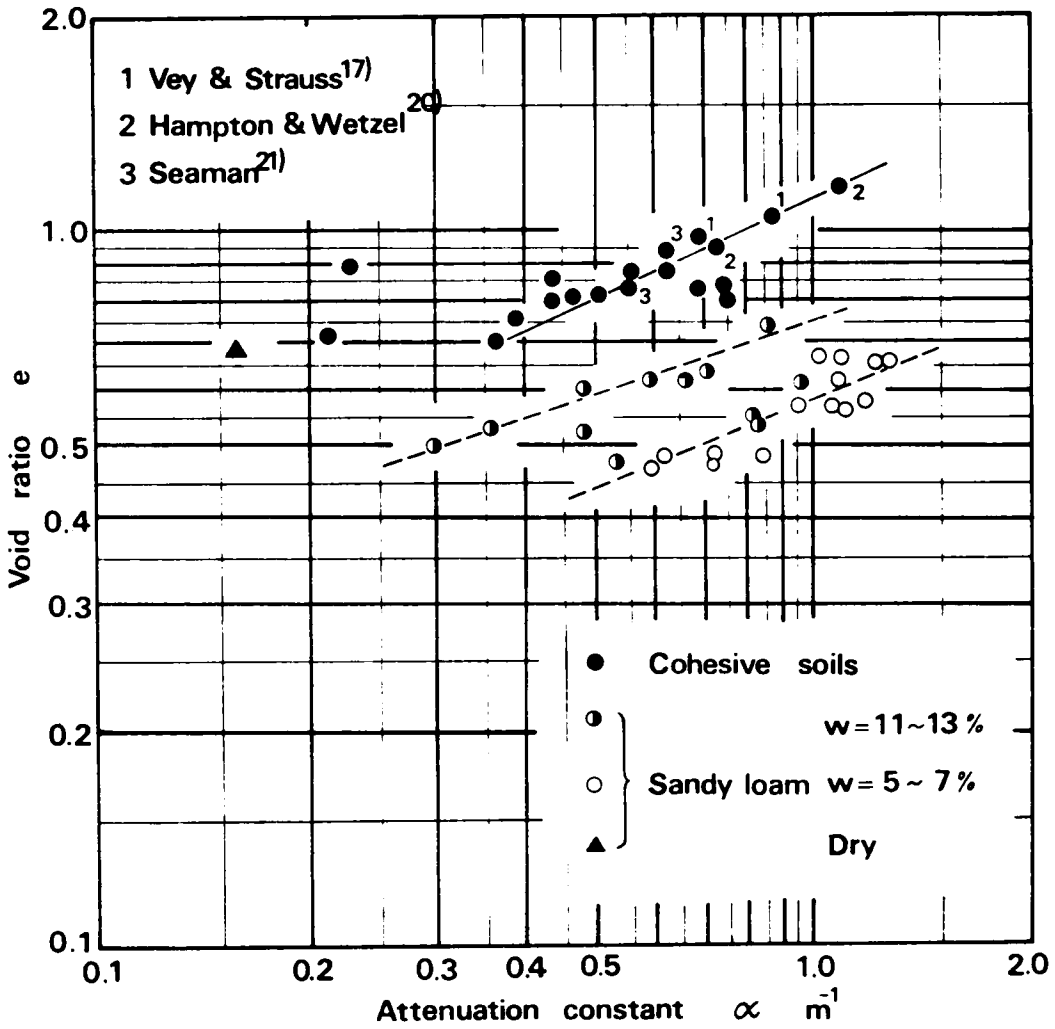

Fig.3.20 Relationship between the attenuation constant and the void ratio.

Table 3.5 Soils and their properties used by various investigators.

investigators	soil	water content %	degree of saturation %	void ratio e	kind of wave
E. Vey [17] L. V. Strauss	EPK-clay	34.1	93.0	0.97	rod wave
D Hampton R.A.Wezel [20]	EPK-clay	29.7	73.9	1.07	rod wave
	EPK-clay	33.2	93.1	0.95	rod wave
L.Seaman [21]	Kaolinite	34.7	88.4	1.02	compressional wave
	Kaolinite	31.7	87.8	0.94	compressional wave
	Kaolinite	18.8	58.9	0.83	compressional wave

0.68.

The attenuation of cohesive soils is smaller than the sandy loam, in spite of the large void ratio. In Fig.3.20, the experimental results obtained by the other investigators from the similar experimental method are also plotted. The soil properties, types of wave and experimental conditions used by investigators are presented in Table 3.5.

3.7 Conclusions

This chapter has dealt with the shock tube technique of the one-dimensional wave propagation tests for soils. Two kinds of tests were carried out: the compressional wave propagation test for sandy loam and the rod wave propagation test for silty loam.

The obtained wave characteristics were considered from two points of view. The first is the wave velocity of the wave front which is considered to exhibit the instantaneous elastic response of the soil for a dynamic external force. Therefore, the moduli calculated from the wave front velocity can be considered to be the dynamic modulus of elasticity of the soil at the infinitesimally small strain level. These moduli were discussed with respect to the confining pressure, the void ratio and the shear strength. The second is the attenuation of peak stress and the changes of wave form with wave propagation which indicate the nature of energy loss due to internal friction of soils. The attenuation constant was used as a parameter which expressed the quantity of attenuation of the peak stress per unit distance, and was discussed with respect to the physical properties of soils such as the void ratio, the dry density and moisture content. Furthermore, it was noticed from observation of wave forms that there existed a critical stress level below which the rate of attenuation was very small and the noticeable changes of traveling wave forms were not seen. By comparing this

critical stress level with the triaxial compressive strength, it was found that this corresponded to the interesting strain level for classification of machanical behaviors of soils according to the strain level.

Throughout this chapter, conclusions are:

(1) A compressional wave velocity through partially saturated soils is strongly dependent upon the void ratio and the degree of saturation. The velocity decreases with increase in the void ratio and the degree of saturation.

(2) The relationship between a rod wave velocity c_R through saturated cohesive soil and an effective confining pressure p_c is given by the following formula:

$$C_R = m \cdot p_c^{\,n}$$

From experimental results, the constants of m and n were determined to be 280 and 0.39 respectively (p_c *in* kg/cm^2). That is, the rod wave velocity is proportional to the two-fifth power of the effective confining pressure. Taking into account the void ratio as a factor which influences the shear wave velocity c_S, the relationship between c_S, p_c and e is given by

$$c_S = F(e) \cdot p_c^{\,0.25}$$

where, $F(e)$ is a linear function of e.

(3) A dynamic modulus of elasticity E_d from a rod wave velocity is linear with p_c. Its magnitude is 3 to 6 times larger than the initial tangent modulus E_s of a stress-strain curve from the static triaxial compression test. Therefore, it can be seen that the behaviors of cohesive soil are strongly strain rate dependent.

The ratio of the dynamic shear modulus G_d to the shear strength s_u of the soil specimen is 773 from experiments.

(4) A stress-strain relationship of the clayey soil at propagation of wave shows a large hysteresis curve at the strain level of 10^{-3}, but any permanent strain is not created during the test. A dynamic modulus of elasticity E_d from the wave velocity coincides with the initial tangent modulus of elasticity E_i.

(5) The relationship between the attenuation constant and the dry density of sandy loam is closely related with the characteristic of compaction of the soil. In the case of the samples with moisture content of 5-7 %, the attenuation constant decreases with increase in the dry density, and in 11-13 % which includes the optimum moisture content, it is smallest at the dry density of about 1.75 g/cm^3. Its dry density is slightly smaller than the maximum dry density at the optimum moisture content.

The attenuation constant decreases with decrease in the void ratio. Its relationship is linear in log-log scale in the experimental range of the void ratio.

(6) In the rod wave propagation test for clayey soil, it was found that the rate of attenuation becamesmall below a certain stress level. This critical stress level corresponds to the stress of 20 to 25 % of the triaxial compressive strength, q_{max}, and also corresopnds to the strain level of 0.1 % in the static stress-strain curves. The author concludes that below this stress or strain level, elastic or viscoelastic property is more predominant in soils than plastic one.

The relationship between the attenuation constant of the rod wave and the void ratio is also linear in log-log scale similar to one of the sandy loam.

References

1) Akai, K., T. Adachi, M. Hori, T. Shimogami and H. Nakagawa: On Design of Triaxial Compression Chamber Connected to the Shock Tube, Preprint, 8th Conf. of JSME, 1973, pp.363-366(in Japanese).

2) Akai, K., M. Hori and T. Shimogami: Study on Stress Wave Propagation through Saturated Cohesive Soils by Means of Triaxial Shock Tube(under contribution to Proc. of JSCE).

3) Kolsky, H.: Stress Waves in Solids, Dover Publications, Inc., 1963, pp.41-86.

4) Hori, M.: Shock Tube Study on Stress Wave Propagation in Confined Soils, Master Thesis of Kyoto University, 1971, pp.19-30.

5) Akai, K., M.Hori, N. Ando and T. Shimogami: Shock Tube Study on Stress Wave Propagation in Confined Soils, Proc. of JSCE, No.200, April, 1972, pp.127-141.

6) Biot, M. A.: Theory of Propagation of Elastic Waves in a Fluid-Saturated Porous Solid, Low-Frequency Range, J. Accoust. Soc. Am., Vol.28, 1956, pp.168-178.

7) Hardin, B. O. and F. E. Richart, Jr.: Elastic Wave Velocities in Granular Soils, Proc. ASCE, Vol.89, No.SM1, 1963, pp.33-65.

8) Akai, K., M. Hori and F. Oka: Stress Wave Propagation Test by Means of the Shock Tube(2nd Report), Preprint, 27th Conf. JSCE, 1972, pp.201-204 (in Japanese).

9) Ishiguro, Y.: Effect of the Stress-Anisotropy on the Shear Wave Velocity in Soils, Annuals of the Disaster Prevention Res. Inst., Kyoto Univ., No.14B, 1971, pp.631-641(in Japanese).

10) Stokoe, K. H. and R. D. Woods: In Situ Shear Wave Velocity by Cross-Hole Method, Proc. ASCE, Vol.98, No.SM5, 1972, pp.443-460.

11) Hardin, B. O. and W. L. Black: Vibration Modulus of Normally Consolidated Clay, Proc. ASCE, Vol.94, No.SM2, 1968, pp.353-369.

12) Marcuson, W. F. and H. E. Wahls: Time Effects on Dynamic Shear Modulus of Clays, Proc. ASCE, Vol.98, No.SM12, 1972, pp.1359-1373.

13) Nishigaki, Y.: Changes of Young's Modulus of Clay with Strain Level, Preprint, 26th Conf. of JSCE, 1971, pp.93-96(in Japanese).

14) Shibata, T. and M. Hasegawa: Considerations on the Dynamic Behavior of Clay , Preprint, 8th Conf. of JSME, 1973, pp.355-358(in Japanese).

15) Seed, H. B. and I. M. Idriss: Soil Moduli and Damping Factors for Dynamic Response Analyses, Report No.EERC70-10, Univ. of Calif., Berkeley, Calif., Dec., 1970, pp.10-13.

16) Shibata, T. and Y. Ishiguro: On the Dynamic Shear Modulus of Elasticity of Soils, Preprint, 26th Conf. of JSCE, 1971, pp.167-170(in Japanese).

17) Vey, E. E. and L. V. Strauss: Stress-Strain Relationships in Clay Due to Propagating Stress Wave, Proc. Int. Symp. Wave Propagation and Dynamic Properties of Earth Materials, Univ. New Mexico, 1967, pp.575-586.

18) Collins, F. and C. C. Lee: Seismic Wave Attenuation Characteristics from Pulse Experiments, Geophysics, Vol.21, No.1, Jan., 1956, pp.16-40.

19) Hirobe, K.: Study on the Characteristics of Wave Attenuation with Fourier Analysis, Graduation Thesis of Kyoto University, 1974(under printing).

20) Hampton, D. and R. A. Wetzel: Stress Wave Propagation in Confined Soils, Proc. Int. Symp. on Wave Propagation and Dynamic Properties of Earth Materials, 1967, pp.433-442.

21) Seaman, L.: One-Dimensional Stress Wave Propagation in Soils, Stanford Res. Inst., AD-632106, DASA-1757, 1966, pp.19-40.

Chapter 4 Viscoelastic Approach to Stress Wave Propagation through Soils

4.1 Introduction

Numerous experiments have shown that whenever a soil is mechanically strained, the imparted elastic energy is never fully recoverable. Some conversion from mechanical to heat energy always occurs and therefore, real behaviors of soil are far from those of a perfectly elastic body. This non-elastic behavior within the Hooke's law region is called "anelasticity", and the various mechanisms which cause the non-elastic properties have been grouped under the term of "internal friction". The study of the internal friction in soils is very important for wave propagation, because the decrease in the intensity of a seismic wave with distance is caused by the internal friction, and the change in shape of the seismic wave with distance is also, in part, a result of internal friction, specifically, its dependence on frequency of the stress wave.

Due to complexity of the internal friction of soils and lack of experimental data from fields and laboratories, not only an explicit treatment for the internal friction has not been established experimentally and theoretically, but also it is unknown whether the internal friction is due to solid friction or viscous friction. The first approximation to mathematically express the internal friction is to assume a soil as a suitable viscoelastic model. It is sometimes useful to solve problems of soil dynamics, because of simplicity and the experimental results obtained by various procedures can be related.

The experiments described in Chapter 3 gave the interesting results that the dynamic moduli of elasticity of the clayey soils were 3 to 6 times larger than the static moduli(strain rate dependence) and the stress wave

attenuated exponentially with distance(energy damping). In order to consider the above mechanical characteristics of the soils in a small strain level ($<10^{-3}$), the spring-voigt model will be assumed in this chapter, and its viscoelastic constants will be on the discussion.

4.2 Wave Characteristics of Spring-Voigt Model

4.2.1 Selection of Model

The mechanical behaviors of solids are extremely complicated and can not always be expressed by a simple viscoelastic model. To allow for the fact that a number of different relaxation phenomena may be taking place simultaneously in a soild, more complicated models have been considered. These consist of a number of Maxwell models jointed in parallel or a number of Voigt models jointed in series. The solid is thus considered as having a number of different relaxation times, or in the limit a continuous spectrum of relaxation times. This treatment is mathematically equivalent to Boltzmann's approach.

Boltzmann suggested that the mechanical behavior of a solid was a function of its entire previous history, and assumed that when a specimen had undergone a series of deformations, the effect of each deformation was independent of that of the others, so that the resultant behavior could be calculated by a simple addition of the effects that would occur if the deformations took place singly. This assumption has become known as the principle of superposition. One form of the superposition principle is expressed by [1)]

$$\sigma(\varepsilon,t) = F(\varepsilon) - \int_{-\infty}^{t} \varepsilon(T)\cdot f(t-T)\,dT \qquad (4.1)$$

where, $\sigma(\varepsilon,t)$ denotes the stress at time t, $\varepsilon(T)$ the strain at time T and

$f(t-T)$ is called a memory function. $F(\varepsilon)$ is a function of ε. Eq.(4.1) means that the total stress σ is the sum of the components of stress remaining from the entire past history of the specimen together with the stress corresponding to the instantaneous value of the strain ε at time t, $F(\varepsilon)$.

The use of Eq.(4.1) is most general treatment for the behavior of viscoelastic materials. However, the application of Eq.(4.1) to the dynamic problems such as vibrations and wave propagation leads the *extremely* complicated mathematical expressions. Accordingly, the assuming the appropriate finite element viscoelastic model is sometimes useful for the analyses of dynamic problems.

For an aim of selecting a model that simulates a particular behavior from a set of tests which involve an application of a sinusoidally oscillating force, Bland has tabulated these relationships for the eight simplest viscoelastic materials up to four element models. According to this table, one can find an appropriate model to fit the experimentally determined complex moduli or compliances in a particular frequency.

The author has analytically studied the one-dimensional wave propagation through some simple viscoelastic models such as Voigt, Maxwell and spring-Voigt models as shown in Fig.4.1 in order to know the natures of wave propagation and to examine the influence of the viscoelastic constants on the natures[3),4)]. The analytical solutions of the rod wave propagation in the semi-infinite viscoelastic rods subjected to the spike pulse stress at the end were obtained, by using the way of the Laplace transformation, the inversion integral formula and the contour integral. The spike pulse stress is like as shown in Fig.4.2 which simulates the input surface pressure to the soil specimen obtained by the shock tube in the experiments described in Chapter 3. The calculated results are as follows:

Voigt Model

The wave forms at various distancesin the rod of the Voigt model are

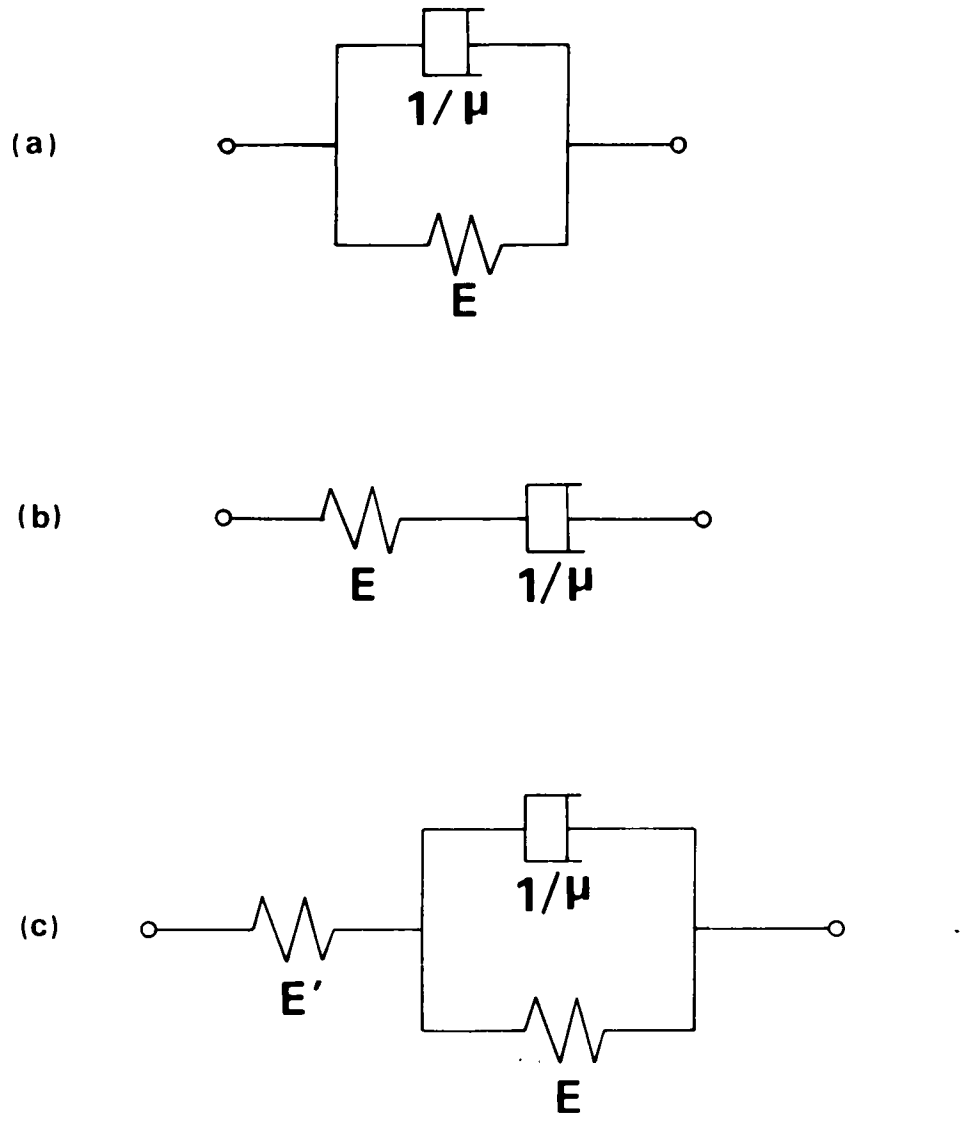

Fig.4.1 (a) Voigt model, (b) Maxwell model and (c) spring-Voigt model(sometimes called as standard linear viscoelastic model).

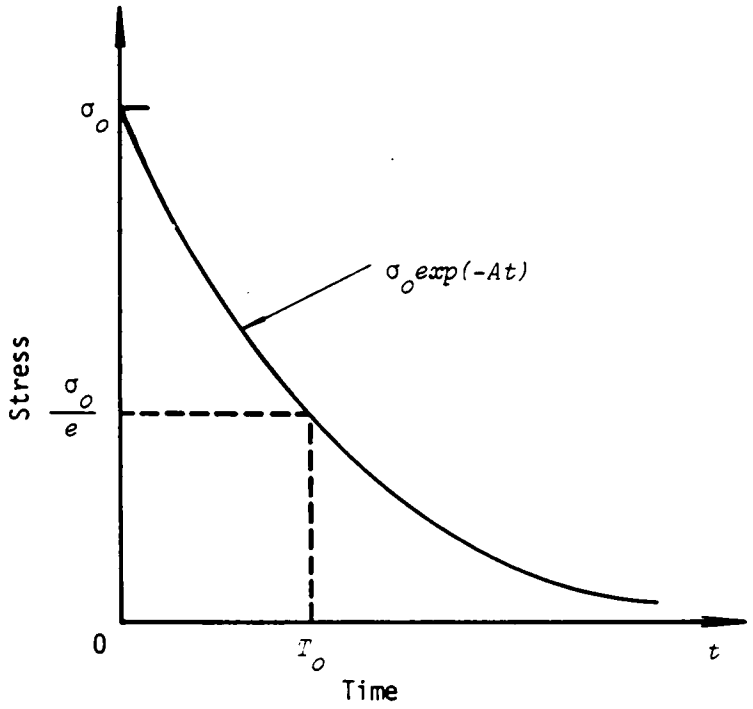

Fig.4.2 Applied spike pulse stress.

indicated in Fig.4.3, where the dimensionless stress Σ', the dimensionless time τ and the dimensionless distance ξ are defined by the following relation;

$$\Sigma' = \frac{\sigma(x,t)}{\sigma_0} \quad , \quad \tau = E\mu t \quad , \quad \xi = (\rho E)^{\frac{1}{2}}\mu x \qquad (4.2)$$

where, $\sigma(x,t)$ denotes the normal stress at time t and distance x, E and μ are the viscoelastic constants as expressed in Fig.4.1 and ρ the mass density. These dimensionless variables will be used for another models in the same way.

Since the behavior of Voigt model becomes perfectly rigid by the shock loading, wave front goes forwards in the medium with infinite velocity. There occurs no shock front at all and the duration time at each situation gradually increases with distance. Thus the wave form in Voigt material becomes flatter as the stress wave propagates into the medium.

Maxwell Model

The wave forms at various distance in the rod of Maxwell model are shown in Fig.4.4. Comparing the figure with Fig.4.3 for Voigt model, there exist remarkable differences, that is, (1) Maxwell model exhibits an instantaneous elastic response and the wave front propagates with an elastic velocity $\sqrt{E/\rho}$, (2) even when the wave proceeds into longer distance, the shock front can be seen, and (3) the wave form at the boundary surface does not change as the wave goes down. Furthermore, it is found from this figure that the attenuation of stress at the wave front is uniquely expressed as $exp(-0.5\tau)$.

Spring-Voigt Model

The response wave form for this model is dependent upon two parameters of k and β defined by

$$k = \frac{E}{E'} \quad , \quad \beta = \frac{1}{E\mu T_0} \qquad (4.3)$$

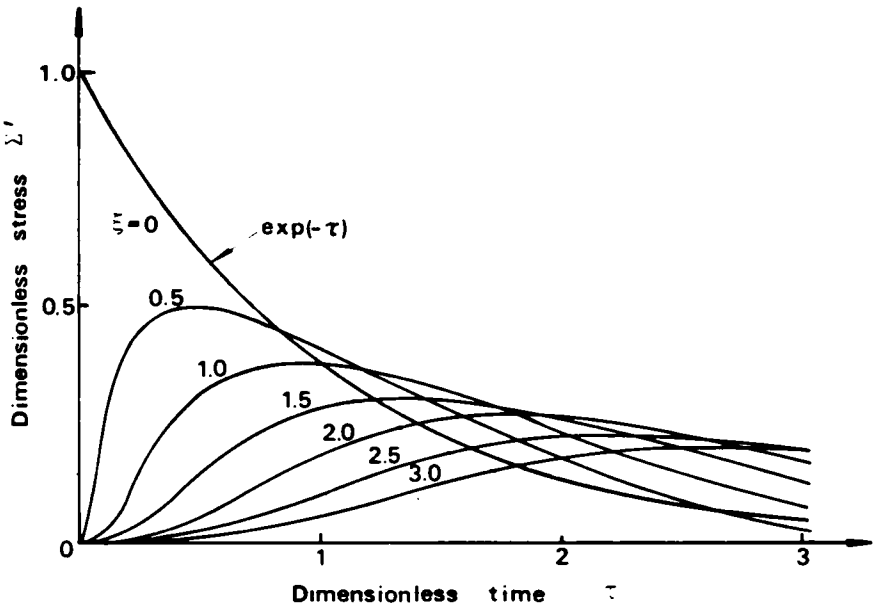

Fig.4.3 Response of Voigt model subjected to spike pulse stress.

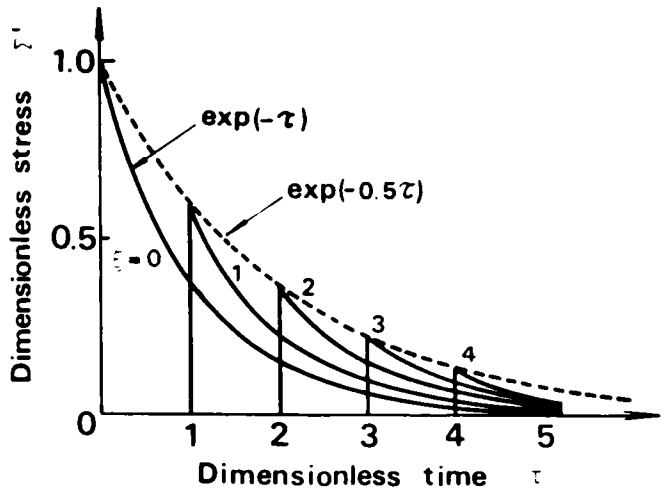

Fig.4.4 Response of Maxwell model subjected to a spike pulse stress.

where, τ_0 is a time as indicated in Fig.4.2. Fig.4.5 shows the features of stress wave propagation in this model in the case of $k=1$ and $\beta=1$[5]. The stress attenuation at the shock front depends upon the parameter k; for this example it decays in the manner of $exp(-0.25\tau)$. As would be anticipated there exist discontinuous stress jumps in the neighbourhood of the surface where the value of ξ is small and, at the same time, there is no change of wave forms in these positions. Thus the medium behaves like Maxwell body there. Reaching $\xi \geq 6.0$, however, there appears some roundness at the wave front and, for still larger value of ξ, the change of wave form being much remarkable. It can be said, therefore, that the medium behaves like Voigt body. Lai and Sauer[6] have called the depth at which this phenomena appears as the critical depth.

Fig.4.6 shows the typical calculated results of the attenuation of peak stress with distance with a parameter k. Furthermore, Fig.4.7 shows the calculated results of attenuation of peak stress with the real variable of distance under the conditions given in the figure. From these figures, one can see that the attenuation increases with increase in the parameter k for a constant value of β. The increase in k implies the decrease in Young's modulus E' of the free spring compared with the Voight spring E in the model. The above phenomenon can be understood by taking into account that Voigt behavior is mainly remarkable with increase in k. Furthermore, it was revealed out from other considerations that the increase in β which implied that the spike pulse became sharp(see Fig.4.2) caused the large amount of attenuation of stress[8], and that the attenuation depended on the product of E and μ as well as E', but not E and μ, individually[4].

Throughout the above analytical study on the rod wave propagation through semi-infinite viscoelastic rods subjected to the spike pulse stress at the end, we can understand that the spring-Voigt model has both characteristics of Voigt and Maxwell models. On the other hand, cohesive soils are

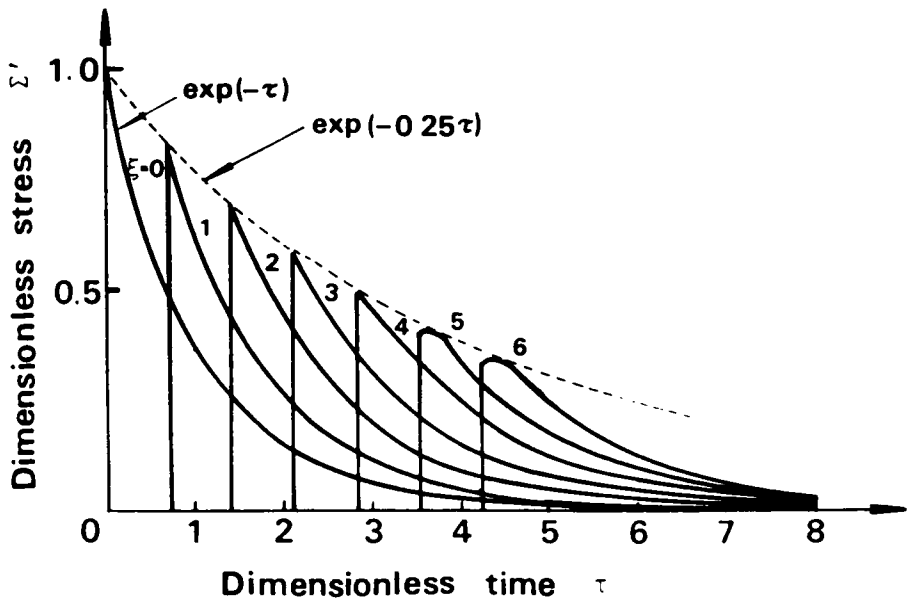

Fig.4.5 Response of spring-Voigt model subjected to a spike pulse(k = 1 and β = 1).

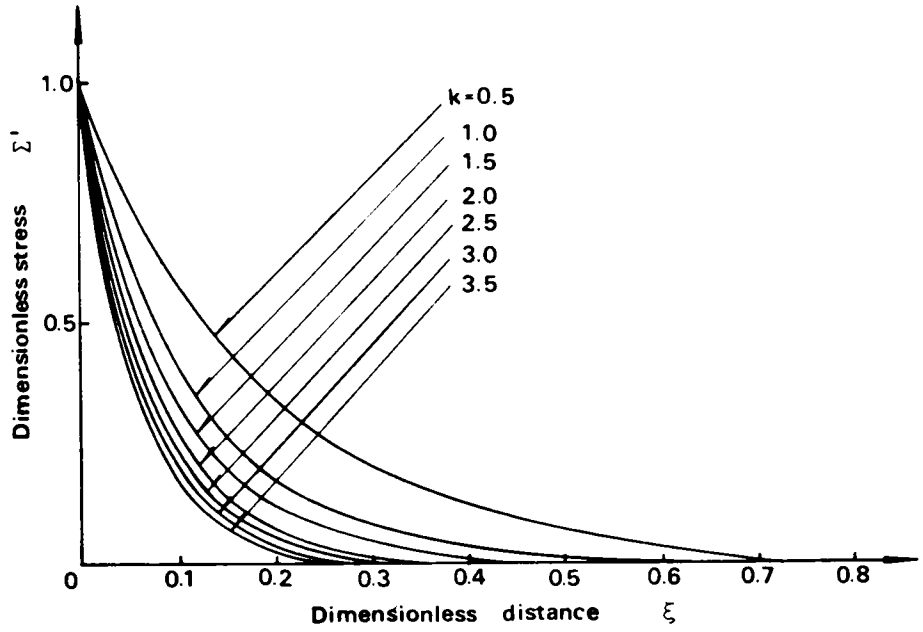

Fig.4.6 Calculated results for attenuation of peak stress in spring-Voigt model(β = 1).

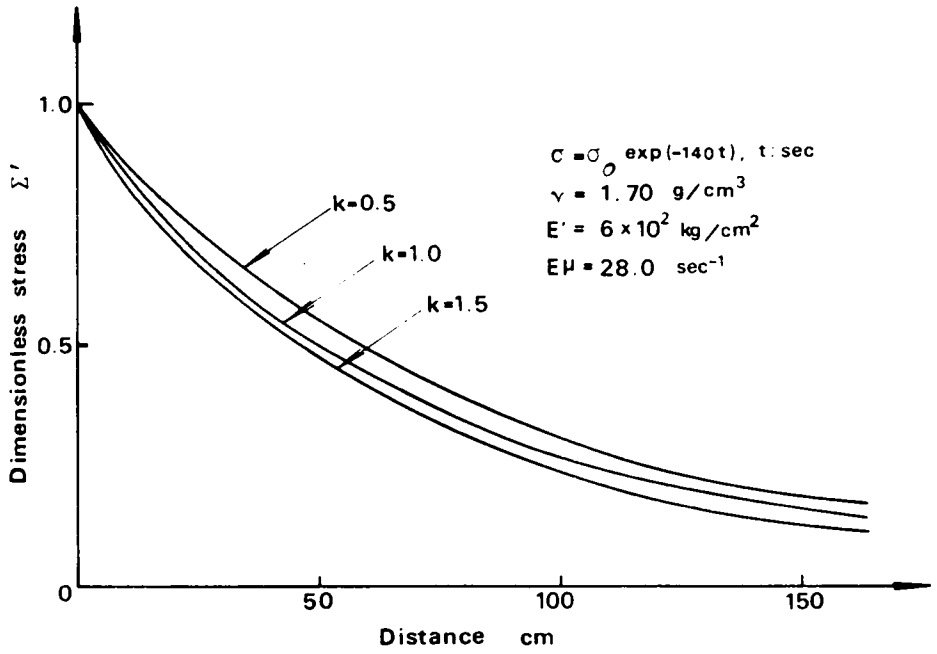

Fig.4.7 Attenuation of stress calculated from Fig.4.6.

considered to have both characteristics of Voigt and Maxwell models in small strain level. These characteristics have been observed in the rod wave propagation tests for the cohesive soils described in Chapter 3, with respect to the instantaneous elastic response, the change of wave forms with travelling distance and the attenuation of peak stress. It was described in 3.6.4 that below the critical stress level defined as the stress of 20 to 25 % of q_{max}, the attenuation rate slowed down and the change of wave form was very small. Assuming the cohesive soil as the spring-Voigt model in this stress level, the author analyses the wave characteristics in the soil as below.

4.2.2 General Behaviors of the Spring-Voigt Model

The constitutive equation of the spring-Voigt model(Fig.4.1(c)) is expressed as

$$\frac{\tau_{sv}}{E'}\dot{\sigma} + \frac{k+1}{kE'}\sigma = \tau_{sv}\dot{\varepsilon} + \varepsilon \qquad (4.4)$$

where, τ_{sv} and k are specific parameters of this model determined by the viscoelastic constants, E, E' and μ, and defined by

$$\tau_{sv} = \frac{1}{E\mu} \quad , \quad k = \frac{E}{E'} \qquad (4.5)$$

τ_{sv} corresponds to the retardation time of the Voigt element of this model.

Strain Rate Dependency on the Stress-Strain Curves

Under the condition of a constant strain rate $\dot{\varepsilon}$, the solution of the linear differential equation, Eq.(4.4), is obtained by

$$\sigma = \frac{k\tau_{sv}E'}{(k+1)^2}\dot{\varepsilon}\left(1 - e^{-\frac{k+1}{k\tau_{sv}}\cdot\frac{\varepsilon}{\dot{\varepsilon}}}\right) + \frac{kE'}{k+1}\varepsilon \qquad (4.6)$$

The stress-strain relations for $\dot{\varepsilon}=\dot{\varepsilon}_1$ and $\dot{\varepsilon}=\dot{\varepsilon}_2$ are schematically shown in Fig.4.8.

In an extreme case, $\dot{\varepsilon}=0$, Eq.(4.6) becomes

$$\sigma = \frac{kE'}{k+1}\varepsilon = \frac{1}{\frac{1}{E}+\frac{1}{E'}}\varepsilon = E_s\varepsilon \tag{4.7}$$

That is, the model behaves as a linear elastic body with the modulus of elasticity E_s called as a static modulus of elasticity. In this case, the dashpot in the Voigt part of the model is inoperative. In the other extreme case, $\dot{\varepsilon}\to\infty$, Eq.(4.6) becomes

$$\sigma = E'\varepsilon \tag{4.8}$$

Also in this case, the model behaves as a linear elastic body with the modulus of elasticity E' called as an instantaneous modulus of elasticity. The Voigt element of the model becomes rigid in this case.

In the range between two extreme cases, the equation to give the tangent modulus of elasticity is expressed as

$$\frac{d\sigma}{d\varepsilon} = \frac{E'}{k+1}e^{-\frac{k+1}{k\tau_{sv}}\cdot\frac{\varepsilon}{\dot{\varepsilon}}} + \frac{kE'}{k+1} \tag{4.9}$$

Therefore, the initial tangent modulus E_i is

$$E_i = \left.\frac{d\sigma}{d\varepsilon}\right|_{\varepsilon=0} = E' \tag{4.10}$$

E_s is obtained by the static tests with the small strain rate, while E' is obtained by the dynamic test with the large strain rate such as the resonant-column method, ultra-sonic pulse method and the shock tube technique in the present study, in which the strain rate of 10^3 %/min. in order is used.

Behaviors under Cyclic Loading

When this model is subjected to a cyclic stress of which amplitude is σ_0, its stress-strain relation is as shown in Fig.4.9. The stress-strain

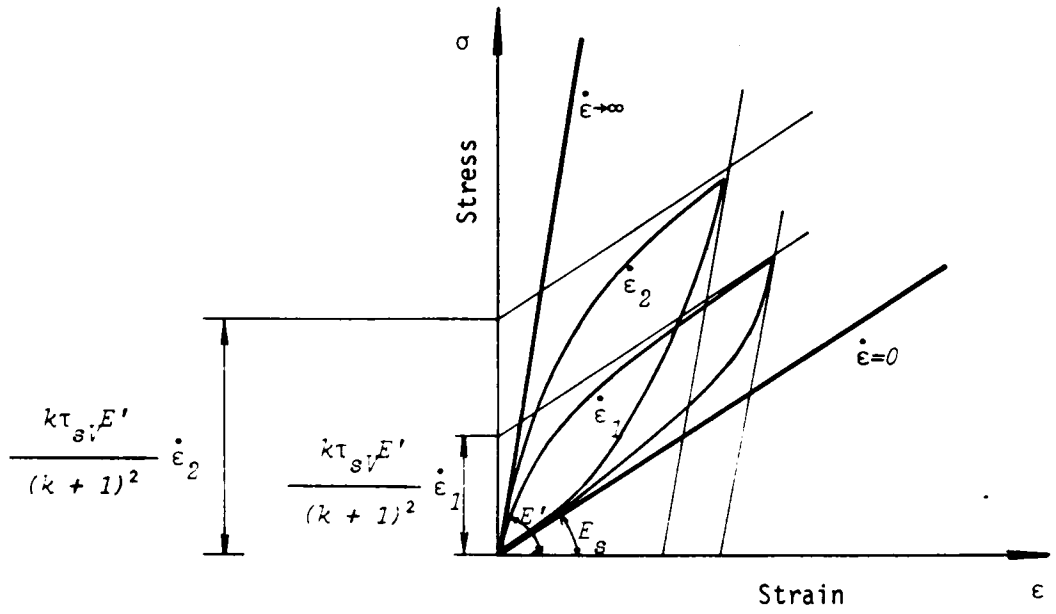

Fig.4.8 Stress-strain relations of spring-Voigt model at a constant strain rate.

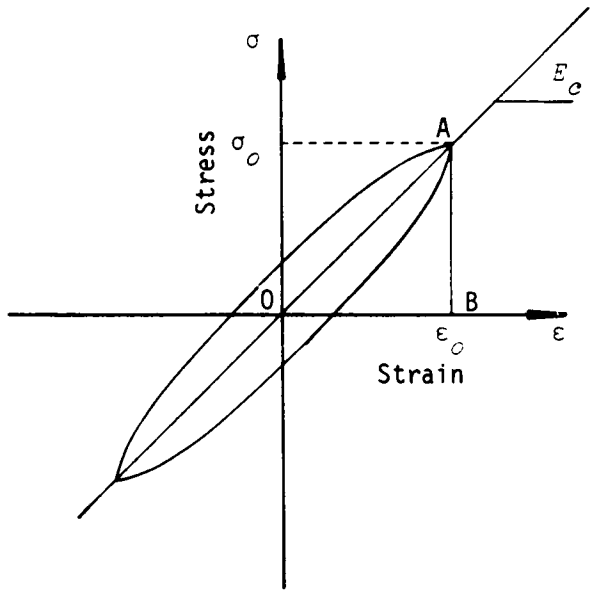

Fig.4.9 Stress-strain relation under cyclic loading.

relation is elliptic and is expressed in mathematical form as

$$\sigma = (Y_1 + i Y_2)\varepsilon \tag{4.11}$$

where, the term of $Y_1 + iY_2$ is called as a complex modulus and, Y_1 and Y_2 are given by

$$Y_1 = \frac{k+1+k\omega^2\tau_{sv}^2}{(k+1)^2+(k\omega\tau_{sv})^2}\ , \quad Y_2 = \frac{k\omega\tau_{sv}}{(k+1)^2+(k\omega\tau_{sv})^2} \tag{4.12}$$

The chord modulus E_c in Fig.4.9 is defined by

$$E_c = \sqrt{Y_1^2 + Y_2^2} \tag{4.13}$$

Furthermore, the specific damping capacity ψ is defined by

$$\psi = \frac{\Delta W}{W} = \frac{2\pi}{Q} = \frac{2\pi Y_2}{Y_1} \tag{4.14}$$

where, ΔW denotes the energy dissipated per cycle(*i.e.*, the area enclosed by the stress-strain curve in Fig.4.9), W the potential energy stored per cycle(*i.e.*, the area of OAB) and $1/Q$ the specific dissipation function[8].

4.2.3 Wave Characteristics

We are concerned with a semi-infinite rod, $x \geq 0$, of spring-Voigt material where the x-coordinate is measured along the length of the rod. Assuming that the longitudinal sections of the rod remain plane and the stress acts uniformly over each section during the passage of waves, we can express the equation of motion as follows;

$$\rho u_{tt} = -\sigma_x \tag{4.15}$$

where, $u(x,t)$ denotes the displacement along the x-direction and the sub-

scripts represent partial differentiation with respect to the corresponding variable. With the assumption of infinitesimal deformation in motion, the kinetic equation is

$$\varepsilon = -u_x \tag{4.16}$$

From Eq.(4.15), Eq.(4.16) and the constitutive equation Eq.(4.4), the wave equation can be obtained as

$$\rho \frac{\tau_{s\sigma}}{E'} \sigma_{xtt} + \rho \frac{k+1}{kE'} \sigma_{tt} = \sigma_{xx} + \tau_{s\sigma} \sigma_{xt} \tag{4.17}$$

The wave equation with respect to the displacement u is same as Eq.(4.17), where u is placed in σ.

In order to know the wave characteristics of infinite harmonic waves through the rod, we try a solution into Eq.(4.17) as follows;

$$\sigma = A \exp\left[i\left\{\omega t - (\phi + i\alpha)x\right\}\right] \tag{4.18}$$

where, A is the stress amplitude, ω the angular frequency, ϕ the wave number and α the attenuation constant. We obtain

$$\phi^2 = \frac{\rho\omega^2}{2E_s E'} \left\{ \left(\frac{E'^2 + E_s^2 \omega^2 \tau_{s\sigma}^2}{1 + \omega^2 \tau_{s\sigma}^2} \right)^{\frac{1}{2}} + \frac{E' + E_s \omega^2 \tau_{s\sigma}^2}{1 + \omega^2 \tau_{s\sigma}^2} \right\} \tag{4.19}$$

$$\alpha^2 = \frac{\rho\omega^2}{2E_s E'} \left\{ \left(\frac{E'^2 + E_s^2 \omega^2 \tau_{s\sigma}}{1 + \omega^2 \tau_{s\sigma}^2} \right)^{\frac{1}{2}} - \frac{E' + E_s \omega^2 \tau_{s\sigma}^2}{1 + \omega^2 \tau_{s\sigma}^2} \right\} \tag{4.20}$$

Furthermore, taking into account that the phase velocity c_p and tangent delta δ_T are defined by

$$C_p = \frac{\omega}{\phi} \quad , \quad \frac{\delta_T}{\pi} = \frac{2\alpha C_p}{\omega} \tag{4.21}$$

where, c_0 is the velocity of propagation at zero frequency so that $c_0 = \sqrt{E_s/\rho}$,

we obtain the following equations from Eqs.(4.19) and (4.20),

$$\frac{c_p}{c_0} = \left(\frac{2}{\sqrt{C} + C'}\right)^{\frac{1}{2}} \tag{4.22}$$

$$\frac{\delta_T}{\pi} = 2\left(\frac{\sqrt{C} - C'}{\sqrt{C} + C'}\right)^{\frac{1}{2}} \tag{4.23}$$

where, C and C' are

$$C = \frac{1 + (\theta_{sV}\,\omega\,\tau_{sV})^2}{1 + (\omega\,\tau_{sV})^2} \quad , \quad C' = \frac{1 + \theta_{sV}\,(\omega\,\tau_{sV})^2}{1 + (\omega\,\tau_{sV})^2} \tag{4.24}$$

and θ_{sV} is the parameter determined by k as follows:

$$\theta_{sV} = \frac{k}{1 + k} \tag{4.25}$$

Fig.4.10 shows the curves obtained on plotting the velocity and the tangent delta against $\omega\tau_{sV}$ with the parameter θ_{sV}=0.1-0.9. It is seen that for small value of ω, c_p approaches $\sqrt{E_s/\rho}$ whilst for very large values of ω, c_p approaches $\sqrt{E'/\rho}$. Thus at frequencies low compared with $1/\tau_{sV}$, the velocity corresponds to the elastic behavior of the two springs in series, while at high frequencies the Voigt spring is inoperative and the velocity depends on the modulus of the free spring. The damping of the wave is given by α and increases with increase in frequency; the tangent delta (or specific loss), however, is proportional to α/ω and it is seen from Fig.4.10 that it approaches zero both for very small and very large values of $\omega\tau_{sV}$, with a maximum value between them. δ_T/π is maximum when $\omega\tau_{sV}$ is about 1.

Fig.4.11 shows the variations of velocity and the tangent delta with frequency for Voigt and Maxwell models obtained by the same way as the above mentioned. In this case, c_p is $\sqrt{E/\rho}$ with use of the spring constant of the

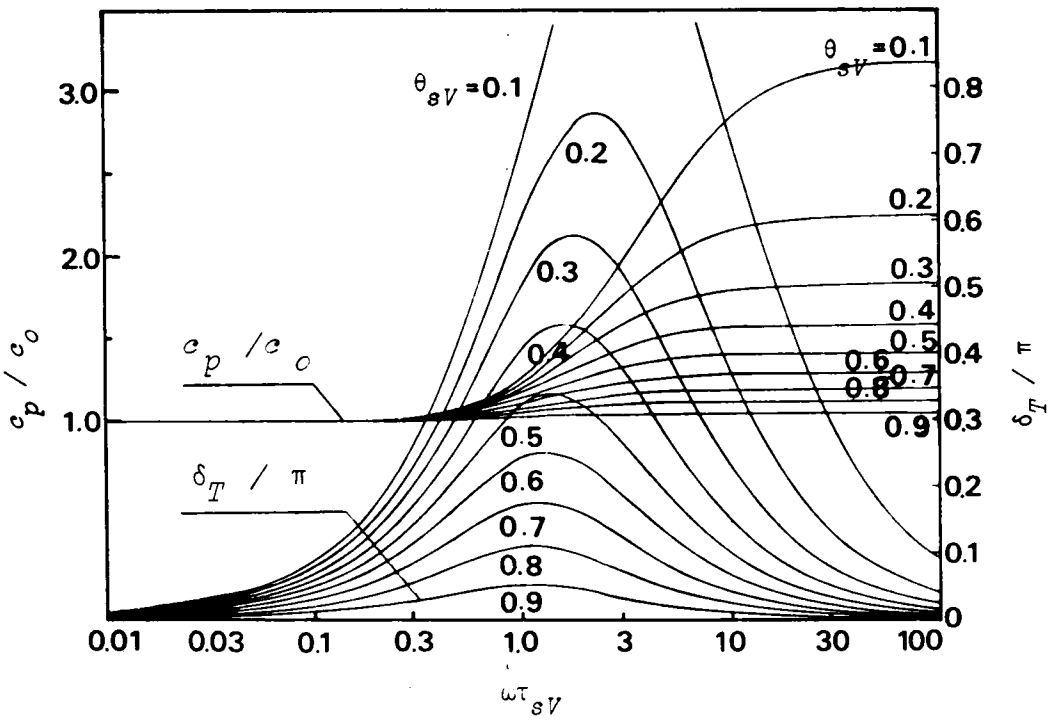

Fig.4.10 The variation of velocity and logarithmic decrement with frequency in a solid which behaves like the spring-Voigt model(θ_{sV} = 0.1 - 0.9).

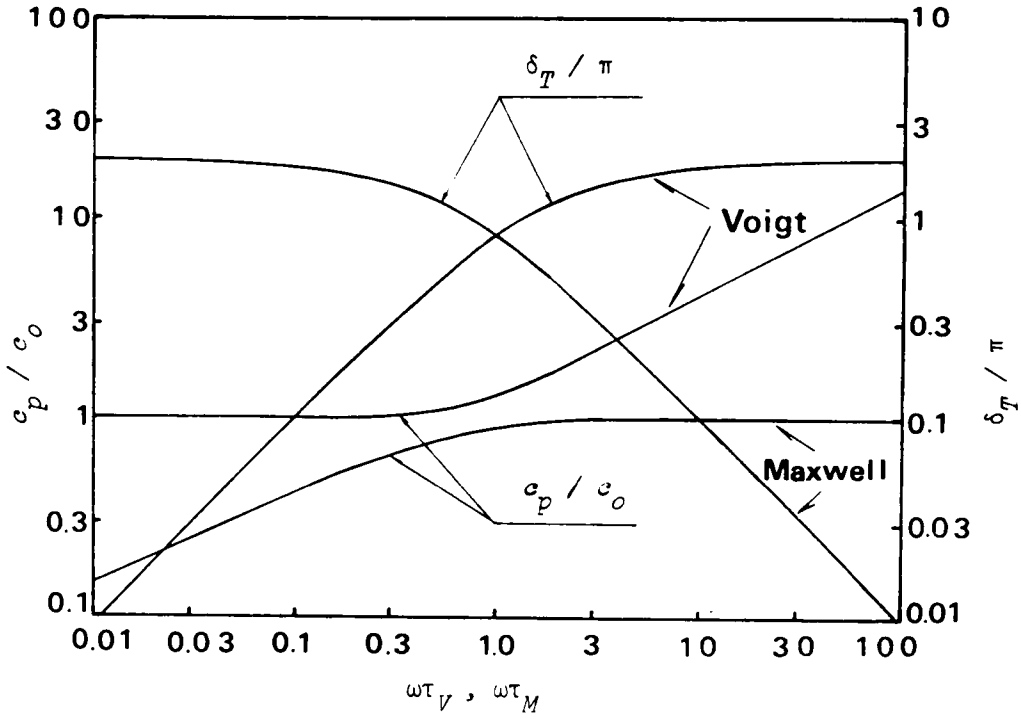

Fig.4.11 Wave characteristics for Voigt and Maxwell models.

corresponding model as indicated in Figs.4.1(a) and (b) respectively. τ_V is the retardation time for Voigt model and τ_M is the relaxation time for Maxwell model, and they are defined by $1/E\mu$. By comparing Fig.4.10 with Fig.4.11, the wave characteristic of the spring-Voigt model is similar to one of Voigt model in a low frequency range and to one of Maxwell model in a high frequency range.

Nishigaki and Hirobe[9] investigated the dependency of the modulus of elasticity and the loss tangent on the strain amplitude by using the soil samples of Osaka diluvial clay by the hysteresis loop method. The frequency range in their tests is 0.001 to 0.3 *cps*. They emphasized that the correlation between the modulus and the loss tangent varied with the applied frequency and its characteristics could be explained by using the spring-Voigt model.

Kondner[10),11)] has tried to represent stress wave propagation phenomena in terms of dynamic response spectra. He pointed out that stress wave propagation in cohesive soils was a function of many factors including moisture content and strength of the soil, applied stress intensity, time characteristics of the applied excitation and the soil, strain level, confining stress, soil density, geometry of the soil-structure system, *etc.*, and that many of complicated aspects of wave propagation could be shown to be compatible and meaningful when viewed and analyzed in terms of dynamic response spectra over wide ranges of the spectrums. In order to unify the results of vibratory steady-state[12)], creep and blast pulse tests[13)], he introduced a parameter $J(\sigma/q,t)$ denoted as the compliance and defined as

$$J_1\left(\frac{\sigma}{q}\cdot t\right) = \frac{\varepsilon q}{\sigma} \qquad (4.26)$$

where, σ is the stress, ε the time or frequency-dependent strain and q the compressive strength of the cohesive soil. Fig.4.12 is a plot of the initial compliance $J_1(\sigma/q,t)$ as a function of the time spectrum. $J_1(\sigma/q,t)$ corresponds to inverse of the initial tangent modulus of stress-strain curve.

t denotes the time(in minute) required when the stress reaches a certain value in the creep tests.

Furthermore, Kondner and Ho[14] investigated the energy dissipation of cohesive soil. Energy dissipation is expressed in terms of the loss tangent by the Fourier transformation of stress relaxation test data. The loss tangent vs. logarithm of frequency relation gives a characteristic single peak bell-shaped distribution as shown in Fig.4.13.

By comparing Figs.4.12 and 4.13 with Fig.4.10, we can easily find that the characteristics concerned with the modulus(or compliance) and the loss tangent of cohesive soils resemble very much those of the spring-Voigt model.

4.3 Similarity of Wave Characteristics in Viscoelastic Materials and Saturated Porous Elastic Media[15]

In general, soil is a mixture which consists of three phases of solid, fluid and void. there are many unknown questions in dynamic characteristics of such a mixture.

Biot explicitly induced the stress-strain relationships and the theory of three-dimensional consolidation of saturated porous elastic media standing on many assumptions[16),17),18)]. Furthermore, he applied his theory to the problem of wave propagation with infinitesimally small amplitudes and found that there existed one shear wave, two compressional waves of the first and the second kind in such a medium[19),20)]. Although Biot's logical inference is unique, there are still left extremely difficult problems how the elastic constants expressed in his study and the amount of mass exchange between the solid and the fluid should be estimated. However, the idea that the dissipative force is proportional to the relative displacement between the solid and the fluid gives us distinct images for the characteristics of energy absorption of soil in dynamic state. While, the Biot's theory is

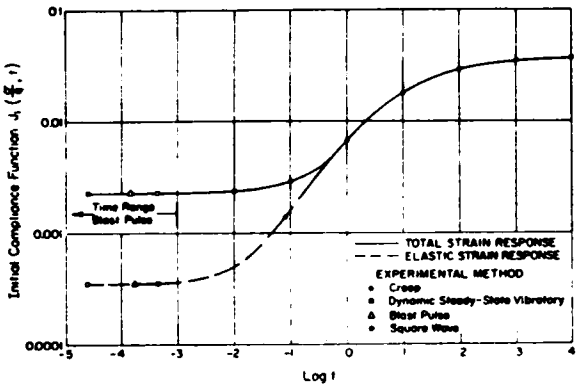

Fig.4.12 Initial compliance correlations for various experimental methods and strain response (after Kondner[10]).

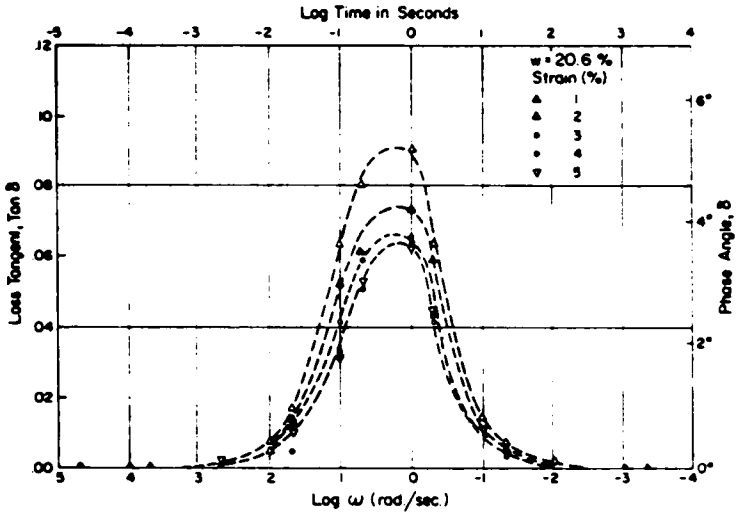

Fig.4.13 Loss tangent from Fourier transformation of stress relaxation response(after Kondner and Ho[14]).

similar to one of viscoelasticity and it is found that the characteristics of the compressional wave of the first kind are equivalent to those in spring-Voigt model[21] and the second kind to Maxwell model[22].

4.3.1 Biot's Approach

Biot considered the general three-dimensional propagation of both shear and compressional waves in a saturated elastic porous medium. The first was assumed to be a compressible liquid free to flow through the pores. Assuming a conservative physical system which was statistically isotropic, Biot derived the following stress-strain relations containing four distinct elastic constants:

$$\begin{aligned} \sigma_{ij} &= \lambda \bar{e} \delta_{ij} + 2G e_{ij} + C_Q \tilde{e} \delta_{ij} \\ -p &= C_Q \bar{e} + C_R \tilde{e} \end{aligned} \tag{4.27}$$

where, σ_{ij} denotes the tensor components of the stress acting on the solid part, $-p$ the total pressure acting on the fluid per unit area of cross-section of porous material, e_{ij} the tensor components of the strain in the solid $\bar{e}$ and $\tilde{e}$ the dilatations in the elastic structure and the fluid, respectively, λ and G the Lame's constants and C_Q and C_R the constants relating to the coupling between the fluid and solid constituents.

When waves with infinitesimally small amplitude propagated in a saturated porous elastic medium, Biot supposed that there occurred mass exchange between the solid and the fluid phase and that the equivalent mass should be added to both phases due to coupling in each other. Consequently, the negative apparent mass has been introduced in his theory. This plays a role as equivalent parts for both phases in kinetic energy and a dissipation function in the Lagrange's equation of motion. Under these assumptions, he derived the following equations of motion[19];

for the solid phase:

$$\sigma_{ij,j} = \frac{\partial^2}{\partial t^2}(\rho_{11} u_i + \rho_{12} U_i) + b \frac{\partial}{\partial t}(u_i - U_i) \tag{4.28}$$

for the fluid phase:

$$-p_{,i} = \frac{\partial^2}{\partial t^2}(\rho_{12} u_i + \rho_{22} U_i) - b \frac{\partial}{\partial t}(u_i - U_i) \tag{4.29}$$

where, u_i denotes the displacement component of the solid and U_i the displacement component of the fluid. Among ρ_{11}, ρ_{12}, and ρ_{22}, the relations exist as

$$\rho_{11} = \rho_1 + \rho_a \quad , \quad \rho_{12} = -\rho_a \quad , \quad \rho_{22} = \rho_2 + \rho_a \tag{4.30}$$

in which ρ_1 and ρ_2 denote the mass of solid and fluid per unit volume of aggregate, respectively, ρ_a the additional mass, and ρ_{12} the additional apparent mass. ρ_1 and ρ_2 are given by the following equations with the terms of mass densities ρ_s and ρ_f for the solid and the fluid and the porosity n:

$$\rho_1 = (1-n)\rho_s \quad , \quad \rho_2 = n\rho_f \tag{4.31}$$

Furthermore, b is given by

$$b = \frac{\eta n^2}{k} \tag{4.32}$$

where, η denotes the fluid viscosity and k the Darcy's coefficient of permeability.

Biot found that there existed one shear wave and two compressional waves in a saturated porous elastic medium. One of these two compressional waves is transmitted through the fluid and designated as the compressional wave of the first kind. It has a velocity of propagation higher than that in water alone. The other is transmitted through the elastic structure and designated

as the compressional wave of the second kind. Its velocity is slightly lower than that of the compressional wave for the dry condition[23]. The former is identified to be a common wave but the latter is found to lose the nature of the wave and to be reduced to a diffusion-type process.

4.3.2 Ishihara's Approach

Biot did not examine throughly the result of his analysis in terms of physical constants that were related to compressibilities of individual constituent material. Ishihara made the Biot's approach to be more realistic and more applicable to practical problems[24].

Ishihara supposed the interacting force proportional to the time rate of relative displacement between the solid and the fluid acting equivalently to the two phases, in place of the mass exchange in Biot's theory. He introduced the equations of motion as

for the solid phase:

$$\rho_s \frac{\partial^2 u_i}{\partial t^2} = \sigma_{ij,j} + b \frac{\partial}{\partial t}(u_i - U_i) \tag{4.33}$$

for the fluid phase:

$$\rho_w \frac{\partial^2 U_i}{\partial t^2} = - p_{,i} - b \frac{\partial}{\partial t}(u_i - U_i) \tag{4.34}$$

where, ρ_s and ρ_w are bulk densities of the solid and the fluid. In his case, b is given by

$$b = \frac{n^2 \gamma_w g}{k} \tag{4.35}$$

where, γ_w denotes the specific mass density of the fluid and g the acceleration of gravity. Furthermore, he expressed the elastic constants in the stress-strain relationships by the terms of four kinds of compressibility

(bulk, solid, pore and fluid compressibilities) which have been proposed by Nagumo[25]. According to Ishihara's approach, it is possible to estimate the elastic constants quantitatively, because the compressibilities of soil can be easily obtained from experiments, and in fact, they have been measured by many investigators.

The equation of wave propagation for the compressional wave of the first kind is derived as

$$\left[b(\rho_s+\rho_w)\frac{\partial}{\partial t}\left(\frac{\partial^2}{\partial t^2}-V_1^2\nabla^2\right)-\rho_s\rho_w\frac{\partial^2}{\partial t^2}\left(\frac{\partial^2}{\partial t^2}-V_n^2\nabla^2\right)\right]e=0 \qquad (4.36)$$

where, e denotes the volumetric strain and V_1 and V_n the phase velocity at the zero and the infinite frequency, respectively. It is found that this equation is equivalent to the following wave equation for the rod wave in a bar whose properties are represented by the spring-Voigt model as shown in Fig.4.1(c);

$$\left[\rho(E+E')\left\{\frac{\partial^2}{\partial t^2}-\frac{EE'}{\rho(E+E')}\frac{\partial^2}{\partial x^2}\right\}-\frac{\rho}{\mu}\frac{\partial}{\partial t}\left(\frac{\partial^2}{\partial t^2}-\frac{E'}{\rho}\frac{\partial^2}{\partial x^2}\right)\right]u=0 \qquad (4.37)$$

In similar, the equation for the wave of the second kind is;

$$\left[\omega_c\frac{\partial}{\partial t}-\frac{\partial^2}{\partial t^2}-V_d^2\nabla\right]e=0 \qquad (4.38)$$

where, ω_c is the characteristic frequency given by

$$\omega_c=\frac{b(\rho_s+\rho_w)V_1^2}{\rho_s\rho_w V_n^2} \qquad (4.39)$$

and, V_d is the phase velocity at the infinite frequency. It is underdtood from Eq.(4.38) that as the contribution of the second-order time derivative is large, it has a nature of hyperbolic partial differential equation, while it shifts to parabolic partial differential equation in the lower frequency range, since the influence of inertia has little role there. Therefore, the

physical phenomenon changes from the wave propagation to the quasi-steady state of consolidation. Eq.(4.38) is equivalent to the following wave equation for a rod wave in the bar whose properties are represented by Maxwell model as shown in Fig.4.1(b);

$$\left[E\mu \frac{\partial}{\partial t} + \frac{\partial^2}{\partial t^2} - \frac{E}{\rho} \frac{\partial^2}{\partial x^2} \right] u = 0 \tag{4.40}$$

Comparing Eq.(4.40) with Eq.(4.38), the terms of $\frac{E}{\rho}$ and $E\mu$ correspond to v_c^2 and ω_c, repectively.

Throughout his investigations, Ishihara concluded that the first kind of wave travelled through the solid-fluid system without causing any change in the pore volume, but the wave of the second kind could progress only when the volume change of pore space took place. It was further suggested that the wave motion usually felt during the earthquake or detonation of explosives was identified to be the first kind of wave at low-frequency range and that the usual consolidation deformation corresponded to the second kind of wave at low-frequency range.

4.3.3 Comparison with the Wave Characteristics of Spring-Voigt Model

It is assumed that the medium is homogeneous, isotropic and viscoelastic, and that its volume change is elastic and the relationship between the deviatoric stress and the deviatoric strain is expressed by the spring-Voigt model as shown in Fig.4.14. The constitutive equations are;

for the volume change:

$$\bar{\sigma} = 3K\bar{e} \tag{4.41}$$

for the deviatoric stress and strain:

$$2G \cdot G' \gamma_{ij} + 2\frac{G'}{\mu} \dot{\gamma}_{ij} = (G + G')\tau_{ij} + \frac{1}{\mu} \dot{\tau}_{ij} \tag{4.42}$$

where, k denotes the bulk modulus and τ_{ij} and γ_{ij} the components of the deviatoric stress and strain. They are related with the stress tensor components σ_{ij} and the strain tensor components e_{ij} by the following equations;

$$\tau_{ij} = \sigma_{ij} - \bar{\sigma}\delta_{ij} \quad , \qquad \bar{\sigma} = \frac{1}{3}\sigma_{kk} \tag{4.43}$$

$$\gamma_{ij} = e_{ij} - \bar{e}\,\delta_{ij} \quad , \qquad \bar{e} = \frac{1}{3}e_{kk} \tag{4.44}$$

where, e_{ij} is given by the following equation by using the displacement components u_i;

$$e_{ij} = \frac{1}{2}(u_{i,j} + u_{j,i}) \tag{4.45}$$

From Eqs.(4.41) and (4.42),

$$\sigma_{ij} = \left\{ K + \frac{\frac{2}{3}G'(G + \frac{1}{\mu}\frac{\partial}{\partial t})}{G + G' + \frac{1}{\mu}\frac{\partial}{\partial t}} \right\} e_{kk}\delta_{ij} + \frac{2G'(G + \frac{1}{\mu}\frac{\partial}{\partial t})}{G + G' + \frac{1}{\mu}\frac{\partial}{\partial t}} e_{ij} \tag{4.46}$$

Substituting Eq.(4.46) into the equation of motion

$$\rho\ddot{u}_i = \sigma_{ij,j} \quad , \tag{4.47}$$

we obtain

$$\rho\frac{\partial^2 u_i}{\partial t^2} = \frac{G'(G + \frac{1}{\mu}\frac{\partial}{\partial t})}{G + G' + \frac{1}{\mu}\frac{\partial}{\partial t}}\nabla^2 u_i + \left\{ K + \frac{\frac{1}{3}G'(G + \frac{1}{\mu}\frac{\partial}{\partial t})}{G + G' - \frac{1}{\mu}\frac{\partial}{\partial t}} \right\} \mathrm{grad}\cdot\mathrm{div}\,\boldsymbol{u} \tag{4.48}$$

where, $\boldsymbol{u}$ denotes the displacement vector. Applying the divergence operator to Eq.(4.48), we obtain the equation for the compressional wave

$$\rho\frac{\partial^2 \bar{e}}{\partial t^2} = \left\{ K + \frac{\frac{4}{3}G'(G + \frac{1}{\mu}\frac{\partial}{\partial t})}{G + G' + \frac{1}{\mu}\frac{\partial}{\partial t}} \right\} \nabla^2 \bar{e} \tag{4.49}$$

On the other hand, using the curl operator to Eq.(4.48) becomes

$$\rho \frac{\partial^2 \omega}{\partial t^2} = \frac{G'(G + \frac{1}{\mu}\frac{\partial}{\partial \tau})}{G + G' + \frac{1}{\mu}\frac{\partial}{\partial \tau}} \nabla^2 \omega \qquad (4.50)$$

where, ω is the rotation of the displacement vector u. By solving Eqs.(4.49) and (4.50), the phase velocities and the logarithmic decrement are obtained, by means of infinite harmonic waves as follows;

Compressional Wave

$$\frac{V_C}{V_s} = \left(\frac{2}{\sqrt{P} + P'}\right)^{\frac{1}{2}}, \quad \frac{\delta_C}{\pi} = 2\left(\frac{\sqrt{P} - P'}{\sqrt{P} + P'}\right)^{\frac{1}{2}} \qquad (4.51)$$

where, P and P' are given by

$$P = \frac{1 + \theta_C^2 \tau_C^2 \omega^2}{1 + \tau_C^2 \omega^2}, \quad P' = \frac{1 + \theta_C \tau_C^2 \omega^2}{1 + \tau_C^2 \omega^2} \qquad (4.52)$$

Rotational Wave

$$\frac{V_H}{V_s} = \left(\frac{2}{\sqrt{Q} + Q'}\right)^{\frac{1}{2}}, \quad \frac{\delta_H}{\pi} = 2\left(\frac{\sqrt{Q} - Q'}{\sqrt{Q} + Q'}\right)^{\frac{1}{2}} \qquad (4.53)$$

where, Q and Q' are given by

$$Q = \frac{1 + \theta_H^2 \tau_H^2 \omega^2}{1 + \tau_H^2 \omega^2}, \quad Q' = \frac{1 + \theta_H \tau_H^2 \omega^2}{1 + \tau_H^2 \omega^2} \qquad (4.54)$$

Throughout Eqs.(4.51) to (4.54), V_C and V_H denote the phase velocities, δ_C and δ_H the logarithmic decrements related with the attenuation constants, α_C and α_H, by

$$\delta_C = \frac{2\pi V_C \alpha_C}{\omega}, \quad \delta_H = \frac{2\pi V_H \alpha_H}{\omega} \qquad (4.55)$$

V_l and V_s are the phase velocities at zero frequency expressed by

$$V_l^2 = \frac{K}{\rho} + \frac{\frac{4}{3}G'G}{\rho(G+G')} \quad , \quad V_s^2 = \frac{G'G}{\rho(G+G')} \tag{4.56}$$

The phase velocities V_n and V_p at the infinite frequency are respectively given by

$$V_n^2 = \frac{K + \frac{4}{3}G'}{\rho} \quad , \quad V_p^2 = \frac{G'}{\rho} \tag{4.57}$$

θ_C and θ_H are parameters defined by

$$\theta_c = \left(\frac{V_l}{V_n}\right)^2 \quad , \quad \theta_H^2 = \left(\frac{V_s}{V_p}\right)^2 \tag{4.58}$$

Finally, τ_C and τ_H are given by

$$\tau_C = \frac{\frac{1}{\mu}(K + \frac{4}{3}G')}{G(K + \frac{4}{3}G') + KG'} = \frac{\frac{1}{\mu}}{G + G'} \cdot \frac{1}{\theta_c} \tag{4.59}$$

$$\tau_H = \frac{1}{\mu G} \tag{4.60}$$

Fig.4.15 shows the calculated results from Eqs.(4.51) and (4.53) in the range of θ_C and θ_H of 0.1 to 0.9. The wave characteristics of both compressional and rotational waves are identical in the expression. If τ_C is replaced by the reciprocal of the characteristic frequency given by Eq.(4.39) as

$$\frac{1}{\omega_c} = \frac{\rho_s \rho_w V_n^2}{b(\rho_s + \rho_w) V_l^2} = \frac{\rho_s \rho_w}{b(\rho_s + \rho_w)} \cdot \frac{1}{\theta_c} \tag{4.61}$$

in the compressional wave, while τ_H is replaced by the reciprocal of the characteristic frequency as

$$\frac{1}{\omega_H} = \frac{\rho_w}{b} \tag{6.62}$$

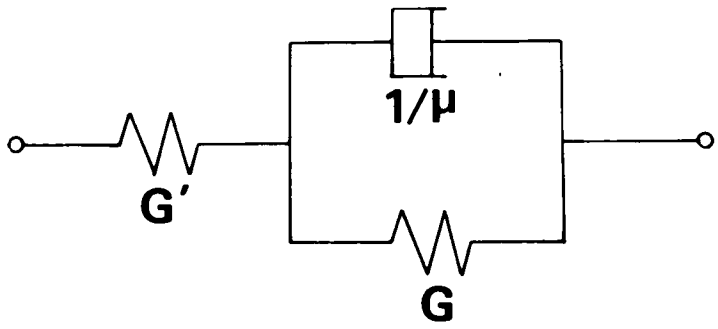

Fig.4.14 Spring-Voigt model for the relationship between the deviatoric stress and the deviatoric strain.

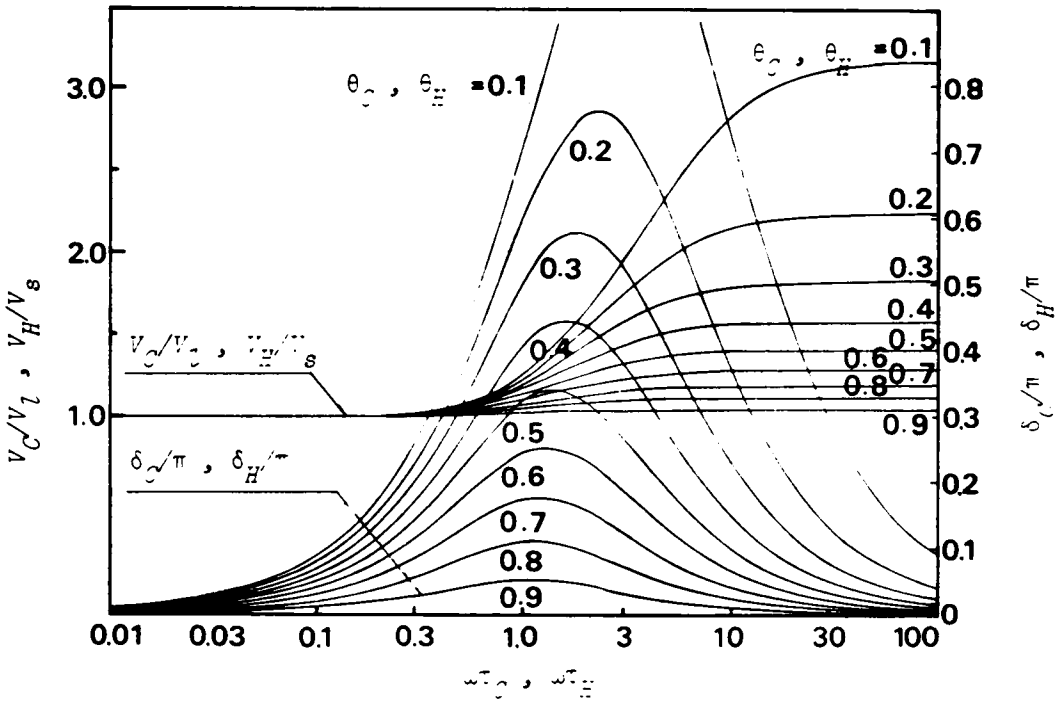

Fig.4.15 Wave characteristics of the assumed model.

in the rotational wave, then the characteristics shown in Fig.4.15 are similar to those in the saturated porous elastic medium proposed by Ishihara[21]. Furthermore, if τ_C or τ_E is replaced by the retardation time, τ_{sV}, defined by Eq.(4.5), Fig.4.15 is identical to Fig.4.10 for the characteristics of the rod wave.

Comparing Eqs.(4.59) and (4.60) with Eqs.(4.61) and (4.62) with each other, it is understood that the viscoelastic constants, E'/μ, J and G', are related with the coefficient k given by Eq.(4.35) for the saturated porous elastic medium. In other words, the viscoelastic constants depend upon the coefficient of permeability and the porosity(or void ratio). Furthermore, we may conclude that, if soil is assumed as the spring-Voigt model in a dynamic state, the free spring in the model expresses the behavior which is independent of the coupling between solid and fluid phases, while the Voigt element expresses the coupling behaviors depending on the relative displacement between two phases.

4.4 Experimental Results and Discussions

As understood in the previous sections, the mechanical characteristics of the spring-Voigt model are uniquely determined by E', τ_{sV} and k. In this section, these constants are obtained from various tests such as the rod wave propagation test presented in Chapter 3 and the forced vibration test, and their dependencies on the confining pressure and the frequency are discussed.

4.4.1 Determination of the Viscoelastic Constants of the Spring-Voigt Model

The velocity of wave front and the attenuation constant have been obtained in the rod wave propagation test for the clayey soil samples. At the same time, the static triaxial compression tests have been carried out using the same soil samples and the static moduli of elasticity have been obtained.

These test results are tabulated in Table 4.1, where c_p is the velocity of wave front and c_0 is the velocity calculated from the initial tangent modulus E_s of the static stress-strain curve and the mass density ρ in the formula $\sqrt{E_s/\rho}$. Wave characteristics of the stress pulse propagation in the experiment are considered to be far from those of the sinusoidal stress propagation in the theoretical analysis in Section 4.2.3. However, according to Fourier analyses of the stress pulse propagation by Hirobe[26], its wave characteristics correspond to those of the sinusoidal stress wave with the frequency of about 120 *cps*. Therefore, in this section, the particular frequency of the present stress wave propagation is assumed as 120 *cps*. δ_T/π in Table 4.1 is calculated from Eq.(4.21) with the values of α, c_p and $\omega=2\pi\cdot 120$. The simultaneous equations of Eqs.(4.22) and (4.23) are solved with the experimental results of c_p/c_0 and δ_T/π and then, k and τ_{sV} are obtained. The calculated viscoelastic constants are tabulated in Table 4.2.

The pre-consolidation pressure of the clayey soil samples is about 0.74 kg/cm^2 as described in Section 3.5.2. So that, the soil samples in test series of 11-a to 14-a and 19-a correspond to normally consolidated clays (N.C.C.), while those in test series of 15-a to 18-a correspond to over-consolidated clays(O.C.C.). From Table 4.2, it is found that θ_{sV} is 0.1-0.2 for N.C.C. and 0.2-0.3 for O.C.C.. The variations of the calculated constants with p_c are shown in Figs.4.16, 4.17 and 4.18. E' increases linearly with the increase in the confining pressure. This relationship is similar to that between E_d and p_c shown in Fig.3.11. However, the relationships between E and $1/\mu$, and p_c change at the pre-consolidation pressure marked as p_i in these figures. The rate of increase in E with p_c less than p_i is steeper than that with p_c larger than p_i. $1/\mu$ is nearly constant with p_c less than p_i, but increases with p_c larger than p_i. These tendencies of the viscoelastic constants with the confining pressure state that E' is independent of the pre-consolidation pressure, but the damping characteristics which are related

Table 4.1 Experimental results by the rod wave propagation test presented in Chapter 3.

No.	p_c kg/cm^2	c_p m/sec	c_c m/sec	c_p/c_c	α m^{-1}	δ_T/π
11-a	2.11	365	130	2.80	0.21	0.203
12-a	1.37	290	123	2.36	0.46	0.354
13-a	1.21	300	127	2.36	0.39	0.311
14-a	0.90	240	115	2.08	1.06	0.675
15-a	0.54	200	108	1.86	0.45	0.239
16-a	0.40	180	91	1.98	0.57	0.272
17-a	0.26	155	75	2.08	0.63	0.259
18-a	0.16	130	76	1.70	0.23	0.079
19-a	1.06	280	114	2.46	0.44	0.327

Table 4.2 Calculated viscoelastic constants.

No.	θ_{sV}	k	τ_{sV} sec	E_d kg/cm^2	E_s kg/cm^2	E' kg/cm^2	E kg/cm^2	$1/\mu$ kg·sec/cm^2
11-a	0.126	0.144	0.0449	2620	316	2620	377	16.93
12-a	0.169	0.203	0.0172	1570	274	1622	329	5.66
13-a	0.171	0.206	0.0196	1360	264	1544	318	6.23
14-a	0.174	0.211	0.0068	1060	237	1363	288	1.96
15-a	0.278	0.385	0.0137	695	184	695	193	2.64
16-a	0.244	0.323	0.0143	643	157	644	157	2.25
17-a	0.222	0.285	0.0171	465	126	567	126	2.15
18-a	0.288	0.404	0.0045	327	102	354	102	0.46
19-a	0.157	0.186	0.0206	1730	252	1730	272	5.60

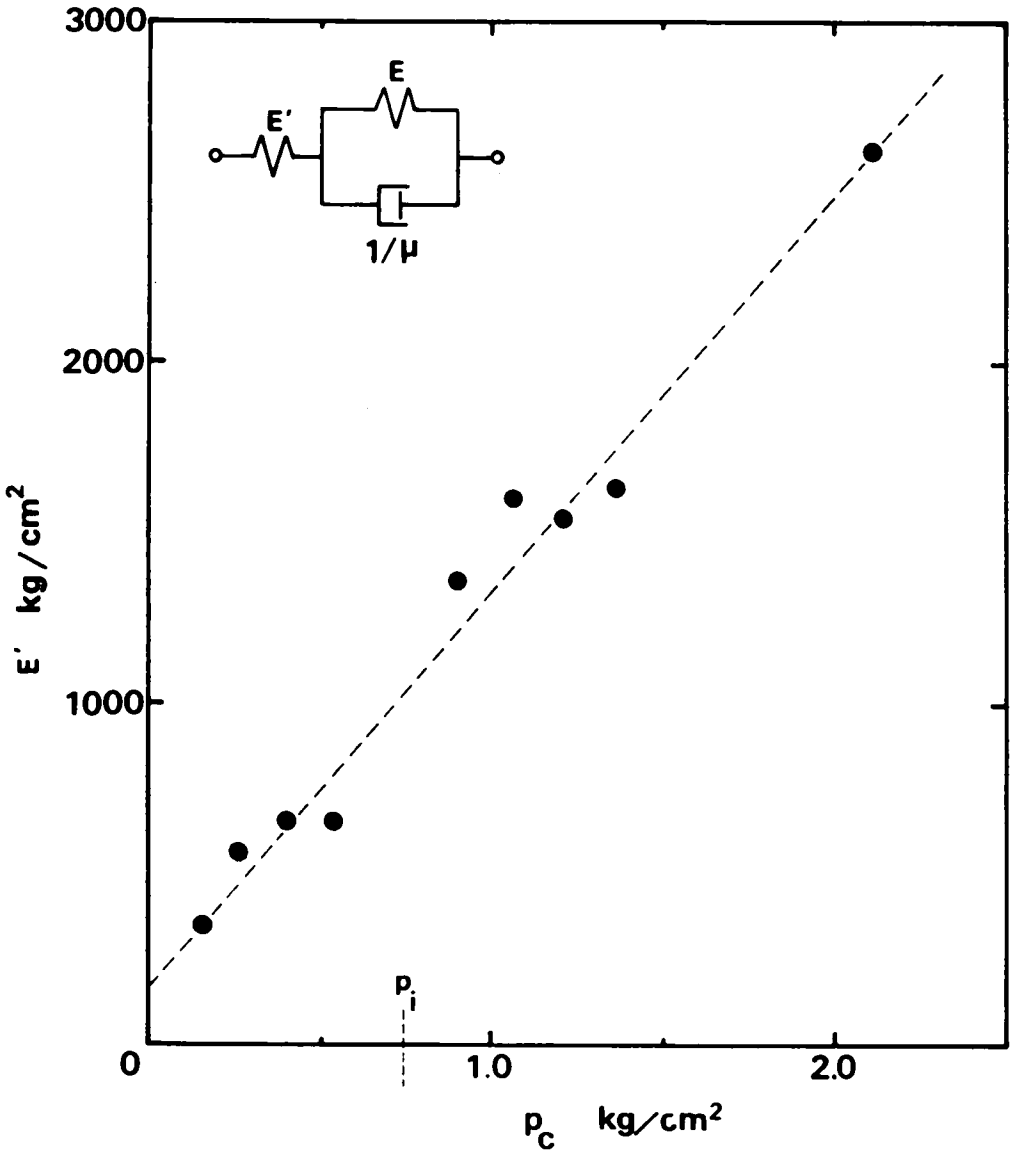

Fig.4.16 Variation of E' with the confining pressure(p_i : the pre-consolidation pressure).

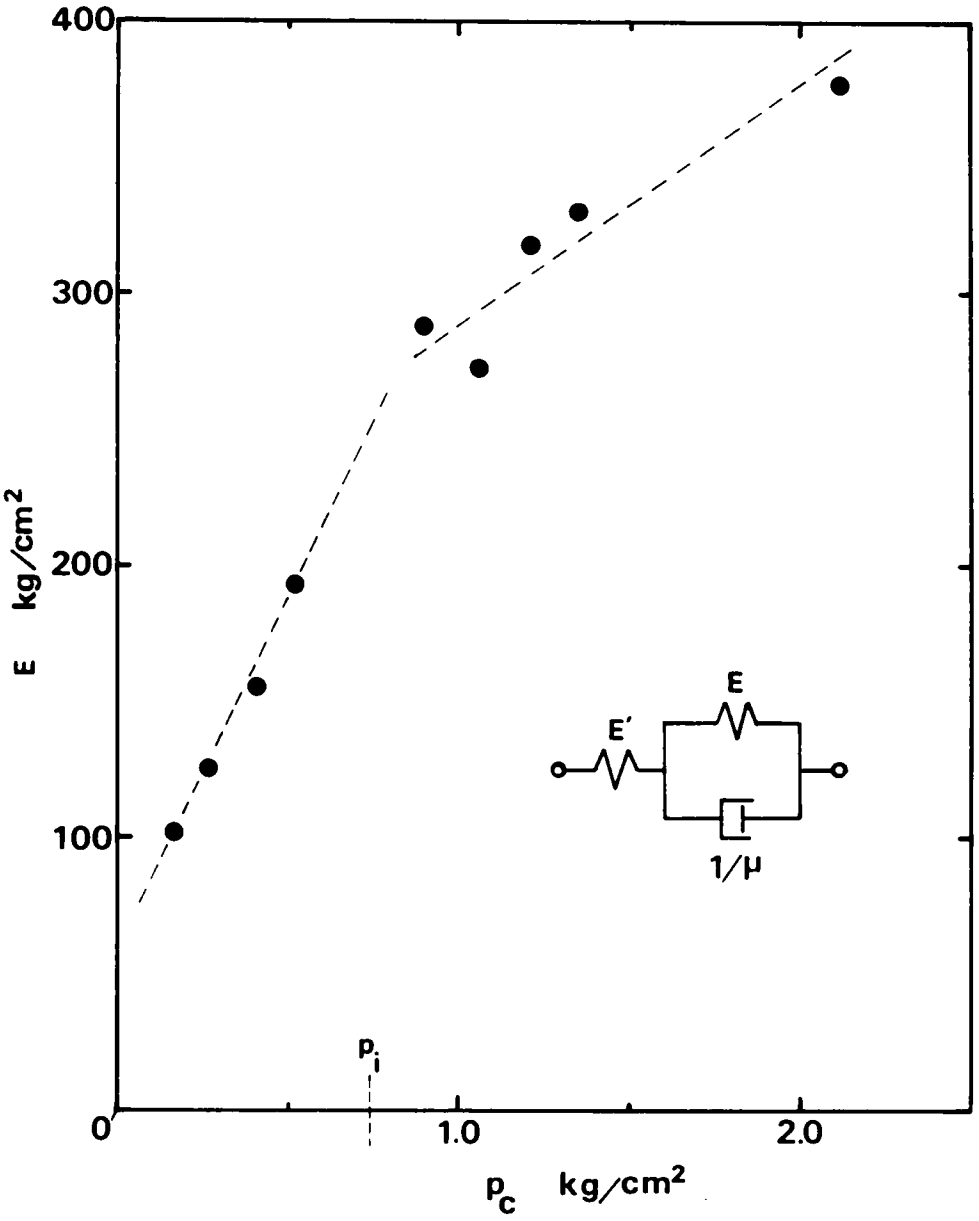

Fig.4.17 Variation of E with the confining pressure(p_i : the pre-consolidation pressure).

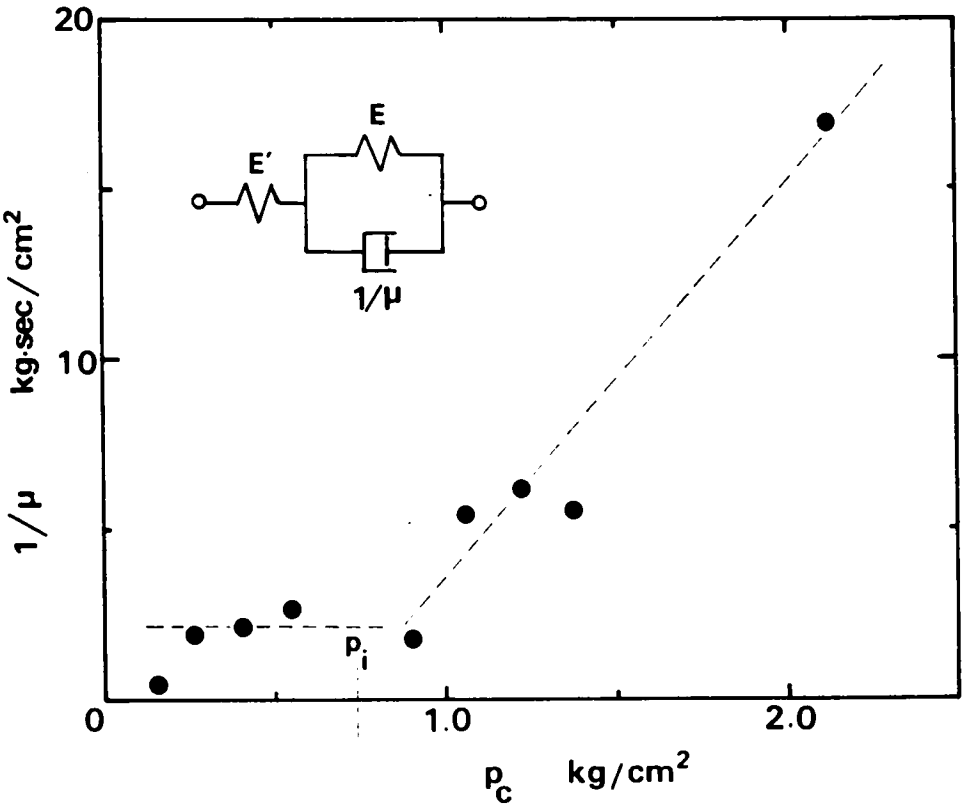

Fig.4.18 Variation of $1/\mu$ with the confining pressure(p_i : the pre-consolidation pressure).

with E and $1/\mu$ depend upon the pre-consolidation pressure. In other words, the instantaneous elasticity E' is not influenced by the changes of soil structure but is determined only by the effective confining pressure, while the retardation elasticity expressed by the Voigt element in the model which depends on the coupling between the solid particles and the pore water, is strongly dependent upon the changes of soil structure[27]. ξ_{∞}/τ of O.C.C. is smaller than that of N.C.C. as found in Table 4.1. Furthermore, c_p/c_s of O.C.C. is near unity, namely, the strain rate dependency is relatively minor. These facts are identical to the general concepts that the elastic behaviors are predominant in the over-consolidated clays compared with the normally consolidated clays.

4.4.2 Estimation of E'

E' is the spring constant which expresses the instantaneous elastic response of the model. Therefore, this modulus is considered to be corresponding to the dynamic modulus of elasticity obtained from the dynamic tests with the high strain rate such as the resonant-column method, ultra-sonic pulse method and the shock tube technique. As already described in the previous section, E' is independent upon the pre-consolidation pressure and is determined only by the confining pressure applied to the soils. The relationship between E'(or E_d in Chapter 3) and the confining pressure is linear.

It has been known that the main factors which influence the dynamic shear modulus, G_d, are the void ratio e and the mean effective principal stress σ_m' of a soil at infinitesimally small strain level, and that the relationship among them is given by

$$G_d = F'(e)\,\sigma_m'^{0.5} \tag{4.63}$$

where, $F'(e)$ denotes a function of e. For instance, its forms are presented in Table 3.3.

As a consequence, $E'(E_d$ or $G_d)$ is influenced only by the void ratio and the mean effective principal stress and can be estimated by the relation of Eq.(4.63).

4.4.3 Estimation of the Time Constant

The time constant, τ_{sV} in Eq.(4.5), τ_e in Eq.(4.59) or τ_H in Eq.(4.60), is a important parameter which is related with the time-responsibility of the model. Fig.4.19 shows the relationship between τ_{sV} and p_c obtained from the rod wave propagation tests. We can see from this figure that τ_{sV} is in the order of 10^{-2} sec and that it slightly increases with p_c.

For further estimation of the time constant, the forced vibration tests were performed by means of the apparatus of the vibrational triaxial compression test under the frequency range of 0.04 to 4 cps. The soil sample is the saturated Fukakusa clay consolidated under the pressure of 1.0 to 2.5 kg/cm^2. The amplitude of shear strain was in the range of 2.4×10^{-4} to 1.4×10^{-3}. Measuring the area surrounded by the hysteresis loop in the shear stress-strain curve, the time constant $\tau_H=\frac{1}{\mu G}$ in Eq.(4.60) was calculated from the relation[28],

$$\tau_H = \frac{\Delta W}{\pi \omega \tau_0 \gamma_0 \left\{ 1 - \frac{1}{2}\left(\frac{\Delta W}{\pi \tau_0 \gamma_0}\right)^2 \right\}} \tag{4.64}$$

where, ΔW denotes the area surrounded by the hysteresis loop, γ_0 the amplitude of shear strain and τ_0 the amplitude of shear stress. Fig.4.20 shows the relationship between the frequency and τ_H calculated from the above equation. In this figure, there are also expressed the time constant, τ_{sV} in Fig.4.19, and the data calculated from the viscoelastic constants of Burgers model shown

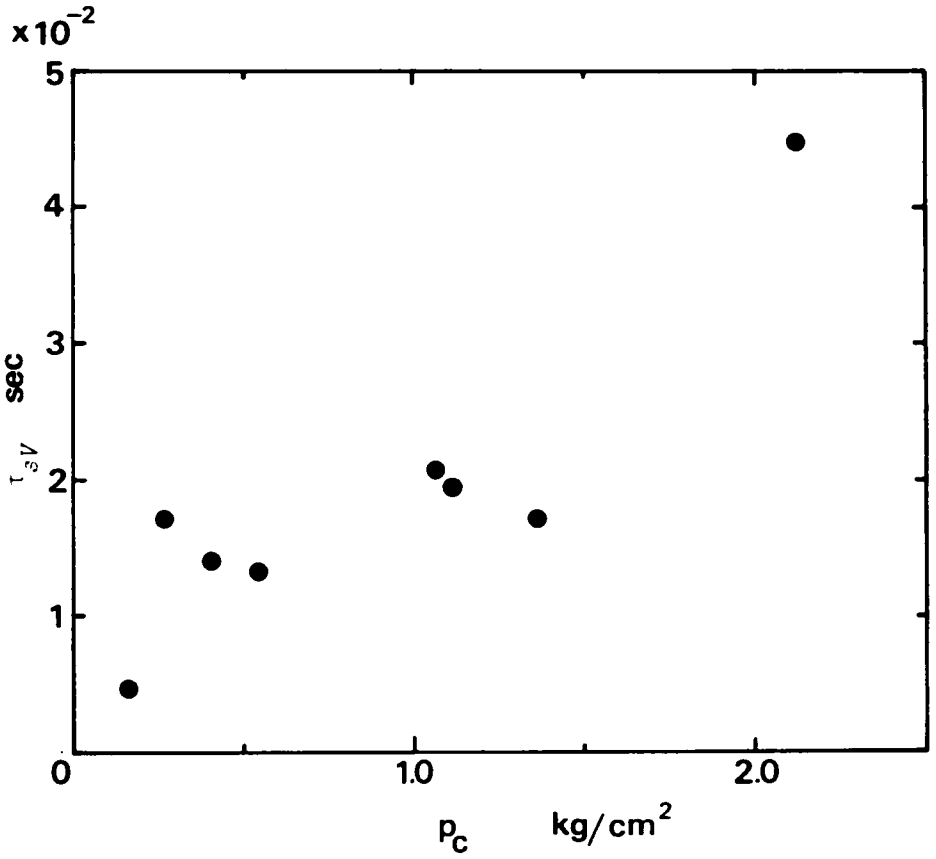

Fig.4.19 Relationship between τ_{sV} and p_c obtained from the rod wave propagation tests.

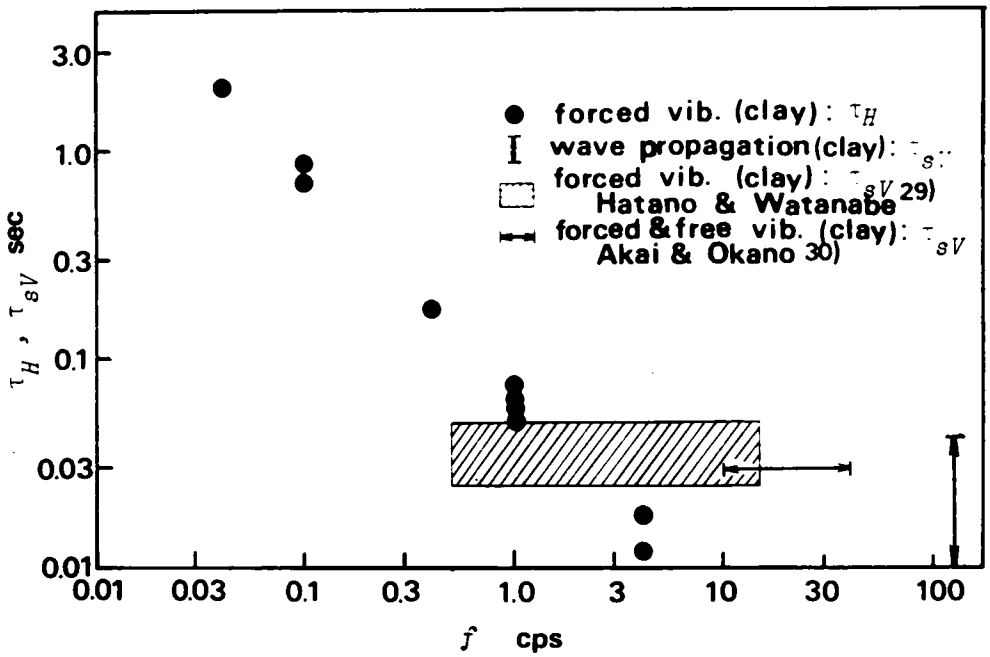

Fig.4.20 Variation of the time constant with frequency.

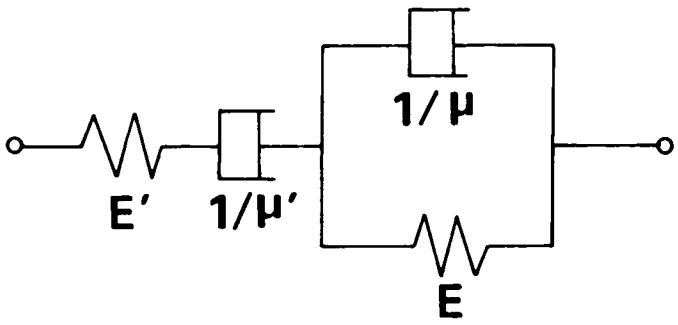

Fig.4.21 Burgers model used by Hatano and Watanabe[29].

in Fig.4.21 which Hatano and Watanabe[29] obtained by the forced vibration tests and also from the experimental results by Akai and Okano[30]. From Fig.4.20, we find a distinct relation that the time constant increases linearly with decrease in the frequency in the range less than 1 *cps* and tends to be constant with the average value of 3×10^{-2} *sec* in the range more than 1 *cps*. The mechanical behaviors of soils will be classified into three states by the frequency; quasi-static, transitional and dynamic states. The creep and relaxation phenomena belong to the quasi-static state. In the transitional state, $f\tau_H$ or $f\tau_{sV}$ is almost constant. Furthermore, in the dynamic state, τ_H or τ_{sV} is nearly constant. Its bounded frequency between the transitional and dynamic states is about 1 *cps*. On the other hand, Hardin[31] tried to express the mechanism of the damping in dry sands by the Voigt model. According to his experimental results, the value of $\omega/\mu G$, in which μ and G denote the viscoelastic constants of the model, varies between 0.01 and 0.07 for shear strain amplitudes in the order of 10^{-6} to 10^{-4} and for confining pressures between 500 *psf* and 3000 *psf*. And also his value of $\omega/\mu G$ is approximately independent of frequency.

According to Ishihara[24], the order of the reciplocal of the characteristic frequency for the saturated porous material, ω_c defined by Eq.(4.39) which is considered to be equivalent to the time constant in the present model, is 10^{-3}(*sec*) in the case of sand and 10^{-7} - 10^{-8}(*sec*) in clay. These values are extremely smaller than the values shown in Fig.4.20. The coefficient b in Eq.(4.39) has been derived by assuming the Poiseuille flow and Darcy's law for the water in the void. However, it is well known that the effective porosity through which the pore water can flow under certain hydraulic gradient is extremely smaller than the total porosity[32]. Consequently the true value of b becomes much smaller, so that the calculated results of $1/\omega_C$ or $1/\omega_H$ becomes larger as known from Eqs.(4.61) or (4.62), and should correspond to the experimental results as shown in Fig.4.20 obtained from the

present viscoelastic approach.

4.4.4 Estimation of k

k is another parameter which determined the characteristics of the model and is defined by Eq.(4.5). The calculated values of k in Table 4.2 are depicted in Fig.4.22. k slightly decreases with increasing in p_c and its value is between 0.1 and 0.4. Tsai[33] used the values of k between 0.01 and 1.0 in his earthquake ground response analysis, when he assumed the earth materials as the spring-Voigt model. Akai and Okano[30] reported that the experimental results due to the forced vibration test and the free vibration test could be well explained by assuming the soils follow the spring-Voigt model, if the values of k between 0.5 and 1.0 were used. According to Hatano and Watanabe's experimental data[29], however, k defined by E/E' in the model as shown in Fig.4.21 is in the range of 1 to 4 for clay samples under the frequency of 0.5 to 15 *cps*.

4.4.5 Estimation of the Logarithmic Decrement

The logarithmic decrement is one of the indices which express the amount of energy loss in a soil under dynamic states such as wave propagation and vibrational loading. If the energy loss is small, the logarithmic decrement δ can be approximately related with other indices as follows;

$$\frac{\delta}{\pi} = \frac{\psi}{2\pi} = \frac{\Delta W}{2\pi W} = \frac{1}{Q} = 2h = \frac{2c\alpha}{\omega} \qquad (4.65)$$

where, ψ, Q, ΔW and W have been already defined by Eq.(4.14) and, h denotes the damping ratio, α and c the attenuation constant and the velocity respectively.

Seed and Idriss[34] have emphasized that the damping ratio as well as the

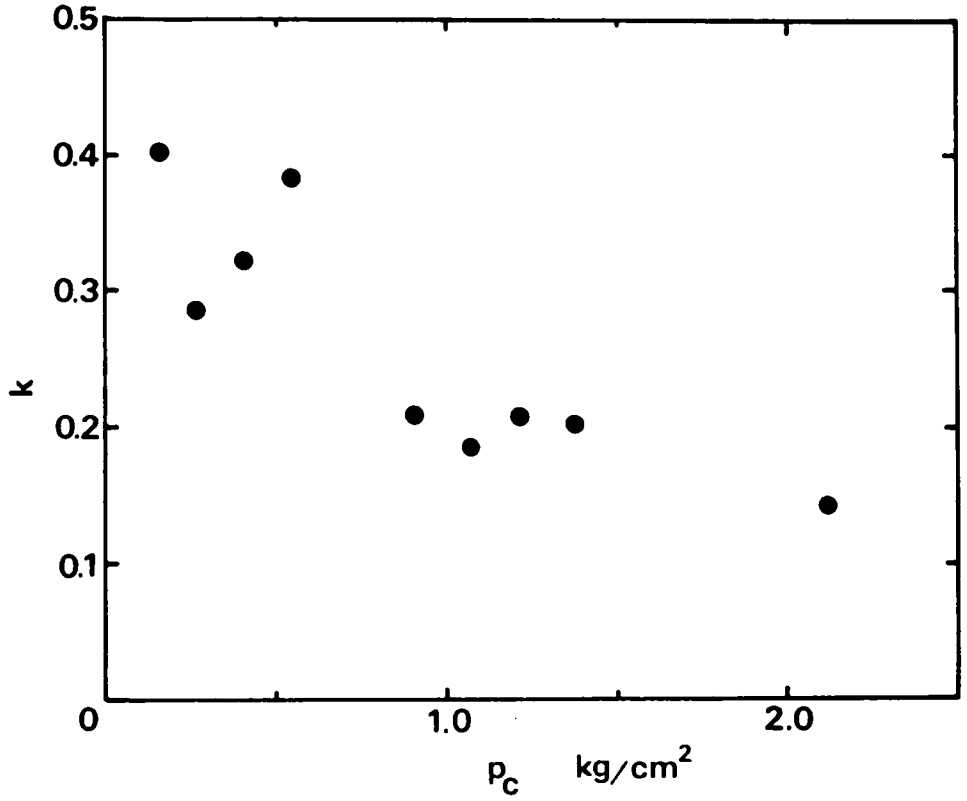

Fig.4.22 Relationship between the parameter k and the confining pressure p_c.

deformation modulus is strongly dependent upon the strain amplitude. Generally speaking, the damping ratio rapidly increases with increase in the amplitude of shear strain as shown in Fig.4.23. From Eq.(4.65), the damping ratio h is half of δ/π.

The logarithmic decrements obtained from various tests are plotted in Fig.4.24. The logarighmic decrements can be directly obtained in the free vibration test[30] and in the forced vibration test they can be calculated from Eq.(4.65) by measuring ΔW and W in the stress-strain relations under cyclic loading. For reference, the broken line in this figure represents the case of θ_{SV} or $\theta_H=0.35$ in the viscoelastic approach in the previous sections. Referring Fig.4.23, we can understand that the experimental results in Fig.4.24 offer the data for the strain level of 10^{-3}.

4.5 Conclusions

The mechanism of energy loss in soils is very complicated and is not clarified sufficiently. The first-order apploximation of the energy loss is the mechanism of linear viscous damping. However, it is also known that the energy loss of soils can not be explained by some simple viscoelastic models.

In this chapter, the soil has been assumed to be the spring-Voigt model. This model consists of the free spring as the instantaneous elasticity and the Voigt element as the retardation elasticity in parallel. The mechanical behaviors exhibit those of both the Voigt and Maxwell models. The analytical approach on the one-dimensional rod wave propagation to the spike pulse for the spring-Voigt model showed that the velocity of wave front was finite, and in the short distance there was no change of wave forms such as seen for the Maxwell model, while in the long distance the change of wave form was remarkable as seen in the rod of the Voigt model.

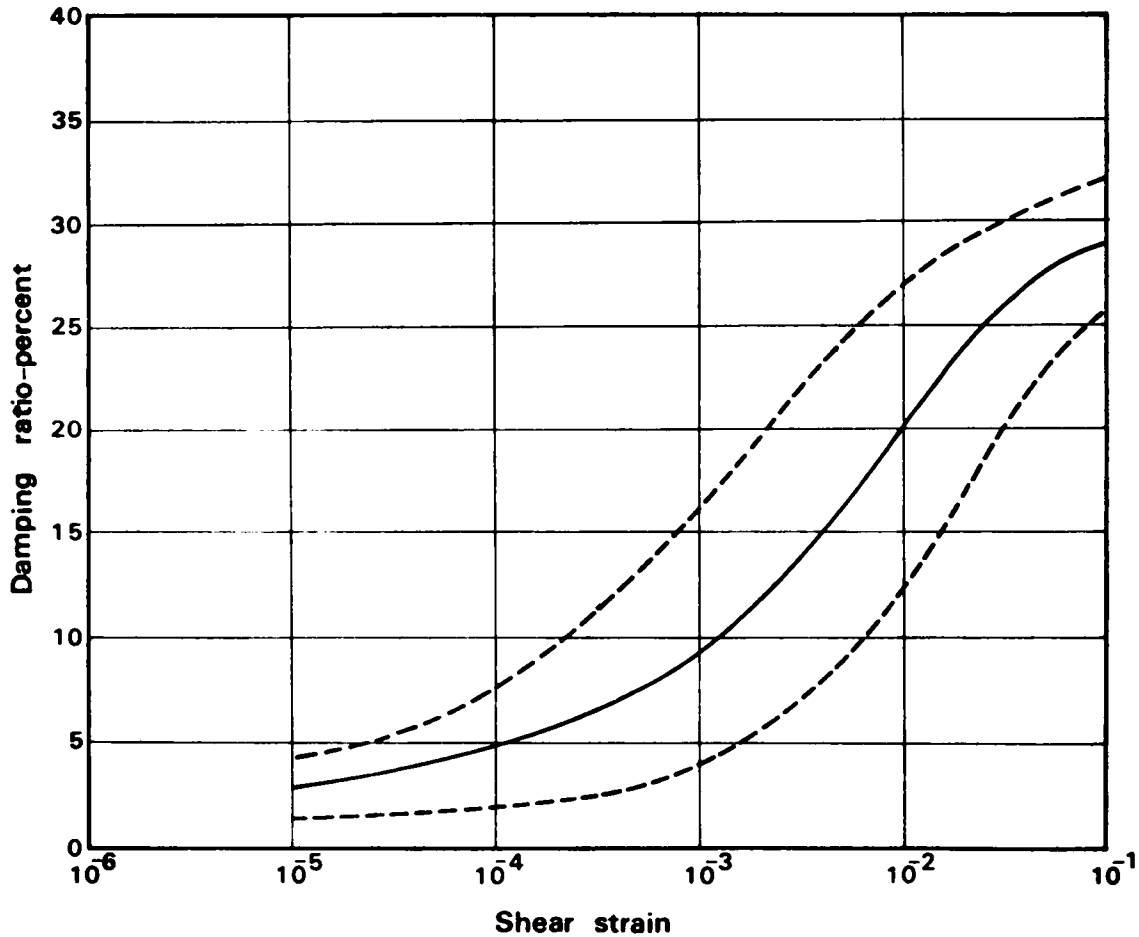

Fig.4.23 Variations of damping ratio with the amplitude of shear strain for clays(after Seed and Idriss[34]).

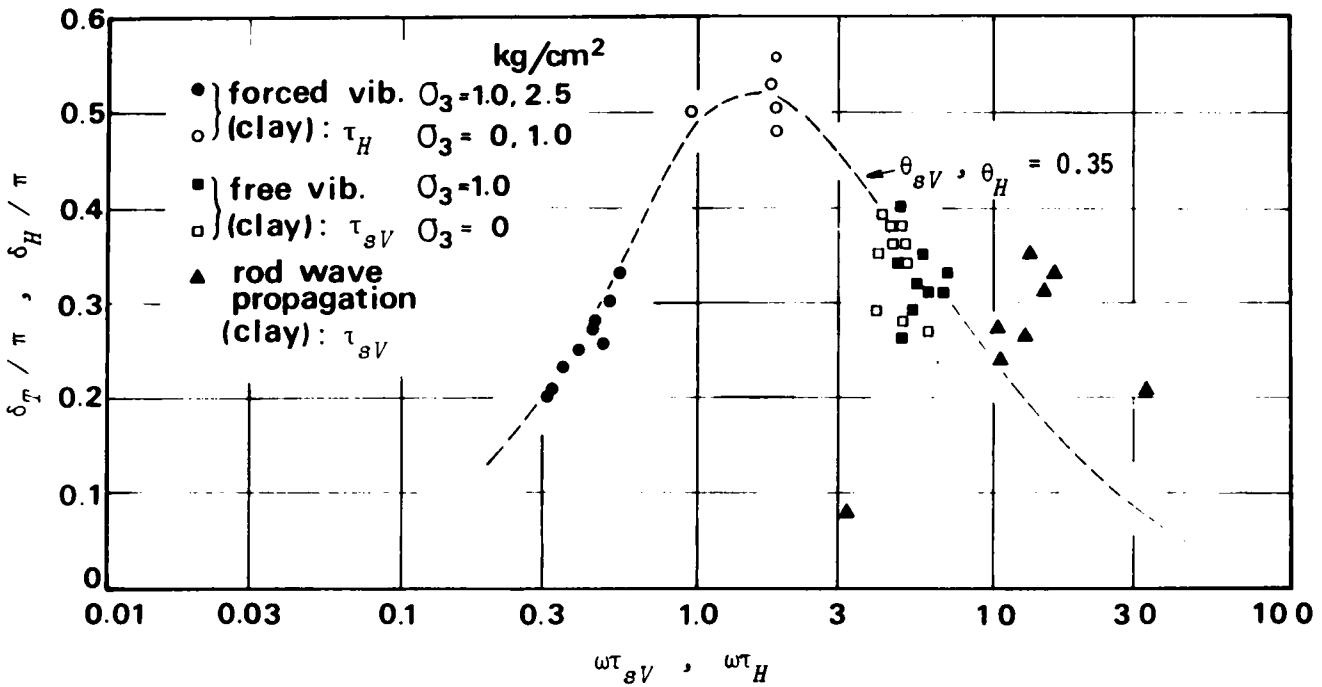

Fig.4.24 Logarithmic decrement obtained from various tests.

Furthermore, the wave characteristics of this model have been investigated. As the results, it can be understood that they are determined only by the two parameters of τ_{sV} and θ_{sV}, and that the phase velocity increases monotonously with $\omega\tau_{sV}$ and the distribution on the logarithmic decrement for $\omega\tau_{sV}$ is the single peak bell-shaped. Its peak appears near at $\omega\tau_{sV}=1.0$. These characteristics well represent the experimental results according to Kondner *et al.*[10),14)]. Kondner introduced the concept of dynamic response spectrum in order to estimate the dynamic characteristics taking into account the various properties of soils. According to his plotting of the initial compliance as a function of the time spectrum, its tendency is similar to one of the phase velocity for the spring-Voigt model. He obtained the loss tangent from the dynamic relaxation test and found that the loss tangent vs. logarithm of frequency relation was a single peak bell-shaped distribution as similar as the distribution of the logarithmic decrement for the spring-Voigt model. His experimental results suggest that the characteristics of soil in the wide frequency range are approximated by the spring-Voigt model.

One of reasons why the mechanical behaviors and the dynamic characteristics of soils are very complicated is that the soil is a mixture consisting of solid, fluid and void. Biot initiated to investigate the problem of wave propagation through the saturated porous elastic medium. Throughout his investigations, it has been found that in such medium there exist two compressional waves and one shear wave. Ishihara has extended the Biot's approach and made it to be more realisticand more applicable to practical problems. The characteristics of the compressional wave of the first kind are same as those of the material of which volume change obeys elasticity and the relationship between the deviatoric stress and the deviatoric strain is expressed by the spring-Voigt model. And the characteristics of the compressional wave of the second kind are similar to those of the rod wave in the Maxwell material.

The experimental results obtained from the rod wave propagation test for clayey soil specimens as described in Chapter 3 were examined from the viewpoint of viscoelasticity. The maximum strain amplitude of the soil during propagation of rod wave was controlled in the level of 10^{-3}. In the strain level less than 10^{-3}, the mechanical behaviors of soil would be viscoelastic. The viscoelastic constants and the parameters of the spring-Voigt model were discussed with our experimental results. The obtained conclusions are:

(1) The parameter ϑ_{sV} is 0.1 - 0.2 for the normally consolidated clays and 0.2 - 0.3 for the over-consolidated clays. By considering that the difference between the static and the dynamic modulus for O.C.C. is smaller than that for N.C.C. and that the logarithmic decrement is smaller, it is concluded that the elastic properties of O.C.C. are remarkable compared with N.C.C..

(2) The free spring E' is almost identical to the dynamic modulus of elasticity E_d calculated from the velocity of the wave front. E' is linearly dependent upon the confining pressure. E' can be estimated only by the void ratio and the confining pressure.

The constants of E and $1/\mu$ are not linearly dependent upon the confining pressure but their relations change at the pre-consolidation pressure of the clayey soil. These experimental results conclude that E and $1/\mu$, which are considered to relate with the coupling effect between the solid particles and the water, are influenced by the change of the soil structure.

(3) The time constant τ_{sV} changes with the frequency. Its value is a few seconds or more in the quasi-static state with the frequency range less than 10^{-2} *cps* and is a constant of about 3×10^{-2} *sec* in the frequency range more than 1 *cps*. In the transitional state, $f\tau_{sV}$ is constant. Therefore, the creep or relaxation phenomena of soils could not be in the dynamic state more than 1 *cps*.

(4) The ratio of E to E', k, obtained from the present experiments is between 0.1 and 0.4. Furthermore, according to the experimental data by other investigators, k is considered to be a value less than 1.0, while only the experimental data by Hatano and Watanabe[29] shows k between 1.0 and 4.0.

References

1) Kolsky, H.: Stress Waves in Solids, Dover Publications, Inc., 1963, pp. 106-129.

2) Bland, D. R. : The Theory of Linear Viscoelasticity, Pergamon Press, New York, 1960.

3) Akai, K. and M. Hori : A Viscoelastic Approach to the Problem of Stress Wave Propagation in Cohesive Soils, Proc. of JSCE, No.185, Jan., 1971, pp. 95-103.

4) Akai, K. and M. Hori : Analytical Study on Stress Wave Propagation in Viscoelastic Materials Subjected to Spike Pulse, Proc. of JSCE, No.195, Nov., 1971, pp. 101-108.

5) Akai, K. and M. Hori : Consideration of Viscoelasticity on the Dynamic Behavior and the Stress Propagation of Saturated Clay, Proc. of 3rd JEES, 1970, pp. 255-262(in Japanese).

6) Lai, W. and F. M. Sauer : Propagation of Stress Pulses in Standard Linear Viscoelastic Materials, Stanford Res. Inst., SU-2917, DASA 1266-1, 1961, pp. 15-56.

7) Akai, K. and M. Hori : A Viscoelastic Approach to the Problem of Stress Wave Propagation in the Ground(2nd Report), Prepring, 26th Conf. JSCE, 1971, pp. 133-136(in Japanese).

8) Johnson, J. W. : Dynamic Response of Clay under Axial Cyclic Loading, Ph. D. Thesis, Univ. of Calif., Berkeley, 1965, pp. 26-40.

9) Nishigaki, Y. and T. Hirobe : Characteristics of Hysteresis of Osaka Diluvial Clays, Preprint, 8th Conf. JSME, 1973, pp. 359-362(in Japanese).

10) Kondner, R. L. : Stress Wave Propagation Phenomena in Terms of Dynamic Response Spectra, Proc. Int. Symp. Wave Propagation and Dynamic Properties of Earth Materials, Univ. New Mexico, 1967, pp. 483-490.

11) Kondner, R. L. : Dynamic Soil Behavior in Terms of Response Spectra, Proc.

Int. Symp. Wave Propagation and Dynamic Properties of Earth Materials, Univ. New Mexico, 1967, pp. 293- 304.

12) Kondner, R. L. and M. K. Ho : Viscoelastic Response of a Cohesive Soil in the Frequency Domain, Trans. Soc. of Rheology, Vol.9, Prat2, 1965, pp. 329-342.

13) Kondner, R. L. and J. B. Forrest : Dynamic Compression of Clay under an Explosive Pulse, Trans. Soc. of Rheology, Vol. 10, Part 1. 1966, pp. 253-273.

14) Kondner, R. L. and M. K. Ho : Energy Dissipation of a Cohesive Soil by the Fourier Transformation of Stress Relaxation Response, Trans. Soc. of Rheology, Vol.9 Part 1, 1965, pp. 145-157.

15) Akai, K. and M. Hori : Considerations of Wave Characteristics in Soil Assumed as Viscoelastic Material, Proc. of JSCE, No.221, Jan., 1974.

16) Biot, M. A. : General Theory of Three-Dimensional Consolidation, J. Appl. Phys., Vol.12, 1941, pp. 155-164.

17) Biot, M. A. : Theory of Elasticity and Consolidation for a Porous Anisotropic Solid, J. Appl. Phys., Vol.26, 1955, pp. 182-185.

18) Biot, M. A. and D. G. Willis : The Elastic Coefficients of the Theory of Consolidation, J. Appl. Mech., Vol.24, 1957, pp. 594-601.

19) Biot, M. A. : Theory of Propagation of Elastic Waves in a Fluid-Saturated Porous Solid, Low-Frequency Range, J. Acoust. Soc. Am., Vol.28, 1956, pp. 168-178.

20) Biot, M. A. : Mechanics of Deformation and Acoustic Propagation in Porous Media, J. Appl. Phys., Vol.33, 1962, pp. 1482-1498.

21) Ishihara, K. : Approximate Forms of Wave Equations for Water-Saturated Porous Materials and Related Dynamic Modulus, Soils and Foundations, Vol.10, No.4, 1970, pp. 10-38.

22) Akai, K. and M. Hori : Comparison and Consideration of Wave Characteristics in Linear Viscoelastic Materials and Porous Elastic Media,

Preprint, 7th Conf. JSME, 1972, pp. 261-264(in Japanese).

23) Richart, F. E., Jr., J. R. Hall, Jr. and R. D. Woods : Vibrations of Soils and Foundations, Prentice-Hall, Inc., 1970, pp. 132-136.

24) Ishihara, K. : Propagation of Compressional Waves in a Saturated Soil, Proc. Int. Symp. Wave Propagation and Dynamic Properties of Earth Materials, Univ. New Mexico, 1967, pp. 451-467.

25) Nagumo, S. : Effect of Pore for Deformation and Failure of Porous Media, Bull. Earthq. Res. Inst., Vol.43, 1965, pp. 317-338.

26) Hirobe, K. : Study on the Characteristics of Wave Attenuation with Fourier Analysis, Graduation Thesis of Kyoto University, 1974 (in Japanese).

27) Akai, K., M. Hori and T. Shimogami : Stress Wave Propagation Test by Means of the Shock Tube(3rd Report), Preprint, 28th Conf. JSCE, 1973, pp. 147-148(in Japanese).

28) Onogi, S. : Theory of Viscoelasticity, Maki Shoten, 1971, pp. 205-209 (in Japanese).

29) Hatano, T. and H. Watanabe : Dynamic and Static Viscoelastic Constants and Poisson's Ratio of Clay, Sand and Crushed Stone, Proc. of JSCE, No.164, April, 1969, pp. 33-49(in Japanese).

30) Akai, K. and M. Okano : Consideration of Damping Characteristics on Cohesive Soils by Theory of Linear Viscoelasticity, Preprint, 26th Conf. JSCE, 1971, pp. 143-146(in Japanese).

31) Hardin, B.O. : The Nature of Damping in Sands, Proc. ASCE, Vol.91, No.SM1, Jan., 1965, pp. 63-97.

32) Akai, K. and T. Uno : Study on the Quasi-One-Dimensional, Non-Steady Seepage Flow through Soil, Trans. JSCE, No.127, March, 1966, pp. 14-22(in Japanese).

33) Tsai, N. C. : Influence of Local Geology on Earthquake Ground Motion, Ph. D. Thesis, California Institute of Technology, Pasadena, 1969.

34) Seed, H. B. and I. M. Idriss : Soil Moduli and Damping Factors for Dynamic Response Analyses, Report No.EERC70-10, Univ. of Calif., Berkeley, Calif., Dec., 1970, pp. 10-14.

Chapter 5 Analysis of Earthquake Motions of Inhomogeneous Elastic Surface Layer with Application of Multiple Reflection Theory

5.1 Introduction

It is known that damages to engineering structures during earthquakes depend on the nature of the arriving seismic waves as well as on the properties of the structures. The characteristics of ground shaking which are of major interest to engineers for purposes of design are the intensity, the frequency composition and the total duration. Generally, such features are functions of the following three factors:

(1) the source mechanism,

(2) the material properties of the earth media along the various paths through which the seismic waves travel, and

(3) the local geological conditions of the site under considerations.

The complicated nature of the earthquake source mechanism, the highly irregular structure of the earth's mantle and crust, and the difficulty of making significant measurements make it difficult to elucidate the real influences on the ground motion. For the purpose of designing earthquake resistant buildings and analysing ground shaking, however, (2) and (3) of above three factors are especially significant in earthquake engineering. As development of computers, detailed local geology conditions and dynamic properties of earth materials have been taken into account in response analysis of the ground during earthquakes. Consequently the following question arises; how does the local geology actually affect the incoming seismic waves and under what conditions will it be significant in engineering problems? In 1972, "The International Conference on Microzonation" was held at Seattle in U.S.A., where a large number of papers on observations of earthquakes at various places of the world and analyses in which the local geology was taken into account were reported[1].

In 1930, Sezawa and Kanai pointed out the possible effects of superficial soil layers on observed ground motions[2),3)]. Since then, extensive research works have been carried out both theoretically and experimentally to study this problem[4),5)]. By considering a simple layered model, namely, two layered strata composed of a base rock and a superficial soil layer, they explained the possibility of prominent vibration of the superficial soil layer caused by the multiple reflections of the body waves in it. This approach is called the "multiple reflection theory of waves" or the "wave propagation method". The principle of multiple reflections has been mainly used when analysing the problems of the ground vibration during earthquakes.

On the other hand, Parmelee et al.[6)], and Idriss and Seed[7)] treated the layered system as a shear beam because of the analogy between the governing differential equations for these two systems. The shear beam is lumped into a discrete mechanical system and a technique of modal analysis or direct numerical integration is applied to analyse the system. The irregularities and inhomogeneities of the geometric configurations and the material properties of the local subsoil media, such as non-linear hysteretic stress-strain law, can be taken into account by this lumped mass model. In this model, however, the deformability of base rock is not considered and, therefore, the fact that a portion of wave energy transmitted from the superficial layered system goes back into the base rock, so called "geometrical dissipation", is neglected.

Now, a question arises whether the above two techniques, the wave propagation method and the lumped mass model, are equivalent and lead to the same results or not. In recent years the accuracy of modal superposition in the lumped mass model is examined by Whitman et al.[8)]. Furthermore, the comparison between these two techniques has been investigated by Arango and Dietrich[9)]. They concluded that although the maximum accelerations at the ground surface by the two techniques were almost identical, there appeared to be some differences in time histories of accelerations, and that the

values of stress and strain obtained by the two techniques also showed relatively poor agreement. Tsai[10] assumed a non-viscous shear beam model connected at its base by a viscous dashpot, of which a damping coefficient equals to a characteristic impedance of the base rock. This model could be considered as an analog for a unit-area vertical column of the laterally infinite layered system. By using this model, he reported that the deformability of the base rock could be taken into account even in the conventional shear beam model.

Whenever we calculate the response of the superficial soil layer, we need the incident earthquake motions all the way from the base rock to the surface. Although it is very important and interest to observe earthquake motions both on and under the ground at the same time in order to know the behaviors of the ground during an earthquake, up to now most of the observations have been carried out only on the ground surface. Therefore, the incident motions at the base rock must be inferentially calculated from an observed earthquake motions on the ground surface. For this purpose, the wave propagation method is a powerful technique. Toki investigated the technique to calculate the vertical distribution of shear stress, shear strain and acceleration in the superficial soil layer during an earthquake from the observed earthquake record on the ground surface by means of the relationship between the root mean square (r.m.s.) distribution of seismic response and the autocorrelation function of the ground surface motion[11]. Kagami and Kobayashi carried out the numerical response analysis of the multi-layered system in applying the multiple reflection theory of waves[12].

In general, the ground formation near the surface is very complicated and the dynamic properties of earth materials vary with the confining pressure as investigated by Hardin and Richart[13]. Furthermore, it is known that the dynamic moduli and the densities of the earth material increase with the depth in the ground. When we take into account such a complex geological

condition for the response analysis, it is convenient for dynamic properties and densities of the system to distribute with the continuous function which increases monotonously with depth. Bhattacharya[14], and Upadhyay and Negi[15] studied the problem of the response characteristics of such an inhomogeneous elastic soil layer due to SH-wave which is incident vertically to it, and obtained, under any inhomogeneous condition, the exact solutions which can be expressed in terms of hypergeometric, Whittaker, Bessel and exponential functions. Meanwhile, Kobori et al.[16] obtained the exact solutions for the wave transfer functions of inhomogeneous viscoelastic soil layers and presented some numerical examples of the characteristics of ground shaking in inhomogeneous elastic soil layers.

In this thesis, for the purpose of engineering applications an approximate technique in analysing the response of inhomogeneous elastic superficial soil layer for incident motions at the base rock and calculating the underground motions from the observed earthquake records at the surface will be presented. This is based on the multiple reflection theory of wave. Comparing the numerical results by this technique with the exact one on the characteristics of ground shaking, it is found that the approximate technique has a high accuracy.

5.2 Definition of Base Rock

In analysing the response characteristics of ground for earthquakes, the base rock of the site under consideration is defined as the layer under which the effects of superficial soil layers can not be significant in the response for earthquakes. In other words, seismic waves arrive equally to the base rock from the source and the characteristics of ground shaking are determined only by the geometric configuration of the local superficial soil layers.

Iwasaki[17] studied the base rocks in Osaka area. By calculating the response of the ground by the modal analysis, he concluded that the granitic

bed beneath Kobe and Nijo Group, about 1.5 km deep, should be considered as the base rock because its impedance ratio is smallest through the layered system in Osaka area. In addition, he concluded that it was possible to consider Osaka Group 0.5 km deep, as the base rock if we paid attention only for maximum acceleration and maximum velocity in response analysis.

As described in Section 5.1, there are two ways to calculate the response of layered system. The frist is the wave propagation method and the second the lumped mass model. The former is based on the theory of wave propagation, in which the base rock is considered to be a deformable half space foundation and the geometrical dissipation is taken into account. The latter is based on the theory of vibration. In this case, since the layered system is replaced by a vibration system with a finite degree of freedom, the base rock is regarded as a rigid base. Therefore, this method does not take into account the deformability of the base rock. In this sense, when definiting the base rock, the smaller an impedance ratio of the adjacent layer to the selected base rock is, the higher an accuracy is in calculation of response.

Tsai and Housner[18] considered the shear beam model which was connected at its base to the excitation $2y(t)$ through a viscous dashpot D as shown in Fig.5.1. The dashpot has a damping coefficient equal to $\rho_{N+1} c_{N+1}$. The transfer function of this model is same as one of the layered system overlying an elastic half space. By this model, the deformability of the base rock can be taken into account in response analysis by means of shear beam model. When the rigidity of

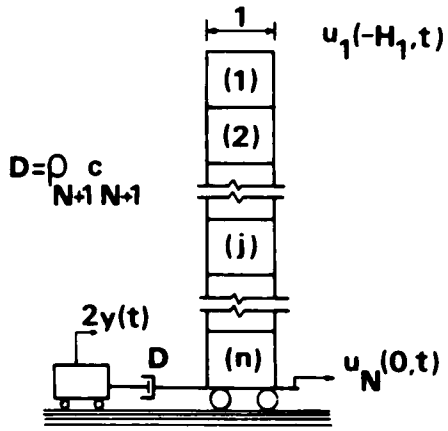

Fig.5.1 The shear beam model presented by Tsai and Housner[18].

the base rock is very large compared with the rigidity of the adjacent layer, the coefficient of the dashpot is large and the model approaches the conventional shear beam model.

If Tsai and Housner's idea is adopted, the layer, of which the characteristic impedance is largest through the geological configuration of the site under consideration and which lies broad area, should be considered as the base rock.

5.3 Basic Equations of Multiple Reflection Theory in Multi-Layered System

We consider the ground consisting of horizontal multi-layers overlying an elastic half-space as shown in Fig.5.2. H_i and ρ_i are the thickness and the density, and U_i and D_i are the ascendeing wave and the descending wave in i^{th} layer, respectively. A set of n coordinates, z_i, $i=1, 2, \ldots n$, is defined as shown in Fig.5.2. A relationship between shear wave velocity c_i and traveling time τ_i is

$$\tau_i = \frac{H_i}{c_i} \tag{5.1}$$

The transmission and reflection coefficients of wave at the boundary between the i^{th} and the $i+1^{th}$ layers are defined as shown in Fig.5.3. The impedance ratio α_i is given by

$$\alpha_i = \frac{\rho_i c_i}{\rho_{i+1} c_{i+1}} \tag{5.2}$$

Each coefficient shown in Fig.5.3 is expressed in term of α_i as follows;

$$\gamma_i = \frac{2}{1+\alpha_i} \quad , \quad \gamma_i' = \frac{2\alpha_i}{1+\alpha_i}$$

$$\beta_i = \frac{1-\alpha_i}{1+\alpha_i} \quad , \quad \beta_i' = \frac{\alpha_i - 1}{1+\alpha_i} \tag{5.3}$$

The equation of shear wave which propagates vertically only, is indicated as

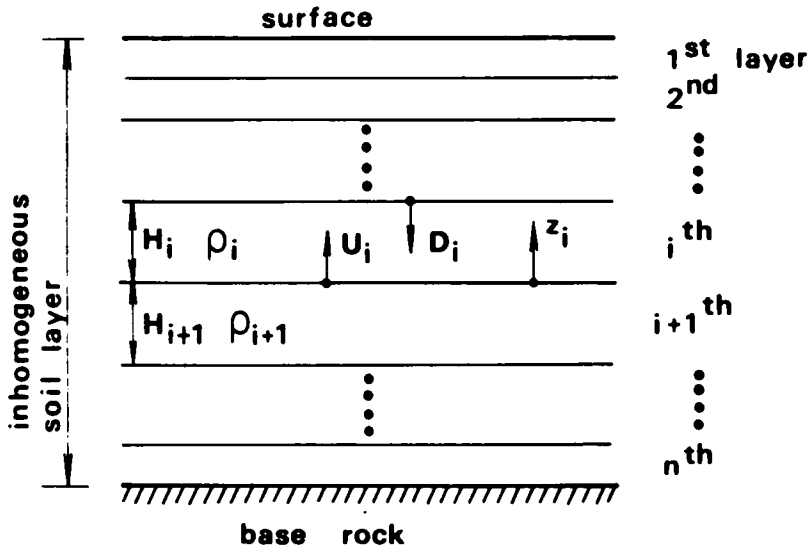

Fig.5.2 Multi-layered system.

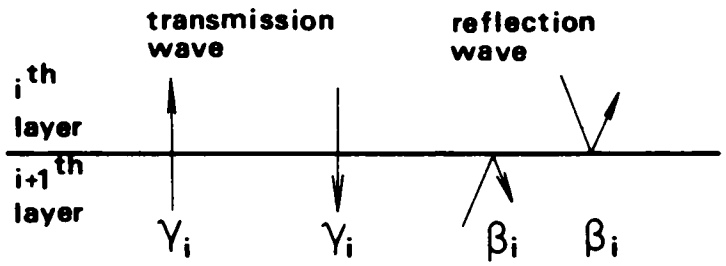

Fig.5.3 Definition of transmission and reflection coefficients.

$$\frac{\partial^2 u_i(t, z_i)}{\partial t^2} = \frac{G_i}{\rho_i} \frac{\partial^2 u_i(t, z_i)}{\partial z_i^2} \tag{5.4}$$

Its solution is denoted by sum of the ascending and the descending waves

$$u_i(t, z_i) = U_i\left(t - \frac{z_i}{c_i}\right) + D_i\left(t - \tau_i + \frac{z_i}{c_i}\right) \tag{5.5}$$

where, $u_i(t, z_i)$ is horizontal displacement at time t and coordinate z_i in the i^{th} layer and G_i is shear modulus. The displacements at the boundaries, $z_i=H_i$ and $z_i=0$ as shown in Fig.5.4, are given by

$$\begin{aligned} u_i(t, H_i) &= U_i(t-\tau_i) + D_i(t) \\ u_i(t, 0) &= U_i(t) + D_i(t-\tau_i) \end{aligned} \tag{5.6}$$

If the observed record at the ground surface is given by $u_s(t)$, there holds the following relation between the ascending and the descending waves at the surface because of free shear stress;

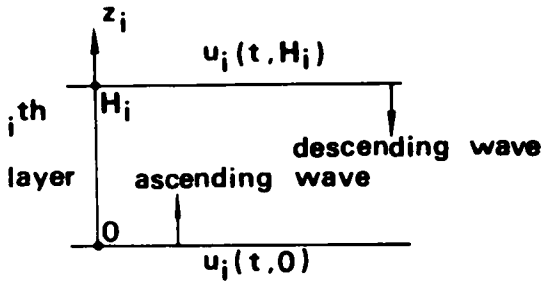

Fig.5.4 The i^{th} layer.

$$U_1(t-\tau_i) = D_1(t) = \frac{1}{2} u_s(t) \tag{5.7}$$

In general, there are the following relationships among the ascending and the descending waves[19];

$$U_i(t) = \gamma_i U_{i+1}(t-\tau_{i+1}) + \beta_i' D_i(t-\tau_i) \tag{5.8}$$

$$D_i(t) = \beta_{i-1} U_i(t-\tau_i) + \gamma_{i-1}' D_{i-1}(t-\tau_{i-1}) \tag{5.9}$$

The relationship between the incident wave $u_0(t)$ and the ascending and the descending waves in the n^{th} layer is given by

$$u_0(t) = \frac{1}{\gamma_n}\left\{ U_n(t) - \beta_n' D_n(t-\tau_n) \right\} \qquad (5.10)$$

If either $u_s(t)$ or $u_g(t)$ is known, the transient motion in all layers during an earthquake can be calculated successively in time region by solving the simultaneous equations of Eqs.(5.7), (5.8), (5.9) and (5.10).

Though the equations described above are derived with respect to displacement, the same relationships also hold for velocity and acceleration of earthquake motion, because the all equations become similar forms even if differentiated with respect to time.

5.4 Calculation of Underground Motion from Surface Record of Earthquake Motion

5.4.1 Derivation of Approximate Equations

In this section, the approximate equations to calculate underground motions during an earthquake from the observed record $u_s(t)$ at the ground surface will be derived with the assumption that the superficial soil layer is inhomogeneous, namely the elastic moduli and the density can be expressed by a suitable function of depth which monotonously increases in depth.

Instead of the direct approach to the inhomogeneous soil layer, the another technique is used; that is, the inhomogeneous soil layer of which thickness is H, is divided into n homogeneous layers. The recurrent equation to express the motion in arbitrary layer in terms of the known surface motion $u_s(t)$ is derived by means of the multiple reflection theory as described in the previous section. By approaching the thickness of the each divided layer to an infinitesimally small thickness, and letting the number of layers approach infinity, the recurrent equation can be transformed into the inte-

gral form. In the stage of obtaining the recurrent equation, the terms of combinations of the transmission coefficients γ_i, γ_i', $i=1, 2, \ldots i$ and the reflection coefficients β_i, β_i', $i=1, 2, \ldots i$, will appear in the equation. Since the characteristic impedance increases in depth as assumed above, an impedance ratio α_i is in the range of

$$0 < \alpha_i \leq 1 \tag{5.11}$$

At the limit, where n goes to infinity, α_i approaches unity. Therefore, it is found from Eq.(5.3) that γ_i and γ_i' approach unity, β_i is positive value and approaches zero, and β_i' is negative value and also approaches zero. In deriving the approximate equations as described below, only the terms of first and second order of the reflection coefficients β_i and β_i', $i=1, 2, \ldots i$, are considered and the terms of the higher order are neglected because they are infinitesimally small quantities.

From Eq.(5.7),

$$U_1(t) = \frac{1}{2} u_s(t+\tau_1) \quad , \quad D_1(t) = \frac{1}{2} u_s(t) \tag{5.12}$$

The ascending wave in the 2^{nd} layer can be expressed by the following equation from Eqs.(5.8) and (5.12);

$$U_2(t) = \frac{1}{2\gamma_1} \left\{ u_s(t+\tau_1+\tau_2) - \beta_1' u_s(t-\tau_1+\tau_2) \right\} \tag{5.13}$$

Upon repeated application of the above recurrent equation,

$$U_3(t) = \frac{1}{2} \left\{ \frac{1}{\gamma_1\gamma_2} u_s(t+\tau_1+\tau_2+\tau_3) - \frac{\beta_1'}{\gamma_1\gamma_2} u_s(t-\tau_1+\tau_2+\tau_3) \right.$$
$$\left. - \frac{\beta_2'\gamma_1'}{\gamma_2} u_s(t-\tau_1-\tau_2+\tau_3) - \frac{\beta_1\beta_2'}{\gamma_1\gamma_2} u_s(t+\tau_1-\tau_2+\tau_3) \right\}$$

$$U_4(t) = \frac{1}{2} \left\{ \frac{1}{\gamma_1\gamma_2\gamma_3} u_s(t+\tau_1+\tau_2+\tau_3+\tau_4) - \frac{\beta_1'}{\gamma_1\gamma_2\gamma_3} u_s(t-\tau_1+\tau_2+\tau_3+\tau_4) \right.$$
$$\left. - \frac{\gamma_1'\beta_2'}{\gamma_2\gamma_3} u_s(t-\tau_1-\tau_2+\tau_3+\tau_4) - \frac{\gamma_1'\gamma_2'\beta_3'}{\gamma_3} u_s(t-\tau_1-\tau_2-\tau_3+\tau_4) \right.$$

$$- \frac{\beta_1 \beta_2'}{\gamma_1 \gamma_2 \gamma_3} u_s(t+\tau_1-\tau_2+\tau_3+\tau_4) - \frac{\beta_2 \beta_3'}{\gamma_1 \gamma_2 \gamma_3} u_s(t+\tau_1+\tau_2-\tau_3+\tau_4)$$

$$- \frac{\gamma_2' \beta_1 \beta_3'}{\gamma_1 \gamma_3} u_s(t+\tau_1-\tau_2-\tau_3+\tau_4) \Big\}$$

. . . . . .

we finally arrive at Eq.(5.15) in an arbitrary i^{th} layer by taking into account Eq.(5.14),

$$\beta_i = -\beta_i' \qquad i = 1, 2, \cdots, i \tag{5.14}$$

$$U_i(t) = \frac{1}{2}\Big\{ \Big(\prod_{k=1}^{i-1} \frac{1}{\gamma_k}\Big) u_s\Big(t + \sum_{k=1}^{i} \tau_k\Big)$$

$$+ \sum_{k=1}^{i-1} \beta_k \Big(\prod_{j=k}^{i-1} \frac{1}{\gamma_j}\Big)\Big(\prod_{l=1}^{k-1} \gamma_l'\Big) u_s\Big(t + \sum_{k=1}^{i} \tau_k - \sum_{m=1}^{k} \tau_m\Big)$$

$$+ \sum_{p=1}^{i-1} \sum_{q=1}^{i-1} \beta_p \beta_q \Big(\prod_{r=1}^{p} \frac{1}{\gamma_r}\Big)\Big(\prod_{s=p+1}^{q-1} \gamma_s'\Big)\Big(\prod_{t=q}^{i-1} \frac{1}{\gamma_t}\Big) u_s\Big(t + \sum_{k=1}^{i} \tau_k \quad 2\sum_{m=p+1}^{q} \tau_m\Big)\Big\} \tag{5.15}$$
$(p<q)$

Similarly, for the descending wave in the i^{th} layer

$$D_i(t) = \frac{1}{2}\Big\{ \Big(\prod_{k=1}^{i-1} \gamma_k'\Big) u_s\Big(t - \sum_{k=1}^{i} \tau_k\Big)$$

$$+ \sum_{k=1}^{i-1} \beta_k \Big(\prod_{j=1}^{k} \frac{1}{\gamma_j}\Big)\Big(\prod_{l=k+1}^{i-1} \gamma_l'\Big) u_s\Big(t - \sum_{k=1}^{i} \tau_k + 2\sum_{m=1}^{k} \tau_m\Big)$$

$$+ \sum_{p=1}^{i-1} \sum_{q=1}^{i-1} \beta_p \beta_q \Big(\prod_{r=p}^{q} \frac{1}{\gamma_r}\Big)\Big(\prod_{s=1}^{p-1} \gamma_s'\Big)\Big(\prod_{t=q+1}^{i-1} \gamma_t'\Big) u_s\Big(t - \sum_{k=1}^{i} \tau_k + 2\sum_{m=p+1}^{q} \tau_m\Big)\Big\} \tag{5.16}$$
$(p<q)$

At the limit of bringing n divided layers to infinity, that is, the thickness of each layer to infinitesimally small, Eqs.(5.15) and (5.16) can be expressed by the integral forms

$$U(t,x) = \lim_{\substack{i\to\infty \\ \tau_1, \tau_2, \cdots \tau_i \to 0}} U_i(t) = \frac{1}{2} A(x)\Big\{ u_s\Big(t + \int_0^x \frac{dx}{c(x)}\Big)$$

$$+ \int_0^x B(y)\, u_s\Big(t + \int_0^x \frac{dx}{c(x)} - 2\int_0^y \frac{dy}{c(y)}\Big)$$

$$+ \int_0^x B(z) \int_0^z B(w)\, u_s\Big(t + \int_0^x \frac{dx}{c(x)} - 2\int_w^z \frac{dw}{c(w)}\Big) dw\, dz \Big\} \tag{5.17}$$

$$D(t,x) = \lim_{\substack{i\to\infty \\ \tau_1,\tau_2\cdots\tau_i\to 0}} D_i(t) = \frac{1}{2}A(x)\left\{ u_s\left(t - \int_0^x \frac{dx}{c(x)}\right)\right.$$
$$+ \int_0^x B(y)\, u_s\left(t - \int_0^x \frac{dx}{c(x)} + 2\int_0^y \frac{dy}{c(y)}\right)$$
$$\left. + \int_0^x B(z)\int_0^z B(w)\, u_s\left(t - \int_0^x \frac{dx}{c(x)} + 2\int_w^z \frac{dw}{c(w)}\right) dw\, dz \right\} \qquad (5.18)$$

In the above equations, we changed the coordinate system of inhomogeneous soil layer as shown in Fig.5.5. As described in the next subsection, $A(x)$ and $B(x)$ are functions of depth and they correspond to the transmission and the reflection coeffients, respectively, $c(x)$ is the distribution function of shear wave velocity. From Eq.(5.5), the displacement $u(t,x)$ at the arbitrary depth is given by

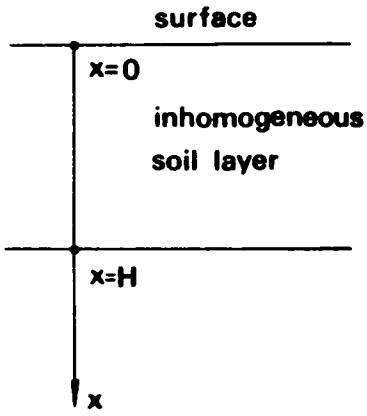

Fig.5.5 Coordinate system for inhomogeneous soil layer.

$$u(t,x) = U(t,x) + D(t,x) \qquad (5.19)$$

Also, the incident motion $u_0(t)$ is given by

$$u_0(t) = \frac{1}{\gamma_n}\left\{ U(t,H) + \beta_n D(t,H)\right\} \qquad (5.20)$$

where, γ_n and β_n are the transmission and the reflection coefficients at the interface between the superficial soil layer and the base rock.

5.4.2 Discussion about $A(x)$ and $B(x)$

$A(x)$ is the limit value of the product of the transmission coefficients and expressed by

$$A(x) = \lim_{i\to\infty} \prod_{k=1}^{i-1} \frac{1}{\gamma_k} = \lim_{i\to\infty} \prod_{k=1}^{i-1} \gamma_k' \tag{5.21}$$

From Eq.(5.3)

$$\frac{\gamma_k'}{\gamma_k} = \alpha_k \tag{5.22}$$

so that

$$\frac{\prod_{k=1}^{i-1} \gamma_k'}{\prod_{k=1}^{i-1} \gamma_k} = \prod_{k=1}^{i-1} \alpha_k = \frac{\rho_1 c_1}{\rho_2 c_2} \cdot \frac{\rho_2 c_2}{\rho_3 c_3} \cdots\cdots \frac{\rho_{i-2} c_{i-2}}{\rho_{i-1} c_{i-1}}$$

$$= \frac{\rho_1 c_1}{\rho_{i-1} c_{i-1}} \tag{5.23}$$

If the distribution function of the characteristic impedance is given by $\chi(x)=\rho(x)c(x)$, we obtain the following equation from Eq.(5.23);

$$\lim_{i\to\infty} \prod_{k=1}^{i-1} \alpha_k = \frac{\chi(0)}{\chi(x)} \tag{5.24}$$

Consequently, $A(x)$ can be expressed by $\chi(x)$ from Eqs.(5.21) and (5.23) as

$$A(x) = \left\{ \frac{\chi(0)}{\chi(x)} \right\}^{\frac{1}{2}} \tag{5.25}$$

The characteristic impedance $\alpha(x)$ which is a function of x is difined by

$$\alpha(x) = \lim_{dx\to 0} \frac{\chi(x-dx)}{\chi(x)}$$

$$\doteqdot \frac{\chi(x) - \chi'(x)dx}{\chi(x)} \tag{5.26}$$

where, $\chi'(x)$ means $\frac{d\chi(x)}{dx}$. The reflection coefficient $\beta(x)$ is given by substituting Eq.(5.26) into Eq.(5.3)

$$\beta(x) = \frac{1-\alpha(x)}{1+\alpha(x)}$$

$$\doteqdot \frac{\chi'(x)}{2\chi(x)} dx \tag{5.27}$$

So that, $B(x)$ is expressed by

$$\beta(x) = \frac{\chi'(x)}{2\chi(x)} \tag{5.28}$$

5.4.3 Characteristics of the Ground Shaking and Considerations on Accuracy of the Approximate Equations

The purpose of sinusoidal steady-state analysis is to compute the response of a given superficial soil layer subjected to excitation of steady-state sinusoidal waves. This analysis is capable of indicating precisely the frequency selective property of a given superficial soil layer.

The characteristics of the ground shaking are investigated with two models of inhomogeneous soil layers. In order to examine the accuracy of the approximate equations derived in the previous subsection, the models used are same as those by Kobori et al.[16]. The characteristics calculated by the approximate equation are compared with the exact solutions.

The dimensionless variable ξ is defined by the following expression in order to unify the expression of conditions of inhomogeneity;

$$\xi = \frac{x}{H} \tag{5.29}$$

where, H is the thickness of inhomogeneous soil layer. The notations of displacement, shear modulus, density and wave velocity of superficial layer and base rock are shown in Fig.5.6. The two models used are shown in Fig.5.7(a) and (b). The former is the model of which inhomogeneity is relatively small and the latter is one of relatively large inhomogeneity.

Substituting Eqs.(5.17) and (5.18) into Eq.(5.20), the incident motion $u_0(t)$ can be expressed by the surface motion $u_s(t)$ as follows;

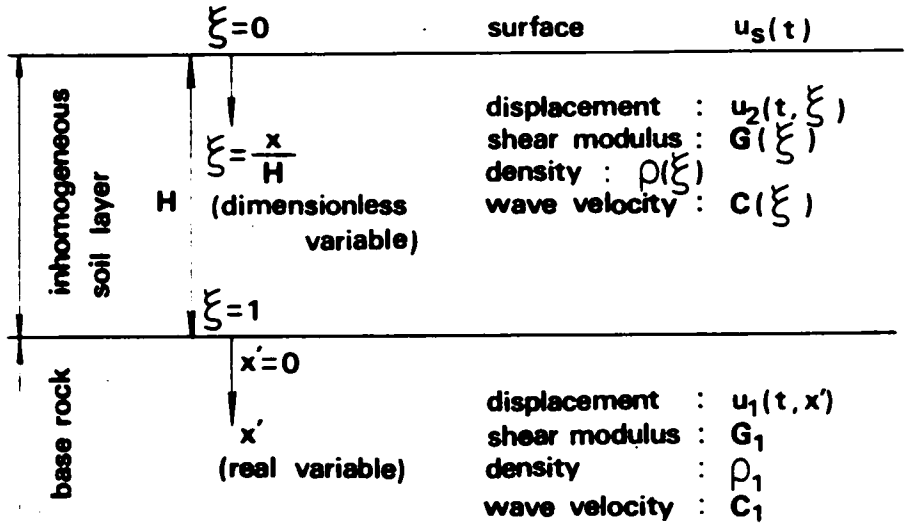

Fig.5.6 Notations of variables and properties in an inhomogeneous soil layer.

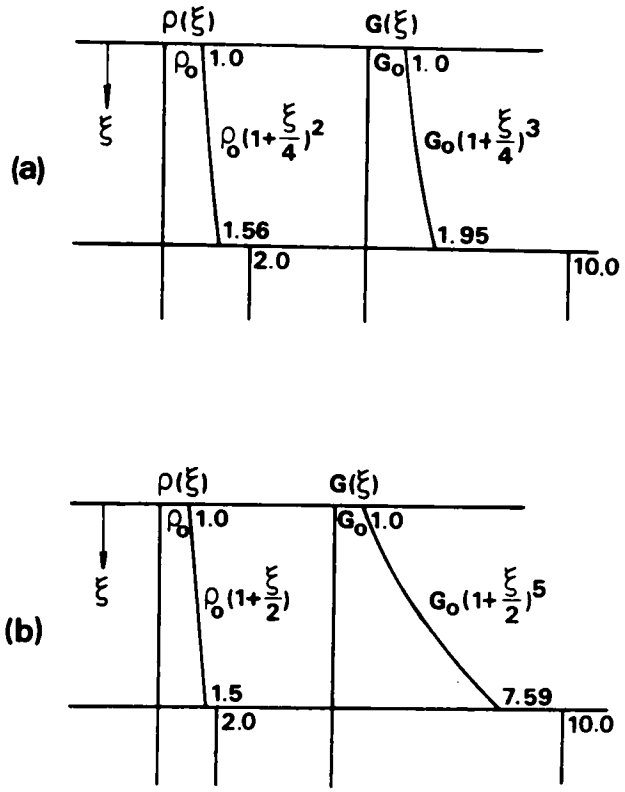

Fig.5.7 The models used in the analysis[16].

$$u_0(t) = \frac{A(1)}{2\gamma_n}\left[u_s\left(t+H\int_0^1 \frac{d\xi}{c(\xi)}\right) + \int_0^1 B(\eta)\, u_s\left(t+H\int_0^1 \frac{d\xi}{c(\xi)} - 2H\int_0^\eta \frac{d\eta}{c(\eta)}\right)d\eta \right.$$

$$+\int_0^1 B(z_1)\int_0^{z_1} B(\mu)\, u_s\left(t+H\int_0^1 \frac{d\xi}{c(\xi)} - 2H\int_\mu^{z_1} \frac{d\mu}{c(\mu)}\right)d\mu dz_1$$

$$+\beta_n\left\{ u_s\left(t-H\int_0^1 \frac{d\xi}{c(\xi)}\right) + \int_0^1 B(\eta)\, u_s\left(t-H\int_0^1 \frac{d\xi}{c(\xi)} + 2H\int_0^\eta \frac{d\eta}{c(\eta)}\right)d\eta \right.$$

$$\left.\left. +\int_0^1 B(z_1)\int_0^{z_1} B(\mu)\, u_s\left(t-H\int_0^1 \frac{d\xi}{c(\xi)} + 2H\int_\mu^{z_1} \frac{d\mu}{c(\mu)}\right)d\mu dz_1 \right\}\right] \tag{5.30}$$

Substituting the following equations into the above equation, the response of the surface in sinusoidal steady-state for the infinite harmonic wave is examined

$$u_0(t) = a\, e^{i\omega t} \quad , \quad u_s(t) = A_s\, e^{i\omega t} \tag{5.31}$$

where, a and A_s are the amplitudes of displacement of the incident and the surface motions, respectively, i the imaginary unit and ω the angular frequency. The ratio of the amplitudes is given by the complex equation

$$\frac{A_s}{a} = \frac{2}{A(1)} \cdot \frac{1}{p + i\alpha_n q} \tag{5.32}$$

where,

$$p = \cos\left(a_0\int_0^1 \frac{d\xi}{f(\xi)}\right) + \int_0^1 B(\eta)\cos\left\{a_0\left(\int_0^1 \frac{d\xi}{f(\xi)} - 2\int_0^\eta \frac{d\eta}{f(\eta)}\right)\right\}d\eta$$

$$+\int_0^1 B(z_1)\int_0^{z_1} B(\mu)\cos\left\{a_0\left(\int_0^1 \frac{d\xi}{f(\xi)} - 2\int_0^{z_1} \frac{d\mu}{f(\mu)}\right)\right\}d\mu dz_1 \tag{5.33}$$

$$q = \sin\left(a_0\int_0^1 \frac{d\xi}{f(\xi)}\right) + \int_0^1 B(\eta)\sin\left\{a_0\left(\int_0^1 \frac{d\xi}{f(\xi)} - 2\int_0^\eta \frac{d\eta}{f(\eta)}\right)\right\}d\eta$$

$$+\int_0^1 B(z_1)\int_0^{z_1} B(\mu)\sin\left\{a_0\left(\int_0^1 \frac{d\xi}{f(\xi)} - 2\int_\mu^{z_1} \frac{d\mu}{f(\mu)}\right)\right\}d\mu dz_1 \tag{5.34}$$

and α_n is the impedance ratio at the interface between the inhomogeneous soil layer and the base rock. a_0 is the dimensionless frequency defined by

$$a_0 = \frac{\omega H}{c_0} \tag{5.35}$$

where, c_0 is the shear wave velocity at the surface and $f(\xi)$ is the function of ξ and shows the distribution of shear wave velocity and is defined by

$$f(\xi) = \frac{c(\xi)}{c_0} \tag{5.36}$$

The amplitude characteristic of the surface is given by the following equation from Eq.(5.32);

$$\left| \frac{A_s}{a} \right| = \frac{2}{A(1)} \cdot \frac{1}{(p^2 + \alpha_n^2 q^2)^{\frac{1}{2}}} \tag{5.37}$$

and the phase characteristic of the surface is

$$\varphi_s = \tan^{-1} \frac{\alpha_n q}{p} \tag{5.38}$$

By the same method as in the homogeneous elastic two layered system, the amplitude characteristics at the bottom boundary can be calculated from

$$\left| \frac{A_H}{a} \right| = A(1) \cdot |p| \cdot \left| \frac{A_s}{a} \right| \tag{5.39}$$

where, A_H is the amplitude of sinusoidal steady-state displacement at the depth H. The functional forms for density, shear modulus, shear wave velocity, $f(\xi)$, characteristic impedance, $A(\xi)$ and $B(\xi)$ used in calculation of Eqs. (5.33) and (5.34), are summarized in Table 5.1 for models A and B shown in Figs.5.7(a) and (b), respectively.

Model A In this model, the inhomogeneity is relatively little and the difference of rigidity between the superficial layer and the base rock is

Table 5.1 The functional forms for the properties of inhomogeneous soil layers about the models A and B.

	model A	model B
$\rho(\xi)$	$\rho_0(1+\frac{\xi}{4})^2$	$\rho_0(1+\frac{\xi}{2})$
$G(\xi)$	$G_0(1+\frac{\xi}{4})^3$	$G_0(1+\frac{\xi}{2})^5$
$C(\xi)$	$C_0(1+\frac{\xi}{4})^{\frac{1}{2}}$	$C_0(1+\frac{\xi}{2})^2$
$f(\xi)$	$(1+\frac{\xi}{4})^{\frac{1}{2}}$	$(1+\frac{\xi}{2})^2$
$\chi(\xi)$	$\rho_0 C_0(1+\frac{\xi}{4})^{\frac{5}{2}}$	$\rho_0 C_0(1+\frac{\xi}{2})^3$
$A(\xi)$	$(1+\frac{\xi}{4})^{-\frac{5}{4}}$	$(1+\frac{\xi}{2})^{-\frac{3}{2}}$
$B(\xi)$	$\frac{5}{16}(1+\frac{\xi}{4})^{-1}$	$\frac{3}{4}(1+\frac{\xi}{2})^{-1}$

fairly large. Under the inhomogeneous condition presented in Table 5.1, Eqs.(5.33) and (5.34) become

$$
\begin{aligned}
p = {} & \cos\left(g(1)a_0\right) + \frac{5}{2}\Big[\cos\left(16a_0 + g(1)a_0\right)\left\{C_i\left(8\sqrt{5}\,a_0\right) - C_i\left(16a_0\right)\right\} \\
& + \sin\left(16a_0 + g(1)a_0\right)\left\{S_i\left(8\sqrt{5}\,a_0\right) - S_i\left(16a_0\right)\right\}\Big] \\
& + \frac{25}{8}\int_0^1 \frac{1}{4+\zeta}\Big[\cos\left(8\sqrt{4+\zeta}\,a_0 - g(1)a_0\right)\left\{C_i\left(8\sqrt{4+\zeta}\,a_0\right) - C_i\left(16a_0\right)\right\} \\
& + \sin\left(8\sqrt{4+\zeta}\,a_0 - g(1)a_0\right)\left\{S_i\left(8\sqrt{4+\zeta}\,a_0\right) - S_i\left(16a_0\right)\right\}\Big]\,d\zeta
\end{aligned}
\tag{5.40}
$$

$$
\begin{aligned}
q = {} & \sin\left(g(1)a_0\right) + \frac{5}{2}\Big[\sin\left(16a_0 + g(1)a_0\right)\left\{C_i\left(8\sqrt{5}\,a_0\right) - C_i\left(16a_0\right)\right\} \\
& - \cos\left(16a_0 + g(1)a_0\right)\left\{S_i\left(8\sqrt{5}\,a_0\right) - S_i\left(16a_0\right)\right\}\Big] \\
& + \frac{25}{8}\int_0^1 \frac{1}{4+\zeta}\Big[\cos\left(8\sqrt{4+\zeta}\,a_0 - g(1)a_0\right)\left\{S_i\left(8\sqrt{4+\zeta}\,a_0\right) - S_i\left(16a_0\right)\right\} \\
& - \sin\left(8\sqrt{4+\zeta}\,a_0 - g(1)a_0\right)\left\{C_i\left(8\sqrt{4+\zeta}\,a_0\right) - C_i\left(16a_0\right)\right\}\Big]\,d\zeta
\end{aligned}
\tag{5.41}
$$

where, $g(1)$ is given by

$$
g(1) = \int_0^1 \frac{d\xi}{\left(1 + \frac{\xi}{4}\right)^{\frac{1}{2}}} \tag{5.42}
$$

and $S_i(x)$ and $C_i(x)$ are the sine and cosine intergrals respectively, defined by the formula

$$
S_i(x) = \int_0^x \frac{\sin t}{t}\,dt \quad , \quad C_i = -\int_x^\infty \frac{\cos t}{t}\,dt \tag{5.43}
$$

The numerical results of the amplitude and phase characteristics are obtained

and shown in Fig.5.8. Compared with the exact solution by Kobori et al.[16], the approximate technique was found to have a high accuracy. It is seen from Fig.5.8 that the characteristics of the ground shaking do not differ so much from the one of the simple layered system composed of homogeneous two layers.

Model *B* In this model, the inhomogeneity is relatively large and the difference of rigidity between the superficial layer and the base rock is small. Similarly as model *A*, under the inhomogeneity condition, Eqs.(5.33) and (5.34) become

$$
\begin{aligned}
p = {} & \cos\left(g(1)a_0\right) + \frac{3}{2}\Big[\cos\left(4a_0 - g(1)a_0\right)\left\{C_i(4a_0) - C_i\left(\frac{8}{3}a_0\right)\right\} \\
& + \sin\left(4a_0 - g(1)a_0\right)\left\{S_i(4a_0) - S_i\left(\frac{8}{3}a_0\right)\right\}\Big] \\
& + \frac{9}{4}\int_0^1 \frac{1}{2+\zeta}\Big[\cos\left(g(1)a_0 + \frac{8a_0}{2+\zeta}\right)\left\{C_i(4a_0) - C_i\left(\frac{8a_0}{2+\zeta}\right)\right\} \\
& + \sin\left(g(1)a_0 + \frac{8a_0}{2+\zeta}\right)\left\{S_i(4a_0) - S_i\left(\frac{8a_0}{2+\zeta}\right)\right\}\Big]\, d\zeta
\end{aligned}
\tag{5.44}
$$

$$
\begin{aligned}
q = {} & \sin\left(g(1)a_0\right) + \frac{3}{2}\Big[\cos\left(4a_0 - g(1)a_0\right)\left\{S_i(4a_0) - S_i\left(\frac{8}{3}a_0\right)\right\} \\
& - \sin\left(4a_0 - g(1)a_0\right)\left\{C_i(4a_0) - C_i\left(\frac{8}{3}a_0\right)\right\}\Big] \\
& + \frac{9}{4}\int_0^1 \frac{1}{2+\zeta}\Big[\sin\left(g(1)a_0 + \frac{8a_0}{2+\zeta}\right)\left\{C_i(4a_0) - C_i\left(\frac{8a_0}{2+\zeta}\right)\right\} \\
& - \cos\left(g(1)a_0 + \frac{8a_0}{2+\zeta}\right)\left\{S_i(4a_0) - S_i\left(\frac{8a_0}{2+\zeta}\right)\right\}\Big]\, d\zeta
\end{aligned}
\tag{5.45}
$$

where, $g(1)$ is given by

$$
g(1) = \int_0^1 \frac{d\zeta}{\left(1 + \frac{\zeta}{2}\right)^2} \tag{5.46}
$$

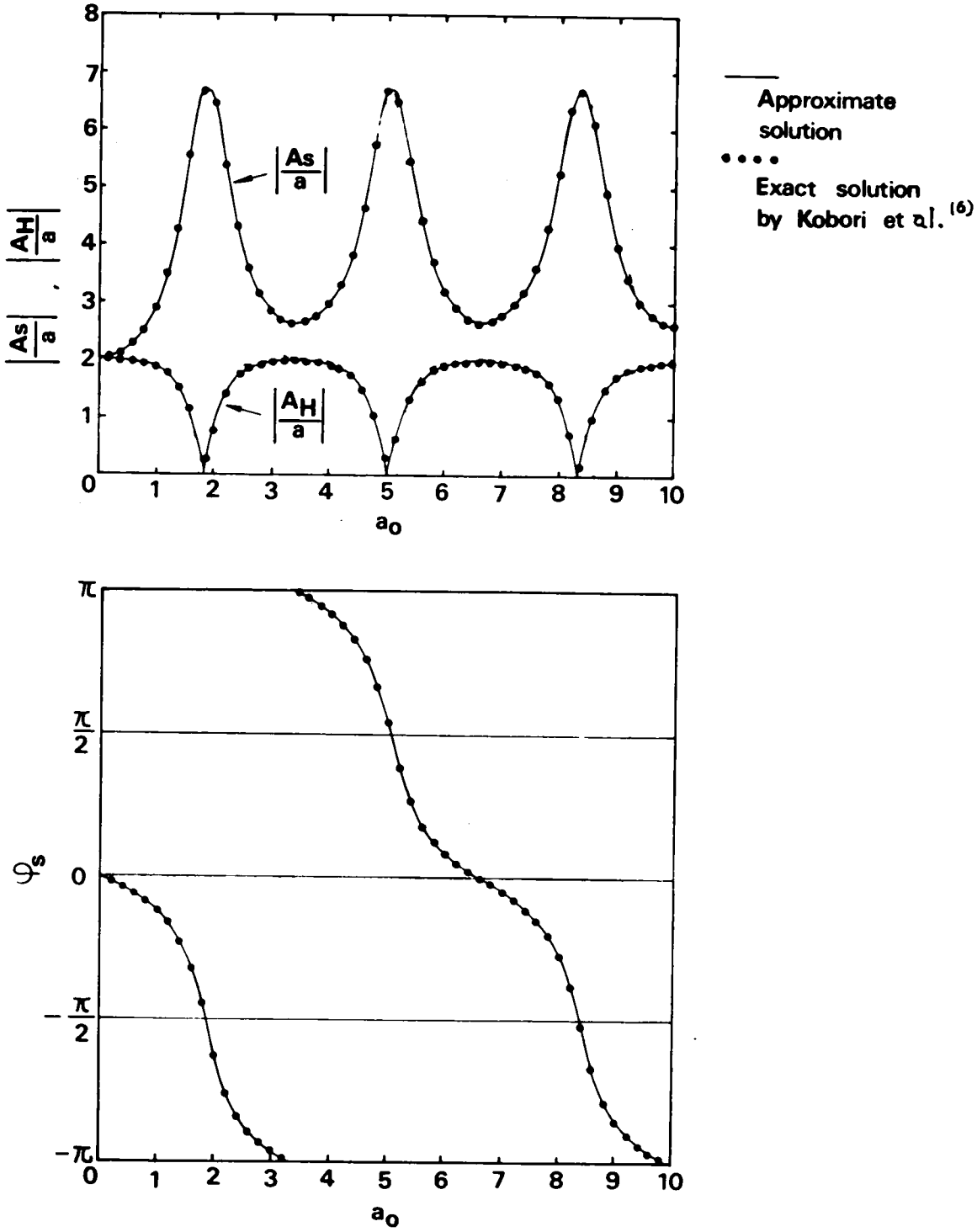

Fig.5.8 The amplitude and phase characteristics of model A.

The numerical results of the characteristics of ground shaking are shown in Fig.5.9. Compared with the exact solution, it is found that a little discrepancy appears only in the low frequency range. It is about as high as 3 %. The tendencies of the amplitude and the phase characteristics of this model are so much different from those of homogeneous two layered system[20].

5.4.4 Numerical Examples

The underground motions in the time domain are inferentially calculated from the observed earthquake record on the ground surface and compared with the observed one.

As the one of Abeno re-development projects, Osaka, three seismometers were placed at three different depths in the ground; the ground surface, 10 *m* and 30 *m*, in the campus of Medical Science of Osaka Municipal University. Microtremors and earthquakes were observed from December, 1970 to March, 1971[21]. The one of earthquakes observed in that period is Atsumi Hanto Oki earthquake of January 5,1971, of which magnitude is 6.3, and the maximum acceleration at the surface is 11.84 *gal*.

A typical configuration for a distribution of S-wave velocity at the observed point is shown in Fig.5.10. Though its distribution is very complicated, the distribution function of S-wave velocity is assumed as $c(x)=200(1+\frac{x}{4H})^3$ for simplicity, and the layer which lies 35 *m* under the ground and in which S-wave velocity is 500 *m/sec*, is regarded as the base rock. The density in each layer is in the range of 1.8 to 1.9 g/cm^3 and considered to be constant through the layered soil in the analytical calculation. The amplitude characteristic of this ground is obtained by the manner described in the last subsection as shown in Fig.5.11. It is found from this figure that the amplification at the surface is relatively small. The fundamental predominant frequency is considered to be 2 *cps* by using the values of $c_0=200$ *m/sec* and $H=35$ *m*.

The recorded accelerogram at the surface is shown in Fig.5.12(a). From that, the underground accelerations are computed by using Eqs.(5.17) to (5.19)

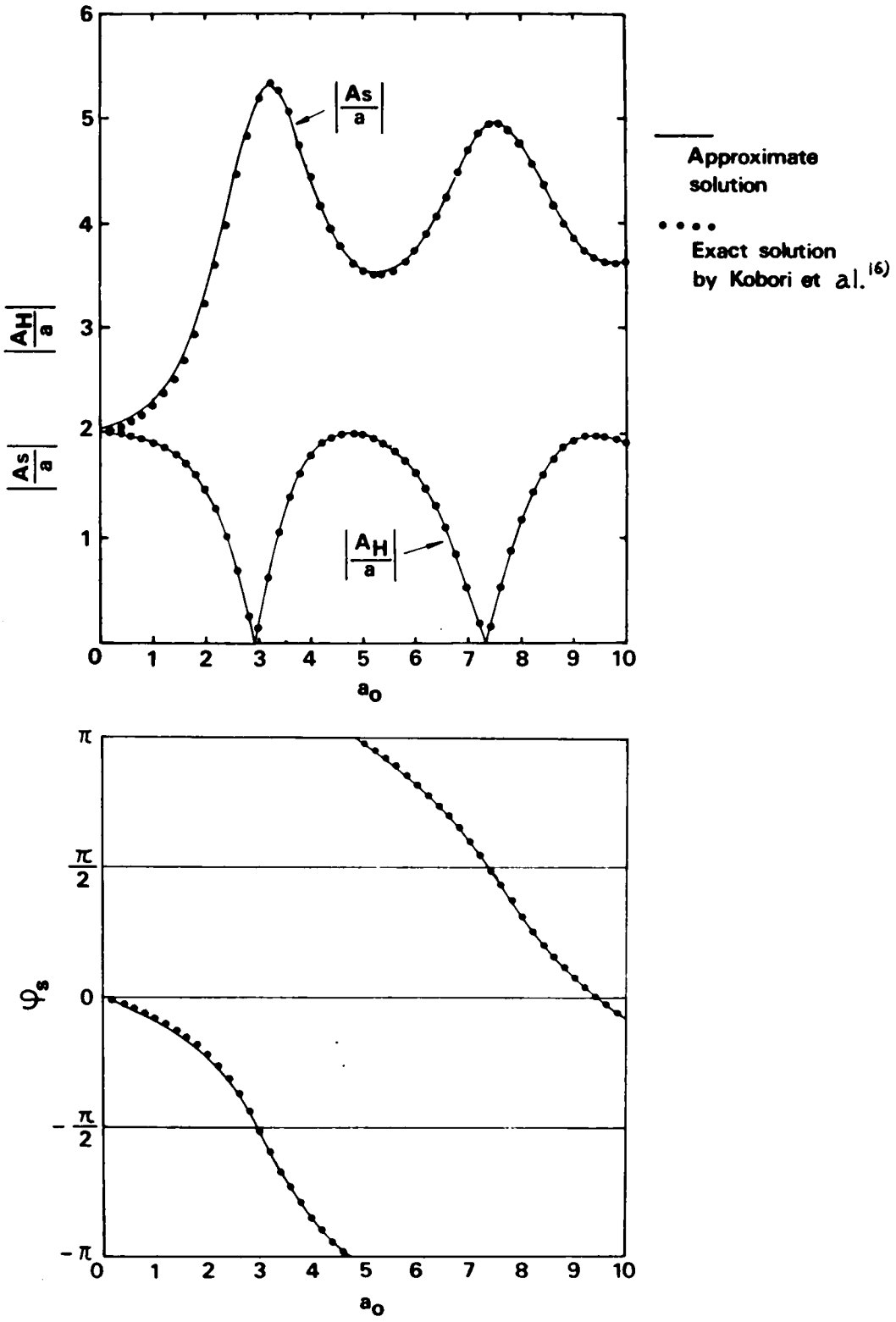

Fig.5.9 The amplitude and phase characteristics of model B.

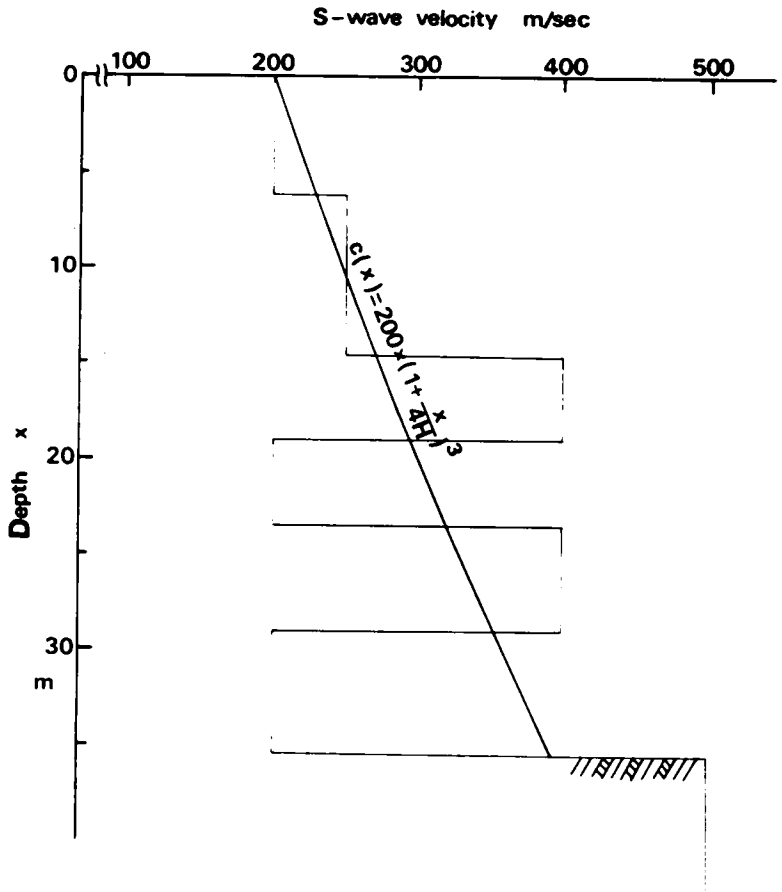

Fig.5.10 Distribution of S-wave velocity at Abeno site.

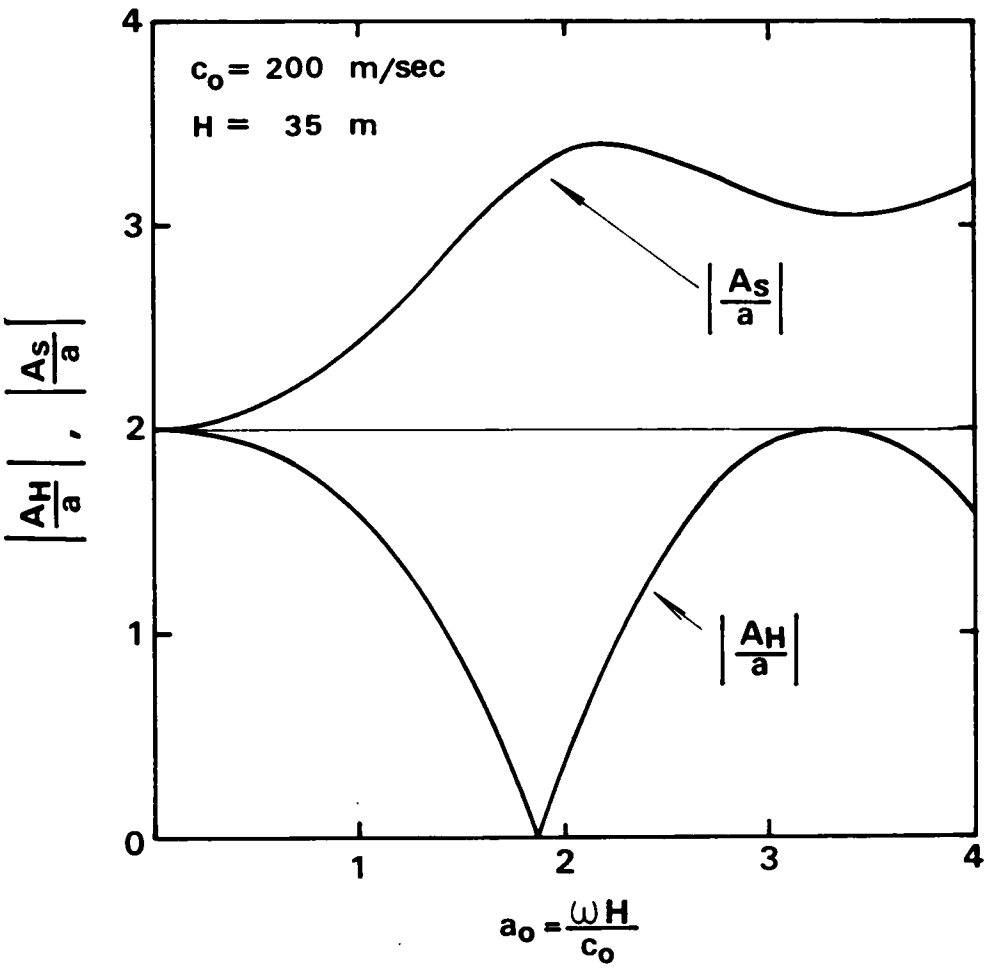

Fig.5.11 Calculated amplitude characteristic of the ground at Abeno site.

The calculated accelerograms at 10 m and 30 m under the ground are compared with the observed one, as shown in Figs.5.12 (b) and (c), respectively. The computation can be done very quickly. In these figures, we can see a good agreement in the wave shapes. Figs.5.13 (a), (b) and (c) show the power spectrum density functions $S(f)$ for the observed and the calculated accelerograms in Fig.5.12. We come to conclusions that the component of frequency $f = 1.1$ *cps* is prominent in all accelerograms, and that the component of frequency 2.1 *cps* is prominent in the surface accelerogram in spite of inferiority in the accelerogram at 30 m under the ground.

5.4.5 Conclusions

The ground formation near the surface is very complicated and the dynamic properties of earth materials vary with the confining pressure. The dynamic moduli and the densities of the earth materials increase with the depth beneath the ground surface in general. There are many cases where the distributions of dynamic properties and densities of the layered soil system can be replaced by a suitable continuous function of depth which increases monotonously with depth.

When designing underground structures such as tunnels or structural foundations, we must know the underground motions during an earthquake. In this section, the approximate approach to calculate the underground earthquake motions in an inhomogeneous soil layer from the surface record has been presented. This is based on the multiple reflection theory. An inhomogeneous soil layer can be regarded as a special case of multi-layered system, that is, it is composed of infinite multi-layers with an infinitesimally small thickness and its dynamic moduli and densities distribute continuously with depth. So that the waves which are incident vertically to the inhomogeneous soil layer may repeat transmission and reflection everywhere in the inhomogeneous soil layer. However, because of the smooth variation of the impedance

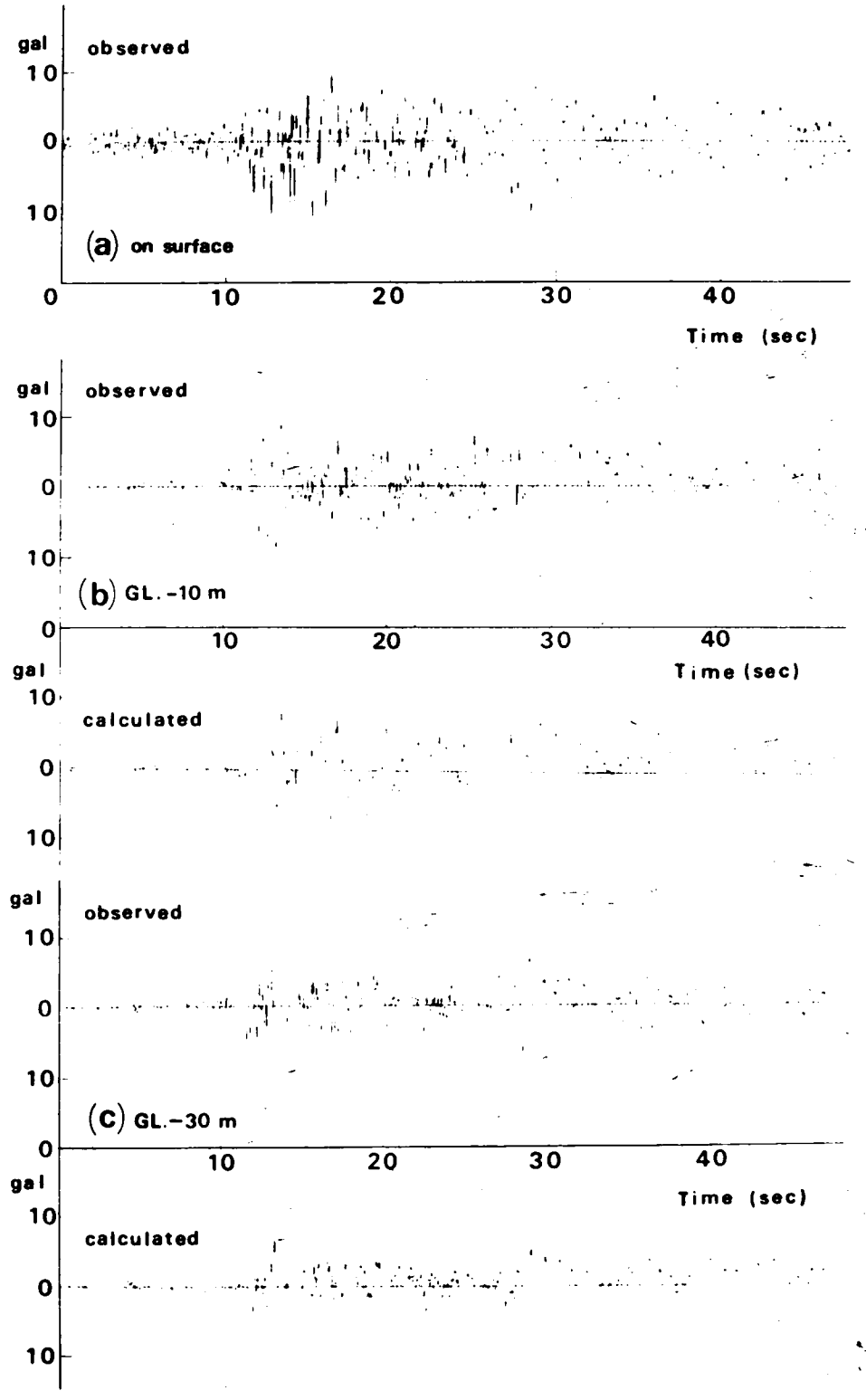

Fig.5.12 Observed and calculated accelerograms of Atsumi Hanto Oki earthquake.

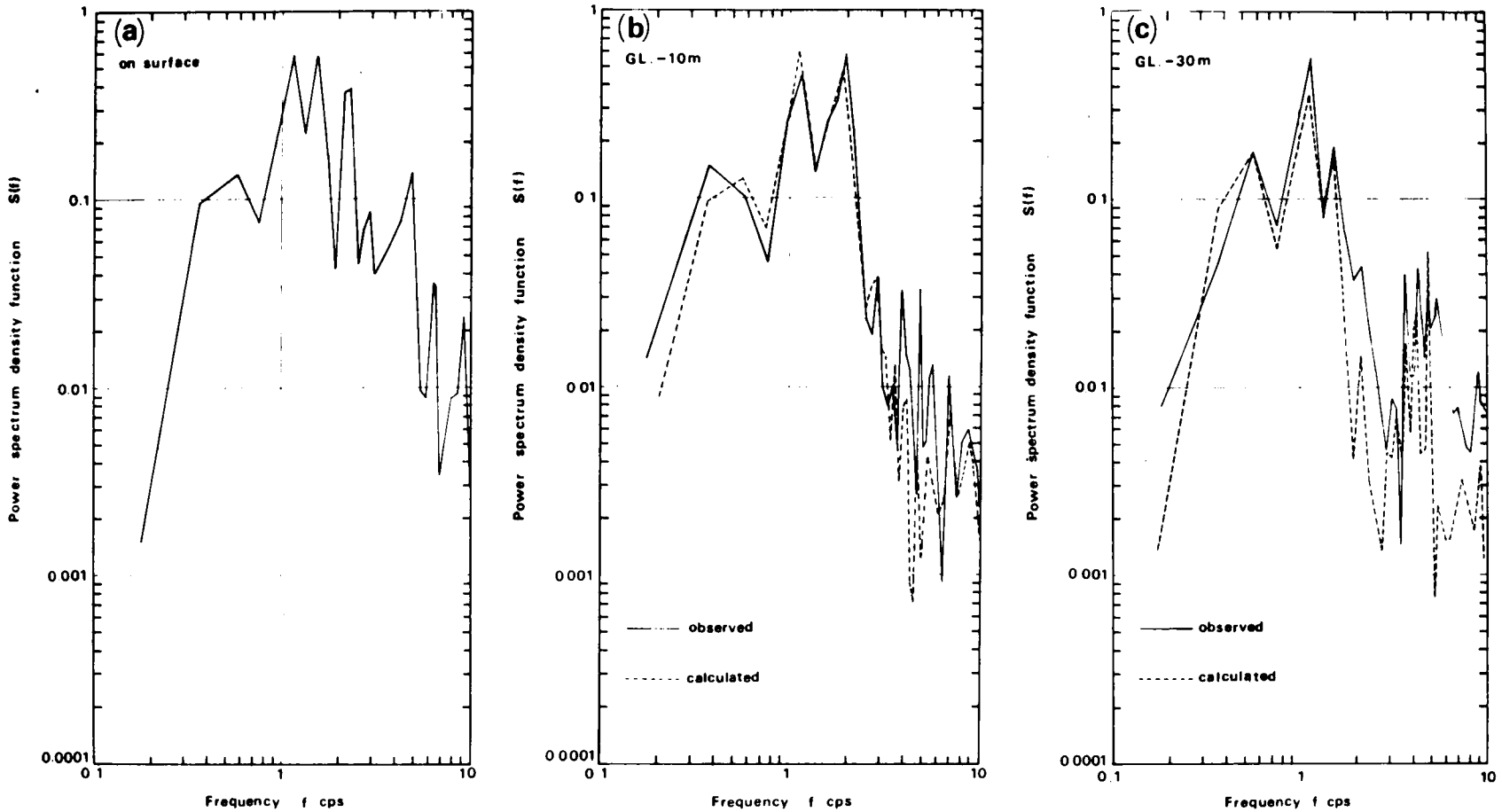

Fig.5.13 Comparison of power spectrum density functions of the observed and the calculated accelerogram.

ratio, the influence due to reflection waves for the results reduces as they reflect so many times. In the approximate approach presented in this section, only the direct transmission wave and the waves which reflect up to twice are considered in the analysis. As a consequence, approximate equations (5.17) and (5.18) are derived. The physical meaning of each term in these equations is visualized in Figs.5.14(a), (b) and (c).

Conclusions are:

1) When the distribution of the elastic moduli and the densities in the ground can be expressed by a suitable continuous and monotonously increasing function, we can calculate the underground earthquake motions from the past surface record by Eqs.(5.17) and (5.18).

2) Even if we only take into account the direct transmission wave and the first and the second order reflection waves, the accuracy of the approximate approach is satisfactory in the engineering purpose. According to the characteristics of the ground shaking for the selected inhomogeneous soil layer models, the approximate solutions almost agree with the exact one.

3) The characteristics of ground shaking for the inhomogeneous soil layer are very different from that for the homogeneous elastic two layered system, as the inhomogeneity of the ground is remarkable.

4) We can compute the underground earthquake motions by this approximate approach in very short computation time. According to the numerical example by Atsumi Hanto Oki earthquake record at Abeno site in Osaka, it is found that the calculated underground motions agree with the observed one.

5.5 Response of Inhomogeneous Surface Layer Subjected to Excitation of Earthquake Motion

In this section, we study the response of the inhomogeneous elastic soil layer subjected to an excitation of earthquake motion at the base rock.

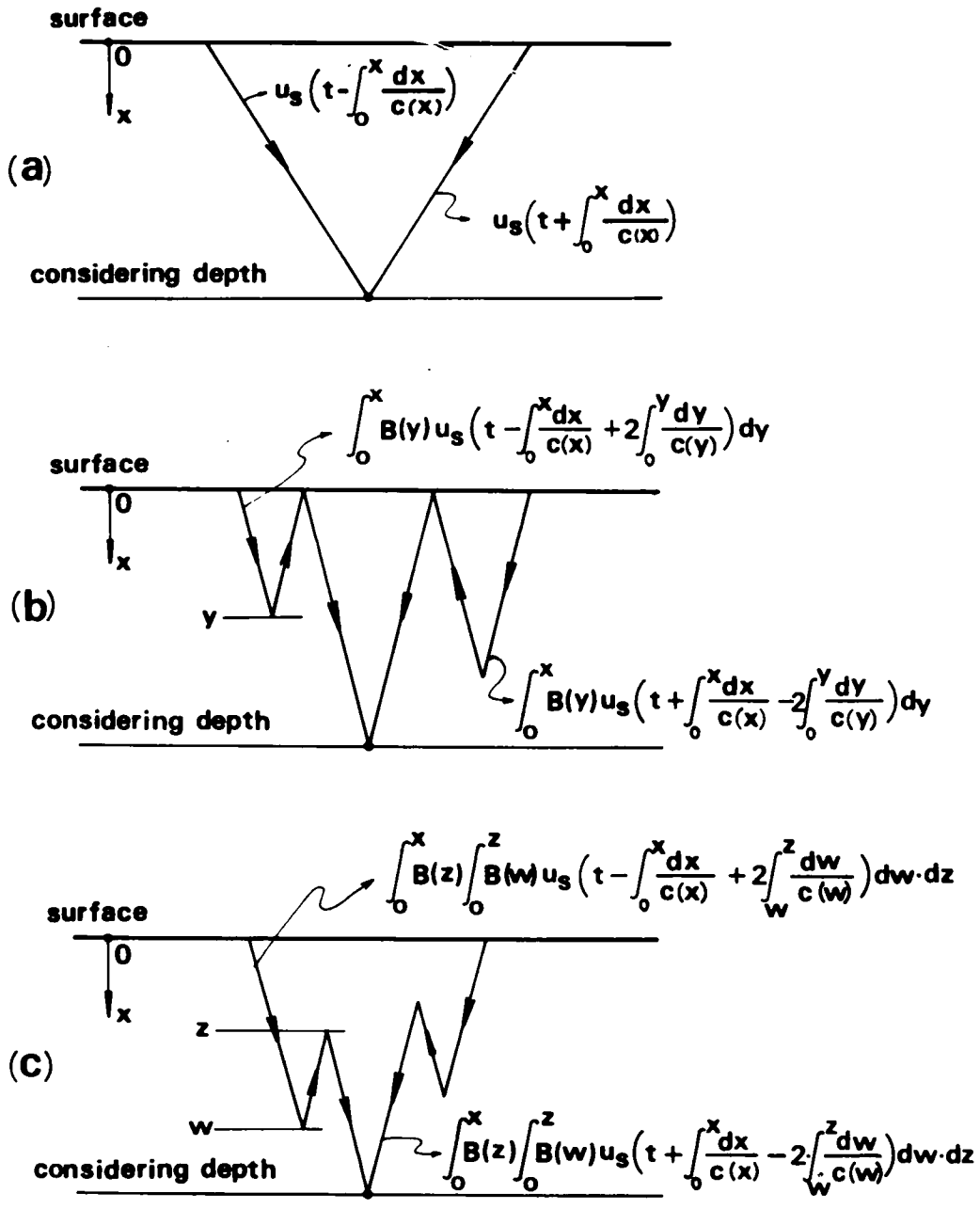

Fig.5.14 (a) direct transmission wave, (b) the first order reflection wave and (c) the second order reflection wave.

We assume that SH-wave is incident vertically to the surface layer and the incident earthquake motion is known.

5.5.1 Derivation of Equations for Response Analysis

The wave which is incident to the inhomogeneous layer, essentially reflects many times at the free surface and the interface between the superficial layer and the base rock, as shown in Fig.5.15. The wave energy is gradually absorbed by the base rock.

In order to calculate the surface motion as the response for the incident motion $u_0(t)$, we must calculate $u_{s1}(t)$, $u_{s2}(t)$, ..., etc. as indicated in Fig.5.15. Then, the final surface motion $u_s(t)$ is given by

$$u_s(t) = u_{s1}(t) + u_{s2}(t) + u_{s3}(t) + \cdots\cdots \tag{5.47}$$

If we adopt the approximation described in the previous section, $u_2(t)$, $u_3(t)$, ..., etc. can be related with $u_{s1}(t)$, $u_{s2}(t)$, ..., etc., respectively, according to Eq.(5.18). Now, we compute $u_{s1}(t)$, $u_{s2}(t)$, ..., etc. one by one from the known function $u_0(t)$.

At first, $u_1(t)$ can be related with $u_0(t)$ as

$$u_1(t) = \gamma_n u_0(t) \tag{5.48}$$

Eq.(5.17) for the ascending wave holds between $u_1(t)$ and $u_{s1}(t)$ and the new relation is given by

$$u_1(t) = \frac{1}{2} A(H) \left\{ u_{s1}\left(t + \int_0^H \frac{dx}{C(x)}\right) + \int_0^H B(y)\, u_{s1}\left(t + \int_0^H \frac{dx}{C(x)} - 2\int_0^y \frac{dy}{C(y)}\right) dy \right.$$

$$\left. + \int_0^H B(z) \int_0^z B(w)\, u_{s1}\left(t + \int_0^H \frac{dx}{C(x)} - 2\int_w^z \frac{dw}{C(w)}\right) dw\, dz \right\} \tag{5.49}$$

This equation is applicable when we know $u_{s1}(t)$. However, we know only

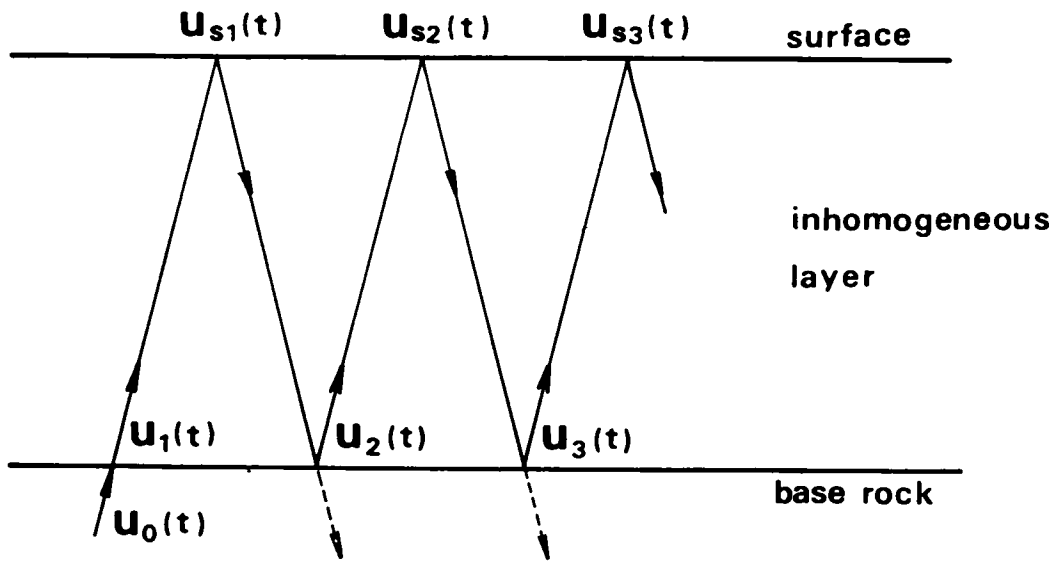

Fig.5.15 Multiple reflection of waves.

$u_1(t)$ from Eq.(5.48). Then, in order to transform Eq.(5.49) to the equation to give $u_{s1}(t)$ in terms of $u_1(t)$, we introduce the Fourier transform. The Fourier transformation of $u_1(t)$ is given by

$$U_1(i\omega) = \frac{1}{\sqrt{2\pi}} \int_{-\infty}^{\infty} u_1(t) e^{-i\omega t} dt \tag{5.50}$$

Similarly, for $u_{s1}(t)$,

$$U_{s1}(i\omega) = \frac{1}{\sqrt{2\pi}} \int_{-\infty}^{\infty} u_{s1}(t) e^{-i\omega t} dt \tag{5.51}$$

By the Fourier transfomation of Eq.(5.49), we obtain

$$U_{s1}(i\omega) = \frac{z\, U_1(i\omega)}{A(H)} \cdot \frac{1}{F(i\omega, H)} \tag{5.52}$$

where,

$$F(i\omega, H) = e^{-i\omega \int_0^H \frac{dx}{C(x)}} \left\{ 1 + \int_0^H B(y) e^{zi\omega \int_0^y \frac{dy}{C(y)}} dy + \int_0^H B(z) \int_0^z B(w) e^{zi\omega \int_w^z \frac{dw}{C(w)}} dw dz \right\} \tag{5.53}$$

$u_2(t)$ can be obtained in terms of $u_{s1}(t)$ by

$$u_2(t) = -\frac{1}{z} A(H) \beta_n \left\{ u_{s1}\left(t - \int_0^H \frac{dx}{C(x)}\right) + \int_0^H B(y)\, u_{s1}\left(t - \int_0^H \frac{dx}{C(x)} + 2\int_0^y \frac{dy}{C(y)}\right) dy + \int_0^H B(z) \int_0^z B(w)\, u_{s1}\left(t - \int_0^H \frac{dx}{C(x)} + 2\int_w^z \frac{dw}{C(w)}\right) dw dz \right\} \tag{5.54}$$

By the Fourier transformation of this equation, we obtain

$$U_2(i\omega) = -\frac{1}{z} A(H) \beta_n\, U_{s1}(i\omega)\, G(i\omega, H) \tag{5.55}$$

where, $U_2(i\omega)$ is the Fourier transform of $u_2(t)$. $G(i\omega, H)$ is given by

$$G(i\omega, H) = e^{i\omega\int_0^H \frac{dx}{C(x)}} \left\{ 1 + \int_0^H B(y) e^{-2i\omega\int_0^y \frac{dy}{C(y)}} dy \right.$$

$$\left. + \int_0^H B(z) \int_0^z B(w) e^{-2i\omega\int_w^H \frac{dw}{C(w)}} dw dz \right\} \qquad (5.56)$$

The similar relations as Eqs.(5.52) and (5.55) hold between $U_{s2}(i\omega)$, $U_{s3}(i\omega)$, ... , etc. and $U_3(i\omega)$, $U_4(i\omega)$, ... , etc., respectively, as follows;

$$U_{s2}(i\omega) = \frac{2U_2(i\omega)}{A(H)} \cdot \frac{1}{F(i\omega, H)}$$

$$U_{s3}(i\omega) = \frac{2U_3(i\omega)}{A(H)} \cdot \frac{1}{F(i\omega, H)}$$

..... (5.57)

and

$$U_3(i\omega) = -\frac{1}{2} A(H)\beta_n U_{s2}(i\omega) G(i\omega, H)$$

$$U_4(i\omega) = -\frac{1}{2} A(H)\beta_n U_{s3}(i\omega) G(i\omega, H)$$

..... (5.58)

The Fourier transform of Eq.(5.48) is given by

$$U_1(i\omega) = \gamma_n U_0(i\omega) \qquad (5.59)$$

From Eqs.(5.52), (5.55), (5.57), (5.58) and (5.59),

$$U_{s1}(i\omega) = \frac{2\gamma_n}{A(H)} U_0(i\omega)$$

$$U_{s2}(i\omega) = -\frac{2\gamma_n}{A(H)} U_0(i\omega) \cdot \frac{\beta_n G(i\omega, H)}{\{F(i\omega, H)\}^2}$$

$$U_{s3}(i\omega) = \frac{2\gamma_n}{A(H)} U_0(i\omega) \cdot \frac{\{\beta_n G(i\omega, H)\}^2}{\{F(i\omega, H)\}^3}$$

..... (5.60)

Therefore, we obtain the surface motion, $U_s(i\omega)$, in the Fourier transform from Eq.(5.47) as follows;

$$U_s(i\omega) = U_{s1}(i\omega) + U_{s2}(i\omega) + U_{s3}(i\omega) + \cdots$$

$$= \frac{2\gamma_n}{A(H)} U_0(i\omega) \cdot \frac{1}{F(i\omega,H)} \left[1 - \frac{G(i\omega,H)}{F(i\omega,H)} \beta_n + \left\{ \frac{G(i\omega,H)}{F(i\omega,H)} \beta_n \right\}^2 - \cdots \right.$$

$$= \frac{2\gamma_n}{A(H)} U_0(i\omega) \cdot \frac{1}{F(i\omega,H) + \beta_n G(i\omega,H)} \tag{5.61}$$

In the above equation, $F(i\omega,H) + \beta_n G(i\omega,H)$ reduces further to

$$F(i\omega,H) + \beta_n G(i\omega,H) = \gamma_n (p' + i\alpha_n q') \tag{5.62}$$

where, p' and q' are similar as p and q in Eqs.(5.33) and (5.34), respectively, and expressed as

$$p' = \cos\left(\omega \int_0^H \frac{dx}{C(x)}\right) + \int_0^H B(y) \cos\left(\omega \int_0^H \frac{dx}{C(x)} - 2\omega \int_0^y \frac{dy}{C(y)}\right) dy$$

$$+ \int_0^H B(z) \int_0^z B(w) \cos\left(\omega \int_0^H \frac{dx}{C(x)} - 2\omega \int_w^z \frac{dw}{C(w)}\right) dw dz \tag{5.63}$$

$$q' = \sin\left(\omega \int_0^H \frac{dx}{C(x)}\right) + \int_0^H B(y) \sin\left(\omega \int_0^H \frac{dx}{C(x)} - 2\omega \int_0^y \frac{dy}{C(y)}\right) dy$$

$$+ \int_0^H B(z) \int_0^z B(w) \sin\left(\omega \int_0^H \frac{dx}{C(x)} - 2\omega \int_w^z \frac{dw}{C(w)}\right) dw dz \tag{5.64}$$

So that, Eq.(5.61) becomes

$$U_s(i\omega) = \frac{2}{A(H)} U_0(i\omega) \cdot \frac{1}{p' + i\alpha_n q'} \tag{5.65}$$

When the surface motion $u_s(t)$ is known, the way to calculate the underground motion $u(t,x)$ from $u_s(t)$, has been presented in the previous section. From Eqs.(5.17), (5.18) and (5.19), this means that the Fourier transform of $u(t,x)$ is expressed in term of $U_s(i\omega)$ as follows;

$$U_x(i\omega) = A(x)\,p''\,U_s(i\omega) \tag{5.66}$$

where, $U_x(i\omega)$ is the Fourier transform of $u(t,x)$. p'' is given by

$$p'' = \cos\left(\omega\int_0^x \frac{dx}{c(x)}\right) + \int_0^x B(y)\cos\left(\omega\int_0^x \frac{dx}{c(x)} - 2\omega\int_0^y \frac{dy}{c(y)}\right)dy$$

$$+ \int_0^x B(z)\int_0^z B(w)\cos\left(\omega\int_0^x \frac{dx}{c(x)} - 2\omega\int_w^z \frac{dw}{c(w)}\right)dw\,dz \tag{5.67}$$

Finally, we can obtain the surface motion $u_s(t)$ and the underground motion $u(t,x)$ in time domain by means of the inverse transform of $U_s(i\omega)$ and $U_x(i\omega)$, as follows;

$$u_s(t) = \frac{1}{\sqrt{2\pi}}\int_{-\infty}^{\infty} U_s(i\omega)e^{i\omega t}d\omega$$

$$u(t,x) = \frac{1}{\sqrt{2\pi}}\int_{-\infty}^{\infty} U_x(i\omega)e^{i\omega t}d\omega \tag{5.68}$$

In the actual computations of the Fourier transform and the inverse transform by computers, it is known to be convenient to use F.F.T..

5.5.2 Numerical Example

As a numerical example, the earthquake response of Osaka area has been examined by the method presented in 5.5.1. Osaka is a controlling city for the west part of Japan, and its population and house density have been heavily increasing. So that, the potential of the earthquake damage becomes increasing. From a point of view of the disaster prevention, Yoshikawa and Iwasaki have thoroughly investigated the history of earthquakes, the response characteristics, the geometrical formation of Osaka area and its dynamic properties[17), 22), 23)]. Furthermore, they computed the ground earthquake response motions by the lumped-mass modal analysis method and concluded that

the computed motions agreed with the recorded motions[23]. Owing to their extensive researches, we may be able to roughly predict the behavior of Osaka ground during earthquakes.

As found later, the vertical distributions of S-wave velocity and the density through the superficial soil layer in Osaka, can be expressed by suitable functions. Therefore, we can easily apply the approximate technique presented in this section. By this technique, the characteristics of ground shaking, response motions and the vertical distributions of maximum accelerations and shear strains during a strong earthquake are computed.

Geological Formation of Osaka Area

Yoshikawa and Iwasaki[23] summarized the results on the dynamic properties of Osaka soils explored by many researchers, and showed the geological formations and their dynamic properties as presented in Table 5.2. Below the top subsurface of alluvium clay and sand layers with 0-40 m thick, 400-800 m thick diluvium layers called as Upper Pleistocene Formations, Osaka Group and Infra Osaka Group consisting of clay, sand and gravel layers and tertiary sand and clay soft rock layers called as Kobe Group and Nijo Group with thickness about 300 m, continue down to the granitic base rock which exists about 700-1400 m below the ground surface[24]. The S-wave velocity and the unit weight of the ground are increasing nearly monotonously with the depth. For the analysis of the response, the distribution functions of the S-wave velocity and the unit weight were determined as indicated in Fig.5.16, where the granitic layer was considered as the base rock. At the interface between the base rock and the bottom boundary of the surface layer, the ratio of the characteristic impedance α_n is 0.187.

Incident Earthquake Motions at the Base Rock

By the principle of the multiple reflection theory, the incident earthquake motion at the base rock was inferentially computed by using the accelerogram of El Centro earthquake of May 18, 1940, which is shown in Fig.5.17.

Table 5.2 The geological formations of Osaka area and their dynamic properties[23].

	thickness m	S wave velocity m/sec	unit weight g/cm^3
Alluvium clay	0 ~ 40	80 ~ 190	1.5 ~ 1.6
Alluvium sand		110 ~ 190	1.5 ~ 1.7
Upper Pleistocene Formations	400~800	200 ~ 600	1.6 ~ 1.9
Osaka Group			
Infra Osaka Group			
Kobe Group Nijo Group	300	500 ~ 800	2.0 ~ 2.1
Grantic base rock		2700~3000	2.7

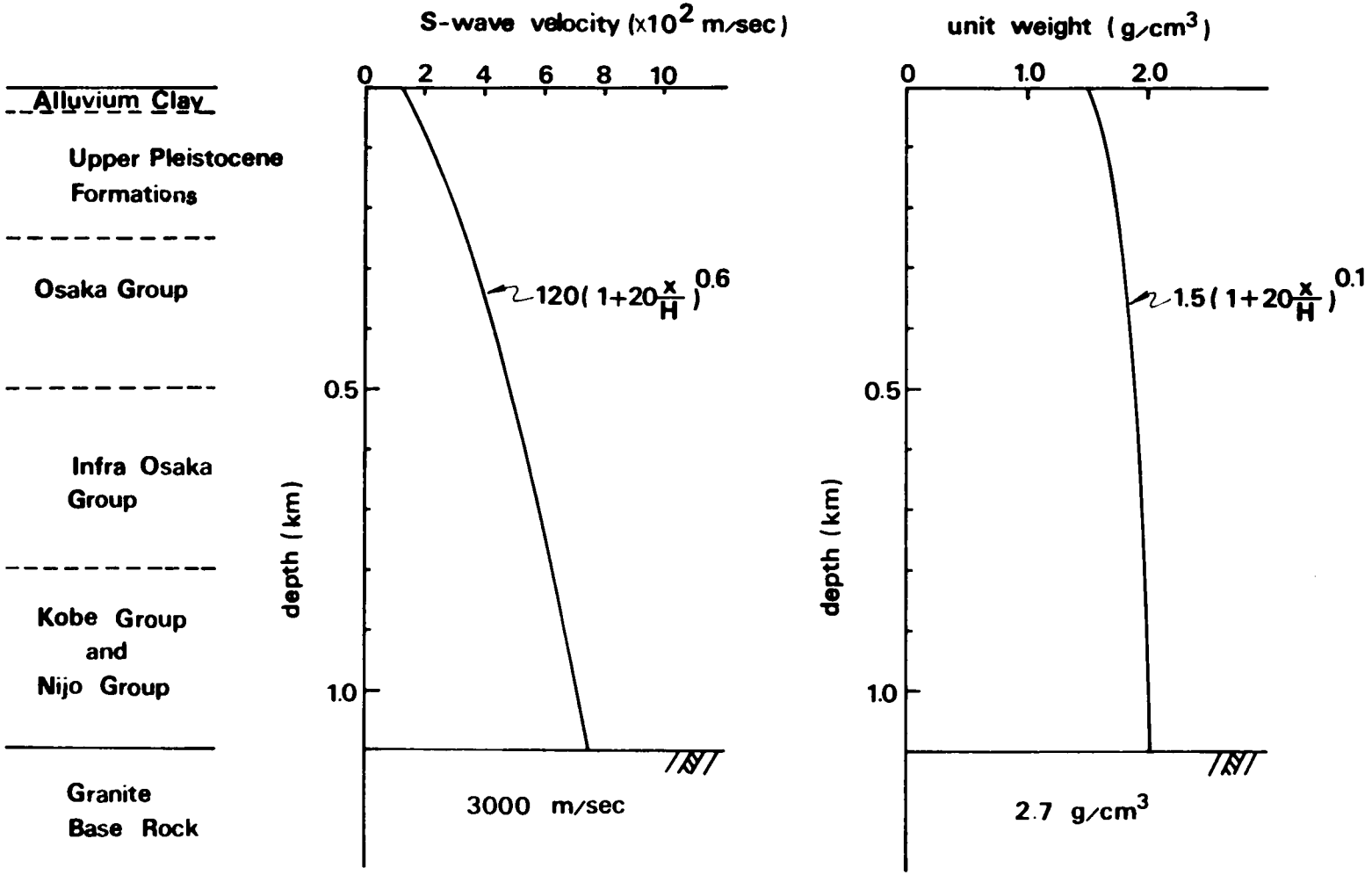

Fig.5.16 The assumed distribution functions of the S-wave velocity and the unit weight in Osaka ground.

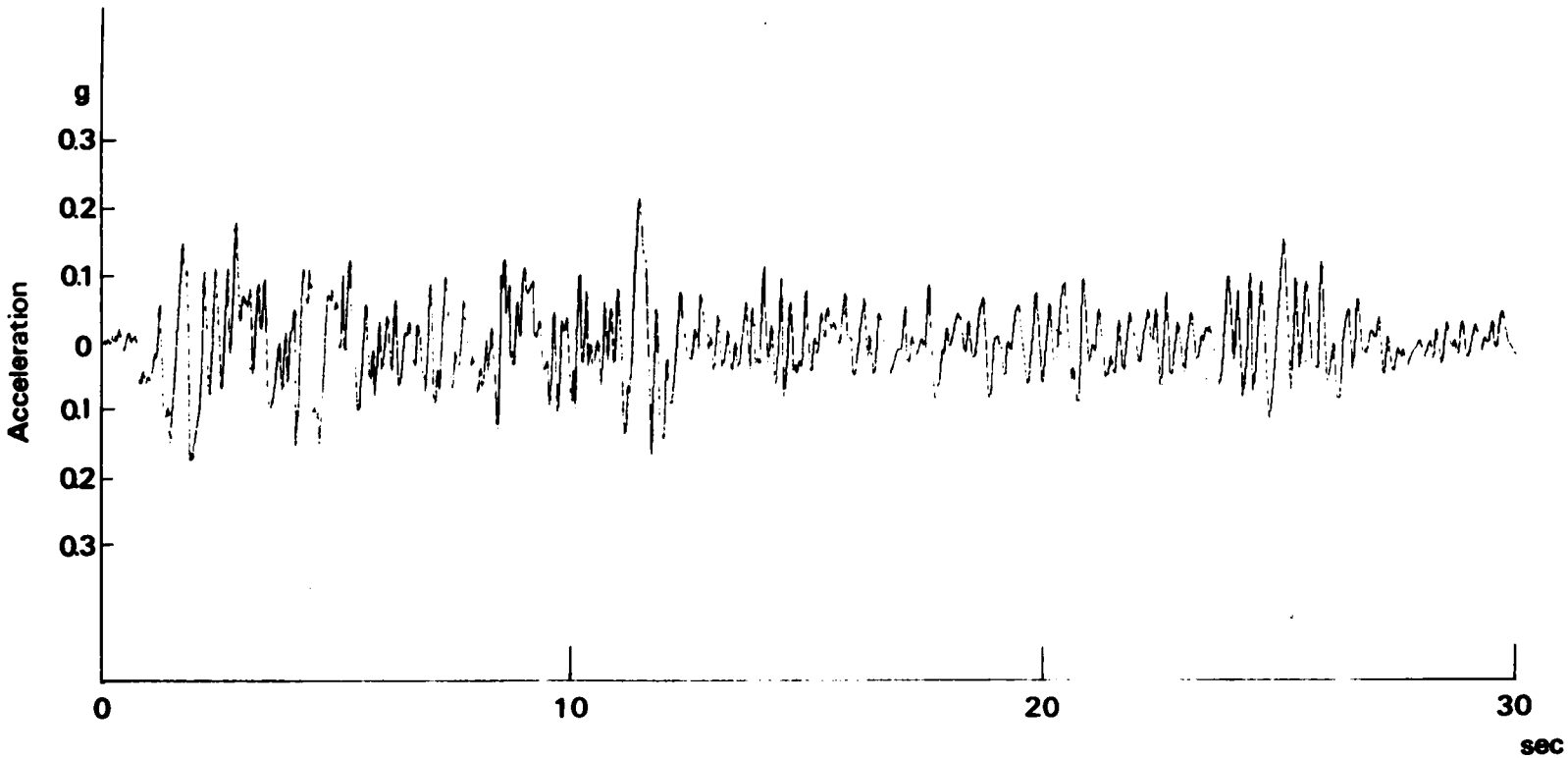

Fig.5.17 The accelerogram of El Centro Earthquake, of May 18, 1940, component EW.

Fig.5.18 shows the power spectrum density function of the accelerogram.

The geological formation for the El Centro location is shown in Fig.5.19 which includes layer thicknesses, wave velocities and densities[25]. The layer which lies 19 m below the surface of the ground, can be considered to be the base rock. The incident motion $u_0(t)$ at the base rock was computed by

$$u_0(t) = \frac{1}{2\gamma}\left\{ u_s(t) + \beta\, u_s(t-2\tau) \right\} \tag{5.69}$$

where, γ and β are the transmission and the reflection coefficients, and $u_s(t)$ is the surface motion. τ is given by

$$\tau = \frac{H_1}{V_s} \tag{5.70}$$

where, V_s is the shear wave velocity of the first layer. The computed incident motion is shown in Fig.5.20. The maximum acceleration is 76 gal (0.078 g) and the prominent period T_p is about 0.3 $sec.$. The power spectrum density function of the motion is shown in Fig.5.21.

The above computed incident motion is used as the base rock motion of Osaka ground in the analysis.

Characteristics of Ground Shaking

The characteristic of ground shaking was calculated under the inhomogeneous conditions as indicated in Fig.5.16, by the way described in 5.4.3. In this case, p and q in Eqs.(5.33) and (5.34) are given by

$$\begin{aligned} p = {} & \cos(g(1)a_0) + \frac{7}{8}\left[\cos\left\{a_0\left(g(1)+\frac{1}{4}\right)\right\}\left\{C_i\left(\frac{21}{4}^{0.4}a_0\right) - C_i\left(\frac{a_0}{4}\right)\right\}\right. \\ & \left. + \sin\left\{a_0\left(g(1)+\frac{1}{4}\right)\right\}\left\{S_i\left(\frac{21}{4}^{0.4}a_0\right) - S_i\left(\frac{a_0}{4}\right)\right\}\right] \\ & + \frac{49}{8}\int_0^1 \frac{1}{1+20z}\left[\cos\left\{a_0\left(g(1)-\frac{1}{4}(1+20z)^{0.4}\right)\right\}\left\{C_i\left(\frac{a_0}{4}(1+20z)^{0.4}\right) - C_i\left(\frac{a_0}{4}\right)\right\}\right. \\ & \left. - \sin\left\{a_0\left(g(1)-\frac{1}{4}(1+20z)^{0.4}\right)\right\}\left\{S_i\left(\frac{a_0}{4}(1+20z)^{0.4}\right) - S_i\left(\frac{a_0}{4}\right)\right\}\right] dz \end{aligned} \tag{5.71}$$

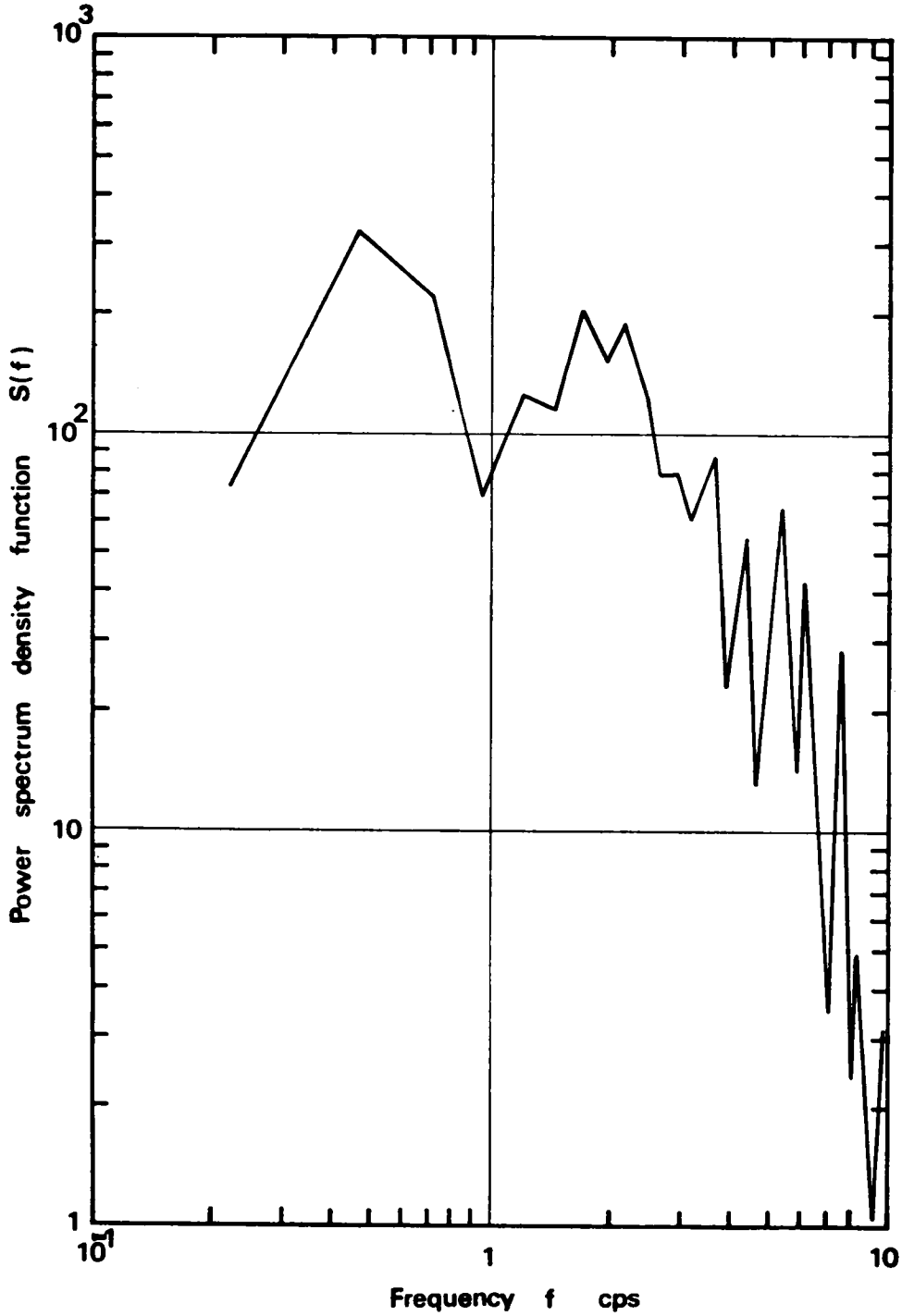

Fig.5.18 The power spectrum density function of the accelerogram for the El Centro.

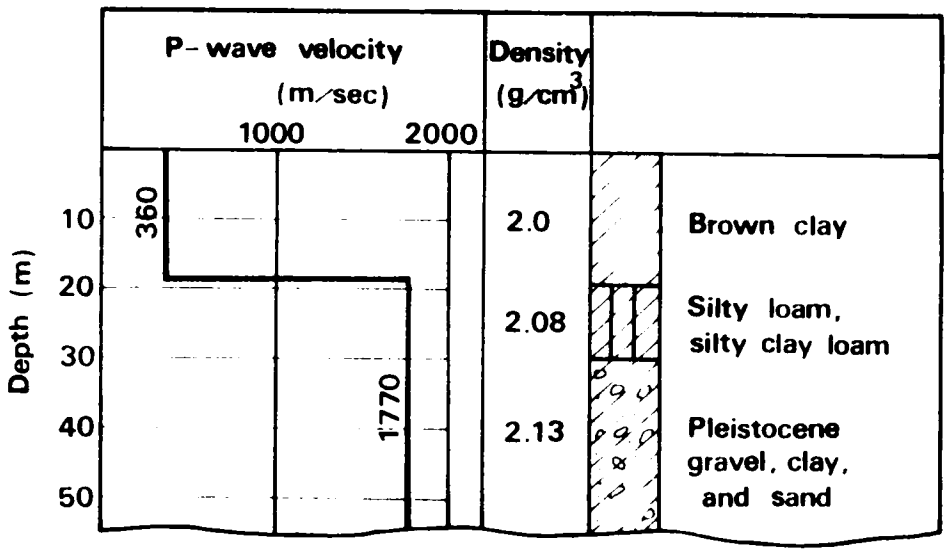

Site	First Layer				Second Layer		
	H_1	V_p	V_s	ρg	V_p	V_s	ρg
El Centro	19	360	157	2.0	1,770	843	2.08

Fig.5.19 Site characteristics at El Centro(after Toki and Cherry[25]).

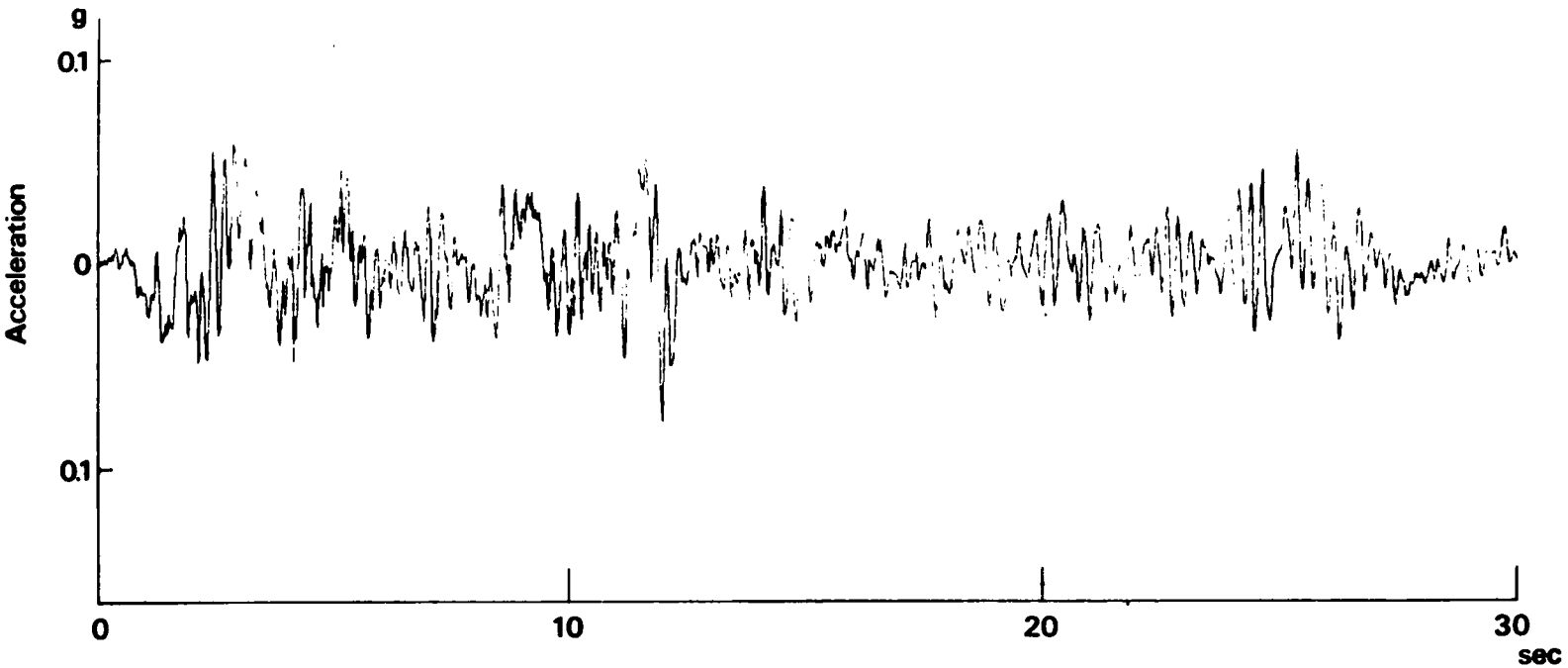

Fig.5.20 Computed incident motion at the base rock for the El Centro.

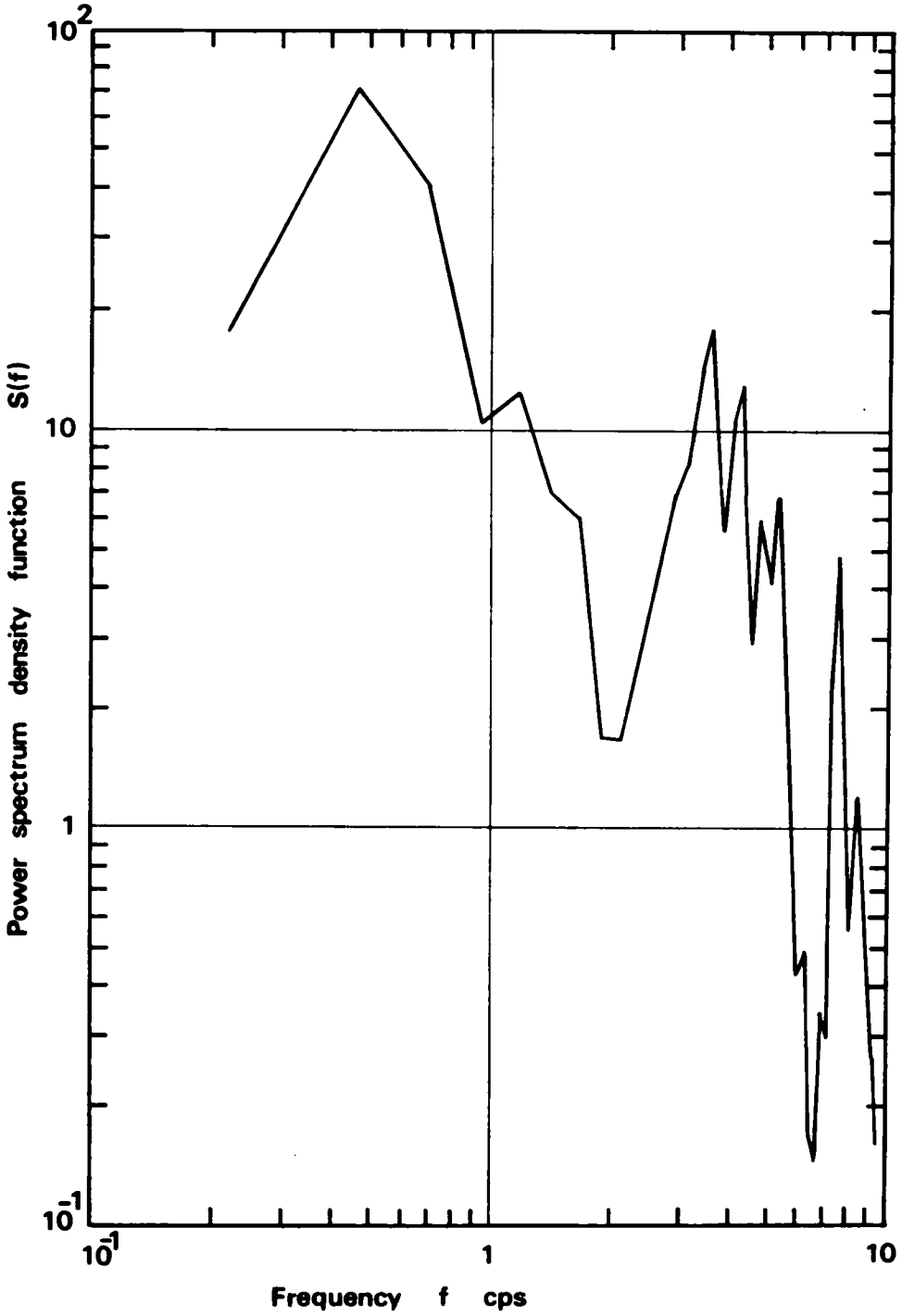

Fig.5.21 Power spectrum density function of the incident motion.

$$
\begin{aligned}
g = \sin\left(g(1)a_0\right) + \frac{7}{8}\Bigg[& \sin\left\{a_0\left(g(1)+\frac{1}{4}\right)\right\}\left\{C_i\left(\frac{21^{0.4}}{4}a_0\right) - C_i\left(\frac{a_0}{4}\right)\right\} \\
& - \cos\left\{a_0\left(g(1)+\frac{1}{4}\right)\right\}\left\{S_i\left(\frac{21^{0.4}}{4}a_0\right) - S_i\left(\frac{a_0}{4}\right)\right\}\Bigg] \\
& + \frac{49}{8}\int_0^1 \frac{1}{1+20\zeta}\Bigg[\sin\left\{a_0\left(g(1) - \frac{1}{4}(1+20\zeta)^{0.4}\right)\right\}\left\{C_i\left(\frac{a_0}{4}(1+20\zeta)^{0.4}\right) - C_i\left(\frac{a_0}{4}\right)\right\} \\
& + \cos\left\{a_0\left(g(1) - \frac{1}{4}(1+20\zeta)^{0.4}\right)\right\}\left\{S_i\left(\frac{a_0}{4}(1+20\zeta)^{0.4}\right) - S_i\left(\frac{a_0}{4}\right)\right\}\Bigg] d\zeta
\end{aligned}
\tag{5.72}
$$

where, $g(1)$ is given by

$$
g(1) = \int_0^1 \frac{d\xi}{(1+20\xi)^{0.6}} \tag{5.73}
$$

and a_0 is the dimensionless frequency defined in Eq.(5.35). The numerical results of the amplitude and the phase characteristics at the surface are shown in Fig.5.22 to Fig.5.24. It is found from these figures that the amplification of the amplitude is considerably large. The fundamental period is 8.06 *sec.* which is a relatively long period because of taking into account the deep geological formations of about 1 *km* below the surface.

Earthquake Response Motions on the Surface and in the Underground

Earthquake response motions on the surface and in the underground were computed by the method described in the preceding subsection. As the incident earthquake motion, the acceleration presented in Fig.5.20 was given at the granitic base rock of Osaka. The computed accelerations at the surface and 500 *m* below the surface are shown in Fig.5.25. The maximum acceleration at the surface is 526 *gal*(0.54 *g*) and the frequency components of 0.45, 0.82 and 3.7 *cps* are prominent as found from Fig.5.26. The distribution of the maximum accelerations in the ground is shown in Fig.5.27. It is found from this figure that the maximum acceleration rapidly decreases at the depth of

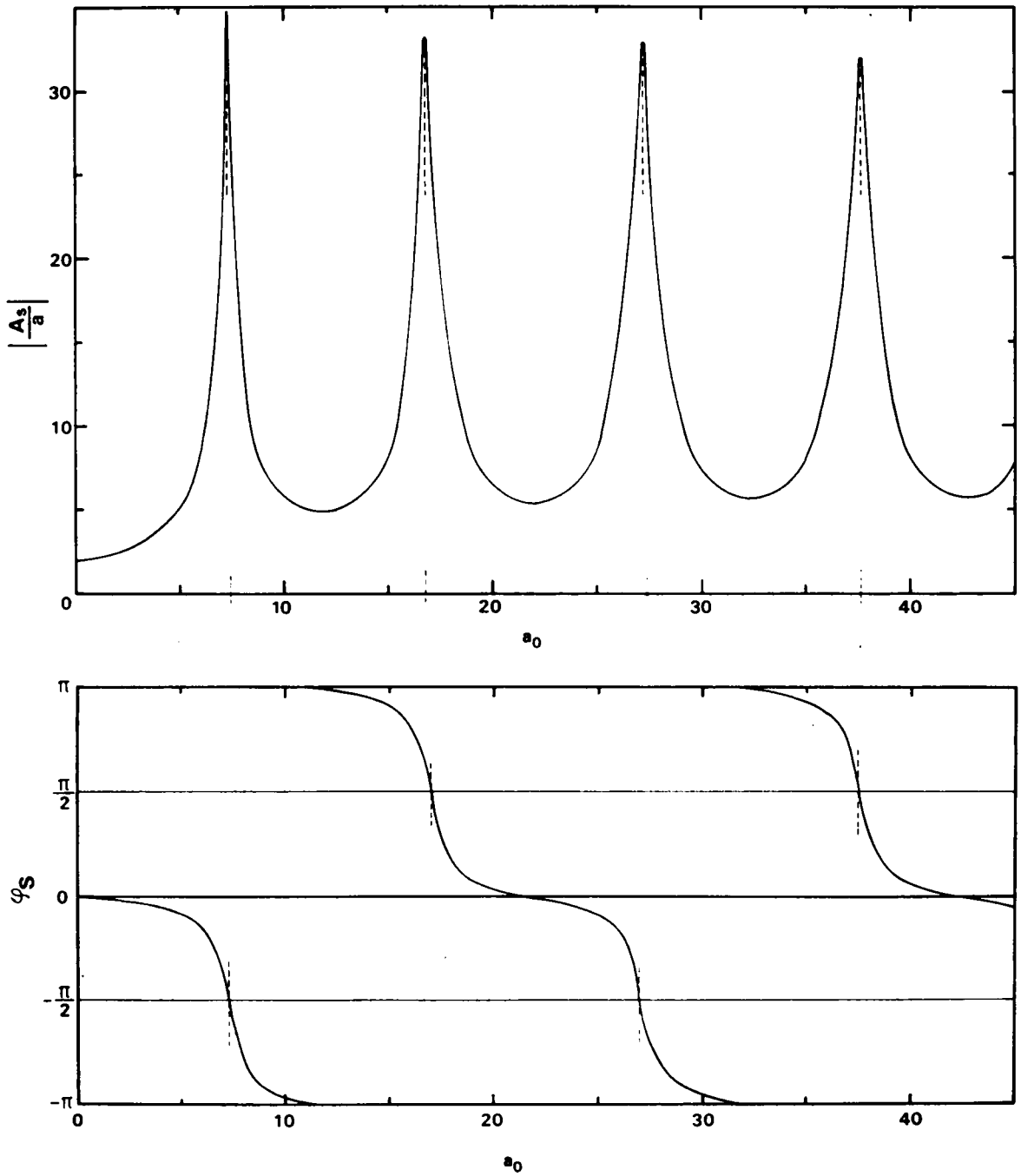

Fig.5.22 Characteristics of ground shaking, a_o= 0 - 45(f = 0 - 0.78cps).

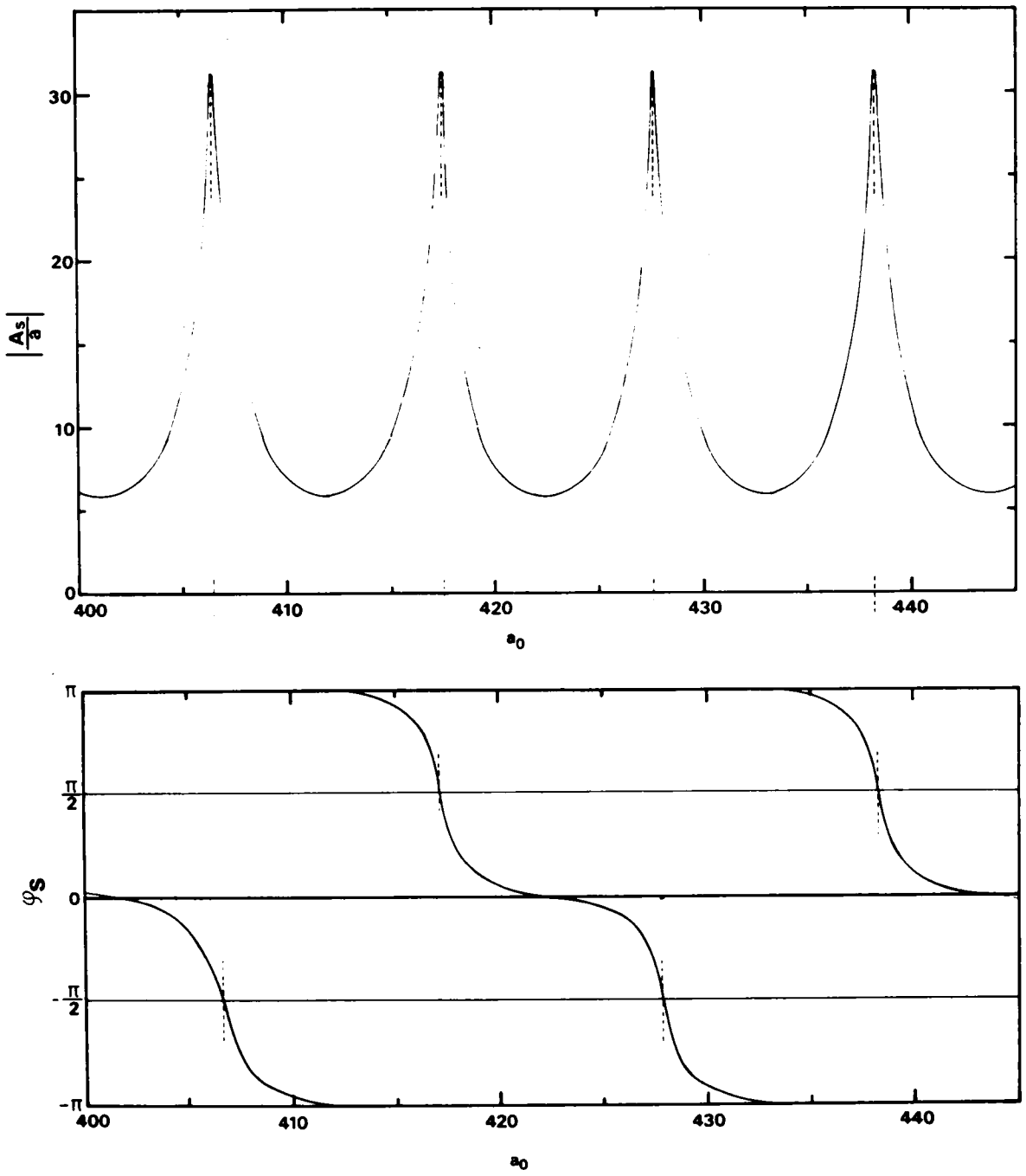

Fig.5.23 Continued, a_o = 400 - 450(f = 6.94 - 7.81cps).

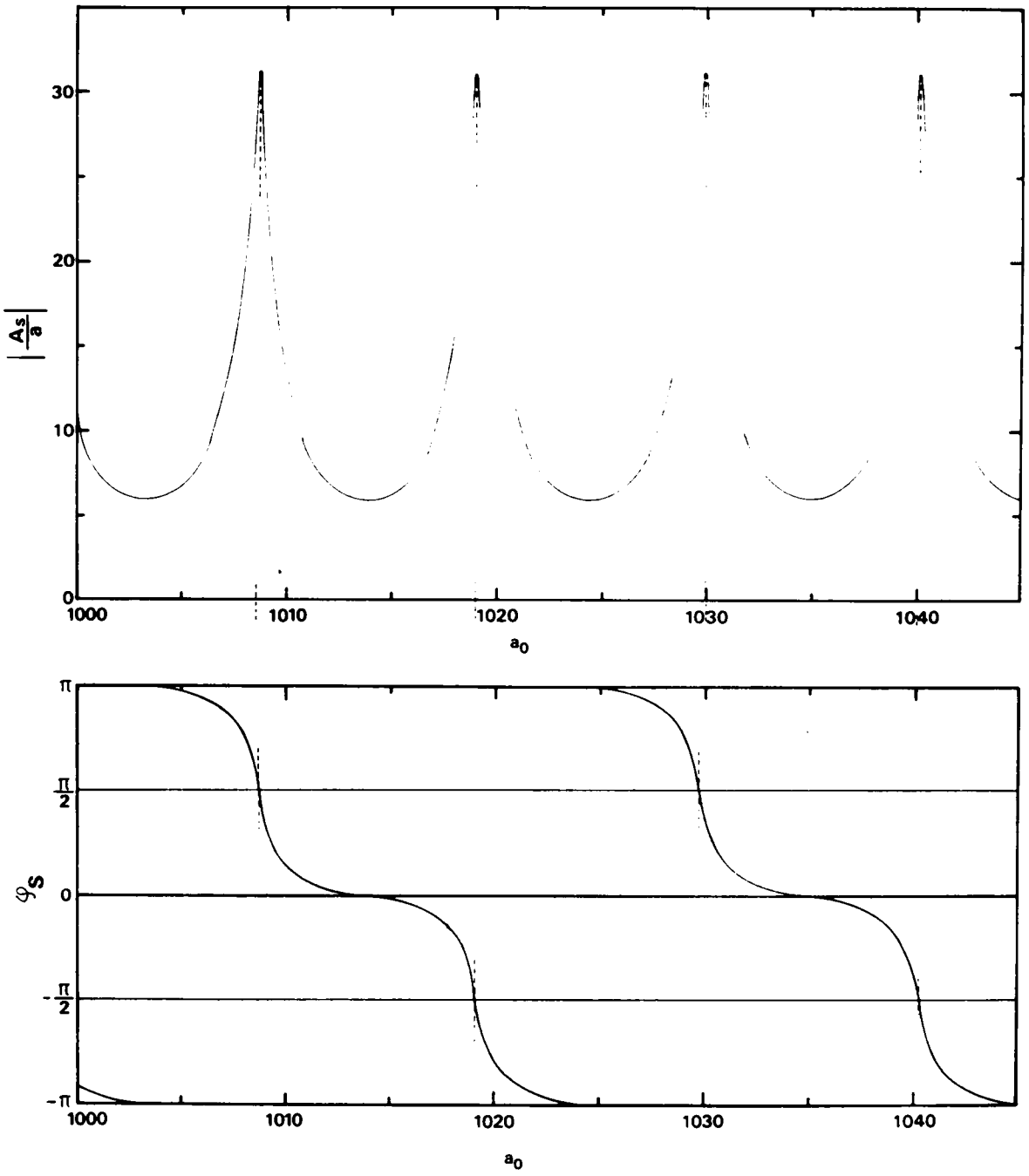

Fig.5.24 Continued, a_o = 1000 - 1045(f = 17.36 -18.14cps).

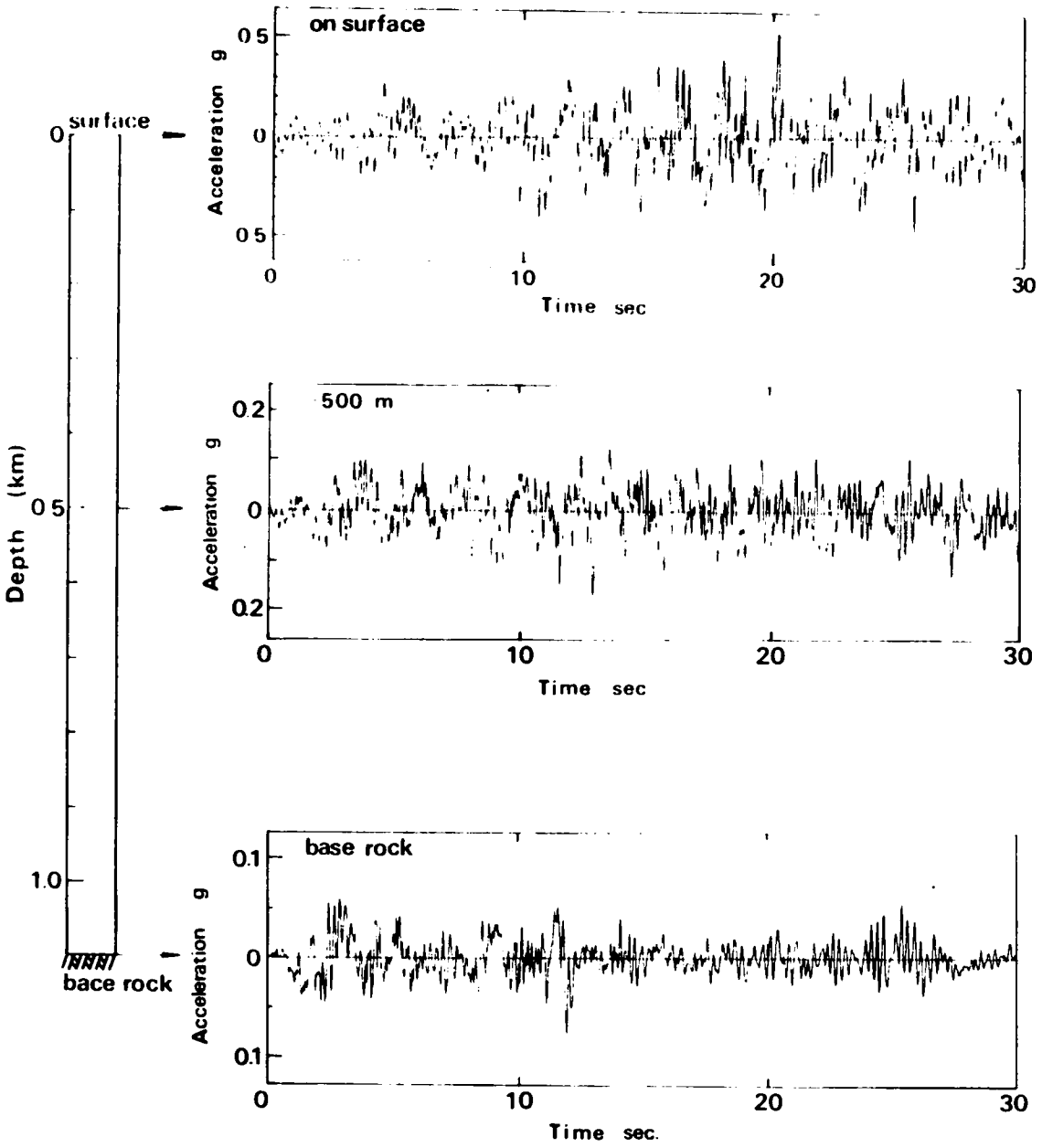

Fig.5.25 Computed accelerations at the surface and 500m in the depth.

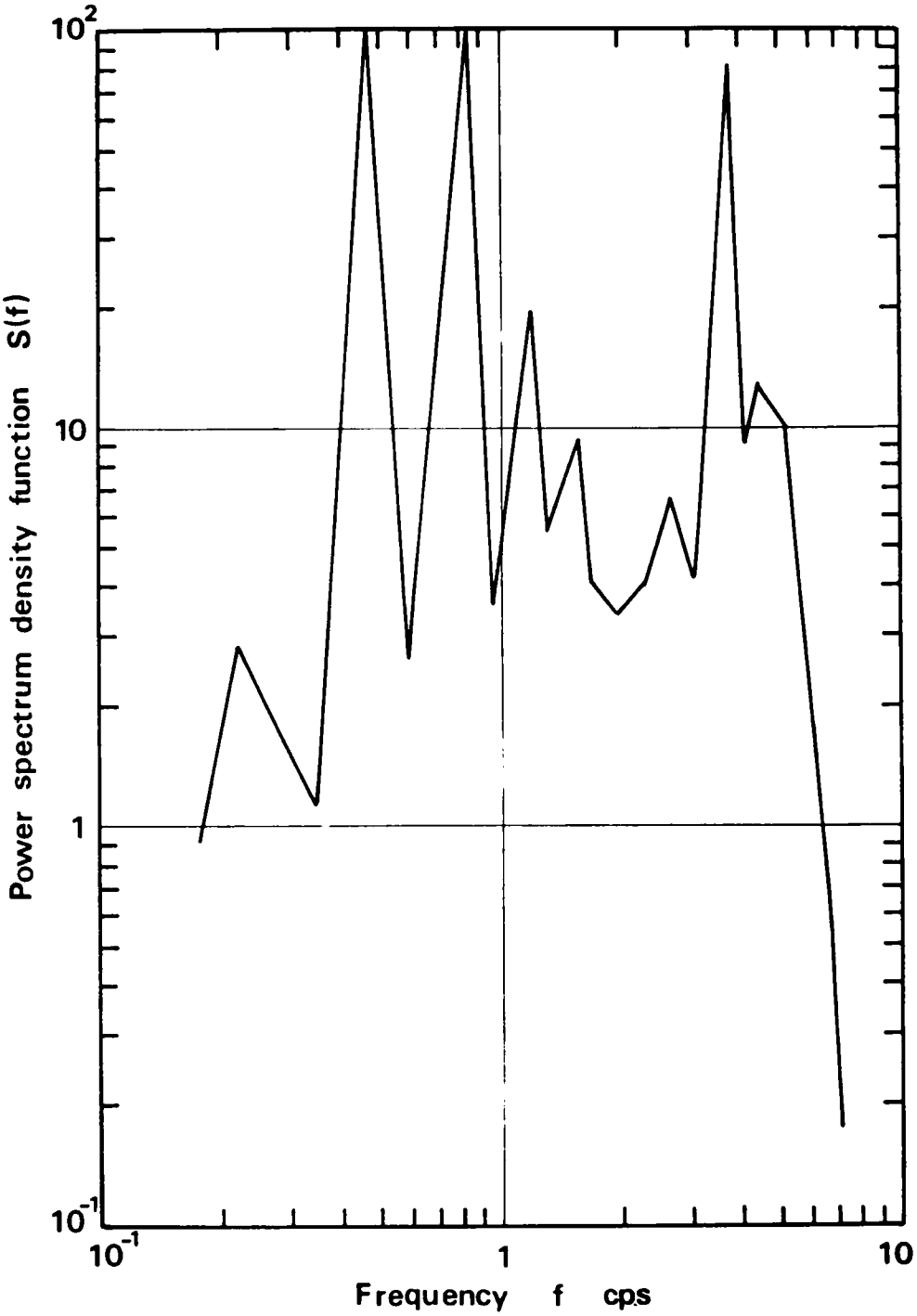

Fig.5.26 Power spectrum density function of the computed accelerogram at the surface.

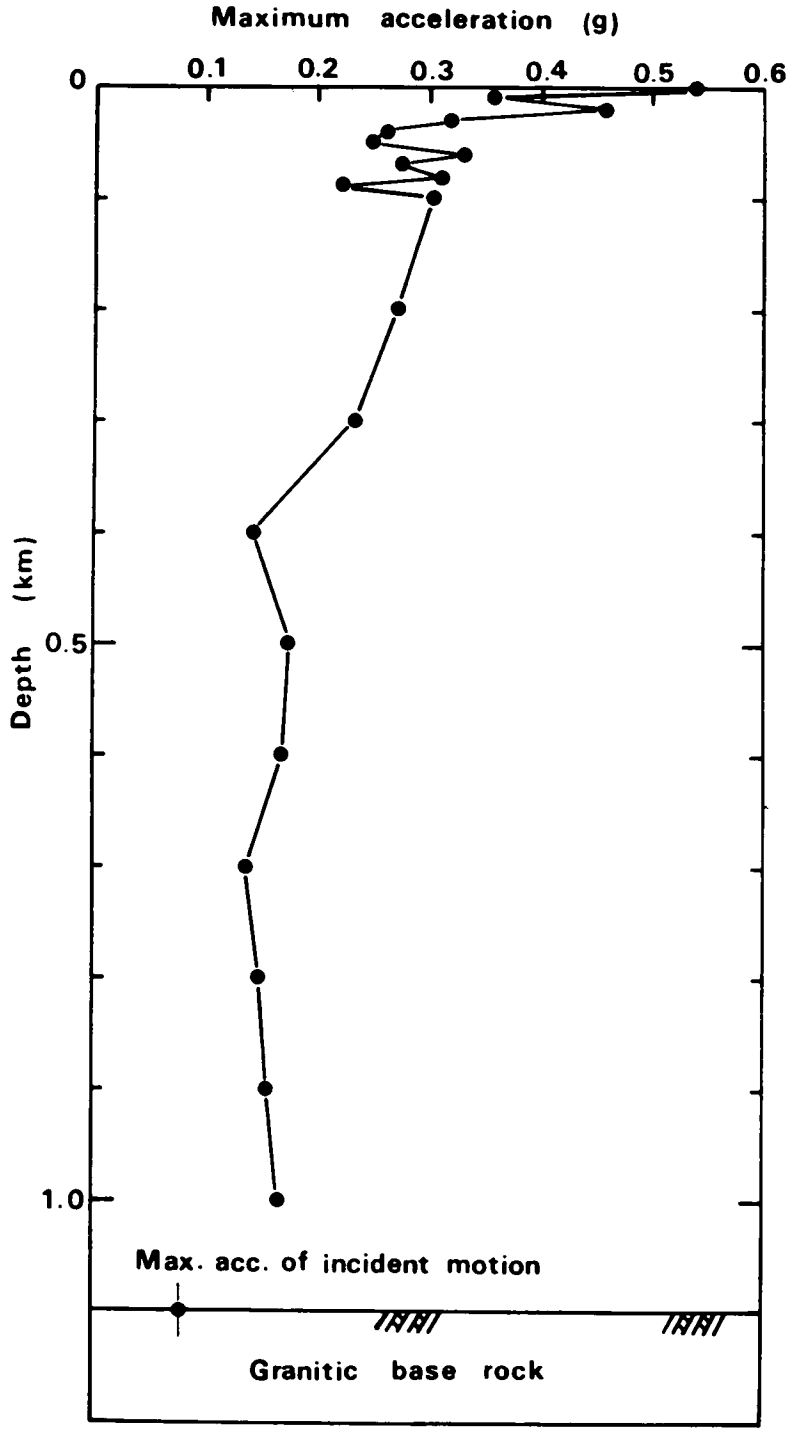

Fig.5.27 Distribution of the maximum acceleration in the ground.

100 m, and 400 m below the surface, it is almost constant of about 0.15 g. That is, the earthquake motions are amplified in the top surface layer of alluvium clay and sand with relatively low rigidity.

Underground Shear Strain

It is interested from a viewpoint of the soil dynamics to know the level of shear strain occurring in the ground during a strong earthquake.

From Eq.(5.6), the equation to calculate the shear strain $\gamma(t,x)$ at the arbitrary depth in the inhomogeneous soil layer can be derived as follows;

$$\begin{aligned}
\gamma(t,x) &= \lim_{\tau_i \to 0} \frac{u_i(t,0) - u_i(t,H_i)}{H_i} \\
&= \lim_{\tau_i \to 0} \frac{U_i(t) - U_i(t-\tau_i) + D_i(t-\tau_i) - D_i(t)}{H_i} \\
&= \lim_{\tau_i \to 0} \frac{1}{\tau_i c_i} \left\{ \tau_i \frac{\partial U_i}{\partial t} - \tau_i \frac{\partial D_i}{\partial t} \right\} \\
&= \lim_{\tau_i \to 0} \frac{1}{c_i} \left(\frac{\partial U_i}{\partial t} - \frac{\partial D_i}{\partial t} \right) \\
&= \frac{1}{c(x)} \left\{ \frac{\partial U(t,x)}{\partial t} - \frac{\partial D(t,x)}{\partial t} \right\}
\end{aligned} \tag{5.74}$$

In this equation, $\frac{\partial U(t,x)}{\partial t}$ and $\frac{\partial D(t,x)}{\partial t}$ correspond to velocities of the ascending and the descending wave, respectively. By using Eq.(5.74), the underground shear strain in time domain was computed, where the time variations of acceleration were integrated to obtain the time variations of velocity. The computed shear strains at the 10 m, 500 m and 1000 m in the depth are shown in Fig. 5.28. At the near surface, the time variation of the strain is complicated. On the other hand, as the depth increases, the time variation of the shear strain is relatively smooth and the long period component is prominent.

From the strain curve at each depth, the maximum value of shear strain was read and plotted in Figs.5.29 and 5.30. Fig.5.29 shows the distribution

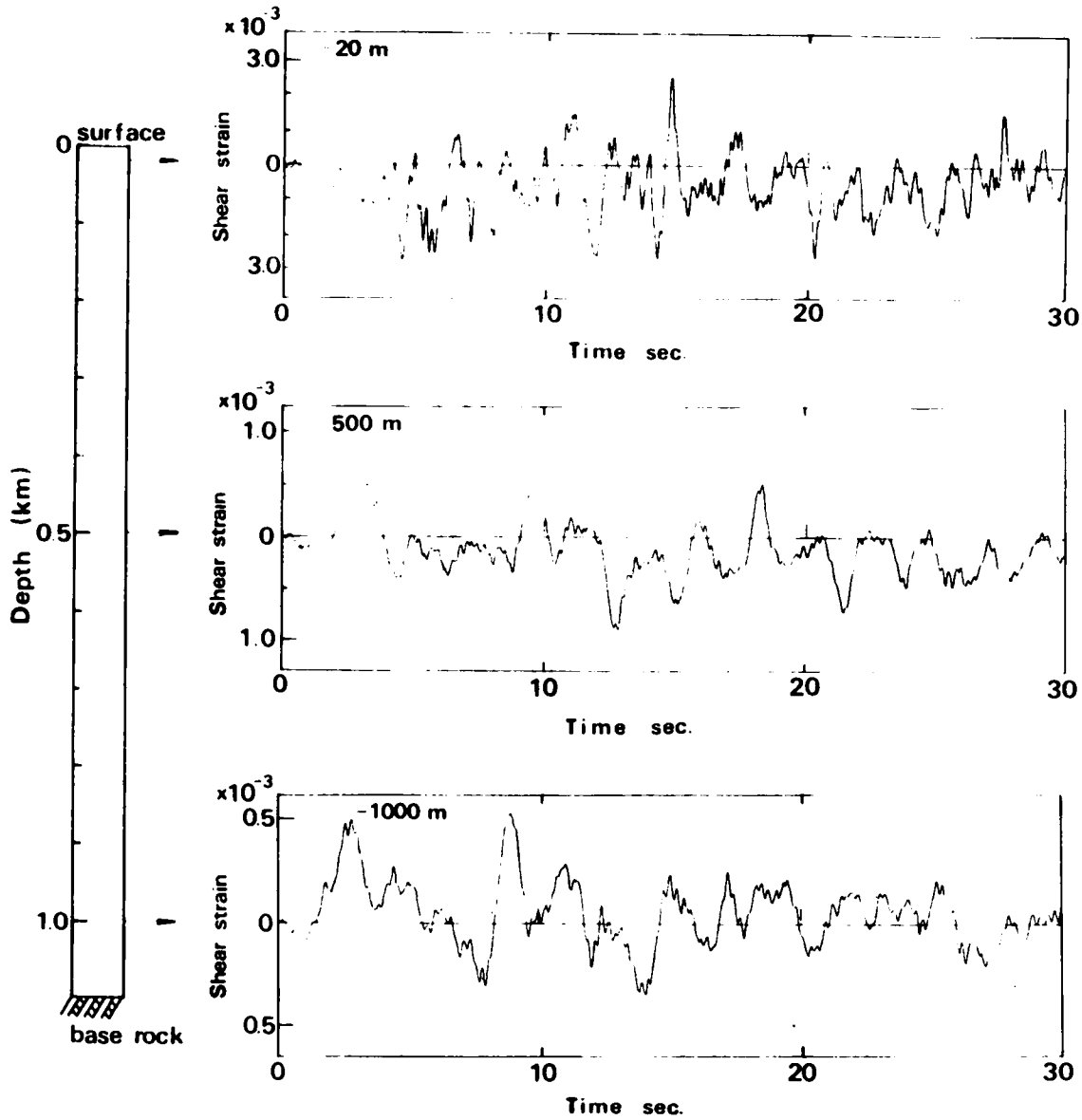

Fig.5.28 Shear strain curves at 10*m*, and 500*m* and 1000*m* in the depth.

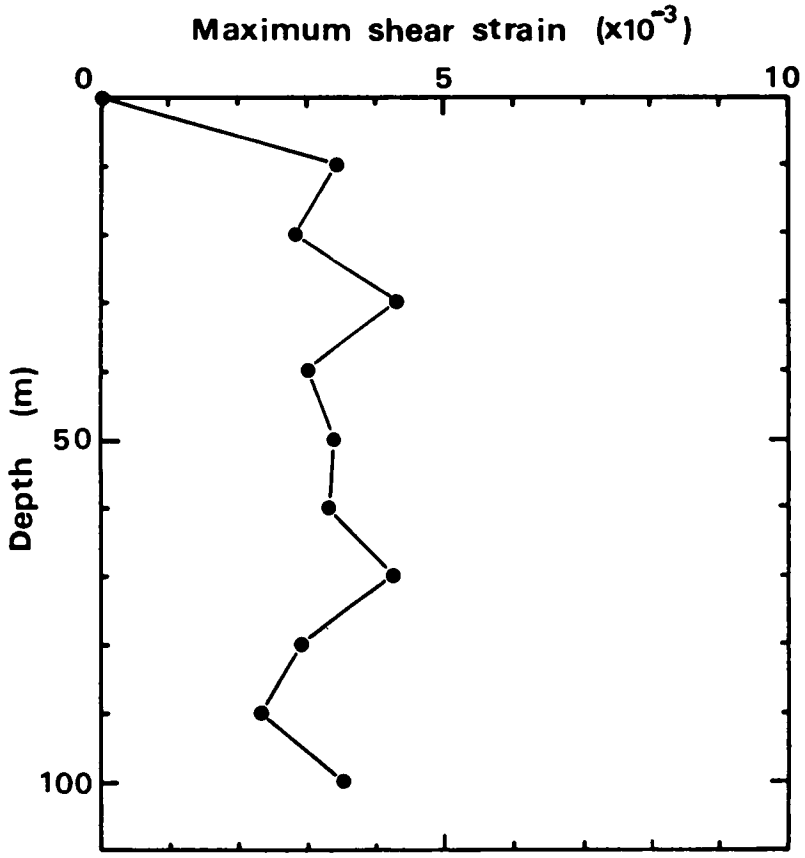

Fig.5.29 Distribution of maximum shear strain in the ground up to 100*m* below the surface.

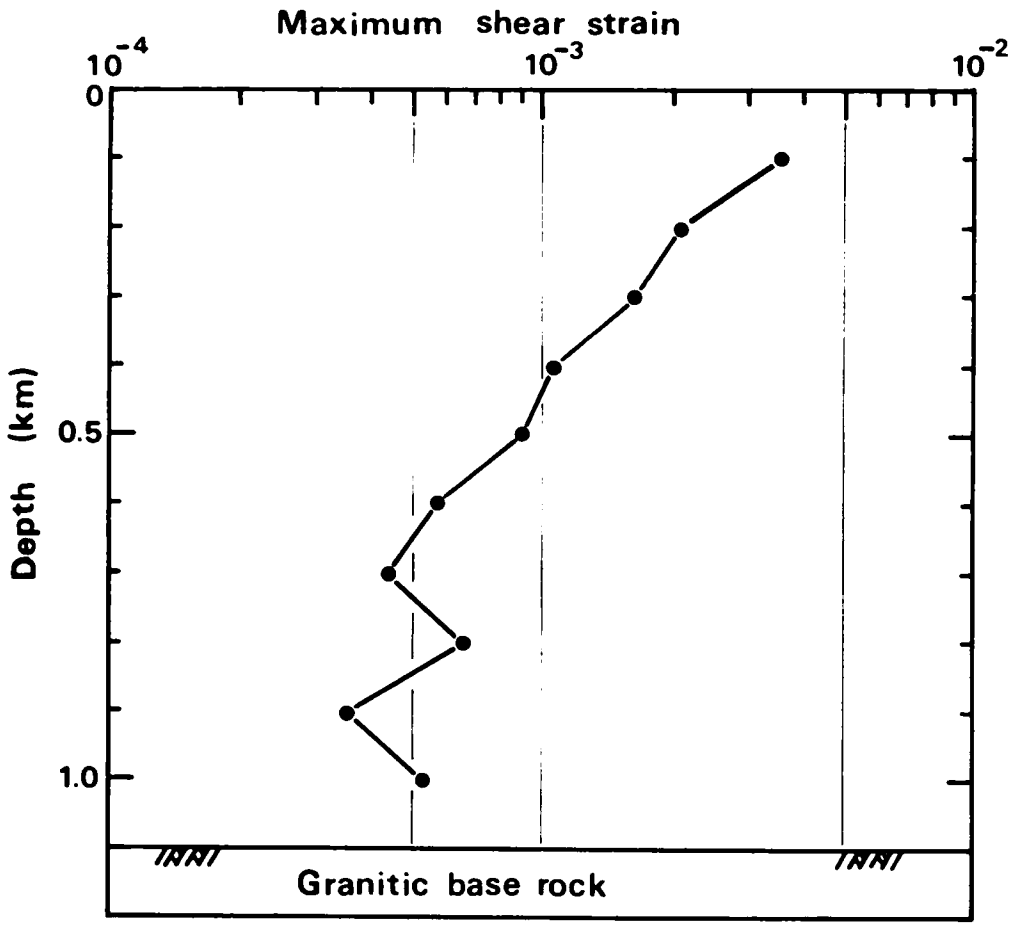

Fig.5.30 Distribution of maximum shear strain in the ground.

of the maximum shear strain in the ground to 100 *m* below the surface, while Fig.5.30 up to 1000 *m* below the surface. It is found from these figures that in the depth of 100 *m*, the maximum shear strain is almost constant and its value is about 3×10^{-3}, and that below 100 *m* in the depth, the shear strain decreases and is less than 10^{-3} strain level below 400 *m*.

The computed maximum shear strains throughout the presented response analysis, are relatively large because the damping characteristics of the soil itself are not taken into account. Below 400 *m* in the depth, the assumption that the soil mechanically behaves as a linear elastic material, can be accepted even for strong earthquake because of the low strain level in that places. In the shallow depth, however, the assumption of a linear elastic body of the soil will not be valid, and it is necessary in the response analysis to take into account the inelastic behaviors of soils such as viscoelastic and elasto-plastic behaviors, and the characteristics of the strain level dependency.

In the soil dynamics, the another important factor to investigate the soil dynamic behaviors is the frequency component. Fig.5.31 shows the Fourier spectrum of the shear strain at the depth of 10 *m*. We can find from this figure that the frequency components of 0.46, 1.2 and 3.5 *cps*. are prominent. Especially, the relatively low frequency component of 0.46 *cps*. is the strongest. In that frequency range the soil is in the transitional state between the static and the dynamic state[26] and shows the creep phenomena.

5.5.3 Conclusions

In the preceding section, the approximate approach to calculate the underground motions in the inhomogeneous elastic soil layer during an earthquake from the observed surface motion has been presented. Also, the accuracy of this approach has been examined. In this section, by using the

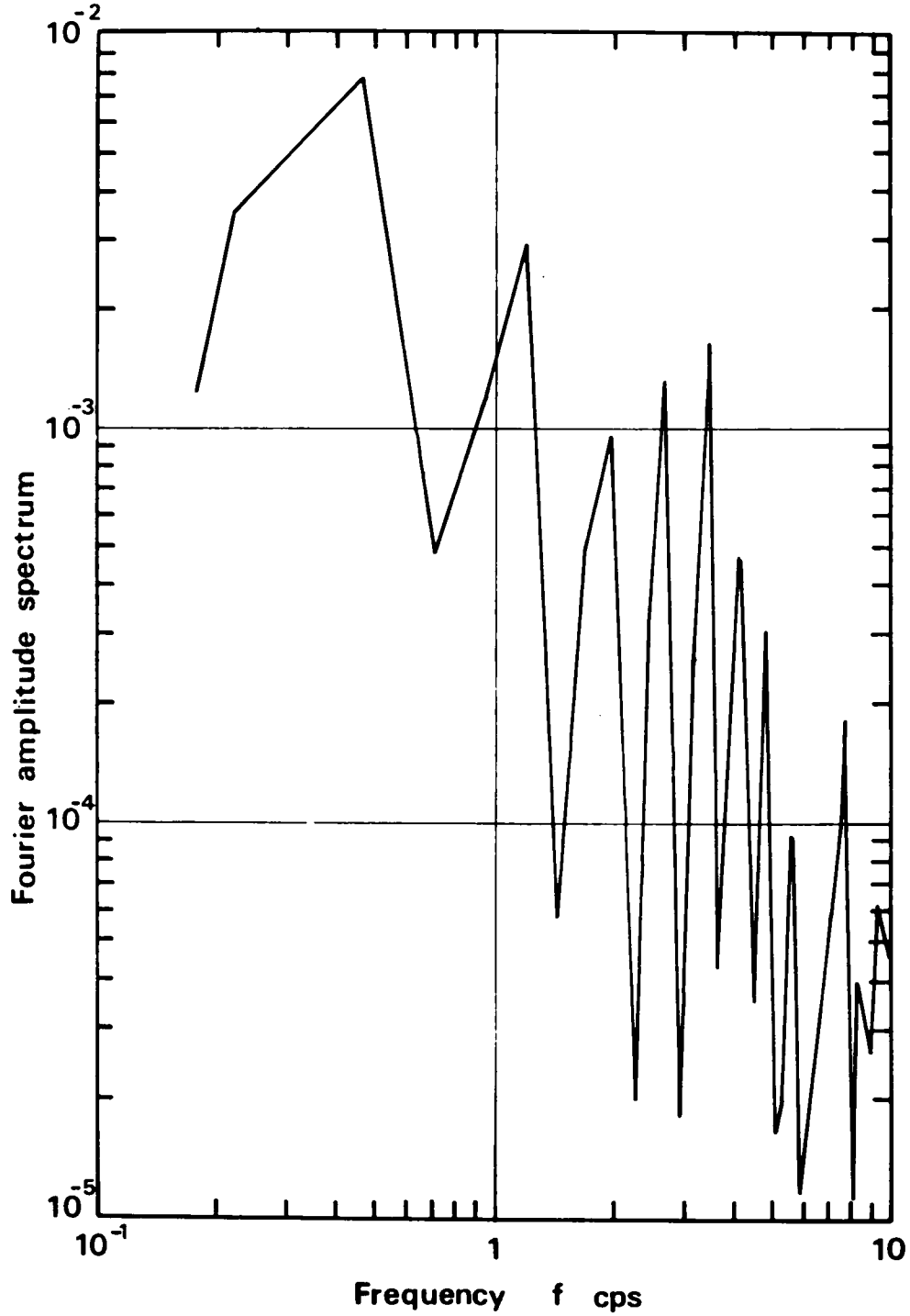

Fig.5.31 Fourier spectrum of shear strain at 10*m* below the surface.

similar approximation as one used in the preceding section, a method to obtain the response of the inhomogeneous elastic soil layer subjected to the incident earthquake motion at the base rock is described. By this method, we can simply calculate the response surface motion and the underground motion with the Fourier transform. Although this approach is limited to the linear elasticity and will give the greater accelerations and strains than expected from the actual strong earthquakes, it is very convenient in the point of being able to simply calculate the response motions in the inhomogeneous soil layer with the short computation time.

The earthquake response motion of Osaka ground was examined by this method. As the inhomogeneous conditions of Osaka ground, the distribution functions of the S-wave velocity and the unit weight were assumed as indicated in Fig.5.16. The acceleration curve at the El Centro base rock which was calculated from the El Centro earthquake of May 18, 1940 was used as the incident motion at the granitic base rock of Osaka. Throughout these response analysis for Osaka ground, the conclusions are obtained as follows;

(1) The fundamental period of Osaka ground is considered to be about 8.0 *sec.*, and the amplification of the amplitudes is considered to be large when we take into account the deep geological formation of Osaka area and regard the granitic layer as the base rock for earthquake analyses.

(2) The computed maximum acceleration at the surface was 526 *gal(0.54 g)* and the prominent frequency components were 0.45, 0.82 and 3.7 *cps.* and their periods were 2.2, 1.2 and 0.27 *sec.*, respectively.

(3) According to the distribution of the maximum acceleration, it decreases quickly in the depth of 100 *m*, and is nearly constant below 400 *m* in the depth.

(4) The time variations of the computed shear strain in the ground are complicated in the shallow depth, but in the deep places, the shear

strains vary with time almost periodically. The maximum shear strains distribute almost constant in the depth of 100 *m*, and their values are about 3.0×10^{-3} strain. Below 100 *m* from the surface, the maximum shear strains decrease with depth and their values become about 5.0×10^{-4} strain below 600 *m*. According to the Fourier spectrum of the shear strain curve at 10 *m* below the surface, we can find that the frequency component of 0.46 *cps*. is prominent, in which frequency range the soil is known to be in the transitional state from the static to the dynamic state.

Although we can understand that the shear strain which occurs in the ground, is at 10^{-3} strain level at most even during a strong earthquake, it is well known that in this strain level, the soil does not behave as a linear elastic material, but behaves viscoelastically or elasto-plastically and is dependent upon the strain level and the strain rate. Therefore, in the future study we must investigate the stress-strain-time characteristics of earth materials and develop the method of the response analysis by which we can take into account these inelastic characteristics and the detailed geological configulations.

References

1) "Proceedings of The International Conference on Microzonation for Safer Construction Research and Application, Vol.1 and 2", Seattle, U.S.A., 1972.

2) Sezawa, K., and K.Kanai: Possibility of Free Oscillations of Strata Excited by Seismic Waves, Bull. Earthq. Res. Inst., Vol.8, 1936, pp.1-11, Vol.10, 1932, pp.1-18 and pp.273-298.

3) Sezawa, K. and K. Kanai: Decay Constant of Seismic Vibrations of a Surface Layer, Bull. Earthq. Res. Inst., Vol.13, 1935, pp.251-265.

4) Kanai, K., T. Tanaka and S. Yoshizawa: Comparative Studies of Earthquake Motions of the Ground and Underground (Multiple Reflection Problem), Bull. Earthq. Res. Inst., Vol.37, 1959, pp.53-87.

5) Kanai, K., T. Tanaka, S. Yoshizawa, T. Morishita, K. Osada, and T. Suzuki: Comparative Studies of Earthquake Motions on the Ground and Underground 2nd Report, Bull. Earthq. Res. Inst., Vol.44, 1966, pp.609-643.

6) Parmelee, R. A., J. Penzien, C. F. Scheffey, H.B. Seed and G. R. Thiers: Seismic Effects on Structures Supported on Piles Extending through Deep Sensitive Clays, Report. No. 64-2, Inst. of Eng. Res., Univ. of California, Berkely, California, 1964.

7) Idriss, I.M. and H.B. Seed: Seismic Response of Horizonal Soil Layers, Proc. ASCE, Vol. 94., No.SM4, 1968, pp.1003-1031.

8) Whitman,R. V., J. M. Roesset, R. Dobry and L. Ayestaran: Accuracy of Modal Superposition for One-Dimensional Soil Amplification Analysis, Proc. Int. Conf. on Microzonation for Safer Construction Research and Application, Vol.2, Seattle, 1972, pp.483-498.

9) Arango, I. and R. J. Dietrich: Soil and Earthquake Uncertainties on Site Response Studies, Proc. Int. Conf. on Microzonation for Safer Construction Research and Application, Vol.2, Seattle, 1972, pp.629-647.

10) Tsai, N. C.: Influence of Local Geology on Earthquake Ground Motion, Ph. D. Thesis, California Institute of Technology, Pasadena, 1969.

11) Toki, K.: Inference of Seismic Ground Motion from Earthquake Records, Proc. JSCE, No.207, 1972, pp.25-36(in Japanese).

12) Kagami, H. and H. Kobayashi: A Method for Local Seismic Intensity Zoning Maps on the Basis of Subsoil Conditions, Proc. Int. Conf. on Microzonation for Safer Construction Researth and Applications, Vol.2, Seattle, 1972, pp.513-528.

13) Hardin, B. O. and F. E. Richart: Elastic Wave Velocities in Granular Soils, Proc. ASCE, Vol.89, No.SM1, 1963, pp.33-65.

14) Bhattacharya, S. M.: Exact Solutions of SH-wave Equation for Inhomogeneous Media, Bull. Seis. Soc. Am., Vol.60, No.5, 1970, pp.1847-1859.

15) Upadhyay, S. K. and J. G. Negi: Effects of Varying Anisotropy Coefficient on SH-wave Dispersion, Bull. Seis. Soc. Am., Vol.60, No.5, 1970, pp.2071-2081.

16) Kobori, T., R. Minai and T. Suzuki: Wave Transfer Functions of Inhomogeneous Linear Viscoelastic Multi-Layered Media, Annuals of the Disaster Prevention Res. Inst., Kyoto Univ., No.13A, 1970, pp.213-232(in Japanese).

17) Iwasaki, Y.: On the Earthquake Base Rock in Osaka, Preprint, 8th Conf. JSME, 1973, pp.637-640(in Japanese).

18) Tsai, N. C. and G. W. Housner: Calculation of Surface Motions of a Layered Half-Space, Bull. Seis. Soc. Am., Vol.60, No.5, 1970, pp.1625-1651.

19) Kanai, K.: Earthquake Engineering, Kyoritsu Shuppan, Co. Ltd., 1970, pp.72-73(in Japanese).

20) Hori, M.: On Approximate Solutions on Characteristics of Inhomogeneous Ground Shaking, Preprint, 8th Conf. JSME, 1973, pp.629-632(in Japanese).

21) Torimi, I.: Report on Ground Suveying in Abeno Re-Development District, 1971.

22) Yoshikawa, S. and Y. Iwasaki: On the Earthquake Response Characteristics and the Distribution of the Intensity of Alluvial Layer, Preprint, 26th Conf. JSCE, 1971, pp.121-124(in Japanese).

23) Yoshikawa, S. and Y. Iwasaki: On the Characteristics of Ground Shaking in Osaka with Considering the Deep Geophysical Formations, Preprint, 27th Conf. JSCE, 1972, pp.221-224(in Japanese).

24) Kobori, T., S. Yoshikawa, R. Minai, T. Suzuki and Y. T. Iwasaki: Effects of Soil and Geological Conditions on Structural Responses in Osaka Area, Proc. Int. Conf. on Microzonation for Safer Construction Research and Application, Vol.2, Seattle, 1972, pp.719-734.

25) Toki, K. and S. Cherry: Inference of Subsurface Acceleration and Strain from Accelerograms Recorded at Ground Surface, Preprint.

26) Akai, K. and M. Hori: Considerations of Wave Characteristics in Soil Assumed as Viscoelastic Material, Proc. of JSCE, No.221, Jan., 1974.

Chapter 6 Conclusions

The purposes of this thesis were :

(1) to develop new experimental laboratory technique, the "shock tube technique", for study on stress wave propagation characteristics through soils;

(2) to investigate the wave characteristics in close relation to the physical properties of soils and to discuss them on the basis of visco-elasticity; and

(3) to develop a method for analyzing the earthquake response of the inhomogeneous ground.

In this chapter, the main conclusions in the previous each chapter are described briefly with a prospect for the continued future study.

A great effort was directed toward the development of the shock tube technique to measure acculately the phenomena of wave propagation through soils. First of all the author devised the condenser-type soil strain meter to measure the one-dimensional soil strain during stress wave propagation. As mentioned in Chapter 2, the amount of change in the electrostatic capacity of the condenser embedded in soils can be transformed into the amount of strain by the simple relation. For this transformation, it only needs to read the initial capacity beforehand the testing, and other troublesome calibration tests are needless. Since the thin needles are used as the electrodes of the condenser, there is no anxiety that the soil is disturbed in forming the condenser in it. It was found from the experiments that the dynamic responsibility of this meter is excellent. When we need to measure the uniaxial strain at an optional point in soils, this type of strain meter surely becomes a convenient tool. However, in order that this meter may become a sure measuring equipment in any environments, there are some problems to be solved.

Since radio frequency is used in this meter, it is easy to be influenced by a man approaching or things. Also since the capacity of the fixed condenser used in the meter is relatively small(100μF), the saturation of electrostatic capacity sometimes occurs in the case of soils with high moisture content.

In Chapter 3, the experimental apparatus of the shock tube technique was described in detail. The shock tube was used as a loading apparatus to the soil specimen. By using this method of loading, it was easy to obtain the uniform pressure like a spike pulse and to control its pressure level. In order to make the conditions for the compressional and the rod wave propagation through the soil specimens, the confining tube for the former case and the triaxial compression chamber for the latter case were designed with appropriate equipments to measure the characteristics of the stress wave propagation. In the design of these apparatus, a great attention was paid to minimize the lateral friction of the specimen. In the case of the compressional wave propagation test the soil column was roled by two teflon sheets not only to minimize the friction but also to perfectly confine the lateral deformation of the soil, and the sandy loam was used as a soil sample. The influences of moisture content, degree of saturation and dry density on the wave characteristics were mainly investigated. On the other hand, in the rod wave propagation test, the bearings were used to support the specimen. The silty loam was used as a sample and the relationships between the wave characteristics and the confining pressure(or consolidation pressure) were obtained. In both tests, the intensity of the input surface pressure was so controlled that the amplitude of strain arised in the soil was less than 10^{-3} in order. The main conclusions obtained from the experiments were:

(1) A compressional wave velocity through partially saturated soils(sandy loam) is strongly dependent upon the void ratio and the degree of saturation. The velocity decreases with increase in the void ratio

and the degree of saturation.

(2) The relationship between a rod wave velocity v_R through saturated cohesive soil and an effective confining pressure p_c is given by the following formula:

$$v_R = m \cdot p_c^{\,n}$$

From experimental results, the constants of m and n were determined to be 280 and 0.39 respectively(p_c : kg/cm^2, v_R : m/sec). That is, the rod wave velocity is proportional to the two-fifth power of the effective confining pressure. Furthermore, assuming Poisson's ratio ν=0.5, the relationship between the shear wave velocity v_s, p_c and the void ratio e is given by

$$v_S = F(e) \cdot p_c^{0.25}$$

where, $F(e)$ is a linear function of e.

(3) A dynamic modulus of elasticity E_d from a rod wave velocity is linear with p_c. Its magnitude is 3 to 6 times larger than the initial tangent modulus E_s of a stress-strain curve from the static triaxial compression test. The ratio of the dynamic shear modulus G_d to the shear strength s_u of the soil specimen tested is 773 from experiments.

(4) A stress-strain relationship of the clayey soil at propagation of wave shows a large hysteresis curve at the strain level of 10^{-3}, but any permanent strain is not created during the test. A dynamic modulus of elasticity E_d from the wave velocity coincides with the initial tangent modulus of elasticity E_i.

(5) The relationship between the attenuation constant and the dry density of sandy loam is closely related with the characteristic of compaction of the soil. In the case of the samples with moisture content of 5-7%, the attenuation constant decreases with increase in the dry

density, and in 11-13% which includes the optimum moisture content, it is smallest at the dry density of about 1.75 g/cm^3. Its dry density is slightly smaller than the maximum dry density at the optimum moisture content. The attenuation constant decreases with decrease in the void ratio. Its relationship is linear in log-log scale in the experimental range of the void ratio.

(6) In the rod wave propagation test for clayey soil, it was found that the rate of attenuation became small below a certain stress level. This critical stress level corresponds to the stress of 20-25% of the triaxial compressive strength σ_{max}, and also corresponds to the strain level of 0.1% in the static stress-strain curves. The author concludes that below this stress or strain level, elastic or viscoelastic property is more predominant in soils than plastic one. The relationship between the attenuation constant of the rod wave and the void ratio is also linear in log-log scale similar to one of the sandy loam.

In Chapter 4, the analytical considerations on the stress wave propagation through soils were performed on the basis of viscoelasticity. For simplicity, the soil was assumed as the spring-Voigt model, and the general behaviors of this model and the boundary value problems of rod wave propagation of spike pulse through it were analyzed mathematically. Furthermore, from comparison of the wave propagation characteristics in between the spring-Voigt model and the saturated porous elastic medium, it was understood that the wave characteristics of the spring-Voigt model are similar to those of the compressional wave of the first kind defined by Biot and Ishihara. By using experimental data of the rod wave propagation test for the silty loam, the viscoelastic constants were obtained and discussed with repect to the confining pressure and the frequency. The obtained conclusions are:

(1) The parameter, which represents the square of the ratio of the phase velocity at zero frequency to that at infinite frequency, ϑ_{sv} is 0.1-0.2 for the normally consolidated clays and 0.2-0.3 for the over-consolidated clays. By considering that the difference between the static and the dynamic modulus for O.C. clay is smaller than that for N.C. clay, and that the logarithmic decrement is smaller, it is concluded that the elastic properties of O.C. clay are remarkable compared with N.C. clay.

(2) The free spring E' in the spring-Voigt model is almost identical to the dynamic modulus of elasticity E_d calculated from the velocity of the wave front. E' is linearly dependent upon the confining pressure and can be estimated only by the void ratio and the confining pressure. While, the remaining parameters E and $1/\mu$ in the model are not linearly dependent upon the confining pressure but their relations change at the pre-consolidation pressure of the clayey soil. These experimental results conclude that E and $1/\mu$, which are considered to relate with the coupling effect between the solid particles and the water, are influenced by the change of the soil structure.

(3) The time constant τ_{sv} changes with the frequency. Its value is a few seconds or more in the quasi-static state with the frequency range less than 10^{-2} *cps* and is a constant of about 3×10^{-2} *sec* in the frequency range more than 1 *cps*. In the transitional state, $f\tau_{sv}$ is constant. Therefore, the creep or relaxation phenomena of soils could not be in the dynamic state more than 1 *cps*.

(4) The ratio of E to E', k, obtained from the present experiments is between 0.1 to 0.4. Furthermore, according to the experimental data by other investigators, k is considered to be a value less than 1.0.

Throughout these viscoelastic approach, it was understood that the mechanical behaviors of soils in the small strain level and in the wide frequency range can be approximated by the spring-Voigt model with the values of the

rheological constants as above estimated.

Although the ground formation near the surface is very complicated in general, it is often that its dynamic modulus and density increase with the depth beneath the ground surface, and that their distribution can be replaced by suitable continuous functions of depth which increase monotonously with depth. In Chapter 5, this particular ground was called as the inhomogeneous ground. The approximate equations to calculate the underground earthquake motions at a certain depth in the inhomogeneous elastic layer from the surface motion were derived in the integral form on the basis of the multiple reflection theory of waves for multi-layered system. The approximate equations consist only of the terms of the direct transmission wave and the first and the second order reflection waves, and the higher order reflection waves were neglected in the derivation. In order to examine the accuracy of the approximation, the results of characteristics of the ground shaking calculated from the approximate equations were compared with the exact one for two particular models of the inhomogeneous ground. It was found from this comparison that the accuracy of the approximation is very high. Furthermore, according to the numerical example by Atsumi Hanto Oki Earthquake record at Abeno site in Osaka, the calculated underground motions remarkably agreed with the observed one. It was confirmed that if irregular distributions of dynamic modulus or densities in the underground can be expressed by certain suitable functions of depth, the underground motions or base rock motions can be simply and accurately calculated with a short computation time from the approximate equations, and the characteristics of ground shaking of an inhomogeneous ground can be also investigated.

Moreover, the analytical method applying the Fourier transform was presented to obtain the response motion of the inhomogeneous elastic layer subjected to an incident earthquake motion at the base rock. The earthquake

response motions of Osaka ground site were calculated by this method. The acceleration curve at the El Centro base rock which was calculated from the El Centro Earthquake of May 18, 1940 was used as the incident motion at the granitic base rock of Osaka site. Throughout these response analyses for Osaka ground, the conclusions were obtained as follows:

(1) The fundamental period of Osaka ground is about 8.0 *sec*, and the amplification of the amplitudes is large when we take into account the deep geological formation of Osaka area and regard the granitic layey as the base rock for earthquake analyses.

(2) The computed maximum acceleration at the surface was 526*gal*(0.54 *g*) and the prominent frequency components were 0.45, 0.82 and 3.7 *cps* and their periods were 2.2, 1.2 and 0.27 *secs*, respectively.

(3) The distribution of the maximum acceleration decreases quickly in the depth of 100 *m*, and is nearly constant below 400 *m*.

(4) The time variations of the computed shear strain in the ground are complicated in the shallow depth, but in the deep places, the shear strains vary with time almost periodically. The maximum shear strains distribute almost constant in the depth of 100 *m*, and their values are about 3.0×10^{-3} strain. Below 100 *m* from the surface, the maximum shear strains decrease with depth and their values become about 5.0×10^{-4} strain below 600 *m*. According to the Fourier spectrum of the shear strain curve at 10 *m* below the surface, we can find that the frequency component of 0.46 *cps* is prominent, in which frequency range the soil is known to be in the transitional state from the static to the dynamic state.

Although we can understand that the shear strain which occurs in the ground, is at 10^{-3} strain level at most even during a strong earthquake, it is well known that in this strain level, the soil does not behave as a linear elastic material, but behaves viscoelastically or elasto-plastically and is

dependent upon the strain level and the strain rate. Therefore, in the future study we must investigate the stress-strain-time characteristics of earth materials and develop the method of the response analysis by which we can take into account these inelastic characteristics and the detailed geological configulations.